takece.com
Continuing Education Simplified!

Course Title: Pregnancy and Fetal Ultrasound

Topic List:-

Chapter 4

Early Pregnancy Ultrasound Assessment of Multiple Pregnancy

Panagiotis Antsaklis, Maria Papamichail, Marianna Theodora, Michael Syndos and George Daskalakis

Additional information is available at the end of the chapter

http://dx.doi.org/10.5772/intechopen.81498

Abstract

As the frequency of multiple pregnancies is increasing, every obstetrician has to know that the correct, accurate, and timely determination of gestational age, chorionicity, and amnionicity has significant importance in the management of a multiple pregnancy. Surveillance, complications, outcome, morbidity, and mortality are totally different in a monochorionic and a dichorionic pregnancy. In this chapter, we will present the sonographic figures that are visualized in the first trimester in a multiple pregnancy and help us define the gestational age, chorionicity, and amnionicity. We will classify them into two periods: the early first trimester, including the 10 first weeks of gestation and the late first trimester including the period between the 10th and 14th week of gestation. Finally, we will review some interesting, although infrequent, cases from the literature, showing that pitfalls in the determination of both chorionicity and amnionicity exist and highlighting the importance of being aware of their subsistence.

Keywords: multiple pregnancy, early ultrasound assessment, gestational age, chorionicity, amnionicity

1. Introduction

It is a well-established fact that multiple pregnancies occur more commonly nowadays than a few decades ago. The progress of reproductive technologies and *in vitro* fertilization has played a major role in this increase. In fact, twins comprise about 3% of all live births in the United States [1]. As we speak about history, the vast majority of multiple pregnancies that occurred

in the past were diagnosed during the intrapartum period [2]. Today, as the use of ultrasound has become a routine in daily medical practice, multiple pregnancies are diagnosed in the initial ultrasound scan [3]. Beyond the diagnosis of early multiple pregnancy, ultrasound scan is more than necessary to define chorionicity, amnionicity, and gestational age [4].

In this chapter, we will present the ultrasound figures that help us determine gestational age, chorionicity, and amnionicity, focused on the 14 first weeks of gestation in multiple pregnancies. We will also focalize the discussion on twin pregnancies, as they comprise >98% of multiple pregnancies and the vast majority of studies today include twin pregnancies [4]. Nonetheless, we will review some cases from the literature that show that situations can be a little more complicated and may lead to a false diagnosis of chorionicity and amnionicity, in order to highlight that when we manage multiple pregnancies, we have to be alert about exceptions despite being infrequent [5].

A twin pregnancy can be either dizygotic (two-third of twin pregnancies), in which two different eggs are fertilized by two different sperms, and in this case, the pregnancy is always dichorionic-diamniotic or monozygotic. A monozygotic pregnancy occurs when an egg is fertilized by one sperm, producing one embryo, which can split any time, more commonly between day 2 and day 13 after fertilization. Chorionicity and amnionicity are differentiated by the timing of embryo splitting. **Table 1** presents this differentiation and the frequency of each type of a monozygotic pregnancy [3].

2. Defining gestational age

The accurate determination of gestational age is critical for pregnancy management as it shows wherever the measurements of the fetus are in line for the estimate gestational age [4]. In addition, a correct pregnancy dating is necessary not only for the appropriate timing for screening and diagnostic testing but also for optimal scheduling of delivery [6]. For women with regular cycles, the date of the last menstrual period is used to estimate gestational age, taking into account the biological variability and correct the cycle length. For IVF pregnancies, the date of the embryo transfer has been used to define pregnancy dating. The vast majority of authors embraced with multiple pregnancies agree that during the second trimester the evaluation of gestational age is more accurate and it is statistically superior to the second trimester [4]. Moreover, there is an agreement that the parameters and formulas that have been used for dating singleton pregnancies are also accurate for dating multiple pregnancies, since studies in this area include a combination of singleton and multiple pregnancies [7–9].

Time of embryo splitting (in days)	Chorionicity	Amnionicity	Frequency (%)
2–3	Dichorionic	Diamniotic	30
3–8	Monochorionic	Diamniotic	70
8–13	Monochorionic	Monoamniotic	<1

Table 1. How the chorionicity and amnionicity are differentiated by the timing of the embryo splitting in monozygotic twins (Table is modified from Simpson L, 2015 [6]).

In the first trimester—before the 14th week of gestation—crown-rump length (CRL) is the parameter that is used in order to estimate gestational age with 5–7 days of deviation [7–9]. If there is a doubt about the reliability of the menstrual cycle or if the woman is administrated late for care, a repeat scan in 3–4 weeks can be helpful to determine pregnancy dating [10].

Modest size discordance is very common in multiple pregnancies [4]. Some studies suggest that pregnancy dating must be defined by using the mean of the fetuses [11]. However, more recent studies agreed that if the gestational age is based on the CRL of the larger twin, the possibility of missing a fetus that might develop intrauterine fetal growth restriction (IUGR) is decreased [12]. Salomon et al. [13] suggested that the CRL of the smallest fetus can estimate more accurately the gestational age, if the intertwin CRL discrepancy is less than the 95th percentile, using charts from studies. An interesting finding is that if the intertwin discordance in CRL is higher than 10%, the possibility of pregnancy loss, aneuploidy, or congenital anomalies is increased [3, 14, 15].

In the second trimester, a combination of parameters is used to define pregnancy dating such as abdominal circumference, femur length, and biparietal diameter [8]. Further discussion about calculating gestational age in second trimester is beyond the scope of this chapter.

3. Defining chorionicity and amnionicity

Early and accurate definition of chorionicity and amnionicity has an undeniably determinant role in the management of multiple pregnancies, since chorionicity plays a key role in the appearance of complications: monochorionic-monoamniotic twins present the highest mortality and morbidity. There is no doubt that the continuous surveillance and the timely intervention can optimize the outcome of the pregnancy [4].

The determination of chorionicity and amnionicity is better to be done in the first trimester [4]. If chorionicity is defined in the first trimester, accuracy is extremely close to 100% and if the definition is carried out in the second trimester, correct assignment decreases to 90% [16, 17].

At this point, we will classify the determination based on gestational age, separated in two periods: the first before the 10th week of gestation and the second that includes the period from week 10 to week 14.

3.1. Before 10 weeks of gestation

Three ultrasound findings can help in the detection of chorionicity: These are (1) the number of observable gestational sacs, (2) the number of amniotic sacs within the chorionic cavity, and (3) the number of yolk sacs [4].

3.1.1. Number of observable gestational sacs

The number of the gestational sacs and the number of fetal heartbeats in early multiple pregnancy scan are strongly related with chorionicity: each gestational sac will form a distinct placenta and chorion. Therefore, visualization of a single gestational sac with two visible heart beats indicates a monochorionic twin pregnancy, while the presentation of two distinctive

gestational sacs implies a dichorionic pregnancy (**Picture 1**) [18]. The number of gestational sacs is the parameter with the highest accuracy to define chorionicity which is extremely close to 100% [16].

3.1.2. Number of amniotic sacs within the chorionic cavity

Identification of the number of amniotic sacs present in a single gestational sac helps define amnionicity in a monochorionic pregnancy. Prior to the 10th week of gestation, the amnions grow outward from the embryonic disk and at that age are not big enough to contact each other and create the intertwin septum [4]. As a result, separate and distinct amnions indicate a diamniotic twin pregnancy (**Pictures 2a**, **b** and **3a**, **b**). The evaluation of the amnion should be done diligently via transvaginal ultrasound since the intertwin membrane is extremely thin and it may be invisible via transabdominal ultrasound. Even when the separate amnions cannot be visualized via the transvaginal ultrasound, their absence can be confirmed by demonstrating umbilical cord enlargement by using pulsed wave Doppler and identifying two distinct heart rates [3]. In addition, the impossible visualization of the intertwin membrane may be technical: if the membrane is parallel to the ultrasound beam or because the ultrasound gain is low, the membrane may be hard to evaluate. This problem can be solved by changing the angle of insonation and increasing gain facilitates visualization [5]. Another way to confirm amnionicity, wherever there is any doubt about the presence of the intertwin membrane, is to suggest a small chain of repeat scans [4].

However, is evaluation of intertwin membrane always that simple? There are two rare yet important situations that may lead to a false diagnosis of monoamniotic twins. The first case

Picture 1. Dichorionic diamniotic pregnancy at 5 weeks of gestation. The two separate gestational sacs with one yolk sac each are visible and a thick septum separates them.

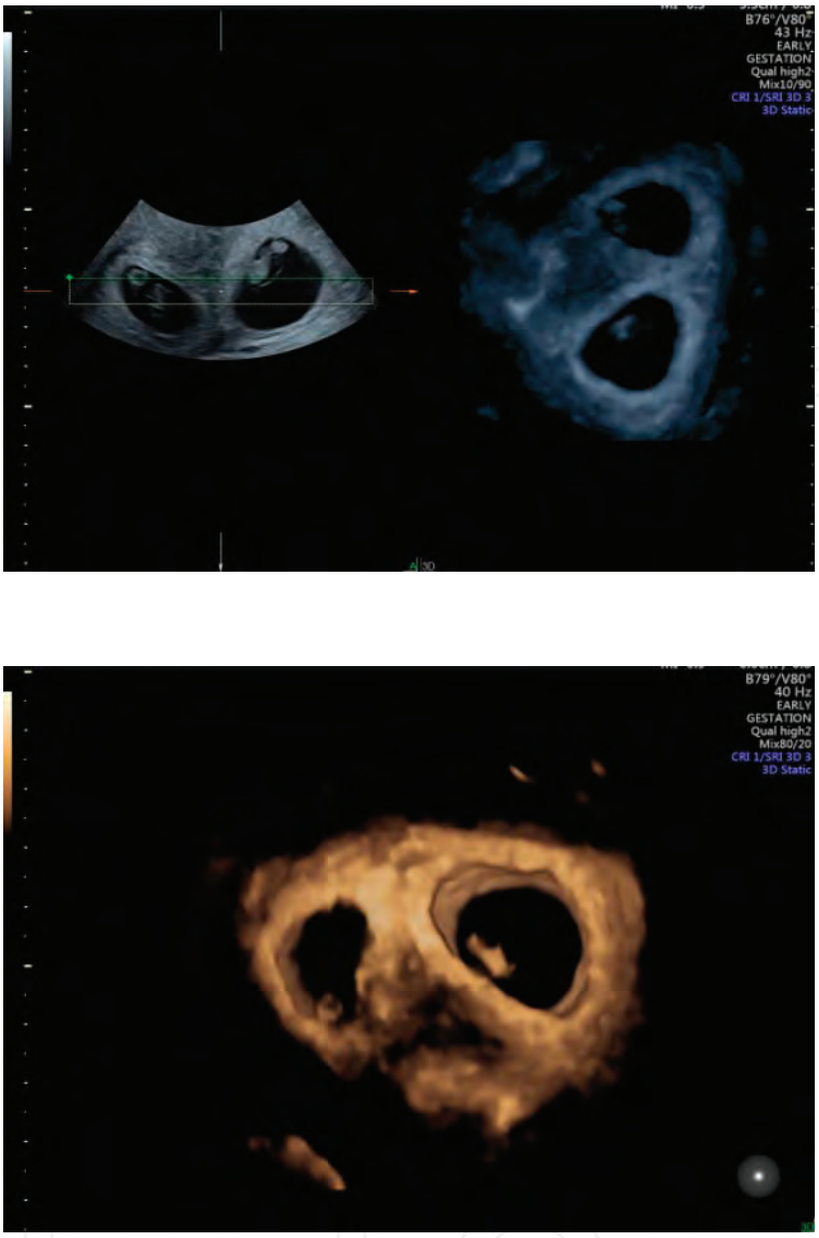

Picture 2. (a) 3D imaging of dichorionic diamniotic pregnancy at 6 weeks of gestation. (b) 3D imaging of dichorionic diamniotic pregnancy at 6 weeks of gestation.

is when the monochorionic-diamniotic twins are complicated with twin-to-twin transfusion syndrome (TTTS) the donor twin has severe oligohydramnios or anhydramnios, and the intertwin membrane collapses resulting in wrapping the donor twin. The collapse of the membrane can be overtaken if we evaluate extremely carefully the wrapping membrane around the limbs of the donor twin. A possible rupture of the intertwine membrane is another case that may lead to "pseudo-MA" twins. Rupture of the membrane may occur spontaneously, but more often is a complication of invasive *in utero* procedures. Discontinuity of the membrane and cord enlargement can be visualized on the ultrasound scan. Other facts helping

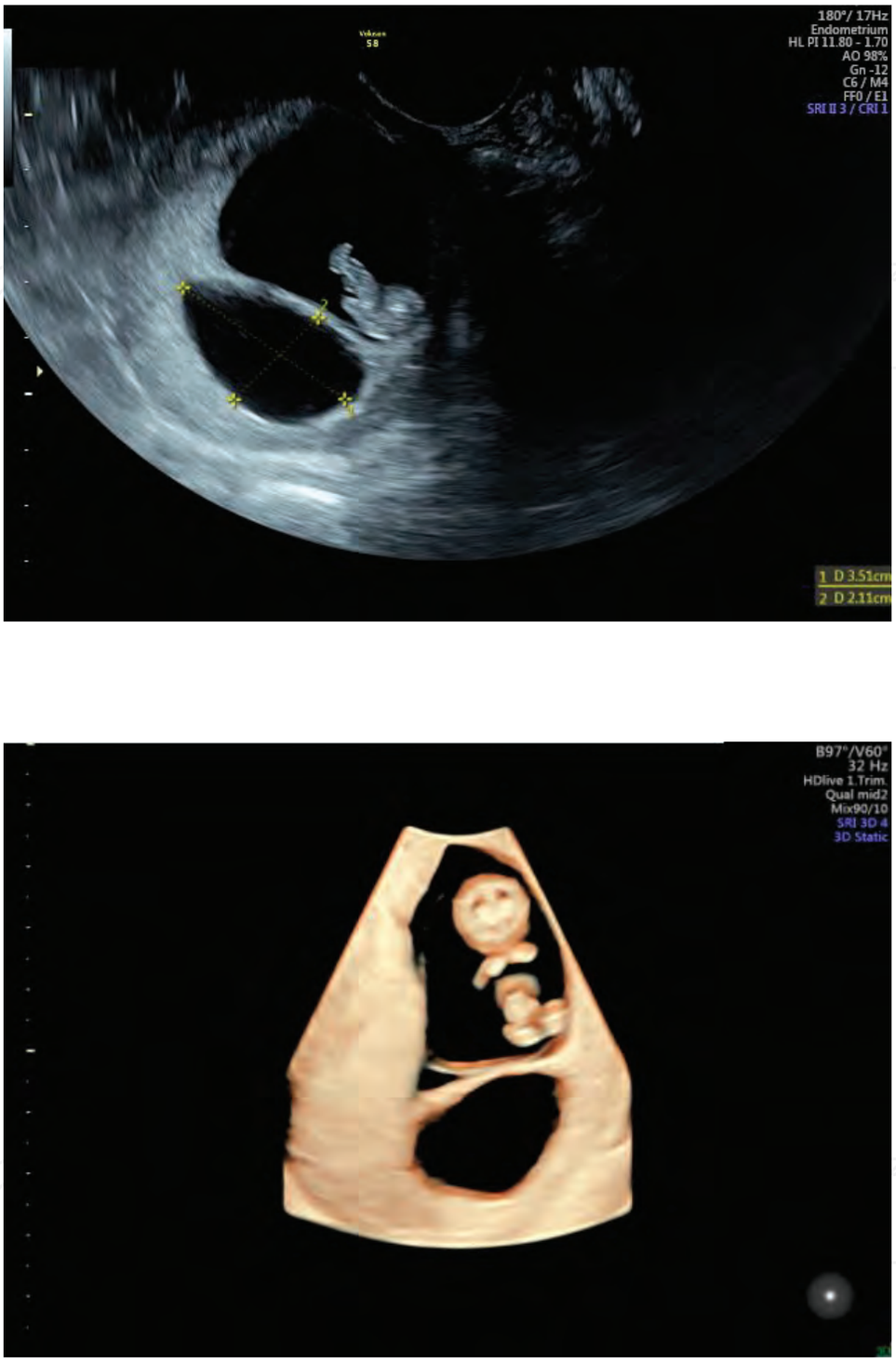

Picture 3. (a) Dichorionic diamniotic pregnancy with one of the pregnancies having miscarried. The size of the empty sac has been measured. (b) 3D imaging of DCDA pregnancy in which one of the sacs appears "empty" due to miscarriage.

in the identification of the membrane rupture are the location of the fetuses in the same side of the warped membrane, the equal quantity of amniotic fluid in both sides of the dividing membrane in a pregnancy, which was complicated with TTTS, and of course a previous diagnosis of a monochorionic-diamniotic twin pregnancy [5].

3.1.3. Number of yolk sacs

Over the past few years, there is an uncertainty regarding the relation between the number of yolk sacs and amnionicity. If there are two yolk sacs present in the extraembryonic coelom, the pregnancy will be regarded as diamniotic. However, a single yolk sac cannot set the definitive diagnosis of a monoamniotic pregnancy. This is well-established since it is known that the differentiation of a yolk sac and an amnion occur very close to each other in time, around 6–8 days after fertilization [5]. If a single yolk sac is detected, a repeat first trimester scan is undertaken, or a refer to a tertiary center with advanced experience in multiple pregnancies can be helpful [3, 4].

3.2. 10th–14th week of gestation

As the pregnancy continues, the ultrasound signs that help in the determination of chorionicity and amnionicity are changing: gestational sacs are now fused and the intertwin membrane is formed. As a result, four other ultrasound figures set the diagnosis of chorionicity and amnionicity. These are: (1) sex discordance, (2) distinct placentas number, (3) intertwin membrane characteristics and (4) chorionic peak sign—'λ' sign.

3.2.1. Sex discordance

If a male and a female fetus are identified in the late first or early second trimester, a dichorionic twin pregnancy is the rule. However, gender discordance is the biggest pitfall for the diagnosis of chorionicity. Discordant fetal sex phenotype can be present in monochorionic twins, leading to a false diagnosis of dichorionic twins.

A false diagnosis of dichorionic twins might be the result of a postzygotic sex chromosome aneuploidy. For instance, there is a 46,XY zygote which splits, but a postzygotic anaphase lag can cause the loss of the Y chromosome in one of the twins. The karyotype of one of the fetuses will be 46,XY which corresponds to a normal male fetus, while the other karyotype will be 45,XO which is a female fetus with Turner syndrome (**Figure 1**). If we want to take our example a step forward, postzygotic nondisjunction after the anaphase lag can lead to mosaicism in the monozygotic twins leading to two embryos with a variety of proportion of 45,XO and 46,XY cells. The phenotype of this individual will correspond to the amount of cells having the abnormal karyotype (**Figure 2**) [19, 20].

A sex discordance in monozygotic twins can also be caused by a trisomic 47,XXY zygote. A process known as trisomy rescue can lead to either the production of a normal 46,XY male fetus (loss of X chromosome) or a normal 46,XX female fetus (loss of Y chromosome) Hence, this mechanism causes the production of two euploids fetuses from a trisomic zygote (**Figure 3**) [21]. In addition, confusion might be caused if a 46,XY zygote splits with nondisjunction of the Y chromosome, producing a male fetus with a 47,XYY karyotype and a female fetus with a 45,XO karyotype, Turner syndrome, and female sex phenotype (**Figure 4**) [22].

Beyond sex chromosome abnormalities, sex discordance may be the result of epigenetic single gene defects in only one of the monoygotic twins, effecting testis-determining genes such as SOX9 which inhibits the expression of SRY gene [23, 24].

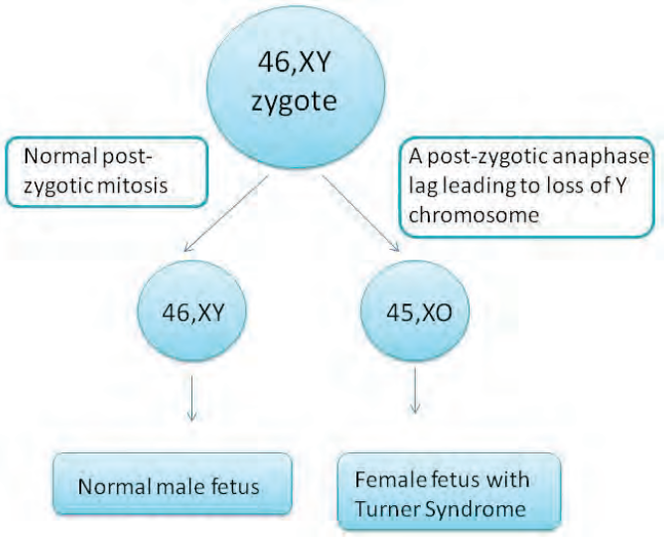

Figure 1. Postzygotic anaphase lag causing sex discordance due to loss of Y chromosome in one of the fetuses.

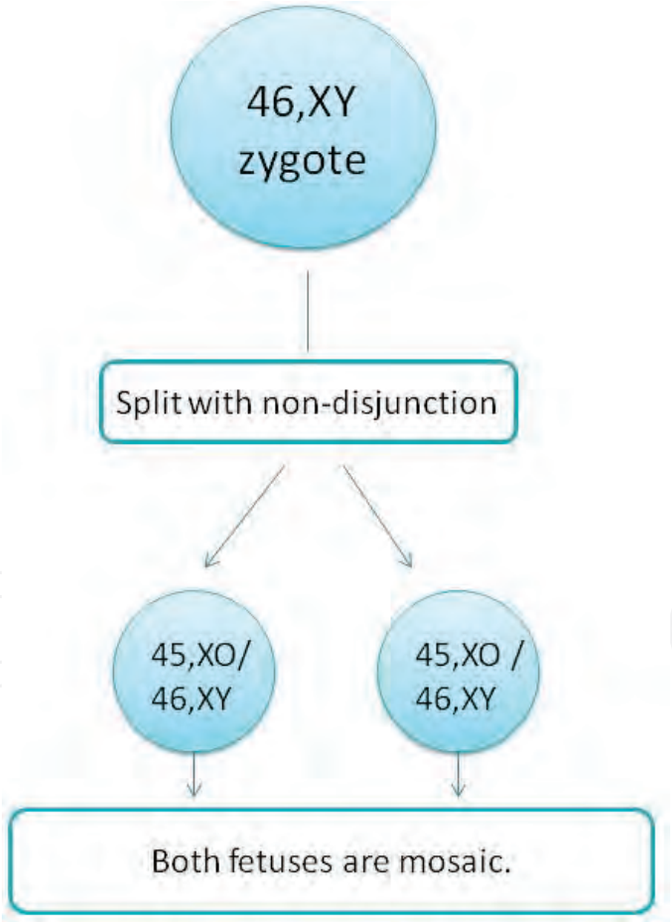

Figure 2. Postzygotic nondisjunction leading to both fetuses with gonadal mosaicism.

Nonetheless, sex discordance may be caused by malformed genitalia unrelated to chromosomal or genetic disorders. It is well established that a monochorionic twin pregnancy is complicated frequently with selective growth restriction [25], and hypospadias is a known complication of

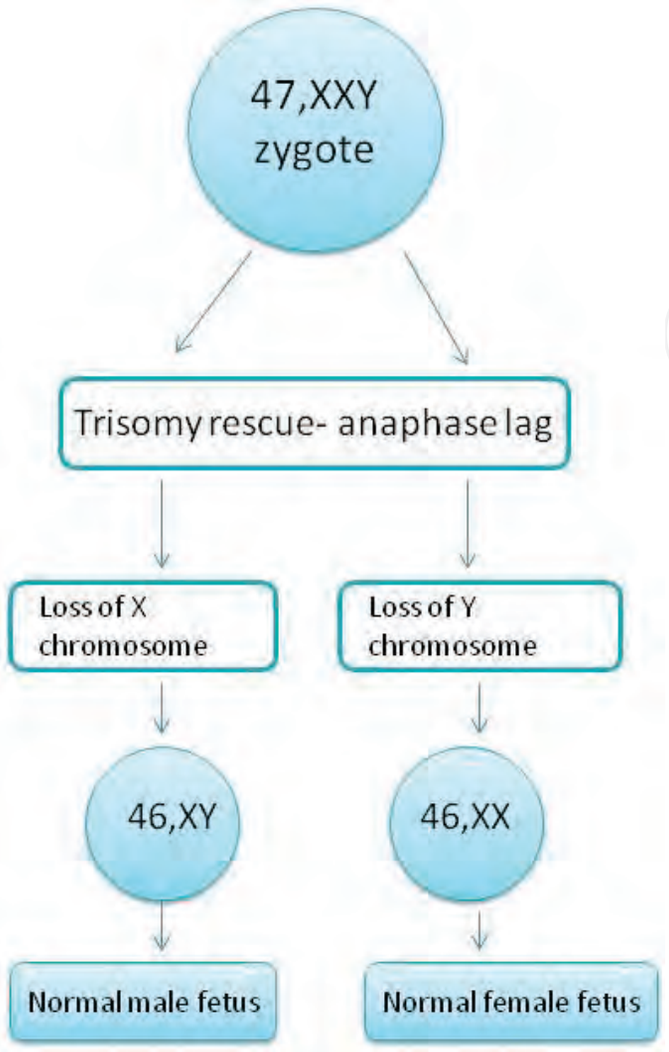

Figure 3. Trisomy rescue.

IUGR [26, 27]. As hypospadias might lead to female sex phenotype, confusion about chorionicity is expected, as the IUCR male fetus will present with female external genitalia, while the normally developing twin will be present as a normal male fetus. Cloacal malformation in one of the female fetuses (karyotype 46,XX) leads to phallus-like structure, causing phenotypically male external genitalia. The outcome is again confusion of chorionicity [28].

A very rare mechanism can cause the transverse situation: a dizygotic twin pregnancy is been diagnosed as monochorionic because of the fusion of the trophoblasts. Two distinct blastocysts produce two distinctive trophoblasts. If these trophoblasts fuse before the implantation, the result is the creation of a placental mass. The fused placenta will form vascular anastomoses, and the twins can exchange blood cells. As a result, blood chimerism of two populations of blood cells will be present in both fetuses [29, 30]. This mechanism is present more frequently in pregnancies carried out from ART because of the disruption of the zona pellucida and spatial proximity of multiple embryos [29, 31]. Dizygotic twins forming a monochorionic placenta have significant importance because these twins are genetically and phenotypically normal and they have to be distinguished from the pathological sex discordance [5].

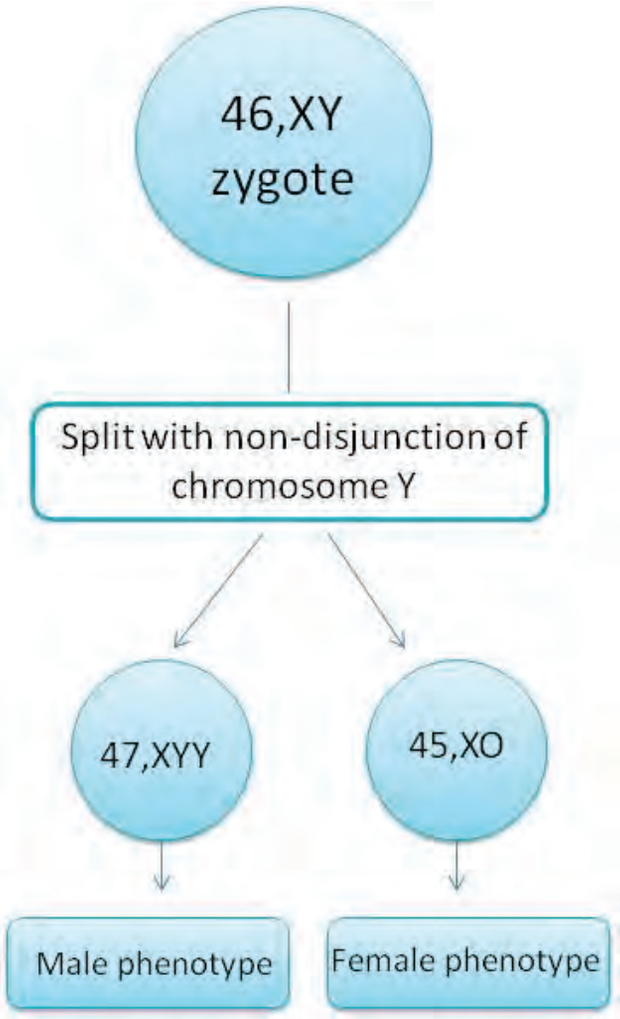

Figure 4. Nondisjunction of chromosome Y.

3.2.2. Number of distinct placentas

It is logical that the visualization of two separate placental masses confirms dichorionicity as a single placenta identifies monochorionicity [4]. Careful ultrasound evaluation has to be done in order to define the presence of a single placenta or two placentas in abutment.

As the pattern above, monochorionic twins may form a bipartite placenta. This sonographic finding is visible in 3% of monochorionic twin pregnancies. As a result, two separated placental masses are present with two nearly equal-sized placental lobes, which can be totally separated or connected by chorion laeve. Things can be more complicated when each placental mass has its own umbilical cord connection. Bipartite placenta can be distinguished from the dichorionic placental masses by using color Doppler and identifying vascular anastomoses that are present between the two lobes. Thus, this leads to the conclusion that if an ostensibly dichorionic pregnancy is complicated with TTTS, the diagnosis of a monochorionic pregnancy with bipartite placenta has to be considered [32–35].

3.2.3. Intertwin membrane characteristics

The intertwin membrane of a dichorionic pregnancy comprises three layers of three membranes: amnion-chorion-amnion, as the monochorionic pregnancy consists only two layers of amnion. Therefore, intertwin membrane in a dichorionic pregnancy is thicker and more echogenic than the intertwin membrane in monochorionic pregnancies. Measuring the thickness of the membrane can help us define chorionicity: a membrane thicker than 2 mm indicates dichorionicity (positive predictive value: 95%), and if the membrane is thinner than 2 mm, the possibility of monochorionic pregnancy is about 90% [4].

The intertwin membrane has to be carefully detected and if it cannot be visualized, a transvaginal ultrasound scan has to be performed, to set the definitive diagnosis of monoamniotic pregnancy [4]. When a single placental mass is visualized and chorionicity is identified as monochorionic, evaluation of the intertwin membrane characteristics is the key to determine amnionicity. The most significant sonographic figure that demonstrates monoamniocity is the demonstration of cord enlargement from the placental or umbilical origin and it is identified easier via color Doppler. Other important findings intimating monoamnionicity are the entanglement of limbs or observation of a limb circumscribing the other, the failure to find the membrane between the two cord insertions in the placenta [4], and the short intercord distance [5].

However, intertwin membrane thickness difference between monochorionic and dichorionic pregnancy decreases during gestation [36]. In addition, the measurement of the thickness of the membrane is not widely accepted since this parameter can be affected by many factors such as the position and the quality of the probe, and as a result, it has poor reproducibility [37]. A rare but significant pitfall may lead to a wrong determination of a monochorionic pregnancy as dichorionic is the intrauterine synechiae in twin pregnancy with a fetus with anencephaly. Intrauterine synechiae can mimic the thick dichorionic membrane [38]. This septum is not the intertwin membrane and does not include the layer of chorion between the layers of amnion.

3.2.4. The chorionic peak sign—the "λ" sign

The chorionic peak sign or the "λ" sign supports strongly dichorionicity, with an accuracy of 99% [5]. It shows a projecting zone of tissue which is as echogenic as the placenta; it has a triangular shape in cross-section; and it is wider at the chorionic surface of the placenta, extending into, and tapering to a point within, the intertwin membrane [39, 40]. The absence of the "λ" sign or the presence of "T" sign indicates monochorionicity. The "T" sign represents the two opposing amnions "standing" at the base of the intertwin membrane [10].

The chorionic peak sign is ideally evaluated during the late first trimester or the very early second trimester, as in second trimester, it is more difficult to be visualized and it might be disappeared at 16–20 weeks of gestation, leading to a false negative "λ" sign. As a result, the impossible depiction of the "λ" sign in late second trimester cannot exclude dichorionicity [41, 42]. Nonetheless, a false positive "λ" sign might also exist. This can be due to umbilical cord insertion into the intertwin membrane or because of the visualization of a hematoma presented along the insertion of the membrane. Another interesting reason that may lead to

a false positive "λ" sign is the presence of an echogenic retrograded yolk sac of the placental junction of the intertwin membrane in a monochorionic-diamniotic twin gestation. The sonographic finding that succors determinate the true "λ" sign is that the true "λ" has been seen along with the whole insertion area, in contrast to the false "λ" sign, which appears in only a small region of the intertwin membrane [43, 44]. Finally, in very rare instances, the placentation may be both monochorionic and dichorionic, and each chorionicity is presented in different regions of the intertwin membrane. Therefore, the same intertwin membrane has parts with two layers of amnions and parts with three layers: amnion-chorion-amnion [45–47]. This situation shows the importance of scanning the whole insertion of the intertwin membrane in early ultrasound assessment of multiple pregnancy.

In some cases and despite the best possible ultrasound assessment, chorionicity is impossible to be defined. In these situations, the pregnancy has to be considered as monochorionic. Therefore, surveillance has to be as close as in monochorionic pregnancies [45], and this is discussed below.

4. Surveillance

Surveillance in multiple pregnancies has a significant importance, as it plays the major role in the detection of complications that are associated with a high-risk pregnancy, and it is well known that multiple pregnancy is a classic example of a high-risk pregnancy. However, the appropriate frequency of the ultrasound assessment in both dichorionic and monochorionic pregnancies, which provides the best balance between cost and effectiveness, is not be established and worldwide accepted [3].

4.1. Dichorionic pregnancies

Finberg et al. [46] suggested repeat scans every 4–6 weeks for noncomplicated dichorionic pregnancies. However, in current daily medical routine, surveillance is closer: follow-up ultrasound assessments are performed every 3–4 weeks [4, 47]. But, if a complication is suspected, and more specifically when CRL, estimated fetal weight or amniotic fluid volume are different between the two fetuses, routine scans have to be repeated every 2 weeks, or within a week [48].

4.2. Monochorionic pregnancies

It is a well-established fact that surveillance in monochorionic pregnancies has to be closer in relation to a dichorionic pregnancy. Finberg et al. [46] recommended ultrasound monitoring for noncomplicated monochorionic twins every 3–4 weeks. As the pattern mentioned previously, nowadays, routine scans are performed more frequently: they are performed every 2–3 weeks, starting from the gestational age of 16 weeks. Finally, in some cases, surveillance is even closer: a follow-up scan can be repeated every 2 weeks.

The parameters that are necessary to be evaluated in these follow-up scans are estimated fetal weight and fetal biometry, amniotic fluid volume, and Doppler assessment of the umbilical artery [49].

5. Conclusion

There is no doubt that multiple pregnancies are now more frequent than a few years before, due to the spreading of artificial reproductive technologies. Determination of gestational age, chorionicity, and amnionicity has to be done as soon as possible and ideally in the first tri-mester of the pregnancy, as the accuracy of the determining sonographic figures is extremely close to 100%, in contrast to the definition in the second trimester whose accuracy is slightly decreased. Last but not least, timely determination of both chorionicity and amnionicity can optimize the outcome of the pregnancy, as the correct and early intervention or a refer to a tertiary center could be really valuable.

Acknowledgements

We would like to thank Kyriaki Savva, PhD student of Cyprus Institute of Neurology and Genetics, for her comments that greatly improved the manuscript.

Author details

Panagiotis Antsaklis[1]*, Maria Papamichail[2], Marianna Theodora[1], Michael Syndos[3] and George Daskalakis[1]
1 Alexandra Maternity Hospital, University of Athens, Athens, Greece
2 University of Athens, Athens, Greece
3 Obstetrics and Gynecology, Alexandra Maternity Hospital, Athens, Greece

References

[1] Martin JA, Hamilton BE, Osterman MJ. Three decades of twin births in the United States, 1980-2009. NCHS Data Brief. 2012;**80**:1-8

[2] Kurtz GR, Keating WJ, Loftus JB. Twin pregnancy and delivery: Analysis of 500 twin pregnancies. Obstetrics and Gynecology. 1995;**6**:370-378

[3] Glanc P, Nyberg DA, Khati NJ, Deshmukh SP, Dudiak KM, Henrichsen TL, Poder L, Shipp TD, Simpson L, Weber TM, Zelop CM. ACR Appropriateness Criteria® Multiple Gestations. Journal of American College of Radiology. 2017;**14**(11):S476-S489

[4] Morin L, Lim K. Ultrasound in twin pregnancies. Journal of Obstetrics and Gynaecology Canada. 2011;**33**(6):643-656

[5] Lu J, Cheng YKY, Ting YH, Law KM, Leung TY. Pitfalls in assessing chorioamnionicity: Novel observations and literature review. American Journal of Obstetrics and Gynecology. 2018;**219**(3):242-254. DOI: 10.1016/j.ajog.2018.02.010

[6] Simpson L. What you need to know when managing twins: 10 key facts. Obstetrics and Gynecology Clinics of North America. 2015;**42**(2):225-239

[7] Kalish RB, Thaler HT, Chasen ST, Gupta M, Berman SJ, Rosenwaks Z, et al. First- and second-trimester ultrasound assessment of gestational age. American Journal of Obstetrics and Gynecology. 2004;**191**:975-978

[8] Tunón K, Eik-Nes SH, Grøttum P, Von Düring V, Kahn JA. Gestational age in pregnancies conceived after in vitro fertilization: A comparison between age assessed from oocyte retrieval, crown-rump length and biparietal diameter. Ultrasound in Obstetrics & Gynecology. 2000;**15**:41-46

[9] Wisser J, Dirschedl P, Krone S. Estimation of gestational age by transvaginal sonographic measurement of greatest embryonic length in dated human embryos. Ultrasound in Obstetrics & Gynecology. 1994;**4**:457-462

[10] Simpson L. Ultrasound in Twins: Dichorionic and Monochorionic. Seminars in Perinatology; 2013;**37**(5):348-358

[11] Chervenak FA, Skupski DW, Romero R, Myers MK, Smith-Levitin M, Rosenwaks Z, et al. How accurate is fetal biometry in the assessment of fetal age? American Journal of Obstetrics and Gynecology. 1998;**178**:678-687

[12] Sebire NJ, D'Ercole C, Soares W, Nayar R, Nicolaides KH. Intertwin disparity in fetal size in monochorionic and dichorionic pregnancies. Obstetrics and Gynecology. 1998;**91**:82-85

[13] Salomon LJ, Cavicchioni O, Bernard JP, Duyme M, Ville Y. Growth discrepancy in twins in the first trimester of pregnancy. Ultrasound in Obstetrics & Gynecology. 2005;**26**: 512-516

[14] D'Antonio F, Khalil A, Pagani G, Papageorghiou AT, Bhide A, Thilaganathan B. Crown-rump length discordance and adverse perinatal outcome in twin pregnancies: Systematic review and metaanalysis. Ultrasound in Obstetrics & Gynecology. 2014;**44**:138-146

[15] Kalish RB, Gupta M, Perni SC, Berman S, Chasen ST. Clinical significance of first trimester crown-rump length disparity in dichorionic twin gestations. American Journal of Obstetrics and Gynecology. 2004;**191**:1437-1440

[16] Carroll SG, Soothill PW, Abdel-Fattah SA, et al. Prediction of chorionicity in twin pregnancies at 10-14 weeks gestation. BJOG. 2002;**109**:182-186

[17] Lee YM, Cleary-Goldman J, Thanker HM, et al. Antenatal sonographic prediction of twin chorionicity. American Journal of Obstetrics and Gynecology. 2006;**195**:863-867

[18] Monteagudo A, Roman AS. Ultrasound in multiple gestations: Twins and other multifetal pregnancies. Clinics in Perinatology. 2005;**32**:329-354, vi

[19] Perlman EJ, Stetten G, Tuck-miiller CM, et al. Sexual discordance in monozygotic twins. American Journal of Medical Genetics. 1990;**37**:551-557

[20] Nieuwint A, Zalen-Sprock R Van, Hummel P, et al. Identical twins with discordant karyotypes. Prenatal Diagnosis. 1999;**19**:72-76

[21] Zech NH, Wisser J, Natalucci G, Riegel M, Baumer A, Schinzel A. Monochorionic-diamniotic twins discordant in gender from a naturally conceived pregnancy through postzygotic sex chromosome loss in a 47,XXY zygote. Prenatal Diagnosis. 2008;**28**:759-763

[22] Bohec C, Douet-Guilbert N, Basinko A, et al. Difficult diagnosis and management of an heterokaryotypic monochorionic twin pregnancy with discordant fetal sex and 45,X/47,XYY karyotypes. Fetal and Pediatric Pathology. 2010;**29**:424-430

[23] Prior HM, Walter MA. SOX genes: Architects of development. Molecular Medicine. 1996;**2**: 405-412

[24] Wolf U. Reorganization of the sex-determining pathway with the evolution of placentation. Human Genetics. 1999;**105**:288-292

[25] De Paepe ME, Shapiro S, Young L, Luks FI. Placental characteristics of selective birth weight discordance in diamniotic-monochorionic twin gestations. Placenta. 2010;**31**: 380-386

[26] Chen M, Macias CG, Gunn SK, Dietrich JE, Roth DR, Schlomer BJ. Intrauterine growth restriction and hypospadias: Is there a connection? International Journal of Pediatric Endocrinology. 2014;**2014**:20

[27] Toufaily MH, Roberts DJ, Westgate M, Hunt A, Holmes LB. Hypospadias, intrauterine growth restriction, and abnormalities of the placenta. Birth Defects Research Journal. 2017;**29**:1-6

[28] Chitrit Y, Vuillard E, Khung S, et al. Cloaca in discordant monoamniotic twins: Prenatal diagnosis and consequence for fetal lung development. American Journal of Perinatology. 2014;**4**:33-36

[29] Mcnamara HC, Kane SC, Craig JM, Short RV, Umstad MP. A review of 21 the mechanisms and evidence for typical and atypical twinning. American Journal of Obstetrics and Gynecology. 2016;**214**:172-191

[30] Souter VL, Kapur RP, Nyholt DR, et al. A report of dizygous monochorionic twins. The New England Journal of Medicine. 2003;**349**:154-158

[31] Miura KNN. Do monochorionic dizygotic twins increase after pregnancy by assisted reproductive technology? Journal of Human Genetics. 2005;**50**:1-6

[32] Lopriore E, Sueters M, Middeldorp JM, Klumper F, Oepkes D, Vandenbussche FP. Twin pregnancies with two separate placental masses can still be monochorionic and have vascular anastomoses. American Journal of Obstetrics and Gynaecology. 2006;**194**:804-808

[33] Kim K, Lage JM. Bipartite diamnionic monochorionic twin placenta with 6 superficial vascular anastomoses: Report of a case. Human Pathology. 1991;**22**:501-503

[34] Altshuler G, Hyde S. Placental pathology casebook: A bidiscoid, monochorionic placenta. Journal of Perinatology. 1993;**13**:492-493

[35] Walsh CA, Wilkinson M, Downey P, Mooney EE, Carroll S. "False" lambda sign in monochorionic twin pregnancy. Ultrasound in Obstetrics & Gynecology. 2015;**46**:376-377

[36] Townsend RR, Simpson GF, Filly RA. Membrane thickness in ultrasound prediction of chorionicity of twin gestations. Journal of Ultrasound in Medicine. 1988;**7**:327-332

[37] Stagiannis KD, Sepulveda W, Southwell D, Price DA, Fisk NM. Ultrasonographic measurement of the dividing membrane in twin pregnancy during the second and third trimesters: A reproducibility study. American Journal of Obstetrics and Gynecology. 1995;**173**:1546-1550

[38] Machin G. Non-identical monozygotic twins, intermediate twin types, zygosity testing, and the non-random nature of monozygotic twinning: A review. American Journal of Medical Genetics. Part C, Seminars in Medical Genetics. 2009;**151C**:110-127

[39] Stenhouse E, Hardwick C, Maharaj S, Webb J, Kelly T, Mackenzie FM. Chorionicity determination in twin pregnancies: How accurate are we? Ultrasound in Obstetrics & Gynecology. 2002;**19**:350-352

[40] Wood SL, St. Onge R, Connors G, Elliot PD. Evaluation of the twin peak or lambda sign in determining chorionicity in multiple pregnancy. Obstetrics and Gynecology. 1996;**88**:6-9

[41] Scardo JA, Ellings JM, Newman RB. Prospective determination of chorionicity, amnionicity, and zygosity in twin gestations. American Journal of Obstetrics and Gynecology. 1995;**173**:1376-1380

[42] Sepulveda W. Chorionicity determination in twin pregnancies: Double trouble. Ultrasound in Obstetrics & Gynecology. 1997;**10**:79-81

[43] Dias T, Arcangeli T, Bhide A, Napolitano R, Mahsud-Dornan S, Thilaganathan B. First-trimester ultrasound determination of chorionicity in twin pregnancy. Ultrasound in Obstetrics & Gynecology. 2011;**38**:530-532

[44] Gueneuc A, Spaggiari E, Bonniere M, Hajal NJ, Ville Y, Salomon LJ. Pitfall in the diagnosis of chorionicity in twin pregnancy at first trimester. Ultrasound in Obstetrics & Gynecology. 2017;**49**:277-278

[45] D'Antonio F, Bhide A. Early pregnancy assessment in multiple pregnancies. Best Practice & Research. Clinical Obstetrics & Gynaecology. 2014;**28**(2):201-214

[46] Finberg H, Mendelson E, Bohm-Velez M, et al. Evaluation of Multiple Gestations. American College of Radiology. 2000;**215**(Suppl):903-914

[47] Vayssiere C, Favre R, Audibert F, et al. Cervical length and funneling at 22 and 27 weeks to predict spontaneous birth before 32 weeks in twin pregnancies: A French prospective multicenter study. American Journal of Obstetrics and Gynecology. 2002;**187**:1596-1604

[48] Modena AB, Berghella V. Antepartum management of multifetal pregnancies. Clinics in Perinatology. 2005;**32**:443-454, vii

[49] Lodeiro JG, Vintzileos AM, Feinstein SJ, Campbell WA, Nochimson DJ. Fetal biophysical profile in twin gestations. Obstetrics and Gynecology. 1986;**67**:824-827

Chapter

Assessment of Fetal Gestational Age in the First Trimester in Normal and Abnormal Pregnancies: Which Sonographic Parameter to Use?

Hong Soo Wong

Abstract

To compare the correlation of various fetal ultrasound parameters to foot length, crown-rump length, and gestational age by date to determine the best estimate at 10–14 completed weeks' gestation and to provide ratios of fetal parameters for assessment of fetal abnormalities in the first trimester. 35 routine obstetric scans were performed at 10–14 completed weeks' gestation for fetal parameters and ratios. The fetal crown-rump length (CRL), biparietal diameter (BPD), head circumference (HC), abdominal circumference (AC), and femur length (FL) showed a linear correlation with the estimated gestational age by date (GA), crown-rump length (CRL), and foot length (FT) ($p < 0.001$), with the least correlation observed with GA and highest with FT. A combination of BPD, HC, AC, and FL correlated best with FT and then CRL and GA ($R^2 = 0.881$, 0.795, and 0.685, respectively, $p < 0.001$). With the addition of CRL, R^2 was 0.859. The ratio of FL/AC and FL/FT to FT, CRL, GA, BPD, and HC increases in an inverse relationship at 10–14 completed weeks' gestation. The combination of BPD, HC, AC, and FL provides a better estimation of gestational age than (and hence may replace) CRL or GA at 10–14 weeks' gestation.

Keywords: ultrasonography, fetus, pregnancy, first trimester, prenatal diagnosis

1. Introduction

The fetal foot is one of the first structures identifiable early in the human embryos. At the end of the fourth week of embryonic development, the limb buds appear as outpouchings from the ventrolateral body wall. At 6 weeks, the terminal portion of the limb buds flattens to form the hand- and footplates and becomes separated from the proximal segment by a circular constriction. It is known that the development of the lower limbs is similar to the upper limbs and lags by only 1–2 days. By 8 weeks (or 56 days), the digital separation is already complete. The fingers and the toes are distinct and separated in the hands and feet [1, 2]. In another word, the fetal hands and feet would be recognizable as distinct formed structures by 8 weeks of embryological development or 10 weeks by the last menstrual period (LMP) according to a 28 day cycle.

About a century ago, Streeter reported a linear correlation between gestational age and foot length in 704 human fetal specimens from around 50 days post-conception until birth [3]. This linear correlation has been confirmed by studies on live fetuses in utero on transabdominal [4–6] or transvaginal scans [7] or on dead fetuses at abortion [8–10] or stillbirth [11, 12], and nomograms have been developed for assessment of fetal gestational age with foot length (FT) from the first trimester to later gestation. Hence, fetal foot length could by itself stand as a proxy for gestational age even in early pregnancy.

Conventionally, crown-rump length (CRL) is used as the reference parameter for assessment of fetal gestational age in the first trimester ultrasound scan [13, 14]. It has been suggested that the ultrasound measurement of the crown-rump length in the embryo or fetus is the most accurate method to establish or confirm gestational age in the first trimester up to 13 + 6 weeks [14]. The use of routine first trimester ultrasound scan has been shown to be associated with a reduction in induction of labor for post-term pregnancy [15]. However, there is little information on the comparison of other fetal parameters including biparietal diameter (BPD), head circumference (HC), abdominal circumference (AC), femur length (FL), and foot length to CRL in the assessment of gestational age in early gestation [16]. This information may be important for the assessment of fetal gestational age in the first trimester and subsequent management of pregnancy.

In order to ascertain the performance of various parameters in assessment of gestational age in the first trimester, in this chapter, the correlation between FT, CRL, and gestational age assessed by date (GA) will be compared from 10 to 14 weeks gestation. The correlation of the other fetal parameters (BPD, HC, AC, and FL) will also be compared to GA, CRL, and FT. Moreover, the ratio of some of these parameters will also be calculated and presented, as the availability of such ratios may be helpful when fetal abnormality is suspected on ultrasound examination in early pregnancy [17–19].

2. Method and material

Transabdominal ultrasound examination was performed as a part of routine antenatal assessment for women attending an obstetric clinic at a gestation of 10–14 + 6 weeks from March 7, 2014, to September 7, 2016 (Accuvix V20 Prestige, Medison with 4–8 MHz volumetric transducer or EPIQ 7, Philips with X6–1 matrix transducer). The following fetal measurements were taken prospectively: crown-rump length (CRL), biparietal diameter (BPD), head circumference (HC), abdominal circumference (AC), femur length (FL), and foot length (FT). Only pregnancies with normal outcomes were included in the analysis and excluded if the entire foot could not be clearly seen during the ultrasound examination. The fetal foot length was measured from the most posterior point of the foot in its long axis to the tip of the first or the second toe whichever was longer (**Figure 1**). The estimated gestational age in weeks (GA) was calculated either from the last normal menstrual period (LMP) or from the first trimester dating scan if there was a discrepancy of more than a week [14]. This was a retrospective analysis involving minimal risk, conforming to the standards established by the NHMRC not requiring ethical review; ethics approval was therefore not sought within the institution [20].

Results for 35 ultrasound scans were analyzed with SPSS statistical package version 20 (SPSS Inc., Chicago, IL, USA). A two-sided probability (p) value of <0.05 was considered statistically significant. The regression models for the fetal measurements were obtained and would be presented in the relevant sections.

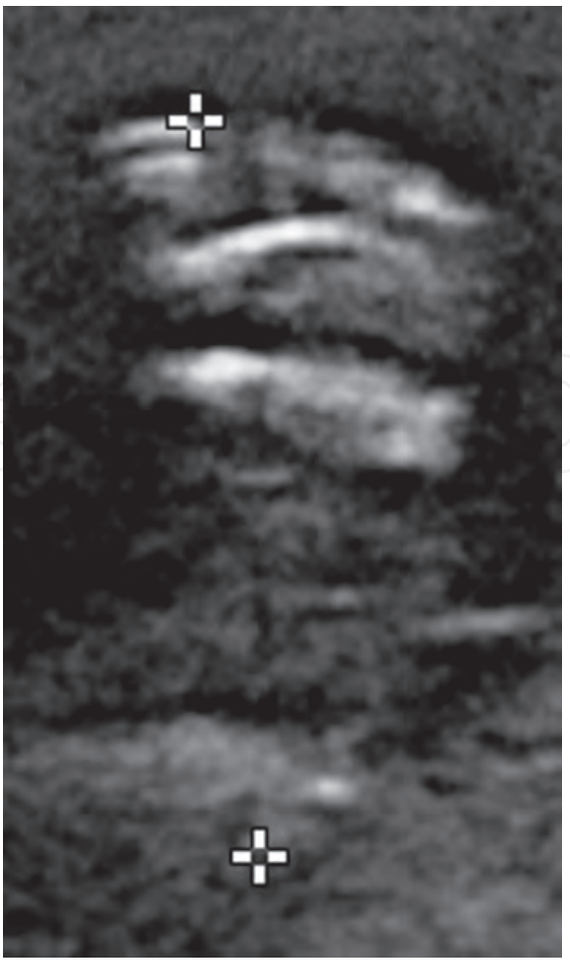

Figure 1.
Fetal foot on first trimester ultrasound scan.

3. Results

3.1 Demographic characteristics

The mean age, gravidity, and parity were 32.0 years, 2.3, and 0.7, respectively (**Table 1**). A total of 32 out of the 35 women were Asians (91.4%) and 3 were Caucasians (8.6%).

3.2 Comparison of the correlation between FT, CRL, and GA

The correlation of foot length, crown-rump length, and the gestational age assessed by date are shown in **Figures 2–4** and tabulated in **Table 2**. FT, CRL, and GA all showed positive correlation with one another in a linear fashion ($p < 0.001$)

	Mean ± S.D.	Range
Age (years)	32.0 ± 4.6	21–44
Gravidity	2.3 ± 1.5	1–8
Parity	0.7 ± 0.7	0–3

SD, standard deviation.

Table 1.
The demographic date of the pregnant women included in the study.

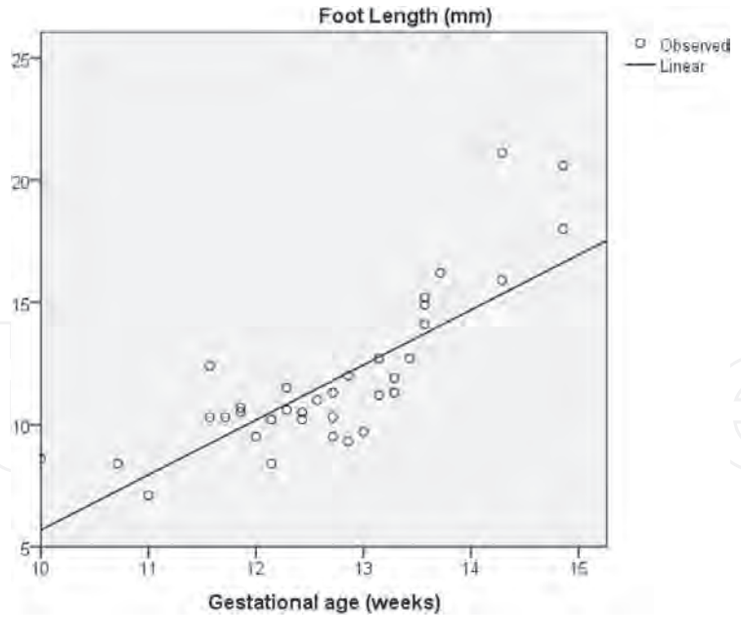

Figure 2.
The graph of fetal foot length against gestational age assessed by date. FT = GA × 2.472−19.44. R^2 = 0.675, p < 0.001. FT, foot length (mm); GA, gestational age assessed by date (weeks); R^2, coefficient of determination of regression; p, probability.

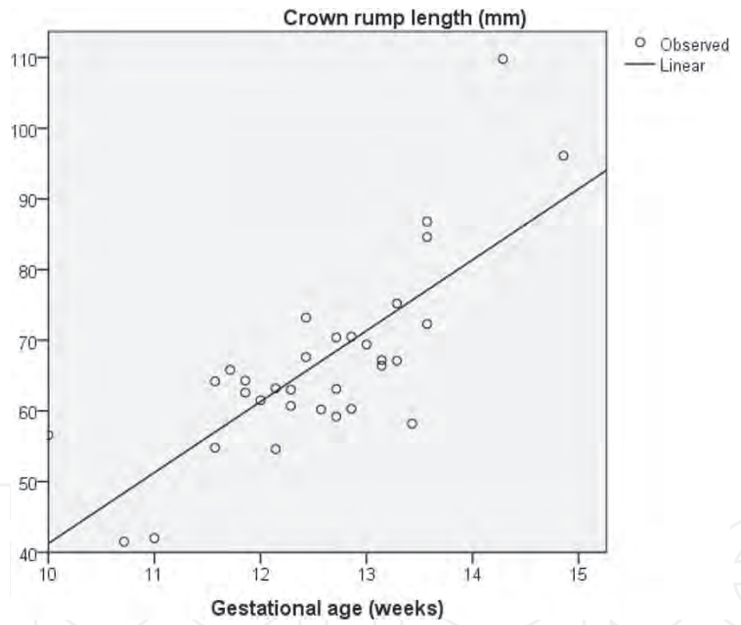

Figure 3.
The graph of fetal crown-rump length against gestational age assessed by date. CRL = GA × 10.464−64.682. R^2 = 0.608, p < 0.001. CRL, crown-rump length (mm); GA, gestational age assessed by date (weeks); R^2, coefficient of determination of regression; p, probability.

(**Figures 2–4**). The coefficient of determination of regression (R^2) was the highest between FT and CRL (0.804), lower between FL and GA (0.675), and the lowest between CRL and GA (0.608) (**Table 2**).

3.3 Comparison of the correlation of BPD, HC, AC, and FL to FT, CRL, and GA

The correlation of BPD, HC, AC, and FL with FT, CRL, and GA is shown in **Figures 5–7, 8–10, 11–13,** and **14–16**, respectively, and summarized in **Table 3**. Correlation in a linear fashion is seen for all (p < 0.001). Overall, the correlation

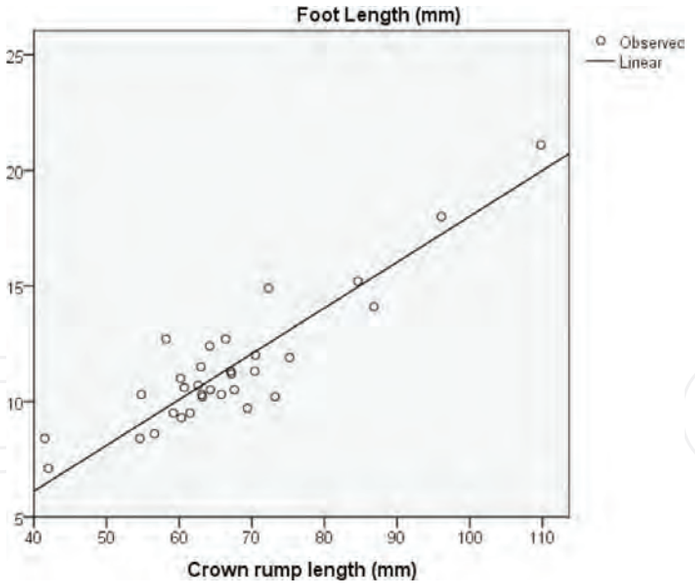

Figure 4.
The graph of fetal foot length against crown-rump length. FT = CRL × 0.187−1.074. R^2 = 0.804, $p < 0.001$. FT, foot length (mm); CRL, crown-rump length (mm); R^2, coefficient of determination of regression; p, probability.

Parameters	FT		CRL		GA	
	R^2	$p^{\dagger}$	R^2	$p^{\dagger}$	R^2	$p^{\dagger}$
FT	–	–	0.804	<0.001*	0.675	<0.001*
CRL	0.804	<0.001*	–	–	0.608	<0.001*
GA	0.675	<0.001*	0.608	<0.001*	–	–

*FT, foot length (mm); CRL, crown rump length (mm); GA, gestational age assessed by date (weeks); R^2, coefficient of determination of linear regression; p, probability; †, ANOVA; *, statistically significant.*

Table 2.
The correlation between fetal foot length, crown-rump length, and gestational age assessed by date.

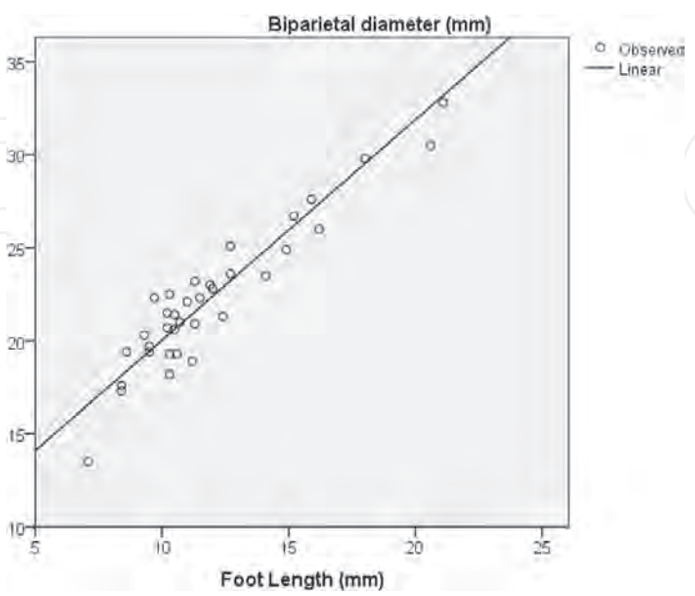

Figure 5.
The correlation of fetal biparietal diameter with foot length. BPD = FT × 1.131 + 8.748. R^2 = 0.884, $p < 0.001$. BPD, biparietal diameter (mm); FT, foot length (mm); R^2, coefficient of determination of regression; p, probability.

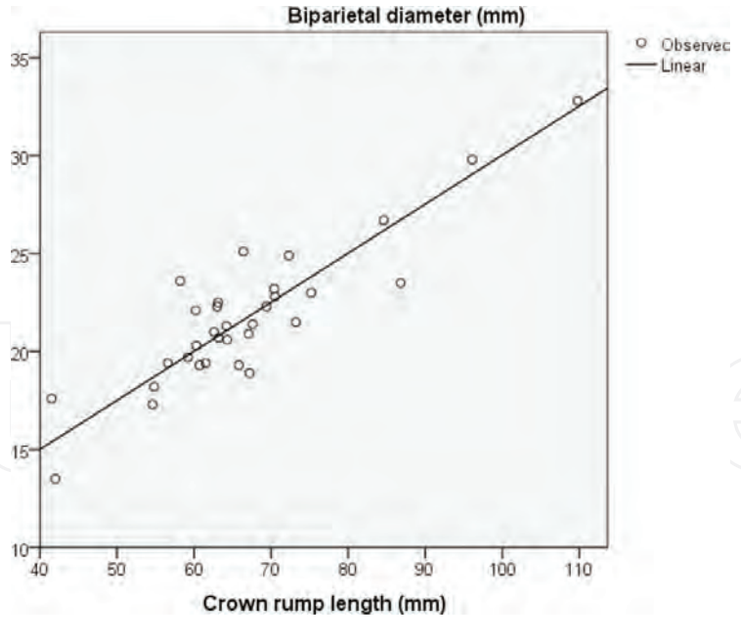

Figure 6.
The correlation of fetal biparietal diameter with crown-rump length. BPD = CRL × 0.239 + 5.78. R^2 = 0.793, p < 0.001. BPD, biparietal diameter (mm); CRL, crown-rump length (mm); R^2, coefficient of determination of regression; p, probability.

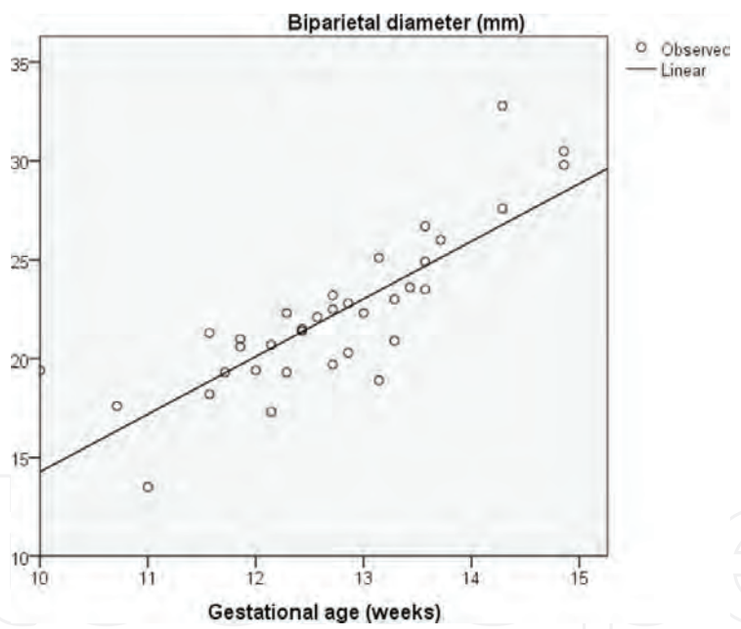

Figure 7.
The correlation of fetal biparietal diameter with gestational age assessed by date. BPD = GA × 3.01–15.967. R^2 = 0.693, p < 0.001. BPD, biparietal diameter (mm); GA, gestational age assessed by date (weeks); R^2, coefficient of determination of regression; p, probability.

of BPD, HC, AC, and FL with FT was the highest, lower with CRL, and the lowest with GA (**Table 3**).

3.4 Comparison of combination of fetal parameters

The correlation of combinations of fetal parameters to FT, CRL, and GA is shown in **Table 4**. The highest correlation was seen between the combination of [BPD,

HC, AC, and FL] and FT (R^2 = 0.881, p < 0.001), followed by correlation to CRL (R^2 = 0.795, p < 0.001), and the least with GA (R^2 = 0.685, p < 0.001). The addition of CRL to the combination yielded a lower R^2 value of 0.859. However, the correlation of the combination, with or without FT, to CRL yielded the same R^2 of 0.795 (p < 0.001).

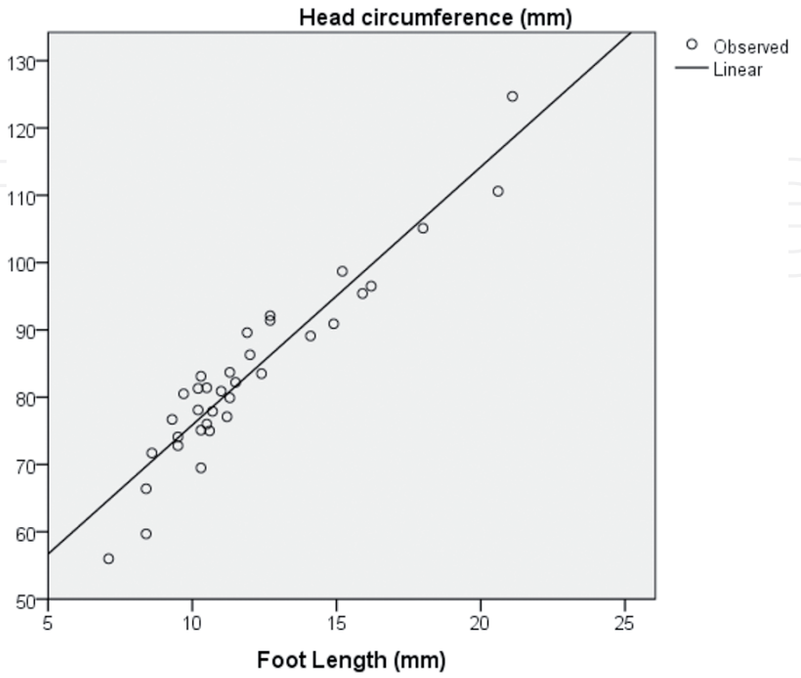

Figure 8.
The correlation of fetal head circumference with foot length. HC = FT × 3.932 + 36.257. R^2 = 0.897, p < 0.001. HC, head circumference (mm); FT, foot length (mm); R^2, coefficient of determination of regression; p, probability.

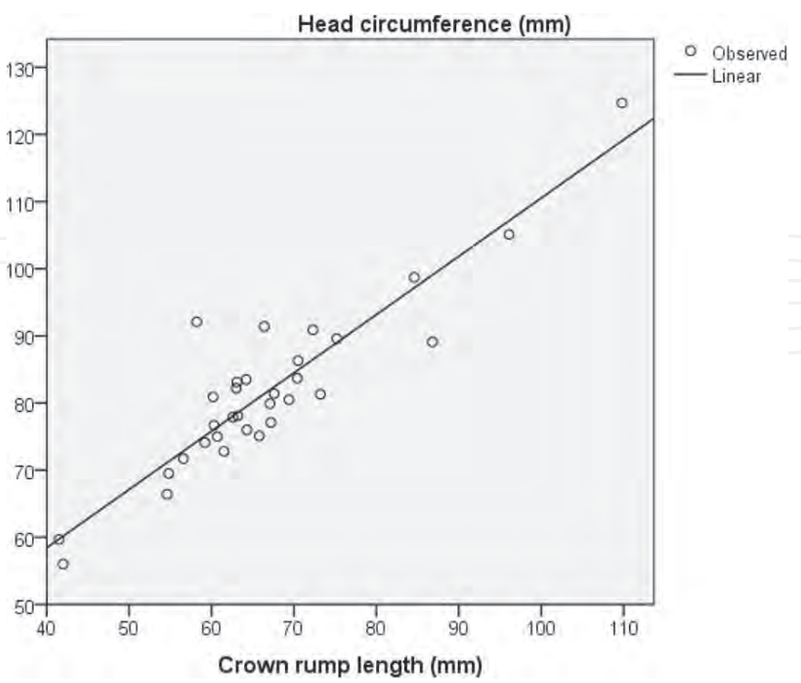

Figure 9.
The correlation of fetal head circumference with crown-rump length. HC = CRL × 0.869 + 23.646. R^2 = 0.834, p < 0.001. BPD, biparietal diameter (mm); CRL, crown-rump length (mm); R^2, coefficient of determination of regression; p, probability.

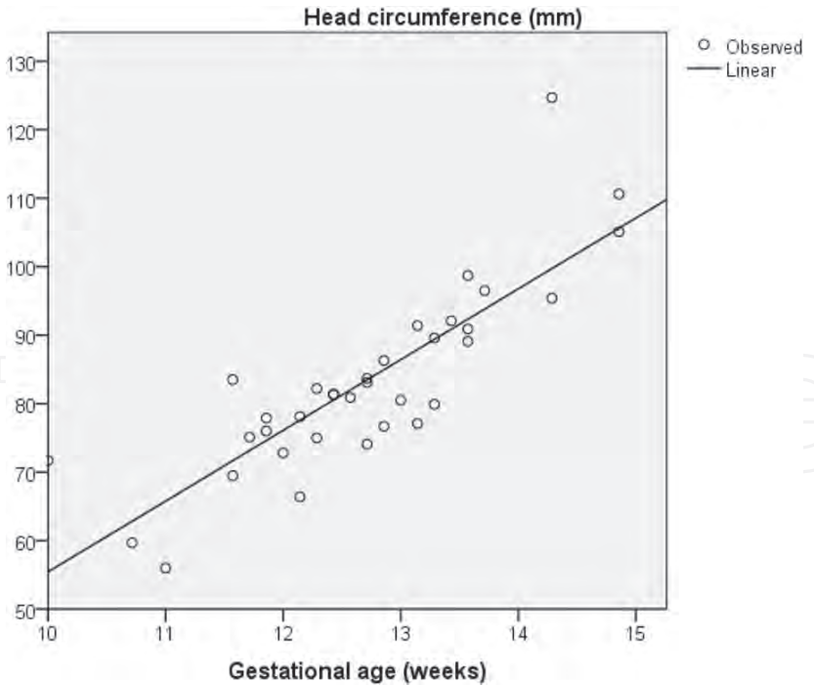

Figure 10.
The correlation of fetal head circumference with gestational age assessed by date. HC = GA × 10.488−49.951. R^2 = 0.706, p < 0.001. HC, head circumference (mm); GA, gestational age assessed by date (weeks); R^2, coefficient of determination of regression; p, probability.

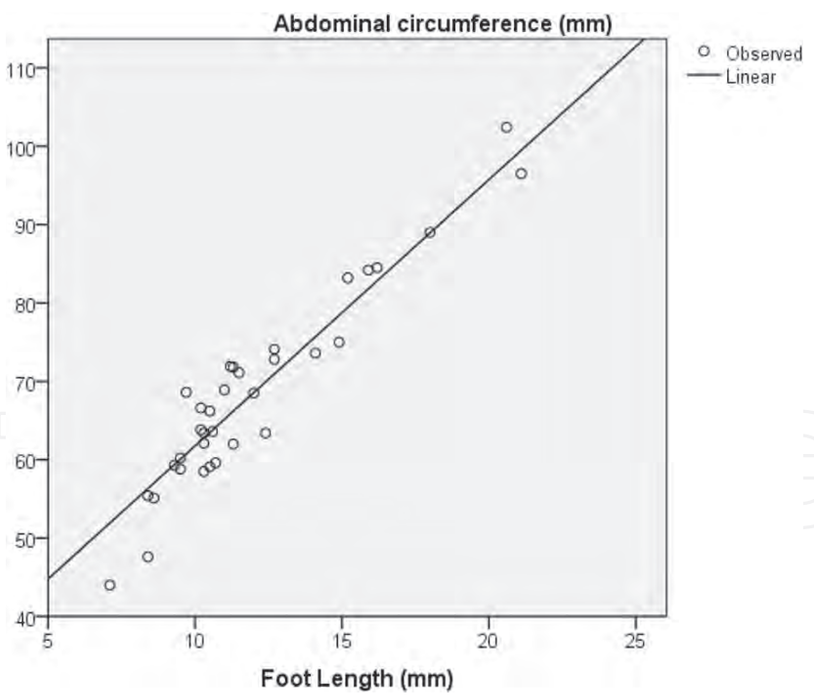

Figure 11.
The correlation of fetal abdominal circumference with foot length. AC = FT × 3.639 + 24.905. R^2 = 0.903, p < 0.001. HC, head circumference (mm); FT, foot length (mm); R^2, coefficient of determination of regression; p, probability.

The combination, in comparison to FT or CRL alone, gave a higher correlation to GA (compare to **Table 2**). However, the correlation of the combination of [BPD, HC, AC, and FL] or FT alone to CRL yielded a similar R^2 (0.795 vs. 0.804, compare **Table 4** to **Table 2**).

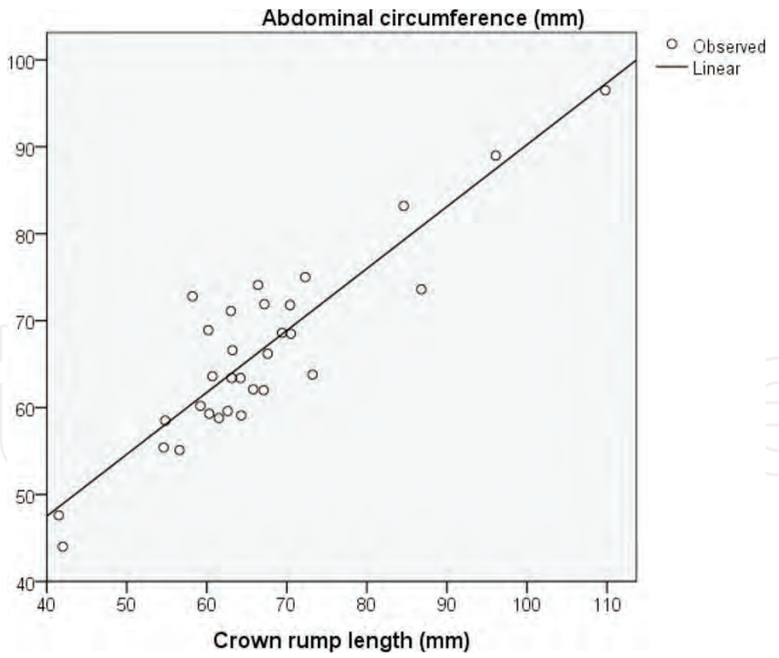

Figure 12.
The correlation of fetal abdominal circumference with crown-rump length. AC = CRL × 0.717 + 18.686. R^2 = 0.811, p < 0.001. AC, abdominal circumference (mm); CRL, crown-rump length (mm); R^2, coefficient of determination of regression; p, probability.

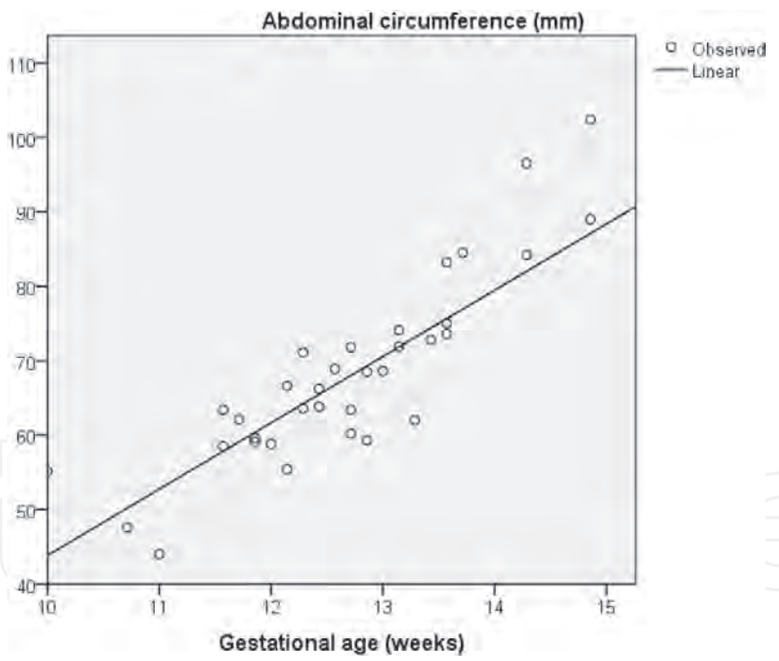

Figure 13.
The correlation of fetal abdominal circumference with gestational age assessed by date. AC = GA × 10.16−60.453. R^2 = 0.772, p < 0.001. AC, abdominal circumference (mm); GA, gestational age assessed by date (weeks); R^2, coefficient of determination of regression; p, probability.

3.5 Ratios of fetal parameters

The ratios of fetal parameters FL/FT and FL/AC to FT, CRL, GA, BPD, and HC are shown in **Figures 17–21** and **22–26**, respectively. The correlation followed an inverse relationship, and the R^2 was higher with HC or BPD or CRL or FT than GA in general (**Table 5**).

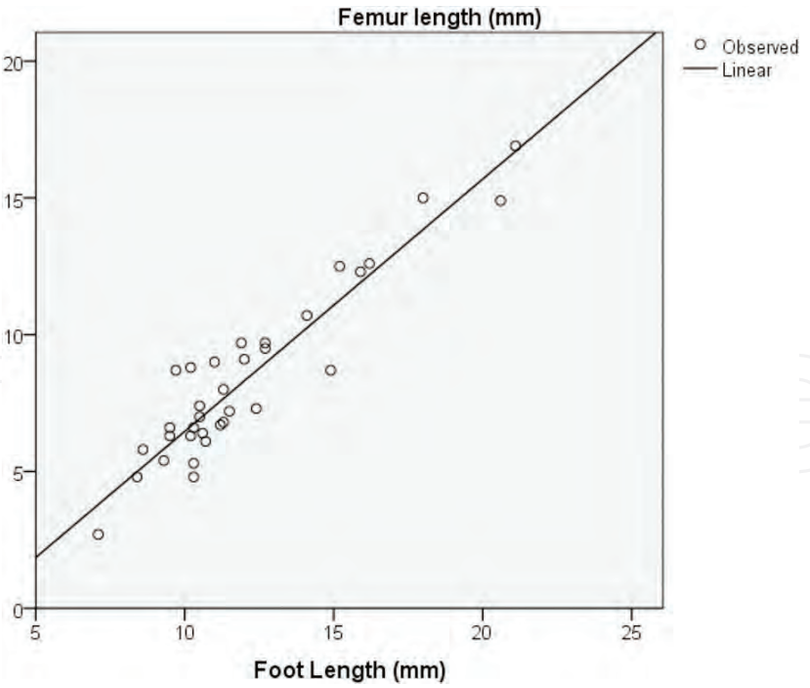

Figure 14.
The correlation of fetal femur length with foot length. FL = FT × 0.922−2.707. R^2 = 0.878, p < 0.001. FL, femur length (mm); FT, foot length (mm); R^2, coefficient of determination of regression; p, probability.

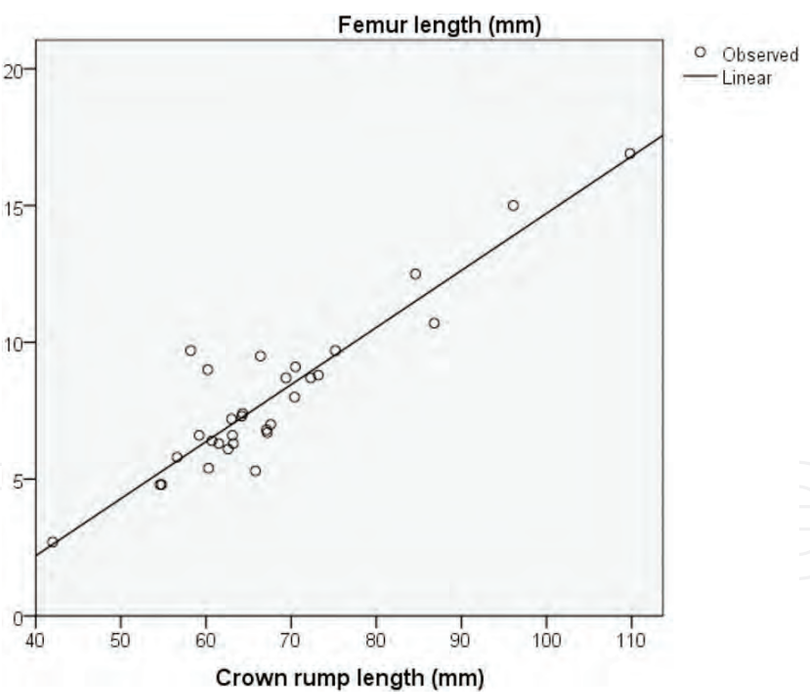

Figure 15.
The correlation of fetal femur length with crown-rump length. FL = CRL × 0.209−6.159. R^2 = 0.843, p < 0.001. FL, femur length (mm); CRL, crown-rump length (mm); R^2, coefficient of determination of regression; p, probability.

3.6 Intra- and inter-observer correlation

The Pearson coefficient for intra-observer correlation was 0.992 ($p < 0.001$) and for inter-observer correlation was 0.990 ($p < 0.001$) in the measurement of fetal foot length.

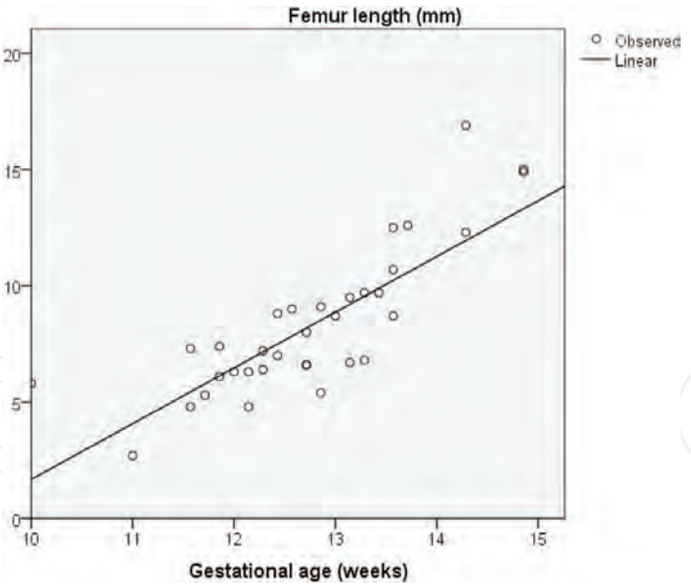

Figure 16.
The correlation of fetal femur length with gestational age assessed by date. FL = GA × 2.56−24.255. R^2 = 0.698, p < 0.001. FL, femur length (mm); GA, gestational age assessed by date (weeks); R^2, coefficient of determination of regression; p, probability.

	FT		CRL		GA	
	R^2	$p^{\dagger}$	R^2	$p^{\dagger}$	R^2	$p^{\dagger}$
BPD	0.884	<0.001*	0.793	<0.001*	0.693	<0.001*
HC	0.897	<0.001*	0.834	<0.001*	0.706	<0.001*
AC	0.903	<0.001*	0.811	<0.001*	0.772	<0.001*
FL	0.878	<0.001*	0.843	<0.001*	0.698	<0.001*
FT	–	–	0.804	<0.001*	0.675	<0.001*
CRL	0.804	<0.001*	–	–	0.608	<0.001*

*FT, foot length (mm); CRL, crown rump length (mm); GA, gestational age assessed by date (weeks); BPD, biparietal diameter (mm), HC, head circumference (mm); AC, abdominal circumference; FL, femur length (mm); R^2, coefficient of determination of regression; p, probability; †, ANOVA; *, statistically significant.*

Table 3.
The correlation of fetal biparietal diameter, head circumference, abdominal circumference, and femur length to foot length, crown-rump length, and gestational age assessed by date.

	FT		CRL		GA	
	R^2	$p^{\dagger}$	R^2	$p^{\dagger}$	R^2	$p^{\dagger}$
BPD, HC, AC, FL, FT, CRL	–	–	–	–	0.560	<0.001*
BPD, HC, AC, FL, CRL	0.859	<0.001*	–	–	0.601	<0.001*
BPD, HC, AC, FL, FT	–	–	0.795	<0.001*	0.685	<0.001*
BPD, HC, AC, FL	0.881	<0.001*	0.795	<0.001*	0.685	<0.001*

*BPD, biparietal diameter (mm); HC, head circumference (mm); AC, abdominal circumference (mm); FL, femur length (mm): FT, fetal foot length (mm); CRL, crown rump length (mm); R^2, coefficient of correlation of regression; p, probability; †, ANOVA; *, statistically significant.*

Table 4.
The correlation of multiple fetal parameters to foot length, crown-rump length, and gestational age.

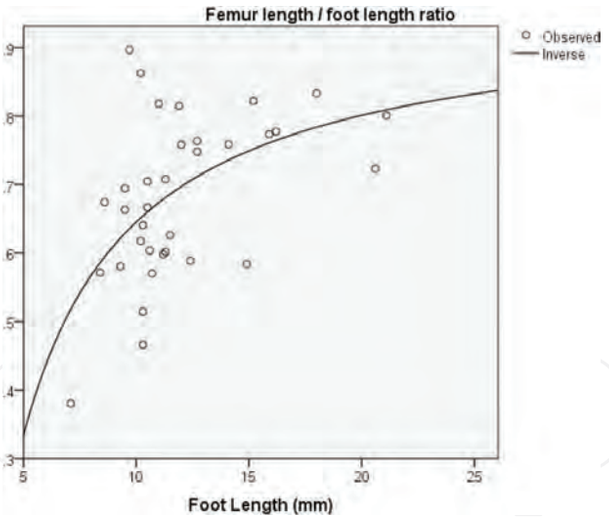

Figure 17.
The correlation of fetal femur length/foot length ratio to foot length. R^2 = 0.283, p = 0.001. R^2, coefficient of determination of regression; p, probability.

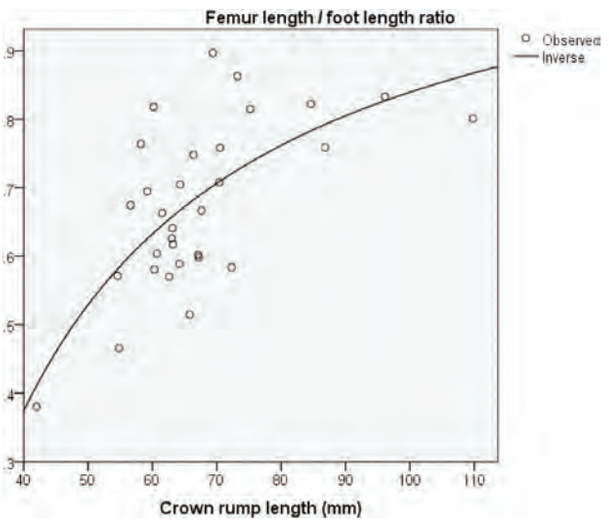

Figure 18.
The correlation of fetal femur length/foot length ratio to crown-rump length. R^2 = 0.458, p < 0.001. R^2, coefficient of determination of regression; p, probability.

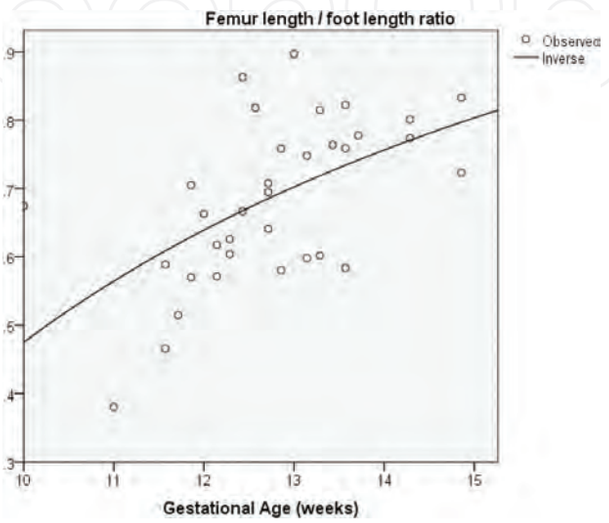

Figure 19.
The correlation of fetal femur length/foot length ratio to gestational age assessed by date. R^2 = 0.309, p = 0.001. R^2, coefficient of determination of regression; p, probability.

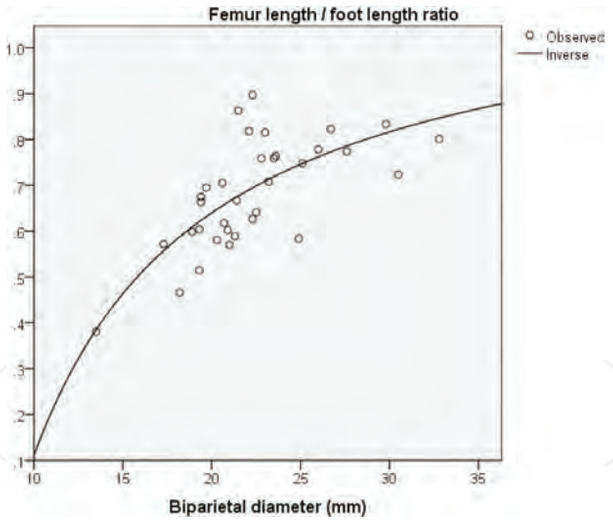

Figure 20.
The correlation of fetal femur length/foot length ratio to biparietal diameter. R^2 = 0.522, $p < 0.001$. R^2, coefficient of determination of regression; p, probability.

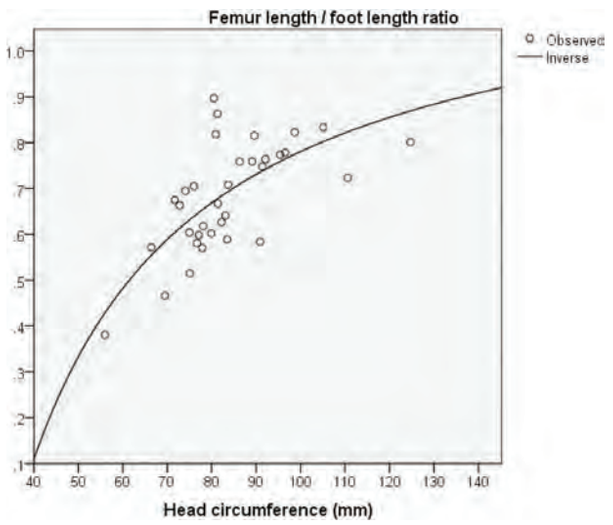

Figure 21.
The correlation of fetal femur length/foot length ratio to head circumference. R^2 = 0.477, $p < 0.001$. R^2, coefficient of determination of regression; p, probability.

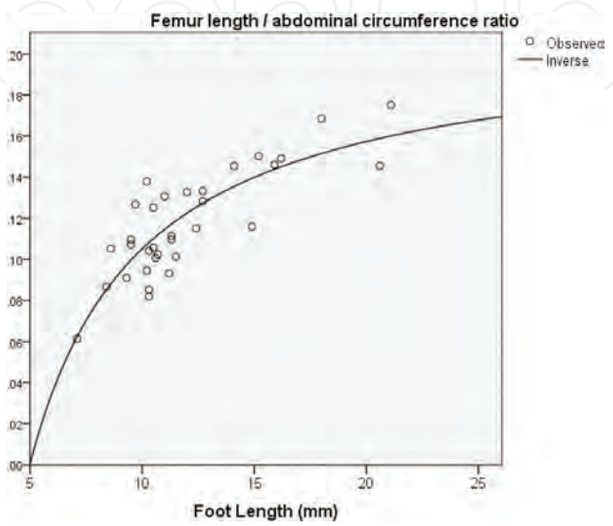

Figure 22.
The correlation of fetal femur length/abdominal circumference ratio to foot length. R^2 = 0.684, $p < 0.001$. R^2, coefficient of determination of regression; p, probability.

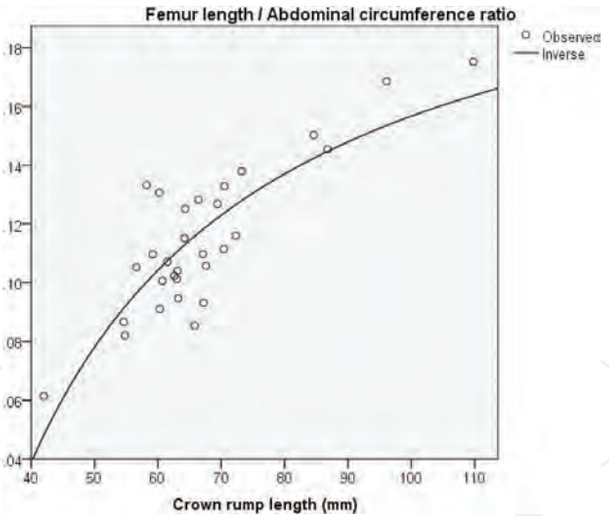

Figure 23.
The correlation of fetal femur length/abdominal circumference ratio to crown-rump length. R^2 = 0.686, $p < 0.001$. R^2, coefficient of determination of regression; p, probability.

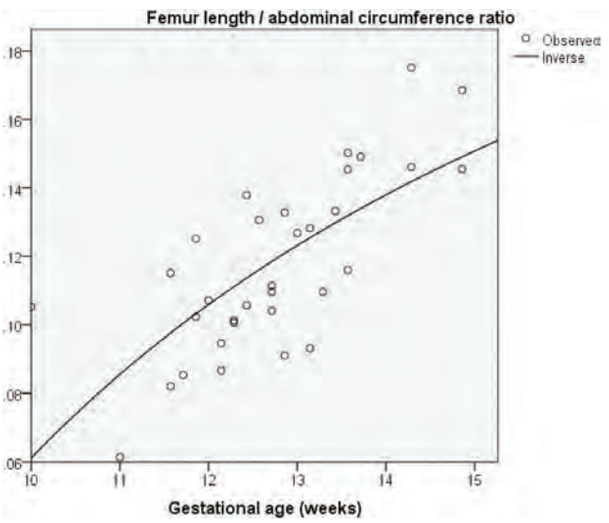

Figure 24.
The correlation of fetal femur length/abdominal circumference ratio to gestational age assessed by date. R^2 = 0.495, $p < 0.001$. R^2, coefficient of determination of regression; p, probability.

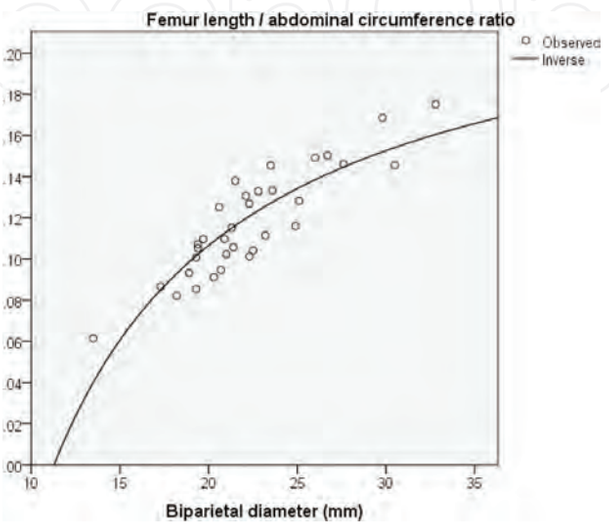

Figure 25.
The correlation of fetal femur length/abdominal circumference ratio to biparietal diameter. R^2 = 0.765, $p < 0.001$. R^2, coefficient of determination of regression; p, probability.

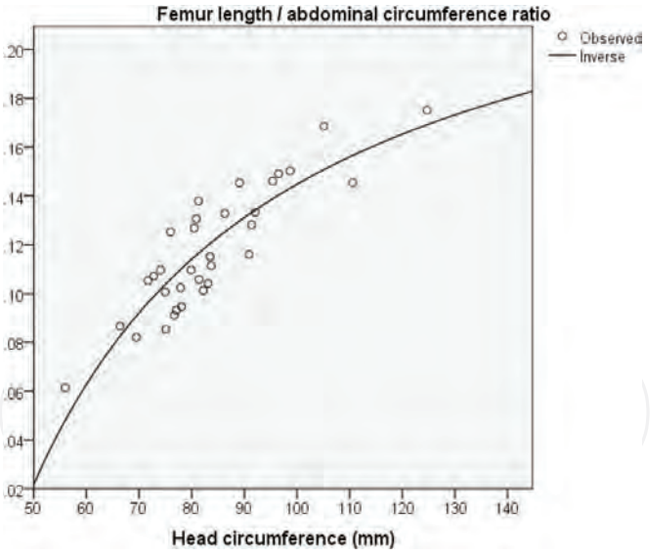

Figure 26.
The correlation of fetal femur length/abdominal circumference ratio to head circumference. $R^2 = 0.773$, $p < 0.001$. R^2, coefficient of determination of regression; p, probability.

	FL/AC		FL/FT	
	R^2	p†	R^2	p†
FT	0.684	<0.001*	0.283	0.001*
CRL	0.686	<0.001*	0.458	<0.001*
GA	0.495	<0.001*	0.309	0.001*
BPD	0.765	<0.001*	0.522	<0.001*
HC	0.773	<0.001*	0.477	<0.001*

*FL, femur length (mm); AC, abdominal circumference (mm); FT, foot length (mm); CRL, crown rump length (mm); GA, gestational age assessed by date (weeks); BPD, biparietal diameter (mm); HC, head circumference (mm); R^2, coefficient of determination of regression; p, probability; †, ANOVA; *, statistically significant.*

Table 5.
The correlation of foot length/abdominal circumference ratio to foot length, crown-rump length, and gestational age assessed by date, biparietal diameter, and abdominal circumference in a reverse relationship.

4. Discussion

An accurate estimation of fetal gestational age in early pregnancy is important for the assessment of the due date [14, 15] and fetal growth [21], the assignment of risk scores for the pregnancy [22], the prediction of fetal abnormality [23], and in the management of twin pregnancies [24]. CRL has been recommended as the standard parameter for assessment of fetal gestational age in the first trimester [14]. It was deduced that CRL gave a better estimation of fetal gestational age than the dates by the observation that it gave a better estimation of the date of delivery [14]. However, it is known that the measurement of CRL could be affected by the fetal posture. Variations in the estimation of fetal gestational age by a few days could be observed for the same gestation with different reference charts derived for CRL [4, 13, 25–28]. Since fetal foot length has been established as an accurate estimate for gestational age [3], it could be used as a proxy for the later. In this study, it could be seen that CRL correlates better with FT than GA. It can therefore be concluded that CRL is a better estimate of fetal gestational age than the date (**Table 2**), consistent

with the previous observations [15]. However, in comparison to FT in the correlation to the other fetal parameters such as BPD, HC, AC, and FL, CRL performs less well in this study. The addition of CRL to the combination also lowers the R^2 (**Table 4**). Therefore, the use of the combination of BPD, HC, AC, and FL could well be applied from 10 to beyond 14 weeks for the estimation of fetal gestational age rather than using CRL below 14 weeks and the combination of BPD, HC, AC, and FL thereafter as in the current obstetrical practice [14]. Similarly when we use ratio of fetal parameters in the assessment of suspected fetal abnormalities, it may be better to use the ratio against fetal parameters such as FT, BPD, HC, or even CRL than against the gestational age by date, as long as the particular reference fetal parameter being used is not significantly affected by the abnormality in question (**Table 5**) [23, 29]. Of note, these ratios may not follow a linear correlation but rather an inverse relationship and vary according to the gestational age in the first trimester as alluded in a previous publication (**Figures 17–21, 22–26**, **Table 5**) [19].

The major limitation of the study is the sample size. The population studied comprised mainly of Asians, and hence there could be a question on generalizability. However, it has already been shown that ethnicity of the population is not an issue in sonographic estimation of fetal gestational age using crown-rump length [26]. Moreover, it has also been shown that less than 3.5% of the total variability of fetal skeletal growth was due to differences between populations when the mothers were adequately nourished [30].

With the advancement of ultrasound technology, small structures could be measured with high accuracy. Rather than relying on CRL, a parameter that could be markedly affected by fetal posture, it is perhaps time to review our ultrasound practice at 10–14 weeks in the first trimester.

5. Conclusion

In the sonographic assessment of fetal gestational age in the first trimester, the use of a combination of fetal parameters such as BPD, HC, AC, and FL is more accurate than CRL or GA at 10–14 weeks gestation in normal pregnancies. The use of these parameters as references for comparison may also be helpful when fetal abnormality is suspected in early pregnancy.

Acknowledgements

I would like to thank Dr. Hoi Yin Mary Tang of the Department of Obstetrics and Gynecology, The University of Hong Kong, for her great kindness in checking the data.

Conflict of interest

Nil to declare.

Author details

Hong Soo Wong
Australian Women's Ultrasound Centre, Hong Kong

References

[1] Moore KL, Persaud V. Chapter 17: The limbs. In: The Developing Human Clinically Orientated Embryology. 7th ed. Philadelphia: Saunders; 2003. pp. 409-425

[2] Sadler TW. Chapter 12: Limbs. In: Langman's Medical Embryology. International Edition. 13th ed. Philadelphia: Wolters Kluwer; 2015. p. 163

[3] Streeter GL. Weight, sitting height, head size, foot length, and menstrual age of the human embryo. In: Contributions to Embryology. Vol. 11. Washington: Carnegie Institute; 1920. p. 143

[4] Mercer BM et al. Fetal foot length as a predictor of gestational age. American Journal of Obstetrics and Gynecology. 1987;**156**(2):350-355

[5] Platt LD et al. Fetal foot length: Relationship to menstrual age and fetal measurements in the second trimester. Obstetrics and Gynecology. 1988;**71**(4):526-531

[6] Goldstein I, Reece EA, Hobbins JC. Sonographic appearance of the fetal heel ossification centers and foot length measurements provide independent markers for gestational age estimation. American Journal of Obstetrics and Gynecology. 1988;**159**(4):923-926

[7] Kustermann A et al. Transvaginal sonography for fetal measurement in early pregnancy. British Journal of Obstetrics and Gynaecology. 1992;**99**(1):38-42

[8] Manjunata B, Nithin ND, Sameer S. Cross sectional study to determine gestational age by metrical measurements of foot length. Egyptian Journal of Forensic Sciences. 2012;**2**:11-17

[9] Croft MS et al. Application of obstetric ultrasound to determine the most suitable parameters for the aging of formalin-fixed human fetuses using manual measurements. Clinical Anatomy. 1999;**12**(2):84-93

[10] Hern WM. Correlation of fetal age and measurements between 10 and 26 weeks of gestation. Obstetrics and Gynecology. 1984;**63**(1):26-32

[11] Conway DL et al. An algorithm for the estimation of gestational age at the time of fetal death. Paediatric and Perinatal Epidemiology. 2013;**27**(2):145-157

[12] Hirst JE, Ha LT, Jeffery HE. The use of fetal foot length to determine stillborn gestational age in Vietnam. International Journal of Gynaecology and Obstetrics. 2012;**116**(1):22-25

[13] Robinson HP, Fleming JE. A critical evaluation of sonar "crown-rump length" measurements. British Journal of Obstetrics and Gynaecology. 1975;**82**:702-710

[14] American College of Obstetricians and Gynecologists. Committee Opinion No. 700: Methods for assessing the due date. Obstetrics and Gynecology. 2017;**129**:e150-e154

[15] Whitworth M, Bricker L, Mullan C. Ultrasound for fetal assessment in early pregnancy. Cochrane Database of Systematic Reviews. 14 Jul 2015;(7)

[16] Wong HS. A comparison of the fetal measurements for sonographic estimation of gestational age at 10 to 14 completed weeks. Indian Journal of Applied Research. 2017;**7**(12):647-650

[17] Khalil A, Pajkrt E, Chitty LS. Early prenatal diagnosis of skeletal anomalies. Prenatal Diagnosis. 2011;**31**(1):115-124

[18] Schramm T et al. Prenatal sonographic diagnosis of skeletal

dysplasias. Ultrasound in Obstetrics & Gynecology. 2009;**34**(2):160-170

[19] Wong HS. A revisit of the fetal foot length and fetal measurements in early pregnancy sonography. International Journal of Women's Health. 2017;**13**(9):199-204

[20] Australian Government National Health and Medical Research Council. National statement on ethical conduct in human research; 2007

[21] Reece EA et al. Dating through pregnancy: A measure of growing up. Obstetrical & Gynecological Survey. 1989;**44**(7):544-555

[22] Bindra R et al. One stop clinic for assessment of risk for trisomy 21 at 11-14 weeks: A prospective study of 15030 pregnancies. Ultrasound in Obstetrics & Gynecology. 2002;**20**:219-225

[23] Bernard JP et al. Combined screening for open spina bifida at 11-13 weeks using fetal biparietal diameter and maternal serum markers. American Journal of Obstetrics and Gynecology. 2013;**209**(3):223.e1-223.e5

[24] El Kateb A et al. First-trimester ultrasound examination and the outcome of monochorionic twin pregnancies. Prenatal Diagnosis. 2007;**27**(10):922-925

[25] McLennan AC, Schluter PJ. Construction of modern Australian first trimester ultrasound dating and growth charts. Journal of Medical Imaging and Radiation Oncology. 2008;**52**:471-479

[26] Papageorghiou AT et al. International standards for early fetal size and pregnancy dating based on ultrasound measurement of crown-rump in the first trimester of pregnancy. Ultrasound in Obstetrics & Gynecology. 2014;**44**:641-648

[27] Napolitano R et al. Pregnancy dating by fetal crown-rump length: A systematic review of charts. BJOG. 2014;**121**(5):556-565

[28] Pexters A et al. New crown-rump length curve based on over 3500 pregnancies. Ultrasound in Obstetrics & Gynecology. 2010;**35**:650-655

[29] Khalil A et al. Biparietal diameter at 11-13 weeks' gestation in fetuses with open spina bifida. Ultrasound in Obstetrics & Gynecology. 2013;**42**(4):409-415

[30] Papageorghiou AT et al. The INTERGROWTH-21st fetal growth standards: Toward the global integration of pregnancy and pediatric care. American Journal of Obstetrics and Gynecology. 2018;**218**(2S):S630-S640

Chapter

Antenatal Diagnosis of Congenital Anomalies on Ultrasound Screening

Callen Kwamboka Onyambu and Norah Mukiri Tharamba

Abstract

Congenital fetal anomalies contribute to the global burden of disease in children. Various screening programs have been used for antenatal screening of these anomalies. Screening targets low risk population and is usually done in the second trimester though some are done at the mother's first antenatal visit especially in resource constrained setting. Mother's who have had a previous pregnancy with congenital anomaly are given targeted elaborate screening. Early diagnosis of this anomalies can lead to early intervention and better outcomes. Diagnosis of the malformations also leads to clinical decision making on mode of delivery thereby avoiding birth related trauma to the mother and the baby. In case of lethal congenital anomalies early diagnosis aids in clinical decision making on the management of the pregnancy.

Keywords: Ultrasound screening, pregnancy, fetal anomalies, fetal well being

1. Introduction

According to the World Health Organization (WHO), the term congenital anomaly includes any morphological, functional, biochemical or molecular defects that may develop in the embryo and fetus that is present at birth, whether detected at that time or not [1].

Major congenital anomalies impair function or greatly interfere with cosmetic value.

They may be life threatening and therefore need immediate management. Major anomalies could have a negative impact on a child's well-being and development, if early corrective surgery is not done. Minor anomalies, on the other hand, may cause little or no functional effects. They do not cause distress in the newborn and hence there is no urgency for their correction in the neonatal period [2].

Congenital anomalies occur in 2–3% of all births and are an important cause of perinatal morbidity and mortality accounting for 20–30% of perinatal deaths.

In a study conducted by Nayab Alia in Madina Teaching Hospital, Faisalabad on gray scale ultrasound, antenatal prevalence of congenital anomalies was 29.75 per 1000 and 2.97% [3]. A similar study in Saudi Arabia showed the antenatal prevalence of congenital anomalies to be 27.96 per 1000. The median maternal age at diagnosis was 27.5 years and the median gestational age at diagnosis was 31 weeks [4].

However, the actual numbers of these anomalies vary among different countries with prevalence of anomalies reported to be 2% in England and 1.49% in South Africa [5]. The reason for the regional difference of congenital anomalies might be attributed to variable factors, such as: maternal risk factors, environmental exposures, ecological, economical and ethnic factors [6, 7].

1.1 Pattern of congenital anomalies

The patterns of congenital anomalies may be different between regions and the actual numbers may vary significantly between countries [8]. In different countries, people have varied cultural and religious practices including exposure during antenatal period to various environmental factors. This may contribute to varied patterns of congenital anomalies. In some instances a common exposure to teratogenic factors or a hereditary condition with variable penetrance, may lead to high numbers of some anomalies, where severely affected individuals were not observed because of fetal/infant mortality [9]. Certain population groups are also regarded as "high risk groups" for congenital anomalies such as those living in heavily polluted industrial zones [10].

According to one study, frequency of congenital anomalies was more in males than females, with CNS anomalies being the most common. The anomalies were more common in gestation age of 29–32 weeks [11]. In a retrospective study of 200 cases of congenital anomalies carried out in Jos, Nigeria, the highest incidence was reported in the gastrointestinal system 61 cases. No association was found between the occurrences of the various congenital anomalies [12].

In yet another study conducted among South African live born neonates at Kalafong Hospital, Pretoria, in which the incidence of congenital anomalies was 11.87 per 1,000 live births, the most commonly affected system was the central nervous system (2.30 per 1,000 live births) [13].

1.2 Risk factors for congenital anomalies

According to WHO, approximately 50% of all congenital anomalies cannot be associated with a specific cause. However, there are some known risk factors which include socioeconomic factors with an estimated 94% of severe birth defects occurring in middle and low income countries. This is because mothers are more susceptible to macronutrient and micronutrient malnutrition and may also have increased exposure to agents that cause or increase the incidence of abnormal prenatal development, especially infection and alcohol. Other known factors are genetic and environmental factors [14, 15]. This is reaffirmed by a study that was conducted in Tanzania, that showed significant association between congenital anomalies and lack of periconceptional use of folic acid, maternal age above 35 years, exposure to pollutants and high birth order above [16].

Women with uterine anomalies have also been found to be at risk for particular CAs. In one study, the risk for some specific defects such as nasal hypoplasia, omphalocele, limb deficiencies, teratomas, and anencephaly was four times higher among offspring of mothers with a bicornuate uterus [17].

1.3 Ultrasound imaging IN congenital anomalies

Many congenital anomalies are identified prenatally on usual work up which includes detailed ultrasound and amniocentesis.

The diagnostic ability of ultrasound is well established by several studies with detection rate dependent on a number of factors which include the type of

abnormality, sophistication of equipment and experience of operator [18]. In a study conducted by Shama Munim at Aga Khan University Hospital (AKUH), Karachi on the accuracy of ultrasound in the diagnosis of congenital abnormalities, antenatal ultrasound successfully diagnosed fetal abnormalities in 48.8% of cases and more than 90% Central Nervous system defects and renal abnormalities [18].

However, a 1997 Report of the Royal College of Obstetricians and Gynecologists Working Party on Ultrasound Screening for Fetal Abnormalities identified that one of the problems with screening scans was the variable way in which they were conducted because there are no clear guidelines about what should, or should not, be examined. In a multicenter study, comparison was made of the precision of sonographic examinations done before 24 weeks gestational age at tertiary ultrasound laboratories contrasted with nontertiary ones. All the institutions were amply furnished with up-to-date equipment and supported with didactic and practical in-service training as required. The study found global sensitivity for sonographically demonstrable fetal abnormalities was 35% in tertiary centers, significantly higher compared to 13% in community hospitals. This further emphasizes that operator experience, competence, and training are vital determinants [19].

Ultrasound imaging is now routinely used in most countries for the purpose of screening pregnancies for fetal malformations but modalities, reliability and value of such screening is controversial [14, 19].

Regarding the time in gestation at which sonographic screening should be done, it is worthy noting that majority of the structural abnormalities are increasingly detected with advancing gestation. In early pregnancy, it is possible to diagnose with confidence certain categories of fetal anomalies, such as anencephaly, which can be reliably demonstrated at 10–14 weeks gestational age [20]. In certain instances, omphalocele and extremity malformations are also detectable using sonography in the first trimester, whereas other structural defects, like urinary system anomalies, are demonstrable later in pregnancy. However, a routine anomaly scan should be performed between 18 and 22 weeks of gestation. This period compromises between dating the pregnancy and the timely detection of major congenital anomalies [21].

Ultrasound examination at 10–14 weeks includes measurement of nuchal translucency, which is the maximum thickness of the subcutaneous translucency between the skin and the soft tissue overlying the cervical spine of the fetus. An increased nuchal translucency is associated with aneuploidy and cardiac malformations [22].

Ultrasound at around 20–21 weeks is done to screen fetuses for morphological anomalies. The utility of second trimester sonographic scan for detection of chromosomal anomalies was first recommended in 1985 [23]. Chromosomal aberrations were increasingly found to be associated with certain ultrasound findings, including biometric parameters (e.g., shortened femur and humerus, pyelectasis, thickened nuchal fold, dilated ventricles, fetal growth retardation) and morphologic features.

Ultrasound is the main diagnostic tool in the prenatal detection of congenital anomalies. It allows examination of the external and internal anatomy of the fetus. Even though a number of women are at increased risk of fetal malformations, either as a result of family history or owing to exposure to teratogens like infection and some drugs, the great majority of fetal abnormaitlies arise in the low risk category. As a result, sonographic evaluation ought to be offered routinely to all pregnant mothers. This is typically performed at 18–23 weeks of gestation, and should be done to a high level of precision. The scan should comprise systematic evaluation of the fetus for the detection of any defects.

2. Systemic review of congenital anomalies on ultrasound

2.1 Central nervous system (CNS)

The frequency of central nervous system anomalies varies according to geographic area and race. It is approximately 1–2:1000 newborns. Survivors are often severely disabled, necessitating long-term care.

The fetal brain undergoes major developmental changes during pregnancy. At 7 weeks of gestation, a sonolucent region is demonstrable in the cranial pole representing the fluid-filled rhombencephalic vesicle. At 9 weeks, demonstration of the convoluted pattern of the three primary cerebral vesicles is possible. The most prominent structures from 11 weeks are the echogenic choroid plexuses which fill the lateral ventricles. In the early second trimester, the lateral ventricles and choroid plexuses decrease in size relative to the brain mass.

Effective ultrasound screening for CNS anomalies can be carried out by examination of two important axial planes through the fetal brain; the transventricular and transcerebellar planes. Therefore, familiarity with the normal appearance of the fetal brain in these planes and at different gestational ages is vital for prompt identification of congenital anomalies.

The transventricular plane is at the level of the ventricular atria, with the echogenic choroid plexus being the dominant landmark. Measurements of atrial diameter made perpendicular to the walls should not normally exceed 10 mm.

This plane is obtained by axial sonogram at the level of the cavum septum pellucidum and shows the lateral margins of the frontal horns, the medial and lateral limits of the posterior horns of the lateral ventricles, and the choroid plexuses. It is used for fetal biometrics and quantification of the ventricular width (**Figure 1**).

The second crucial axial plane is the transcerebellar plane, which allows the examination of the midbrain and posterior fossa. The anatomic landmarks are the inferior portion of the third ventricle and the cerebellar hemispheres, which are outlined by fluid in the cisterna magna. The normal cisterna magna measures 2 to 11 mm in width (**Figure 2**).

A small cisterna magna (<2 mm) suggests a Chiari II malformation. However, it may also occur in massive ventriculomegaly. A large cisterna magna (>11 mm) may be a normal variant (megacisterna magna) or indicate a variety of anomalies. These

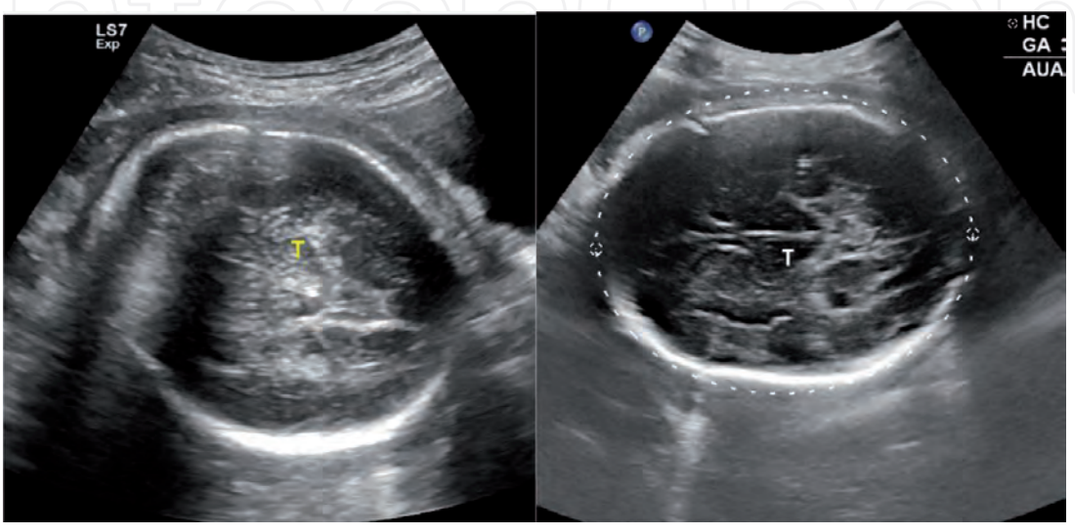

Figure 1.
Obstetric ultrasound showing biometric measurements. Fetal head: *Sonograms of the fetal head at the level of the thalami (T) showing measurement of the head circumference.*

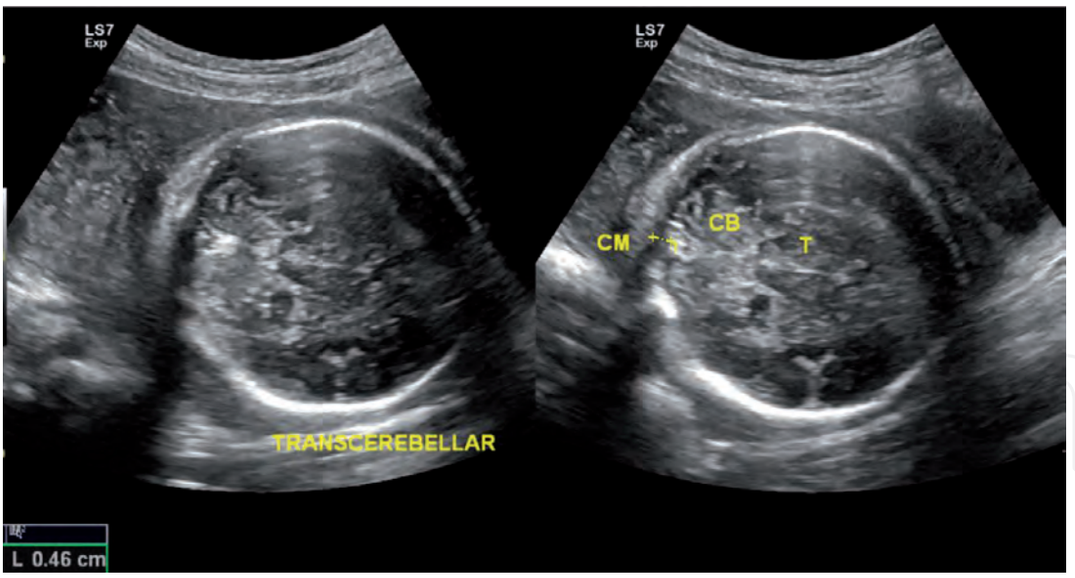

Figure 2.
Obstetric ultrasound; trans-cerebellar plane: This shows the cerebellar hemispheres (CB), cisterna magna (CM, between the two calibers) and thalami (T).

include Dandy-Walker malformation, arachnoid cyst, and cerebellar hypoplasia. When these two planes are anatomically normal, the risk of CNS anomaly is minute (0.005%).

Additional scanning planes along different orientations may be required occasionally, when one needs better definition of intracranial anatomy detail.

A sagittal and/or coronal view of the entire fetal spine should be obtained. In the sagittal plane, the normal spine has a 'double railway' appearance and one can appreciate intact soft tissue above it. In the coronal plane, the three ossification centers of the vertebra are visualized and should tether down into the sacrum. These views are used for assessment of vertebral integrity which rules out spina bifida. The presence and regularity of the whole spine from these views rules out sacral agenesis and scoliosis.

2.2 Cardiovascular system

The heart is the first functional organ in the embryo. It is prominently located and has visible contractions, which has made it the object of study for centuries. However, as recently as the late 1970s and early 1980s, the field of heart development was still in its infancy. In 1984, Dr. Constance Weinstein and colleagues at the National Institutes of Health (NIH) organized a meeting to bring together both cardiologists and basic scientists to summarize what was known about the development of the heart.

Congenital Heart Disease (CHD) is the most common birth defect comprising over 30 types of defects, ranging from mild to severe. It is found in 5–10 per 1,000 live births and in about 30 per 1,000 still births. Some forms of CHD resolve spontaneously, others are fully correctible, while others are life-threatening. Nearly 3 children out of every thousand live births have severe CHD requiring early surgery, while another 13/1000 requires surgery or catheter-based intervention later in childhood.

Precise US diagnosis of fetal heart abnormalities often requires specialized equipment and a high level of expertise.

The examination of the fetal heart begins with the assessment of the disposition of abdominal and thoracic organs. Abnormal disposition is associated with complex

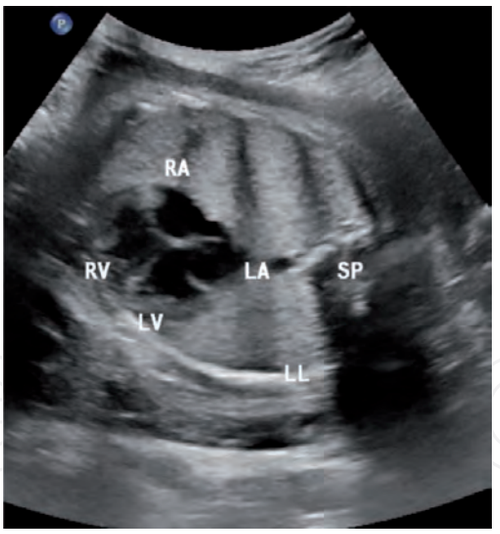

Figure 3.
Obstetric ultrasound; 4-chamber heart. Normal four-chamber view of the heart. Transverse scan through the fetal heart showing right ventricle (RV) anteriorly, left ventricle (LV) on the left, right atrium (RA) on the right and the left atrium (LA) as the most posterior. The spine (SP) and left lung (LL) are demonstrated.

cardiac anomalies. A transverse scan of the upper abdomen allows demonstration of the situation of the liver, stomach and great abdominal vessels. An axial section of the chest demonstration of a four-chamber view of the fetal heart. The heart covers about one third of the thorax. It is shifted to the left part of the thorax with the apex directed to the left.

About 90% of ultrasonographically detectable fetal cardiac defects demonstrate some abnormalities in the four-chamber view. Heart rate and rhythm are assessed subjectively. M-mode is useful for the evaluation of abnormal cases though is of little help in assessing morphology of the heart (**Figure 3**).

2.3 Pulmonary abnormalities

The lungs are interrogated in the same section used for the four-chamber view of the heart. The fetal lungs are uniformly echogenic. At 18–23 weeks, the middle third of the thoracic area at the level of the four-chamber view is occupied by the heart and the remaining two thirds by the lungs.

2.4 Anterior abdominal wall

The prevalence of anterior abdominal wall defects in sub Saharan Africa is not known as there are no population based studies. This could be due to non-availability of prenatal diagnosis and poor outcome of care post-delivery [24]. In a study carried out in a Nigerian tertiary hospital, omphalocele was the most common anterior abdominal wall defect seen [25].

Normal development of the anterior abdominal wall depends on the fusion of four folds (cephalic, caudal and two lateral). Developmental midgut herniation occurs at 8–10 weeks with subsequent retraction into the abdominal cavity at 10–12 weeks.

The integrity of the abdominal wall should always be adequately demonstrated. This is achieved via transverse scans which demonstrate the insertion of the umbilical cord. The urinary bladder should be visualized within the pelvis which rules out bladder exstrophy.

A study conducted to determine the ability of routine obstetric ultrasound to detect and accurately describe fetuses with anterior abdominal wall defects

demonstrated examination between 16 and 22 weeks gestation detected 60% of defects with a false positive rate of 5.3%. Fetuses with gastroschisis were incorrectly assigned as exomphalos in 14.7% of cases recognized before 22 weeks gestation. The diagnosis was completely accurate in 71.6% of cases. Therefore, problems of diagnostic accuracy should be put into consideration when counseling couples with a fetal anomaly.

2.5 Gastrointestinal tract

The fetal abdomen differs from the abdomen of the older child or adult. The fetal abdomen is large in relation to its body dimension compared with the adult. The liver is larger with the left lobe is bigger than the right owing to its greater supply of oxygenated blood. The umbilical vein is an important US landmark. Half the blood it carries goes directly to the inferior vena cava via the ductus venosus. The remainder perfuses the liver via the left portal vein. The gall bladder is visualized as an ovoid cystic structure below the intrahepatic portion of the umbilical vein. The spleen may be demonstrated in a transverse plane posterior and to the left of the stomach. The adrenal glands are up to 20 times larger in relative size because of the presence of a fetal zone. The pelvis is small with the pelvic organs extending into the lower abdomen. Swallowing commences at 11 to 12 weeks gestational age (GA). The fetal stomach is visible from 9 weeks of gestation as a sonolucent cystic structure in the upper left quadrant of the abdomen. It should be filled with swallowed fluid by 18 weeks GA. The small bowel is moderately echogenic and centrally located. Peristalsis in small intestine loops is usually demonstrable by the third trimester. The visualized small gut usually measures just below 6 mm in width and below 15 mm in length. The large bowel is seen after 20 weeks of intrauterine life as a tubular organ in the periphery of the abdominal cavity. It gradually fills up with meconium but does not usually surpass 23 mm in caliber.

The abdominal circumference should be measured in a scan of the abdomen demonstrating the stomach and the portal sinus of the liver. The visceral situs should also be evaluated.

This is done by demonstrating the relative location of the stomach, hepatic vessels, abdominal aorta and inferior vena cava (**Figure 4**).

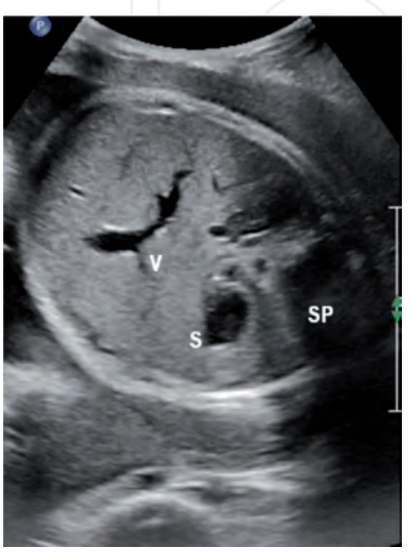

Figure 4.
Obstetric ultrasound showing the fetal abdomen. Fetal abdomen: The stomach (S) and intrahepatic portion of the umbilical vein (V) are demonstrated. The spine (SP) is seen posteriorly.

A case series of gastrointestinal abnormalities in fetuses with echogenic bowel detected during the antenatal period revealed that prenatal diagnosis of bowel abnormalities is challenging owing to the varying appearance of the bowel throughout pregnancy [26].

A related study showed that the prenatal ultrasound scan is unreliable in the detection or exclusion of fetal gastrointestinal malformations (GIM). Therefore clinicians involved in prenatal sonography or counseling should exercise caution in making such diagnoses. In this study, there were 220 confirmed cases of GIM, of which only 35 (16%) had been correctly identified prenatally. However, prenatal ultrasound was quite reliable in the detection of duodenal obstruction with 55% confirmed cases identified prenatally [27].

2.6 Kidneys and urinary tract

Detection of congenital urinary system anomalies is an important aspect of the prenatal ultrasound examination. Prenatal diagnosis of urinary tract abnormalities known to precipitate neonatal urosepsis and sequel such as renal scarring has made it possible to commence early intervention. A complete workup of the infants can be initiated early and before life-threatening complications occur.

The kidneys are visualized on sonography from as early as nine weeks of gestation and in all cases from twelve weeks. Echogenicity is high at nine weeks but reduces with advancing gestational age.

In a longitudinal scan, the kidneys are seen as elliptical structures while on axial sonograms, they are seen as rounded structures on either side of the spine. At 20 weeks, they show a hyperechoic capsule and the cortical area is slightly more echogenic than the medulla. Fat tissue normally accumulates around the kidneys as gestation progresses which enhances the borders of the kidneys in contrast with other organs. Normal ureters are rarely visualized in the absence of distal obstruction or reflux. The fetal bladder can be seen from the first trimester in more than 90% of subjects by 13 weeks (**Figure 5**).

A retrospective review of 56 children with urinary tract abnormalities detected by prenatal ultrasound revealed that more than half of the abnormalities were isolated hydronephrosis or multicystic dysplasia of the kidney [28].

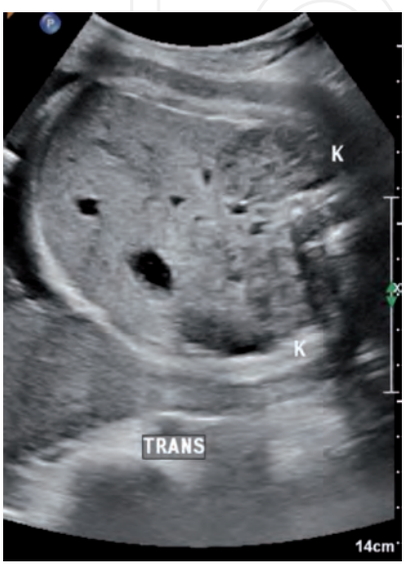

Figure 5.
Obstetric ultrasound showing fetal kidneys. Fetal abdomen at the level of the kidneys: Both kidneys (K) are seen on either side of the spine in this transverse sonogram.

The most frequent causes of hydronephrosis in the antenatal period are ureteropelvic junction (UPJ) obstruction, ectopic ureterocele, and posterior urethral valves (PUV). Renal pelvis of more than 10 mm in anteroposterior diameter or more than half of the anteroposterior diameter of the kidney in transverse section are conclusive evidence of significant hydronephrosis.

2.7 Skeleton

Detection of fetal anomalies is satisfactory for most organ systems but remains poor for cardiac, skeletal, and craniofacial anomalies. In a study to assess the accuracy of the prenatal diagnosis of skeletal dysplasias by Barbara V. Parilla et al., the antenatal diagnosis was correct in 20 (65%) of 31 cases [29]. This suggests that precise antenatal diagnosis of skeletal dysplasia is challenging. However, the antenatal prediction of lethality was highly accurate.

In general, skeletal dysplasias are uncommon. They affect 1 in every 4,000–5,000 births, even though the incidence may be higher since the features may not be apparent until early childhood, at what time short stature, joint abnormalities or other complications become apparent.

Skeletal dysplasias comprise a heterogeneous group of disorders of skeletal growth that result in bones of abnormal size and shape.

Normally, all long bones are consistently seen from 11 weeks and the limbs move about readily at this gestation.

At the 18–23 week scan, the 3 segments of each limb should be visualized. It is nevertheless only necessary to measure the length of one femur. The relationship of the leg and foot should also be evaluated to rule out club foot.

US findings that are highly associated with the presence of a generalized skeletal dysplasia include shortening of extremity bones, fractures, bowing of long bones, demineralization, and a small thorax. A ratio of femur length to foot length of less than 0.9 and femur length–abdominal circumference ratio of less than 0.16 suggest a skeletal dysplasia.

3. Conclusion

Antenatal ultrasound can allow for early detection of fetal anomalies and therefore early intervention as well as appropriate management of the pregnancy.

Author details

Callen Kwamboka Onyambu[1*] and Norah Mukiri Tharamba[2]
1 Department of Diagnostic Imaging and Radiation Medicine, University of Nairobi, Nairobi, Kenya
2 Mathari Teaching and Referral Hospital, Nairobi, Kenya

Available from https://dx.doi.org/10.5772/intechopen.98586

References

[1] R.M. S, D.I. S. Congenital malformations prevalent among Egyptian children and associated risk factors. Egyptian Journal of Medical Human Genetics. 2011.

[2] Samina Shamim, Nadeem Chohan SQ. Pattern of congenital malformations and their neonatal outcome. J Surg Pakistan Int. 2010;15(1):34-37.

[3] Alia N, Ahmed I, Mahais AH, Perveen N. Original Article CONGENITAL ANOMALIES : PREVALENCE OF CONGENITAL ABNORMALITIES IN 2 ND TRIMESTER OF PREGNANCY IN MADINA TEACHING HOSPITAL , FAISALABAD ON GRAY SCALE ULTRASOUND. J Univ Med Dent Coll. 2010;1(1):23-28.

[4] BI S, MS A-H, RA A, AA AS. Antenatal diagnosis, prevalence and outcome of major congenital anomalies in Saudi Arabia: a hospital-based study. Ann Saudi Med. 2008;

[5] Taboo ZA-A. Prevalence and Risk Factors for Congenital Anomalies in Mosul City. Iraqi Postgrad Med J. 2010;11(4).

[6] Barišić I, Group EW. EUROCAT – EPIDEMIOLOGICAL SURVEILLANCE OF CONGENITAL ANOMALIES IN EUROPE. Slov Med J [Internet]. 2018 Feb 14;78(0 SE-Review). Available from: https://vestnik.szd.si/index.php/ZdravVest/article/view/2760

[7] Improved National Prevalence Estimates for 18 Selected Major Birth Defects--United States, 1999-2001. JAMA J Am Med Assoc. 2006;

[8] Arjun Singh RKG. Pattern of Congenital Anomalies in Newborn: A Hospital Based Prospective Study. JK Sci. 2009;11(1):34-36.

[9] Magak P, King CH, Ireri E, Kadzo H, Ouma JH, Muchiri EM. High prevalence of ectopic kidney in Coast Province, Kenya. Trop Med Int Heal. 2004;

[10] Mashhadi Abdolahi H, Kargar Maher MH, Afsharnia F, Dastgiri S. Prevalence of Congenital Anomalies: A Community-Based Study in the Northwest of Iran. Neville H, Rice H, Tokiwa K, editors. ISRN Pediatr [Internet]. 2014;2014:920940. Available from: https://doi.org/10.1155/2014/920940

[11] Padma S, Ramakrishna D, Jijiya Bai P, Ramana P V. Pattern of distribution of congenital anomalies in stillborn: A hospital based prospective study. Int J Pharma Bio Sci. 2011;

[12] Ekwere EO, Mcneil R, Agim B, Jeminiwa B, Oni O, Pam S. A RETROSPECTIVE STUDY OF CONGENITAL ANOMALIES PRESENTED AT TERTIARY HEALTH FACILITIES IN JOS , NIGERIA. JPCS. 2011;

[13] Delport SD, Christianson AL, Van den Berg HJS, Wolmarans L, Gericke GS. Congenital anomalies in black South African liveborn neonates at an urban academic hospital. South African Med J. 1995;

[14] Onyambu CK, Tharamba NM. Screening for congenital fetal anomalies in low risk pregnancy: The Kenyatta National Hospital experience. BMC Pregnancy Childbirth. 2018;18(1).

[15] Parker A, Downs J, Kumar A, Shergill N, Jairaman, Jones AY-M, et al. Congenital anomalies fact sheet N 370. Pediatric Physical Therapy. 2014.

[16] Mashuda F, Zuechner A, Chalya PL, Kidenya BR, Manyama M. Pattern and factors associated with congenital anomalies among young infants

admitted at Bugando medical centre, Mwanza, Tanzania. BMC Res Notes. 2014;

[17] Martinez-Frías ML, Bermejo E, Rodríguez-Pinilla E, Frías JL. Congenital anomalies in the offspring of mothers with a bicornuate uterus. Pediatrics. 1998;

[18] Munim S, Nadeem S, Ali Khuwaja N. The accuracy of ultrasound in the diagnosis of congenital abnormalities. J Pak Med Assoc. 2006;

[19] Todros T, Capuzzo E, Gaglioti P. Prenatal diagnosis of congenital anomalies. Images Paediatr Cardiol [Internet]. 2001 Apr;3(2):3-18. Available from: https://pubmed.ncbi.nlm.nih.gov/22368596

[20] Johnson SP, Sebire NJ, Snijders RJM, Tunkel S, Nicolaides KH. Ultrasound screening for anencephaly at 10-14 weeks of gestation. Ultrasound Obstet Gynecol. 1997;

[21] Salomon LJ, Alfirevic Z, Berghella V, Bilardo C, Hernandez-Andrade E, Johnsen SL, et al. Practice guidelines for performance of the routine mid-trimester fetal ultrasound scan. Ultrasound Obstet Gynecol. 2011;

[22] Nicolaides KH, Azar G, Byrne D, Mansur C, Marks K. Fetal nuchal translucency: Ultrasound screening for chromosomal defects in first trimester of pregnancy. Br Med J. 1992;

[23] Benacerraf BR, Barss VA, Laboda LA. A sonographic sign for the detection in the second trimester of the fetus with Down's syndrome. Am J Obstet Gynecol. 1985;

[24] Ameh EA, Dogo PM, Nmadu PT. Emergency neonatal surgery in a developing country. Pediatr Surg Int. 2001;

[25] Abdur-Rahman L, Abdulrasheed N, Adeniran J. Challenges and outcomes of management of anterior abdominal wall defects in a Nigerian tertiary hospital. African J Paediatr Surg. 2011;

[26] Corteville JE, Gray DL, Langer JC. Bowel abnormalities in the fetus - Correlation of prenatal ultrasonographic findings with outcome. Am J Obstet Gynecol. 1996;

[27] Phelps S, Fisher R, Partington A, Dykes E. Prenatal ultrasound diagnosis of gastrointestinal malformations. In: Journal of Pediatric Surgery. 1997.

[28] Gloor JM, Ogburn PL, Breckle RJ, Morgenstern BZ, Milliner DS. Urinary Tract Anomalies Detected by Prenatal Ultrasound Examination at Mayo Clinic Rochester. Mayo Clin Proc. 1995;

[29] Parilla B V., Leeth EA, Kambich MP, Chilis P, MacGregor SN. Antenatal detection of skeletal dysplasias. J Ultrasound Med. 2003;

Chapter

Fetal Craniospinal Malformations: Aetiology and Diagnosis

Artur Beke, Virág Bartek and Aténé Simonyi

Abstract

The chapter discusses the aetiology and diagnostics of each fetal craniospinal disorder, particularly neural tube defects, ventriculomegaly, Dandy-Walker and Arnold-Chiari malformation, corpus callosum dysgenesis, iniencephaly, holoprosencephaly, microcephaly and kinked-brainstem. We aimed to highlight the usual ultrasound findings and genetic testing options.

Keywords: neural tube defects, anencephaly, exencephaly, spina bifida, ventriculomegaly, encephalocele, hydrocephalus, Dandy-Walker, Arnold-Chiari, corpus callosum, iniencephaly, kinked-brainstem, holoprosencephaly, microcephaly

1. Introduction

Our knowledge of the genetic background of the development of neurodevelopmental disorders is evolving. Today, ultrasound is a gold-standard diagnostic method for diagnosing developmental disorders. In addition to teratogenic causes, an increasing genetic background is being recognised for more and more fetal disorders. In addition to ultrasound diagnostics, the aim of this chapter is to investigate the genetic diagnostics of developmental disorders affecting the nervous system. In the case of malformations involving multiple organ systems, we investigate what chromosomal abnormalities or gene mutations may underlie each multiple disorder.

2. Fetal craniospinal malformations

2.1 Neural tube defects. Anencephaly/exencephaly. Spina bifida. Encephalocele

2.1.1 Epidemiology

Neural tube defects are the second most common structural-developmental malformations [1]. If the failure of neural tube closure is at the cranial end of the developing embryo, the disorder occurs in the form of anencephaly (initially exencephaly), if the failure is more caudal than cranial, it occurs in the form of spina bifida.

The prevalence of neural tube defects (NTDs) is 0.5–2/1000 live births, showing a heterogeneous geographical and ethnic distribution [2]. A genetic cause can be identified in 20% of cases [3].

2.1.2 Fetal morphology and prognosis

The brain of an anencephalic fetus is missing or missing in large parts. The form localising only to the cranium is called meroacrania, and extending to the foramen magnum is called holoacrania. If the spinal cord is also affected, the disorder is called craniorachischis.

The most severe neural tube closure disorder is caused by abnormal closure of the cranial section of the neural tube [4]. Anencephaly is a condition incompatible with life.

Spina bifida develops due to an abnormality in the closure of the neural tube caudally from the cranium. It basically affects the spinal region, with or without nerve tissue involvement. Its mildest form is spina bifida occulta, which is a defect of the vertebral arcs without affecting the underlying nerve tissue, most commonly in the sacral region, and usually causes no symptoms. In the case of spina bifida cystica, the lesion advances cystically. It can be closed (covered with skin or an opaque membrane) or open. If the cyst has meninx and cerebrospinal fluid but no nerve tissue in it, the lesion is called meningocele, if it also contains nerve tissue elements, the term is myelomeningocele [5]. The most severe form is myeloschisis (also known as rachischisis), which is an open lesion, so nothing covers the medullary (neural) plate [5]. After birth, spina bifida occulta usually does not cause symptoms, while spina bifida cystica can lead to paralysis of the lower extremities and urinary problems. Although myelomeningocele is a developmental disorder compatible with life, it is often associated with varying degrees of disability.

In encephalocele, the brain tissue with or without the meninges protrudes hernia-like through a pathological opening in the skull [5]. The most common site of its formation is os occipital [6]. Based on the grouping of Suwanwela and Suwanwela: cranial, frontoethmoidal, and basal encephalocele can be distinguished in addition to the occipital group [7].

2.1.3 Aetiology

To date, no clear genetic defect has been identified in the background of the development of NTDs, however, the role of a number of environmental and genetic predisposing factors is already known. It has been clinically demonstrated that folic acid supplementation significantly reduces the incidence of neural tube defects during the first trimester of pregnancy. Folic acid enrichment of the flour reduced the incidence of NTDs by 18% in 59 countries [8]. Folic acid, which is involved in purine and pyrimidine synthesis, is one of the cornerstones of DNA synthesis. Of course, not only isolated folic acid deficiency but any drug involved in folic acid synthesis may be associated with the development of anencephaly and other neural tube defects. These drugs such as antiepileptics (valproate or carbamazepine) and antimalarials (trimethoprim) are contraindicated during pregnancy without adequate folic acid supplementation, especially, in the first trimester.

In 1999, Shields et al. identified a heat-labile *MTHFR* C677T mutant gene that was present in the homozygous form of TT in 51 (18.8%) of 271 infants with neural tube defects (the homozygous form of CC did not increase the rate, whereas the heterozygous form of CT alone non-significantly increased the incidence of neural tube defects) [9].

Two members of the *SHROOM* gene family, the *SHROOM-2* and *SHROOM-3* genes have also been associated with the development of NTDs.

The role of the *SHROOM-3* gene in complex morphogenesis has long been demonstrated, and a mutation in a Loss of Function (LoF) (p.N594f) may be

associated with the development of neural tube defects. The Shroom-3 protein encoded by the gene is involved in the planar cell polarity (PCP) pathway, and in animal models, it has been found that its main function is to regulate the distribution of myosin II in cells [10].

A Chinese research team, Z. Chen et al. isolated 1.56 times as many rare variants in the *SHROOM-3* gene in live-born children with NTD than in the control group. In addition, the same research has also linked another member of the *SHROOM* family, the *SHROOM-2* gene mutation, to the development of neural tube defects. *SHROOM-2* is a gene localised on the short arm of the X chromosome (Xp22.2), which encodes a protein of the same name, Shroom-2. Shroom-2 is expressed by endothelial cells; its role in facilitating the development of the contractile network in endothelial cells. In infants with NTD cases, 4.5 times as many deleterious missense (D-Mis) variants were identified compared with the control group. In the same study, *SHROOM-2* variants were found in 42 of the 343 NTD cases, of which 15 mutations were identified. More than one *SHROOM-2* mutation was found in five of these samples [1].

Because the convergent extension is a critical point in neural tube closure, mutation of the gene encoding any other protein in the PCP system that regulates it leads to neural tube closure disorders. Mutation of PCP core genes such as *VANGL2* or *CELSR1* has been shown in mouse models to lead to the development of severe NTDs [11]. It is likely that genes encoding other proteins involved in the PCP signalling pathway may also be associated with neural tube closure disorders, however, human orthologs of the genes found in the experimental models have not yet been identified, so this may be part of further research.

Foetuses of untreated diabetic mothers are also more prone to neural tube defects, as elevated blood glucose levels lead to misfolded proteins, their accumulation and apoptosis of cells through non-enzymatic glycosylation.

This causes structural damage to organogenesis, especially the neuroepithelium. In animal models, high-dose folic acid supplementation has also been shown to reduce the incidence of neural tube defects associated with high blood glucose [12]. In terms of other environmental factors, hyperthermia and vitamin A deficiency may also lead to NTD, the former due to heat stress and the latter due to its role in the retinoic acid pathway resulting in the inadequate closure of the neural tube. Maternal obesity increases the chances of developing NTDs through hyperinsulinemia, and metabolic syndrome through its teratogenic effect due to oxidative stress [13].

2.1.4 Diagnostics

Anencephaly can be diagnosed in the first trimester (in this case, exencephaly is shown in the image), but can only be diagnosed with ultrasound in the second trimester with high certainty, median time to prenatal diagnosis is 20 weeks (16–24) [14]. Ultrasound signals that the upper part of the skull is missing and that no parenchymal tissue can be detected in the skull, however, the brainstem and occipital bone can be identified. In the coronal plane, a 'frog eye' or 'Mickey Mouse' symptom is seen, which is due to a lack of cranial bones and a protruding bulbus. In some cases, it is associated with polyhydramnios, which is the result of insufficient amniotic fluid ingestion by the fetus.

Spina bifida can be diagnosed in the second trimester, with a median time of 21 weeks (18–24). The time and accuracy of detection depend largely on the type of spina bifida and the position of the fetus, as certain positions make it very difficult to follow the spinal column. The direct signs are the openness of the vertebral arches and

herniation of the spinal cord, and the indirect signs are the lemon sign, the biconcave os frontale, and the banana sign, which is an abnormally bent, thin shape of the cerebellum. Ventriculomegaly due to cerebrospinal fluid flow disturbance is also common in foetuses with spina bifida, however, this ultrasound signal is not specific for diagnosis. Furthermore, the clivus-supraocciput angle is of diagnostic value; if it is less than 5 percentile, it raises the possibility of a form of neural tube defect associated with Chiari II malformation [15].

Thanks to modern technology, the availability of 3D and 4D ultrasound and MRI make it easier to diagnose neural tube defects so that in case of doubtful ultrasound findings, the diagnosis can be clarified by choosing another imaging modality. However, it should be noted that although these tests are much more accurate than conventional transabdominal and transvaginal ultrasound, their cost and limited availability make it essential to perform 2D ultrasound accurately and precisely, as it is still the most accessible, quickest and most economical method of diagnosis today.

In addition to imaging, laboratory tests can also support the diagnosis, as in 90% of cases, α-fetoprotein (AFP) levels are elevated in maternal blood and amniotic fluid, so this may be an additional tool to imaging. However, with the development of ultrasound, this test has been superseded.

In about one-tenth of cases, a chromosomal aberration or mutation has been identified as the cause of the neural tube defect, i.e., the majority of NTDs have a non-syndromic cause [16]. It can be seen that, although no clear environmental influence or genetic mutation has been identified as the cause of NTDs, it is likely that their development is multifactorial, i.e., genetic predisposing factors and environmental stresses contribute to their development.

2.1.5 Postnatal morphology and associated disorders

Postnatally, the anencephalic infant lacks a cranial bone (skull), the cerebellum is only a mass, shrunken. The ears are low set and deformed. Facial structures such as the eyes, nose and cheeks are large. The neck is short and spinal abnormalities may be present. The limbs are deformed, the thymus is abnormally large and pulmonary hypoplasia is often present. Spina bifida may be present with minimal external signs depending on the severity of the disease (in spina bifida occulta, only a darker patch or patch of hair-covered skin in the sacral region indicates a malformation). Depending on the region affected, a child with spina bifida lacks the structures covering the spinal column at the affected vertebrae and may have a herniated spinal cord; in meningocele and myelomeningocele, the protruding cyst is visible in the occipital region, with or without nerve tissue.

Neural tube defects are most commonly associated with renal abnormalities such as hydronephrosis, polycystic kidney disease, uni- or bilateral agenesis or unilateral hypoplasia. Cardiac malformations range from simple septal defects to complex cardiac malformations [17].

2.2 Congenital ventriculomegaly and hydrocephalus

2.2.1 Epidemiology

Ventriculomegaly is one of the most common pathological findings during antenatal ultrasound screening [18]. In severe cases, we are talking about hydrocephalus. The prevalence of hydrocephalus is 11/1000 live births [19].

2.2.2 Fetal morphology and prognosis

Hydrocephalus develops due to a progressive increase or impaired absorption of intraventricular cerebrospinal fluid (CSF) and its pathomechanism can be either obstructive or communicating [17, 20]. Increased pressure leads to the dilation of the ventricles, i.e., ventriculomegaly. If the brain volume thins due to the growth of the ventricles, we speak of hydrocephalus internus, if the volume of cerebrospinal fluid increases in the subarachnoid spaces, we speak of hydrocephalus externus. Macrocephaly can also develop with the growth of the bony skull [5], and the skull of such a fetus is larger than average.

The CSF is produced by the choroid plexus, circulates in the ventricles, then exits through the fourth ventricle into the subarachnoid space, where it is absorbed by the granulationes arachnoideae and finally drained through the venous sinuses into the systemic circulation. 1/3 of the CSF enters the lymphatic circulation, however, pathological alterations of this have not yet been demonstrated in human models [19].

The prognosis of hydrocephalus depends on its severity and the success of prenatal treatment. Of the 90 cases of hydrocephalus followed up by Yamasaki et al., 17% resulted in death, 21% were diagnosed with severe retardation, 13% with moderate retardation and 26% with mild retardation. A normal phenotype was described in 23% of cases [21].

The classification of ventriculomegaly depends on the degree of dilatation detected on ultrasound: mild ventriculomegaly between 10–12 mm, moderate ventriculomegaly between 13–15 mm and severe ventriculomegaly above 15 mm. The measurement is taken at the atrium of the lateral ventricle, the point where the temporal and posterior horns converge. This is a fixed value between 15 and 40 weeks of pregnancy [22].

If no abnormality is found in genetic testing and no other associated abnormality is present, mild ventriculomegaly is not considered pathological, and postnatally 90% of these cases present a normal phenotype, i.e., the wider ventricle is considered a normal variant [22].

2.2.3 Aetiology

Congenital hydrocephalus can be syndromic or non-syndromic, but in half of the cases, it is idiopathic [20]. The most common form of congenital hydrocephalus is the X-linked monogenic *L1CAM* mutation. The gene product of *L1CAM* is a protein that plays a key role in neuronal migration.

Hydrocephalus due to the *L1CAM* mutation is one of the most severe forms associated with stenosis of the aqueduct of Sylvius, known as HSAS (Hydrocephalus with Stenosis of the Aqueduct of Sylvius). It is often associated with corpus callosum agenesia or hypoplasia, adducted thumb and other structural cerebellar abnormalities [20]. Another form of X-linked congenital hydrocephalus is associated with *AP1S2* mutation [23].

Mutations in the *MPDZ* gene lead to primary ependymal malformations, including hydrocephalus [20]. *MPDZ* encodes a protein that regulates tight junction function and is also likely involved in the PCP pathway [24]. Mutations in this gene at 9p23 lead to autosomal recessive non-syndromic hydrocephalus [25]. Another form of autosomal recessive hydrocephalus is caused by mutations in *CCDC88C*. This gene encodes a protein called Daple, which interacts with Dishevelled protein to regulate cell migration. The Dishevelled protein is a member of the non-canonical Wnt pathway [26].

In addition to these well-studied genes, two others have recently been identified that are associated with the development of hydrocephalus. The *EML1* gene (14q32.2) encodes a microtubule system-related protein that is also involved in the PCP pathway. The gene mutation results in abnormal development of the posterior part of the skull, leading to severe hydrocephalus [23]. Also in this study, Shaheen et al. described another mutation, *WDR81* (17p13.3), which leads to severe hydrocephalus with cerebellar hypoplasia.

Neural tube defects are often associated with hydrocephalus. This may be due to common genetic factors and environmental aetiology, and pathological spinal development may itself be a physical barrier to CSF. Arachnoid cysts may also form a physical barrier in the pathway of cerebrospinal fluid. As arachnoid cysts occur in 15% of Phelan-McDermid syndromes, this syndrome is also often associated with hydrocephalus [19]. Other syndromes include mucopolysaccharidosis, Sotos syndrome and Rothmund-Thomson syndrome. Cytogenetic abnormalities have also been associated with the disorder, such as microdeletion of 9q22.3, partial trisomy of chromosome 1, but hydrocephalus is also common in Patau, Edwards and Down syndromes [19].

Ventriculomegaly/hydrocephalus may occur in isolated cases as a consequence of TORCH (Toxoplasma, Rubeola, Cytomegalovirus, Herpes simplex and other viruses) infection during pregnancy, or in rare cases due to congenital tumours such as choroid plexus papilloma [21].

2.2.4 Diagnostics

In terms of ultrasound diagnostics, it should be noted that in the first trimester, physiological ventricular dilatation is present, so hydrocephalus can only be diagnosed with certainty after the 14th week. The first characteristic ultrasound sign is asymmetry of the choroid plexus [27]. The top of the fourth ventricle may show an abnormal image and the absence of foramina Magendii and Luschka is common [17]. Due to the progressive nature of hydrocephalus, it may develop throughout pregnancy and even after birth without any previous ultrasound signal. Thus, the time to diagnosis also varies widely; Yamasaki et al., in their study of 156 cases of hydrocephalus, found the diagnosis to be made between 13 and 40 weeks (51% of cases were already diagnosed before 28 weeks). Breeze et al., also reported similar data, with a median time to diagnosis of 28 weeks (16–36) [28].

In addition to ultrasound, if ventriculomegaly or hydrocephalus is suspected, a Magnetic Resonance Imaging (MRI) scan may be useful, as it is a more accurate and reliable way of showing the development of brain structures and their possible malformations than ultrasound. However, it should be taken into account that, in addition to the general disadvantages of MRI (difficult availability, high costs), the fact that the fetal movement makes the findings more difficult or impossible to evaluate in antenatal diagnosis is a particular difficulty [29].

2.2.5 Postnatal morphology and associated disorders

The neonate with ventriculomegaly/hydrocephalus has macrocephaly, which may progress postnatally [30]. The disorder is often associated with neural tube defects due to common genetic predisposing factors.

2.3 Dandy-Walker malformation

2.3.1 Epidemiology

The incidence of this malformation is 0.33/1000 live births [31], i.e., it is a relatively rare disorder.

2.3.2 Fetal morphology and prognosis

The Dandy-Walker malformation includes dilatation of the fourth ventricle with hypoplasia or agenesis of the vermis of the cerebellum. A pseudocyst often develops at the base of the posterior fossa. Survival is low (about half of cases) [5].

2.3.3 Aetiology

Genetically heterogeneous in origin, several mutations have been described in recent years. However, one of the main "suspects" are the *ZIC1* and *ZIC4* genes, located at 3q24. In terms of inheritance, autosomal dominant, recessive and X-linked inheritance patterns have been reported, so it may be present as part of trisomy 9 (AR) or 6p (AD), but it may also be associated with Aicardi syndrome.

It is common in Edwards syndrome. However, in addition to genetic causes, a number of environmental factors may contribute to its development, such as maternal alcoholism or severe diabetes mellitus, as well as TORCH infection in the first trimester [17].

2.3.4 Diagnostics

Dandy-Walker malformation can be diagnosed by ultrasound at the earliest at week 11, but it should be noted that isolated dilatation of the fourth ventricle may be physiological during early development. In addition, the cerebellar vermis is not fully developed until the second trimester. In conclusion, an accurate diagnosis is only possible during the second trimester [27].

2.3.5 Postnatal morphology and associated disorders

Since the disorder mainly affects the cerebellum, in case of survival, postnatally the disorder may be marked by muscle movement disorders, learning difficulties and mental retardation. Hydrocephalus and consequent macrocephaly often develop due to inhibition of cerebrospinal fluid drainage [17]. It is often associated with hyperdactyly, syndactyly, renal, hepatic and pancreatic alloplasia and abnormal retina [32].

2.4 Arnold-Chiari malformation

2.4.1 Epidemiology

There are four types of Arnold-Chiari syndrome. Its prevalence is 0.9/1000 live births [33].

2.4.2 Fetal morphology and prognosis

In type I, the cerebellar tonsils are ectopic, with a part of the tonsils pressing into the foramen magnum, often in isolation. In type II, there is cerebellar hypoplasia with myelomeningocele, part of the tonsils and the elongated distal part of the brainstem protruding into the foramen magnum. In type III, the cerebellum is herniated due to the absence of occipital bone and spina bifida. In type IV, the most severe type, the cerebellum itself is hypoplastic [17]. Structural deformities lead to hydrocephalus. A lesion with a poor prognosis.

2.4.3 Aetiology

In the majority of cases, Arnold-Chiari malformation is multifactorial, and external environmental factors may also play a role in the development of the disease.

A precise genetic mutation has not yet been identified. It is assumed to be the result of mutations in proteins involved in the Sonic hedgehog and Wnt pathways, suggesting that there is an overlap at the gene level between mutations causing neural tube defects and Arnold-Chiari malformation, but this requires further research. Its aetiology is probably multifactorial and it cannot be ruled out that various environmental factors also contribute to the development of the phenotype.

Syringomyelia is often described in this pathology. In syringomyelia, the cavity formation observed in the nervous system may be due to residual formations from embryonic age, but may also occur as a result of haemorrhage or inflammation.

2.4.4 Diagnostics

An ultrasound scan in the second trimester of pregnancy can raise suspicion of the lesion, and if necessary, an MRI scan can confirm the diagnosis.

2.4.5 Postnatal morphology and associated disorders

Type I occurs in 3–5% of patients with Klippel-Feil syndrome, suggesting that abnormal *GDF6* and *GDF3* function may also be associated with the development of the syndrome [33].

Syringomyelia, which is often associated with type II, is rarely hereditary and may be associated with the following additional pathological conditions and gene mutations: hydrocephalus (*NF1, NES, GFAP, FGFR2, AQP4*), spina bifida (*GDF6*, *GDF3*) and other spinal deformities (*VDR, POC5, NF1, GH1, GFAP, GDF3*), various neurological tumours: astrocytoma (*NRAS, NF1, NES, GFAP, COL1A1*), neurilemmoma (*NF1, NES, GFAP*), ependymoma (*NES, GFAP*).

In addition, syringomyelia may also be caused by tissue weakness, such as in Ehlers-Danlos syndrome (mutations in *COL1A1, COL1A2, COL3A1, COL5A1, COL5A2, TNXB, ADAMTS2, PLOD1, B4GALT7, DSE, D4ST1/CHST14* genes) or Marfan syndrome (mutation in *FBN1* gene).

2.5 Corpus callosum agenesia/dysgenesis

2.5.1 Epidemiology

The prevalence of malformations of the corpus callosum is 0.25/1000 live births. In terms of aetiology, 30–45% of cases are due to genetic causes, 10% to chromosomal

abnormalities and 20–35% are associated with a genetic syndrome. In some cases, environmental factors (e.g., maternal alcohol consumption) also lead to corpus callosum dys- or agenesis [34].

2.5.2 Fetal morphology and prognosis

The corpus callosum is one of the five major cerebral commissures and is one of the largest white matter-containing tract in the brain. Its role is to connect the right and left hemispheres of the brain, and it is thought that 2–3% of the cortical fibres are passing through it. Its main function is to coordinate the hemispheres of the brain and to integrate sensory and motor functions [35].

Isolated corpus callosum dys- or agenesis is a disorder compatible with life, however, approximately 25% of foetuses with isolated corpus callosum agenesis/dysgenesis diagnosed antenatally will later have an intellectual disability. In addition, mild social or learning deficits may occur even with normal intelligence [35]. If the developmental disorder is part of a syndrome, the outcome of the disease depends on the particular syndrome.

2.5.3 Aetiology

Known chromosomal abnormalities affect chromosomes 1, 4, 6, 8 and 17. The most common type is a deletion, including the 1q42-q44 deletion causing corpus callosum dys- or agenesis of variable severity [35]. As most of the proteins encoded by these regions regulate or are involved in a key moment in nervous system development, corpus callosum dys- or agenesis as an isolated developmental disorder does not occur in any of the chromosomal disorders, but is often associated with microcephaly, hydrocephalus or craniofacial abnormalities.

Inheritance patterns include autosomal dominant, recessive and X-linked hereditary syndromes.

A very severe form of X-linked dominant (XLD) inheritance is Aicardi syndrome, which is incompatible with life in male foetuses but also has high premature mortality in girls. In addition to corpus callosum agenesis, it is associated with infantile seizures (infantile spasm) and the development of chorioretinal lacunes [36].

The autosomal dominant form is frontonasal dysplasia, Goldenhar syndrome; autosomal recessive form is Andermann syndrome, craniotelencephalic dysplasia, Da Silva or Leigh syndrome. Isolated corpus callosum dys- or agenesis can be inherited in an autosomal recessive, X-linked recessive (XLR) or autosomal recessive (AR) manner [17].

2.5.4 Diagnostics

Developmental abnormalities of the corpus callosum are difficult to detect before 18 weeks [35]. Ultrasonography shows colpocephaly, a high-lying enlarged third ventricle with absent or abnormal morphology of the corpus callosum [34]. These may confirm the suspicion, as in ultrasound diagnostics there is always the question of whether the absence of a formula is not only due to the position of the fetus, or possibly to a technician error. In their 2012 study, Santo et al. found that the number of false-positive ultrasound findings can be as high as 20%. An MRI scan after 22 weeks can confirm or refute the ultrasound findings with high certainty [37].

2.5.5 Post-natal morphology and associated abnormalities

Corpus callosum dys- or agenesis is often associated with microcephaly, hydrocephalus or craniofacial abnormalities [17]. Therefore, both the postnatal picture and the associated abnormalities are influenced by the gene mutation that results in the disorder.

2.6 Holoprosencephaly

2.6.1 Epidemiology

Holoprosencephaly is a midline malformation of the cranium and face. Its prevalence is estimated to be between 0.2 and 0.06 per 1000 live births [17, 38].

2.6.2 Fetal morphology and prognosis

The three main types of holoprosencephaly are lobar, semi-lobar and alobar. The most severe form is alobar, where midline separation is completely absent and the blister of the telencephalon does not separate. Typically, the corpus callosum and the third ventricle are absent, and cyclopia and proboscis are present. In the semilobar form, the frontal and parietal lobes are usually not separated bilaterally, but all septations, especially in the posterior region, are observed. Microphtalmia or anophtalmia, nasal malformations may also be associated. In the least severe form, the lobar form, the two hemispheres are essentially retained, with varying degrees of fusion between the two halves. The nose may be depressed with eyes sitting close, but the facial phenotype may be completely normal [39].

The prognosis depends on the severity of the holoprosencephaly. Mortality is high in alobar cases.

2.6.3 Aetiology

As with all neural tube defects, the development of holoprosencephaly is multifactorial, with both genetic and environmental influences contributing to its occurrence [40].

It is often associated with chromosomal abnormalities, most commonly with trisomy (Patau syndrome) or deletion of chromosome 13, but may also be associated with trisomy and deletion of chromosomes 18 and 21. Monogenic syndromes have also been associated with foetuses with holoprosencephaly, such as ARH (autosomal recessive holoprosencephaly), ADH (autosomal dominant holoprosencephaly), Váradi-Papp syndrome (AR), Grote syndrome (AR), Steinfield syndrome (AD) or holoprosencephaly-fetal akinesia syndrome (XL) (Wainwright, 2005). Environmental influences have also been implicated in the development of holoprosencephaly, such as maternal alcohol consumption during pregnancy and insulin-dependent diabetes mellitus.

A clear genetic mutation has been identified in the background of 15–20% of holoprosencephalic disorders [41]. Since the Sonic hedgehog signalling pathway is responsible for the regulation of the ventral phase of nervous system development and for the separation of the brain vesicles, it is understandable that genes affecting this mutation and their dysfunctional protein products would also be involved in this pathway. Mutations in the *SHH* gene itself have been demonstrated to underlie

holoprosencephalic retardation since 1996 [42]. Later, mutations in several members of the signalling pathway were identified, including mutations in *PTCH1* and *GLI2*. The Six-3 protein has not yet been linked to any of the signalling pathways, but mutations in *SIX3* are responsible for about 1.3% of holoprosencephaly cases. Six-3 is thought to play a role in the Wnt pathway [43].

There are also correlations between the development of neural tube defects and holoprosencephaly due to their common predisposing factors. K. Shiota found 14 cases of exencephaly or myeloschisis in 150 embryos with holoprosencephaly, but no correlation was found between holoprosencephaly and the severity of the neural tube defect. Diabetic mothers have a higher risk of developing both holoprosencephaly and neural tube defects [41].

2.6.4 Diagnostics

It can be diagnosed prenatally by transabdominal or transvaginal ultrasound, however, some of the milder lobar forms are difficult to diagnose by ultrasound. The median time to diagnosis of holoprosencephaly is 12 weeks (10–14) [27]. In the alobar type, morphological abnormalities of the face (cyclopia, ethmocephaly, cebocephaly) and absence of the choroid plexus in the lateral ventricles are well diagnosed by ultrasound. Dorsal cysts, ventriculomegaly and absence of the cavum septum pellucidum may also be associated findings [44]. An ultrasound sign of semilobar holoprosencephaly is incomplete separation of the hemispheric nuclei and fused thalamus. Both types are often associated with polydactyly, renal dysplasia, omphalocele and hydrops [44].

2.6.5 Postnatal morphology and associated disorders

Kaliaperumal et al. found a 95% mortality rate in alobar holoprosencephaly after antenatal diagnosis. Even mild cases are associated with severe postnatal complications, often requiring neurosurgery and intensive care [45].

2.7 Microcephaly

2.7.1 Epidemiology

Microcephaly is a deviation of at least three standard deviations of head circumference from the mean for given sex and age at fetal maturity [46]. A microcephaly finding is a clinical finding in itself, not a diagnosis [47]. Primary microcephaly is defined as a diagnosis made before 36 weeks of gestation, secondary microcephaly develops after birth [47]. The incidence of primary microcephaly is 0.16–0.025/1000 live births [17].

2.7.2 Fetal morphology and prognosis

Primary microcephaly is a static condition [48]. Phenotypic microcephaly is associated with varying degrees of cognitive deficits depending on the mutation, in addition, to head circumferential abnormalities, but weight, height and other external variations are not common. Imaging studies show normal brain morphology [48]. The prognosis depends on the type of mutation and is generally good, but in the majority of cases, severe deterioration in the quality of life is to be expected.

2.7.3 Aetiology

In terms of aetiology, microcephaly may be caused by a reduction or absence of neurogenesis (due to Cytomegalovirus (CMV) infection, chromosomal abnormality or primary autosomal recessive microcephaly), a prenatal destructive process (e.g., hypoxia, ischaemia) or a rare genetic syndrome.

TORCH infection suffered antenatally, especially in the first trimester, also increases the chance of developing microcephaly [47]. In addition to TORCH pathogens, the Zika virus has received particularly high press coverage in recent years due to the increased number of cases in the US. The association between Zika virus infection during pregnancy and primary microcephaly was quickly shown to be significant. 41,473 pregnant women infected with Zika virus were studied in Brazil between 2015 and 2016. Of these, 1950 cases of microcephaly associated with infection were recorded [49]. The almost 5% case rate is a huge increase compared to the average of 0.02%, and therefore more attention should be paid to mapping the teratogenic effects of Zika virus and preventing infection.

In particular, exposure to harmful substances such as maternal alcohol consumption in the first trimester increases the risk of developing microcephaly in addition to neural tube defects and hydrocephalus. Since fetal hypoxia during pregnancy can also lead to the development of microcephaly, special attention should be paid to pregnant women with placental insufficiency [47].

Isolated microcephaly is an autosomal recessively inherited disorder. Its pathomechanism is a disorder of neurogenic tissue mitotic activity, with normal cell migration and apoptosis [48]. Currently, 18 genes have been identified in the pathogenesis of primary microcephaly. All are members of the MCPH (autosomal recessive primary microcephaly) gene family.

In addition to the autosomal recessive form, mutations in other gene families are known to lead to primary microcephaly. These include *KIF2A, KIF5C* and *KIF11* from the kinesin family, and *TUBG1*, *TUBB2B* and *TUBA1A* from the tubulin family. The proteins encoded by these genes also contribute to the physiological function of the microtubule system.

Among chromosomal abnormalities, microcephaly is often associated with Patau, Edwards and Down syndromes [17].

2.7.4 Diagnostics

Ultrasound diagnosis is made by calculating the head circumference, calculated from the biparietal diameter and the occipitofrontal diameter. This derived value is compared with the mean value for the developmental stage and sex, and if it is at least two [50], in other sources three [46], standard deviations lower than the mean, it raises the possibility of microcephaly.

However, it is worth noting that individual variations may occur without organic deviation, and therefore further examinations to exclude false positivity is always important in the diagnosis of microcephaly. Other imaging, MRI, 3D or 4D ultrasound may be helpful. If a genetic abnormality is suspected, depending on the gestational age, amniocentesis and detailed genetic testing should be considered, especially if microcephaly is associated with other suspected signs (e.g. Intrauterine Growth Restriction, IUGR).

2.7.5 Postnatal morphology and associated disorders

Microcephaly may be associated with certain syndromes. One of these is the autosomal recessive Meier-Gorlin syndrome, which is caused by mutations in the *ORC1, ORC4, and ORC6, CDT1* or *CDC6* gene. The syndrome is one of the primordial dwarfisms and is characterised by intrauterine growth retardation, absence of patella, small ears and microcephaly. Pulmonary emphysema is common [51]. Other notable conditions include Nijmegen-Breakage syndrome, Ligase IV syndrome, Warsaw-Breakage syndrome, severe combined immunodeficiency (SCID) or Bloom syndrome [52].

2.8 Sacrococcygeal teratoma

2.8.1 Epidemiology

Sacrococcygeal teratoma is the most common neonatal tumour with a prevalence of 0.027/1000 live births. Its origin is pluripotent cell proliferation with tissue from all three germinal discs. The origin of the cells is remnant cells of the primitive streak or primordial germ cells [53]. It is more common in female foetuses, with a 4:1 ratio [54].

2.8.2 Fetal morphology and prognosis

The typical site of the tumour is the sacral region, hence its name, and it can often grow very large. In terms of pathology, it can be benign (mature) or malignant (immature). The majority of tumours (90%) are benign [55]. The tumour may be cystic or solid, as well as mixed in appearance. Often it may degenerate secondarily, calcify, or may contain haemorrhagic or necrotic regions [55].

The Altman classification was established based on the anatomical location of the tumour. Altman I is largely located externally, II has an associated intrapelvic tumour, III is largely located in the abdominal cavity, and IV is predominantly located presacrally, often without an externally visible tumour [56].

At prenatal diagnosis, the prognosis is poor, with frequent intrauterine death, mainly due to cardiac failure. In contrast, the prognosis is excellent after surgical intervention for postnatally diagnosed sacrococcygeal teratomas [54].

2.8.3 Aetiology

Sacrococcygeal teratoma is rarely associated with chromosomal abnormalities. There is literature evidence that sacrococcygeal teratoma can be associated with partial 13q22 trisomy [57]. Mutations associated with the 12p region are common in adult germ cell tumours, but this mutation has not been detected in "pure" sacrococcygeal teratomas [58]. However, the 12p mutation is common in sacrococcygeal teratomas where a yolk sac component is also present in the tumour. Based on this, Emans et al. suggest that sacrococcygeal teratomas should be classified into two groups depending on the absence or presence of the 12p isochromosome [59].

Rarely, sacrococcygeal teratoma may be part of the Currarino triad. It is an autosomal dominant inherited disorder with mutations in the *HLXB9* gene in the 7q36 region and is associated with anorectal malformations and presacral tissue proliferation and tumours

in addition to teratoma. Presacral tumours associated with the Currarino triad have a much lower chance of malignancy than non-syndromic forms [60].

In other rare cases, it may be associated with 3q trisomy, resulting in a Cornelia de Lange syndrome-like phenotype (short stature, bone developmental malformations, mental retardation, facial developmental abnormalities) [59].

2.8.4 Diagnostics

One of the most important suspicious signs is a larger uterus compared to the gestational age. This is caused by the size of the tumour or by the associated polyhydramnios. The visible tumour mass required to confirm the suspicion may be seen on ultrasound from as early as week 13, but its differential diagnosis is difficult, as the visible mass in the sacral region may also be pseudocyst, obstructive uropathy or meconium. In such cases, as is often the case in neurodevelopmental disorders, it is worthwhile to have an additional MRI scan.

An enlarged placenta and/or fetal hydrops may cause the mother to develop a condition similar to eclampsia, maternal mirror syndrome.

2.8.5 Postnatal morphology and associated disorders

The American Academy of Paediatrics Surgical Section (AAPSS) has developed a classification system that allows inferring the chance of malignancy and future complications depending on the presence of presacral and external tumours, the diagnosis, the success of the resection. In the I to IV scheme, grade I is the mildest with the least tendency to malignancy, while grade IV is the most severe and most likely to malign [55].

Associated abnormalities are usually consequential, so obstruction of the urinary tract, hydronephrosis, rectal atresia, bony malformation of the sacral region as well as fetal hydrops may occur [55]. Hip dysplasia and hydronephrosis may also be associated with sacrococcygeal teratoma in an unconsequential manner, so screening for these is essential both ante- and postnatally [56].

2.9 Kinked brainstem

2.9.1 Epidemiology

Kinked brainstem is an extremely rare condition. It is often only recognised postnatally. Precise figures on its incidence are not yet available.

2.9.2 Fetal morphology and prognosis

A kinked brainstem (twisted brainstem, fractured brainstem, also known as a Z-shaped brainstem) is a rare lesion, a sign of severe neurodysgenesis [61] on pre- or postnatal brain MRI scans. It usually occurs in association with other neurodevelopmental disorders and has a poor prognosis [62].

The posterior fossa is formed early during gestation. Brainstem folding occurs between the third and eighth week, with cerebellum development complete by the 16th week of gestation. Between the third and fifth week, the forebrain folds in accordance with the developing brainstem structures, creating the flexura cephalica, flexura pontis and flexura cervicalis. In the kinked brainstem, the angle of the

flexures is increased, normal brainstem and cerebellar development are inhibited, and cerebellar hypoplasia is, therefore, an associated abnormality in almost all cases [61].

2.9.3 Aetiology

So far, three syndromes have been identified in which kinked brainstem is present as an associated disorder: alpha-dystroglycanopathies (e.g., Walker-Warburg syndrome), tubulinopathies and X-linked hydrocephalus.

Alpha-dystroglycanopathies are heterogeneous congenital muscular dystrophies with brain, muscle and eye involvement [63]. At the more severe end of the spectrum is autosomal recessive Walker-Warburg syndrome, a defect in O-mannosyltransferase. It is often associated with ocular abnormalities (e.g. microphthalmia, retinal detachment), but these can often only be diagnosed after birth. Other alpha-dystroglycanopathies include muscle-eye-brain disease, Fukuyama muscular and cerebral dystrophy and muscle-eye-brain disease with bilateral multicystic leukodystrophy.

Alpha-dystroglycanopathy may be suspected if cobblestone lissencephaly is present. The trunks may be enlarged. Encephalocele is not a diagnostic criterion but may confirm suspicion [61, 62].

The genes identified so far that cause alpha-dystroglycanopathy are *FKRP, FKTN, POMT1, POMT2, POMGnT1, LARGE, ISPD, GTDC2, DAG1, TMEM5, B3GALNT2, B3GNT1, GMPPB, SGK196, DPM1, DPM2, DPM3, DOLK* [64].

There are two types of tubolinopathy, a more severe and a milder form. The more severe form is associated with microlissencephaly and 'kinked brainstem', the milder form is associated with more non-specific nervous system abnormalities. Three genes have been identified so far in its background: *TUBA1A* (chromosome 12), *TUBB2B* (chromosome 6) and *TUBB3* (chromosome 16) [65].

X-linked hydrocephalus is caused by the *L1CAM* (X-chromosome) mutation. It is suspected if the fetus is a boy and the cerebral aqueduct is not detectable on MRI even with a high T2 signal (however, this is difficult to diagnose if the fetus is small or moves around a lot during the scan). Spasticity and adduction of the thumbs may be associated (mainly seen on dynamic ultrasound, but not a diagnostic criterion). Usually, the hemispheres and trunks are not affected by the lesion [62].

2.9.4 Diagnostics

The abnormality is usually diagnosed prenatally during an MRI scan for suspected ventriculomegaly or other intracranial lesions. If the anomaly has not been diagnosed prenatally, a newborn with a kinked brainstem will require intensive care and will be in poor condition. Regardless of the associated abnormalities, the newborn presents with a variety of neurological symptoms, hypotonia and seizures [62].

2.9.5 Postnatal morphology and associated disorders

The kinked brainstem refers to the increase in the angle of the pontomesencephalic transition, exact figures have not been described so far. The brainstem may dislocate posteriorly or anteriorly at the midbrain bridge level. It is often associated with other intracranial abnormalities. Cerebellar hypoplasia is almost always present.

Other associated abnormalities may include ventriculomegaly, dys- or agenesis of the corpus callosum, delayed cortical development, neuron migration

disorders (e.g., lissencephaly), Dandy-Walker malformation, vertex encephalocele, abnormal cerebral hemispheres or abnormal head size (micro- or macrocephaly) [61].

Polymicrogyria and cobblestone lissencephaly are strongly suggestive of alpha-dystroglycanopathy, but the assessment of neuronal migration is difficult prenatally because the fetal brain is brainstem-rich until about 16 weeks gestation. Cerebellar cysts may also be present, however, these do not develop until the second week after birth [63].

The complicating factor is the secondary damage to cortical structures due to preexisting ventriculomegaly and hydrocephalus.

In a review of seven cases, Stroustrup et al. found that in two cases, the "kinked brainstem" was misidentified as a cerebellum on ultrasound [61]. Since the posterior fossa and the brainstem area are difficult to examine by ultrasound, it is advisable to request an MRI scan in case of a suspicious finding.

Theoretically, the abnormality can be diagnosed from week 7, but in practice, it is usually detected during the second-trimester screening.

2.10 Iniencephaly

2.10.1 Epidemiology

Iniencephaly is a complex malformation characterised by the absence of a neck, pronounced cervicothoracic lordosis and spina bifida.

Its prevalence is very rare and varies between 1 and 0.02/1000 live births, however, the actual prevalence may be higher, as iniencephaly is not always described as part of complex disorders [66].

2.10.2 Fetal morphology and prognosis

It is characterised by the complete or partial absence of the os occipital scales and of the cervical and thoracic vertebrae, an irregular fusion of the existing vertebrae and absence of the neck due to abnormalities in the closure of the vertebral arch. The foramen magnum is wider, while the posterior fossa is usually smaller. Due to the high degree of lordosis of the cervicothoracic spinal segment, the head is strongly tilted backwards, the face is upward (so-called "stargazing") and the trunk is shortened. It is often associated with other neural tube defects, open spina bifida or anencephaly. The disease has a very poor prognosis. If born alive, the newborn dies within a few hours (although one case has been described where the affected individual survived to adulthood and retained his or her intellect) [67].

We distinguish between two types of iniencephaly, iniencephaly apertus (with encephalocele) and iniencephaly clausus (without encephalocele) [68].

2.10.3 Aetiology

Its occurrence is predominantly sporadic. It is more common in female foetuses. Environmental effects have been described in association with maternal syphilis and drug intoxication. Chen et al. found chromosomal abnormalities in 5 of 16 cases studied (two cases of trisomy 18, two cases of trisomy of chromosome 13 mosaic and one case of monosomy of chromosome X mosaic) [66].

Since this is a type of neural tube defect, adequate folate supplementation can reduce the chances of its development, and all the factors described above as leading to the development of neural tube defects also contribute to the development of iniencephaly.

2.10.4 Diagnostics

Cuillier et al. diagnosed iniencephaly by transvaginal ultrasound at the 9th gestational week as the earliest on the basis of acrania, encephalocele and shortened spine [69]. Iniencephaly can be diagnosed with certainty from gestational week 13. Ultrasound signs include extreme dorsiflexion of the head, abnormally short and deformed spine and occipital meningocele. Polyhydramnios is always present.

In terms of differential diagnosis, it should be distinguished from cervical hyperextension, prenatal teratoma, lymphangioma, cervical myelomeningocele, Klipper-Feil and Jarcho-Levin syndromes.

Klipper-Feil syndrome is caused by a failure of segmentation of the cervical vertebrae early in gestation. There is no spina bifida in this case. There are usually associated neurological symptoms, often associated with deafness. Most cases are sporadic, but autosomal dominant and recessive forms have been described [66]. Klipper-Feil syndrome can be subsequently treated surgically [68].

2.10.5 Postnatal morphology and associated disorders

In 84% of cases, other anomalies are also associated: anencephaly, encephalocele, hydrocephalus, cyclopia, mandibular defect, cleft lip and palate, cardiovascular anomalies, diaphragmatic hernia, omphalocele, gastroschisis, situs inversus, ren polycysticum, arthrogriposis. It may also be associated with an undescribed frequency of Dandy-Walker malformation, hydronephrosis, atresia of the gastrointestinal system and umbilical artery singularis [66].

2.11 The epigenetics of fetal craniospinal malformations

As the cause of craniospinal malformations is usually multifactorial, it is understandable that epigenetic pathways should play an important role in neurulation, although it is yet a poorly researched area. The relation between neural tube defects and epigenetic pathways is the most studied part.

Multiple ways have been identified which affect the formation of neural tubes epigenetically. The most reviewed topic is DNA methylation, although only animal studies are available. In DNA methyltransferases *DNMT3A* and *DNMT3B* knocked-out mice neural tube defects are more common. It is also possible that *DNMT3L* plays a role in the process too, although it is less researched [70]. Mouse models have also been made to examine histone acetyltransferases, and it has been identified that histone acetyltransferases *GCN5* and *CBP* are both play a significant role in neurulation. It is supposed that it has an impact on human neural tube development too. Nucleosome positioning, another example of epigenetic regulation, is also studied in association with NTDs, as a subtype of ATP-dependent chromatin remodelling complex, the SWI/SNF-related nucleosome remodelling BAF complex has been proved to play an important role in the relation of neural tube closing in mice. Also, micro RNAs, like CECR2 have been proven to cause exencephaly in animal models [71].

It is clear that the epigenetic pathways do not function on their own, but rather as a part of a complex system. It would be important to examine and understand more about that as a part of future research.

3. Conclusion

In summary, by the second trimester, developmental disorders affecting the nervous system can be diagnosed with a high degree of certainty by ultrasound, but in case of doubtful findings, additional imaging tests should be performed. The development of these disorders is multifactorial; both environmental and genetic factors play a role. In the case of an abnormal ultrasound finding, genetic testing should be performed to confirm the finding and to rule out inherited mutations in subsequent pregnancies.

Author details

Artur Beke*, Virág Bartek and Aténé Simonyi
Department of Obstetrics and Gynecology, Semmelweis University, Budapest, Hungary

Available from https://dx.doi.org/10.5772/intechopen.103691

References

[1] Chen Z, Kuang L, Finnell RH, Wang H. Genetic and functional analysis of SHROOM1-4 in a Chinese neural tube defect cohort. Human Genetics. 2018;**137**(3):195-202

[2] Colas J-F, Schoenwolf GC. Towards a cellular and molecular understanding of neurulation. Developmental Dynamics. 2001;**221**(2):117-145. DOI: 10.1002/dvdy.1144

[3] Seidahmed MZ, Abdelbasit OB, Shaheed MM, Alhussein KA, Miqdad AM, Khalil MI, et al. Epidemiology of neural tube defects. Saudi Medical Journal. 2014;**35**(Suppl 1):S29-S35

[4] Tafuri SM, Lui F. Embryology, Anencephaly. 2021 May 8. In: StatPearls [Internet]. Treasure Island (FL): StatPearls Publishing; Jan 2022. PMID: 31424828

[5] Papp Z. A szülészet-nőgyógyászat tankönyve. Vol. 4. Budapest, Semmelweis Kiadó; 2009

[6] Horcajadas A, Palma A, Khalon BM. Frontoethmoidal encephalocele. Report of a case. Neurocirugía (Asturias, Spain). 2019;**30**(2):94-99. DOI: 10.1016/j.neucir.2018.02.006

[7] Suwanwela C, Suwanwela N. A morphological classification of sincipital encephalomeningoceles. Journal of Neurosurgery. Feb 1972;**36**(2):201-211. DOI: 10.3171/jns.1972.36.2.0201. PMID: 5008734

[8] Kancherla V, Wagh K, Johnson Q, Oakley GP Jr. A 2017 global update on folic acid-preventable spina bifida and anencephaly. Birth Defects Research. 2018;**110**(14):1139-1147. DOI: 10.1002/bdr1132.1366

[9] Shields DC, Kirke PN, Mills JL, Ramsbottom D, Molloy AM, Burke H, et al. The "thermolabile" variant of methylenetetrahydrofolate reductase and neural tube defects: An evaluation of genetic risk and the relative importance of the genotypes of the embryo and the mother. American Journal of Human Genetics. 1999;**64**(4):1045-1055

[10] McGreevy EM, Vijayraghavan D, Davidson LA, Hildebrand JD. Shroom3 functions downstream of planar cell polarity to regulate myosin II distribution and cellular organization during neural tube closure. Biology Open. 2015;**4**(2):186-196

[11] Murdoch JN, Damrau C, Paudyal A, Bogani D, Wells S, Greene NDE, et al. Genetic interactions between planar cell polarity genes cause diverse neural tube defects in mice. Disease Models & Mechanisms. 2014;**7**(10):1153-1163

[12] Valentin M, Coste Mazeau P, Zerah M, Ceccaldi PF, Benachi A, Luton D. Acid folic and pregnancy: A mandatory supplementation. Annales d'Endocrinologie. 2018;**79**(2):91-94

[13] Avagliano L, Massa V, George TM, Qureshy S, Bulfamante GP, Finnell RH. Overview on neural tube defects: From development to physical characteristics. Birth Defects Research. 2019;**111**(19):1455-1467. DOI: 10.1002/bdr1452.1380

[14] Turhan AH, Isik S. Neural tube defects: A retrospective study of 69 cases. Asian Journal of Neurosurgery. 2019;**14**(2):506-509

[15] Micu R, Chicea AL, Bratu DG, Nita P, Nemeti G, Chicea R. Ultrasound and magnetic resonance imaging in

the prenatal diagnosis of open spina bifida. Medical Ultrasonography. 2018;**20**(2):2018. DOI: 10.11152/mu-1325

[16] Kennedy D, Chitayat D, Winsor EJT, Silver M, Toi A. Prenatally diagnosed neural tube defects: Ultrasound, chromosome, and autopsy or postnatal findings in 212 cases. American Journal of Medical Genetics. 1998;**77**(4):317-321

[17] Wainwright HC. Embryo and Fetal pathology. Color atlas with ultrasound correlation. Journal of Clinical Pathology. 2005;**58**:784. DOI: 10.1136/jcp.2005.026047

[18] D'Antonio F, Zafeiriou DI. Fetal ventriculomegaly: What we have and what is still missing. European Journal of Pediatric Neurology. 2018;**22**(6):898-899. DOI: 10.1016/j.ejpn.2018.11.005

[19] Tully HM, Dobyns WB. Infantile hydrocephalus: A review of epidemiology, classification and causes. Europen Journal of Medical Genetics. 2014;**57**(8):359-368. DOI: 10.1016/j.ejmg.2014.06.002

[20] Saugier-Veber P, Marguet F, Lecoquierre F, Adle-Biassette H, Guimiot F, Cipriani S, et al. Hydrocephalus due to multiple ependymal malformations is caused by mutations in the MPDZ gene. Acta Neuropathologica Communications. 2017;**5**(1):36. DOI: 10.1186/s40478-017-0438-4

[21] Yamasaki M, Nonaka M, Bamba Y, Teramoto C, Ban C, Pooh RK. Diagnosis, treatment, and long-term outcomes of fetal hydrocephalus. Seminars in Fetal and Neonatal Medicine. 2012;**17**(6):330-335. DOI: 10.1016/j.siny.2012.07.004

[22] Fox NS, Monteagudo A, Kuller JA, Craigo S, Norton ME. Mild fetal ventriculomegaly: Diagnosis, evaluation, and management. American Journal of Obstetrics and Gynecology. 2018;**219**(1):B2-B9. DOI: 10.1016/j.ajog.2018.04.039

[23] Shaheen R, Sebai MA, Patel N, Ewida N, Kurdi W, Altweijri I, et al. The genetic landscape of familial congenital hydrocephalus. Annals of Neurology. 2017;**81**(6):890-897. DOI: 10.1002/ana.24964

[24] Assémat E, Crost E, Ponserre M, Wijnholds J, Le Bivic A, Massey-Harroche D. The multi-PDZ domain protein-1 (MUPP-1) expression regulates cellular levels of the PALS-1/PATJ polarity complex. Experimental Cell Research. 2013;**319**(17):2514-2525. DOI: 10.1016/j.yexcr.2013.07.011

[25] Drielsma A, Jalas C, Simonis N, Désir J, Simanovsky N, Pirson I, et al. Two novel CCDC88C mutations confirm the role of DAPLE in autosomal recessive congenital hydrocephalus. Journal of Medical Genetics. 2012;**49**(11):708-712. DOI: 10.1136/jmedgenet-2012-101190

[26] Ishida-Takagishi M, Enomoto A, Asai N, Ushida K, Watanabe T, Hashimoto T, et al. The dishevelled-associating protein Daple controls the non-canonical Wnt/Rac pathway and cell motility. Nature Communications. 2012;**3**:859. DOI: 10.1038/ncomms1861

[27] Blaas HG, Eik-Nes SH. Sonoembryology and early prenatal diagnosis of neural anomalies. Prenatal Diagnosis. 2009;**29**(4):312-325. DOI: 10.1002/pd.2170

[28] Breeze A, Alexander P, Murdoch E, Missfelder-Lobos H, Hackett G, Lees C. Obstetric and neonatal outcome in severe ventriculomegaly. Prenatal Diagnosis. 2007;**27**:124-129. DOI: 10.1002/pd.1624

[29] Pisapia JM, Sinha S, Zarnow DM, Johnson MP, Heuer GG. Fetal ventriculomegaly: Diagnosis, treatment, and future directions. Child's Nervous System. 2017;**33**(7):1113-1123. DOI: 10.1007/s00381-017-3441-y

[30] Kahle KT, Kulkarni AV, Limbrick DD Jr, Warf BC. Hydrocephalus in children. Lancet. 2016;**387**(10020):788-799. DOI: 10.1016/s0140-6736(15)60694-8

[31] Swaiman KF. Swaiman's pediatric neurology: Principles and practice. 6th edition. Edinburgh: Elsevier Saunders; 2012;S199-202

[32] Hunter A, Jimenez C, Tawagi F. Familial renal-hepatic-pancreatic dysplasia and Dandy-Walker cyst: A distinct syndrome? American Journal of Medical Genetics. 1991;**41**(2):201-207

[33] Capra V, Iacomino M, Accogli A, Pavanello M, Zara F, Cama A, et al. Chiari malformation type I: What information from the genetics? Child's Nervous System. 2019;**35**(10):1665-1671. DOI: 10.1007/s00381-019-04322-w

[34] Lieb JM, Ahlhelm FJ. Balkenfehlbildungen. Der Radiologe. 2018;**58**(7):636-645. DOI: 10.1007/s00117-018-0388-2

[35] Palmer EE, Mowat D. Agenesis of the corpus callosum: A clinical approach to diagnosis. American Journal of Medical Genetics. 2014;**166c**(2):184-197. DOI: 10.1002/ajmg.c.31405

[36] Aicardi J. Aicardi syndrome. Brain and Development. 2005;**27**(3):164-171. DOI: 10.1016/j.braindev.2003.11.011

[37] Santo S, D'Antonio F, Homfray T, Rich P, Pilu G, Bhide A, et al. Counseling in fetal medicine: Agenesis of the corpus callosum. Ultrasound in Obstetrics and Gynecology. 2012;**40**(5):513-521. DOI: 10.1002/uog.12315

[38] Ming JE, Muenke M. Multiple hits during early embryonic development: Digenic diseases and holoprosencephaly. American Journal of Human Genetics. 2002;**71**(5):1017-1032. DOI: 10.1086/344412

[39] Tekendo-Ngongang C, Muenke M, Kruszka P. Holoprosencephaly overview. In: Adam MP, Ardinger HH, Pagon RA, Wallace SE, Bean LJH, Stephens K, Amemiya A, editors. GeneReviews(®). Seattle: University of Washington; 1993

[40] Ming JE, Roessler E, Muenke M. Human developmental disorders and the sonic hedgehog pathway. Molecular Medicine Today. 1998;**4**(8):343-349. DOI: 10.1016/s1357-4310(98)01299-4

[41] Cohen MM Jr. Holoprosencephaly: Clinical, anatomic, and molecular dimensions. Birth Defects Research. 2006;**76**(9):658-673. DOI: 10.1002/bdra.20295

[42] Belloni E, Muenke M, Roessler E, Traverso G, Siegel-Bartelt J, Frumkin A, et al. Identification of sonic hedgehog as a candidate gene responsible for holoprosencephaly. Nature Genetics. 1996;**14**(3):353-356. DOI: 10.1038/ng1196-353

[43] Geng X, Speirs C, Lagutin O, Inbal A, Liu W, Solnica-Krezel L, et al. Haploinsufficiency of Six3 fails to activate sonic hedgehog expression in the ventral forebrain and causes holoprosencephaly. Developmental Cell. 2008;**15**(2):236-247. DOI: 10.1016/j.devcel.2008.07.003

[44] Kousa YA, du Plessis AJ, Vezina G. Prenatal diagnosis of holoprosencephaly. American Journal of Medical Genetics Part C: Seminars in Medical Genetics. 2018;**178**(2):206-213. DOI: 10.1002/ajmg.c.31618

[45] Kaliaperumal C, Ndoro S, Mandiwanza T, Reidy F, McAuliffe F,

Caird J, et al. Holoprosencephaly: Antenatal and postnatal diagnosis and outcome. Childs Nervous System. 2016;**32**(5):801-809. DOI: 10.1007/s00381-016-3015-4

[46] Arroyo HA. Microcephaly. Medicina (B Aires). 2018;**78**(Suppl 2):94-100 (Microcefalia.)

[47] Woods CG, Parker A. Investigating microcephaly. Archives of Disease in Childhood. 2013;**98**(9):707-713. DOI: 10.1136/archdischild-2012-302882

[48] Faheem M, Naseer MI, Rasool M, Chaudhary AG, Kumosani TA, Ilyas AM, et al. Molecular genetics of human primary microcephaly: An overview. BMC Medical Genomics. 2015;**8**(Suppl 1(Suppl 1)):S4. DOI: 10.1186/1755-8794-8-s1-s4

[49] de Oliveira WK, de França GVA, Carmo EH, Duncan BB, de Souza Kuchenbecker R, Schmidt MI. Infection-related microcephaly after the 2015 and 2016 Zika virus outbreaks in Brazil: A surveillance-based analysis. Lancet. 2017;**390**(10097):861-870. DOI: 10.1016/s0140-6736(17)31368-5

[50] de Castro M, Doin Trigo LA, Benini-Junior JR, Brito LGO, Marba STM, Amaral E. Ultrasound diagnosis of microcephaly: A comparison of three reference curves and postnatal diagnosis. Archives of Gynecology and Obstetrics. 2019;**300**(5):1211-1219. DOI: 10.1007/s00404-019-05234-5

[51] Bicknell LS, Walker S, Klingseisen A, Stiff T, Leitch A, Kerzendorfer C, et al. Mutations in ORC1, encoding the largest subunit of the origin recognition complex, cause microcephalic primordial dwarfism resembling Meier-Gorlin syndrome. Nature Genetics. 2011;**43**(4):350-355. DOI: 10.1038/ng.776

[52] Alcantara D, O'Driscoll M. Congenital microcephaly. American Journal of Medical Genetics. 2014; **166c**(2):124-139. DOI: 10.1002/ajmg.c.31397

[53] Sadler TW, Langman J. Langman's Medical Embryology. Vol. 1. Philadelphia: Wolters Kluwer Health/Lippincott Williams & Wilkins; 2012. p. c2012

[54] Taguchi T. Sacrococcygeal teratoma: Nationwide survey and guidelines. Pediatrics International. 2019;**61**(7):633. DOI: 10.1111/ped.13933

[55] Graf JL, Albanese CT. Fetal sacrococcygeal teratoma. World Journal of Surgery. 2003;**27**(1):84-86. DOI: 10.1007/s00268-002-6741-6

[56] Kremer MEB, Althof JF, Derikx JPM, van Baren R, Heij HA, Wijnen M, et al. The incidence of associated abnormalities in patients with sacrococcygeal teratoma. Journal of Pediatric Surgery. 2018;**53**(10):1918-1922. DOI: 10.1016/j.jpedsurg.2018.01.013

[57] Dalal SS, Berry T, Pimentel VM. Prenatal Sacrococcygeal Teratoma diagnosed in a Fetus with partial trisomy 13q22. Case Report in Obstetrics and Gynecology. 2019;**2019**:2892869. DOI: 10.1155/2019/2892869

[58] Mylonas KS, Kao CS, Levy D, Lordello L, Dal Cin P, Masiakos PT, et al. Clinicopathologic features and chromosome 12p status of Pediatric Sacrococcygeal Teratomas: A multi-institutional analysis. Pediatric and Development Pathology. 2019;**22**(3):214-220. DOI: 10.1177/1093526618798771

[59] Emerson RE, Kao CS, Eble JN, Grignon DJ, Wang M, Zhang S, et al. Evidence of a dual histogenetic pathway of sacrococcygeal teratomas. Histopathology. 2017;**70**(2):290-300. DOI: 10.1111/his.13062

[60] Emans PJ, Kootstra G, Marcelis CL, Beuls EA, van Heurn LW. The Currarino triad: The variable expression. Journal of Pediatric Surgery. 2005;**40**(8):1238-1242. DOI: 10.1016/j.jpedsurg.2005.05.004

[61] Stroustrup Smith A, Levine D, Barnes PD, Robertson RL. Magnetic resonance imaging of the kinked fetal brain stem: A sign of severe dysgenesis. Journal of Ultrasound in Medicine. 2005;**24**(12):1697-1709. DOI: 10.7863/jum.2005.24.12.1697

[62] Stanislavsky A, Kang O. Kinked brainstem. Reference article, Radiopaedia.org. [Accessed on 25 Mar 2022] DOI: 10.53347/rID-51058

[63] Amir T, Poretti A, Boltshauser E, Huisman TA. Differential diagnosis of ventriculomegaly and brainstem kinking on fetal MRI. Brain Development. 2016;**38**(1):103-108. DOI: 10.1016/j.braindev.2015.05.006

[64] Bönnemann CG, Wang CH, Quijano-Roy S, Deconinck N, Bertini E, Ferreiro A, et al. Diagnostic approach to the congenital muscular dystrophies. Neuromuscular Disorders. 2014;**24**(4):289-311. DOI: 10.1016/j.nmd.2013.12.011

[65] Cabet S, Karl K, Garel C, Delius M, Hartung J, Lesca G, et al. Two different prenatal imaging cerebral patterns of tubulinopathy. Ultrasound in Obstetrics & Gynecology. 2021;**57**(3):493-497. DOI: 10.1002/uog.22010

[66] Chen CP. Prenatal diagnosis of iniencephaly. Taiwanese Journal of Obstetrics and Gynecology. 2007;**46**(3):199-208. DOI: 10.1016/s1028-4559(08)60021-2

[67] Holmes LB, Toufaily MH, Westgate MN. Iniencephaly. Birth Defects Research. 2018;**110**(2):128-133. DOI: 10.1002/bdr2.1082

[68] Tanriverdi EC, Delibas IB, Kamalak Z, Kadioglu BG, Bender RA. A Fetus with Iniencephaly delivered at the third trimester. Case Report in Medicine. 2015;**2015**:520715. DOI: 10.1155/2015/520715

[69] Cuillier F, Koenig P, Lagarde L, Cartault JF. Transvaginal sonographic diagnosis of iniencephaly apertus and craniorachischisis at 9 weeks' gestation. Ultrasound in Obstetrics and Gynecology. 2003;**22**(6):657-658. DOI: 10.1002/uog.895

[70] Greene ND, Stanier P, Moore GE. The emerging role of epigenetic mechanisms in the etiology of neural tube defects. Epigenetics. 2011;**6**(7):875-883. DOI: 10.4161/epi.6.7.16400

[71] Wilde JJ, Petersen JR, Niswander L. Genetic, epigenetic, and environmental contributions to neural tube closure. Annual Reviews of Genetics. 2014;**48**:583-611. DOI: 10.1146/annurev-genet-120213-092208

Chapter

Diagnosis of Ectopic Pregnancy

Subrat Panda, Ananya Das, Kaushiki Singh, Prateeti Baruah and Anusuya Sharma

Abstract

Ectopic pregnancy is defined as the implantation of a fertilised egg outside the uterine cavity. The site of ectopic pregnancy are Fallopian tube. Cervix, ovary, peritoneal cavity, or uterine scars. Other two site of implantation are cornual pregnancy and interstitial pregnancy. Diagnostic tests for ectopic pregnancy include a urine pregnancy tests, Serum beta hcG and ultrasound. The instant result of a urine pregnancy test is a useful pointer for the clinician to suspect an ectopic pregnancy. The test is a useful triage tool for clinicians to rule out a pregnancy when the clinical situation is not clear such as a patient who is not sure of dates, does not remember or is in a state of shock and the history cannot be elicited. Ultrasound remains the mainstay of the diagnosis and high index of suspicion and a detailed history are pre-requisite of scanning. Different ultrasonography feature are diagnostic of different site of implantation. For uterine scar pregnancy ultrasonologic criteria are not validated still now.

Keywords: ultrasound, b HCG

1. Introduction

The proverb black cat in dark night fits into the diagnosis of ectopic pregnancy. To diagnose ectopic pregnancy clinician's mind should be suspicious about ectopic pregnancy. The most common ectopic site of implantation (97%) is the fallopian tube. The most common site for tubal pregnancy is ampulla, followed by isthmus, fimbrial and interstitial. Sometimes twin tubal pregnancy with both embryos in one tube or with one in each tube has been noted [1]. The other sites of ectopic pregnancies are implantation in the cervix, ovary, peritoneal cavity, or uterine scars. A growing ectopic pregnancy in any location can make the tissue vascular, friable and eventually rupture and result in intra-abdominal bleeding. This is a life threatening medical emergency. In history the risk factors like Pelvic inflammatory disease, including pelvic tuberculosis, previous ectopic pregnancy, pregnancy with an intrauterine device, tubal surgeries (ligations, reconstructions, and re-implantations), history of STD, smoking, infertility, ovulation induction and ART procedures should be elicited. The majority of women with ectopic gestation have no identifiable risk factor.

Ectopic pregnancy should be suspected in any woman with child bearing age presenting to the clinic or emergency department with symptoms of amenorrhea,

pain abdomen, and vaginal bleeding [2]. They may present with the complaint of fainting, collapse, breathlessness, or dizziness. Uncommon symptoms include diarrhoea, pain in the shoulder, rectal pressure, urinary symptoms, and anaemia. A small, undisturbed tubal pregnancy, the physical examination might be normal. In these situations, the diagnosis is dependent on investigations. On the other hand, with late presentations, there could be a disturbance of the vital signs and features of shock may be present including tachycardia, tachypnoea, hypotension, and rarely bradycardia. On abdominal examination there may be guarding, rigidity and tenderness. There could be also cervical motion tenderness, adnexal tenderness or fullness in the adnexae and pouch of Douglas. The presence of abdominal signs with altered vital parameters suggests presence of hemoperitoneum and mandates urgent resuscitation and management at a centre with appropriate facilities for blood transfusion and surgery.

Diagnostic tools for ectopic pregnancy are urine pregnancy tests, Serum beta-hCG and transvaginal or trans-abdominal ultrasound. Clinical suspicion combined with these tests plays a very important role in diagnosis and management of ectopic pregnancy. The instant result of a urine pregnancy test is a useful pointer for the practitioner to suspect an ectopic pregnancy. This kit test is easily available at low cost and is reliable. The test is a useful triage tool for clinicians to rule out a pregnancy when the clinical situation is doubtful such as a patient who is not sure of dates, does not remember or is in a state of shock and the history cannot be elicited.

Laboratory tests of a single laboratory value of beta-hCG might not be useful to diagnose the location of a pregnancy. The typical level in a healthy intrauterine pregnancy on the day of the missed period is 50 to 100 IU/L. In a normal intrauterine pregnancy, levels of serum beta-hCG will double every 1.4 to 2.1 days and peak between 50,000 and 100,000 IU/L at 8 to 10 weeks of pregnancy. Compared to the pattern observed in healthy intrauterine pregnancies, the rate of increase between two serum-hCG levels when it is done 48 hours apart is slower.

Progesterone levels are not useful for the diagnosis of an ectopic and maybe used in the prognostication of pregnancy of unknown location.

Ultrasound remains the mainstay of the diagnosis [3]. High index of suspicion and a detailed history are pre-requisite of scanning. The majority of tubal ectopic pregnancies should be visualised on transvaginal ultrasound.

Transvaginal ultrasound has sensitivities of 87.0–99.0% and specificities of 94.0–99.9% for the diagnosis of ectopic pregnancy [4]. Usually most of the ectopic pregnancies will be visualised on the initial ultrasound examination [5]. When no intrauterine or extauterine pregnancy is seen in USG it is called pregnancy of unknown location (PUL). Ectopic pregnancies initially classified as a PUL on the initial scan may be ectopic pregnancies are just too small and too early in the disease process to be visualised on the initial ultrasound examination. Sometimes the limiting value of beta-hCG should be evaluated, below which intrauterine pregnancies cannot be seen on USG. In case of PUL serial beta-hCG level assays adone to identify pattern that indicate either a growing or failing IUP. Without clear evidence for ectopic pregnancy, serial β-hCG level is advised and a level is checked after 48 hours. This wards off unnecessary medical therapy and avoids harming an early normal pregnancy. With more concern for an ectopic gestation, D&C is another option to distinguish an ectopic from a failing IUP. Normal rise B-Hcg does not exclude normal and ectopic pregnancy [6]. Laparoscopy is no longer the gold standard for diagnosis of ectopic pregnancies.

2. USG findings

An inhomogeneous or non cystic adnexal mass is the most common finding, about 50–60% of cases.

An empty extra-uterine gestational sac will be present in around 20–40% [7] of cases and an extra-uterine gestational sac containing a yolk sac and/or embryonic pole that may or may not have cardiac activity will be present in around 15–20% of cases [7].

There is no specific endometrial appearance or thickness, based on which diagnosis of tubal pregnancy can be confirmed. A few of cases, in around 20%, a collection of fluid may be seen within the uterine cavity, known as 'pseudosac'. It is difficult to differentiate pseudosac from an early intrauterine gestational sac. The intradecidual and double decidual signs indicates early intrauterine pregnancy (**Figures 1** and **2**). The intradecidual sign is eccentrically located echogenic area within a markedly thickened decidua [8]. The double decidual sign is described as an intrauterine fluid collection surrounded by two hyper echogenic rings [9]. But practically, it is very difficult to distinguish a 'pseudosac' which is just a collection of fluid in the endometrial cavity from

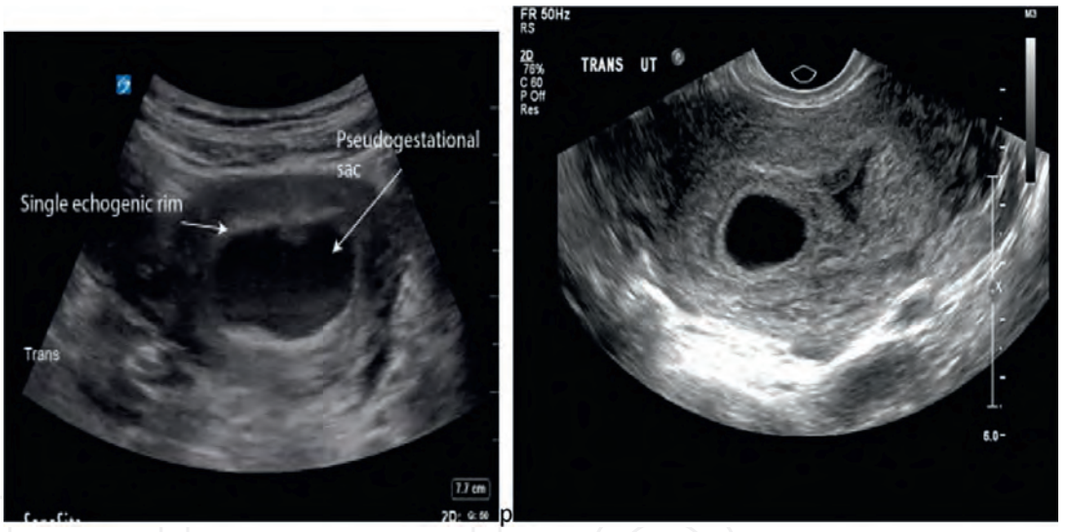

Figure 1.
Double decidual sign.

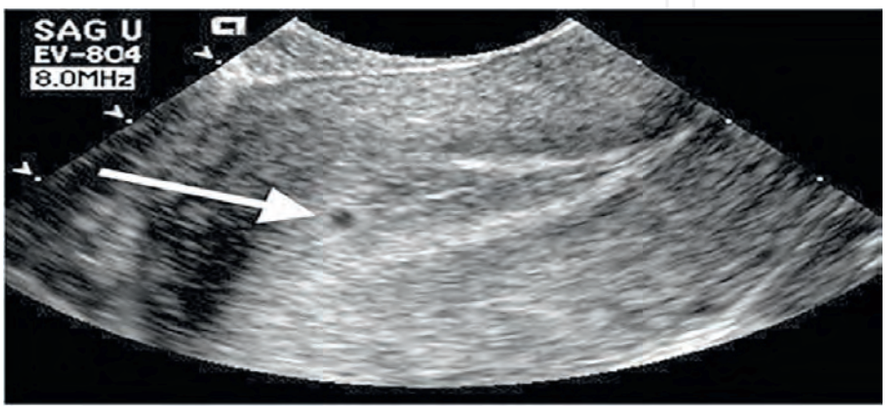

Figure 2.
Intradecidual sign.

an early intrauterine sac. A small anechoic cystic structure is more likely to be an early sac rather than a 'pseudosac'. Positive pregnancy test with and a small anechoic cystic structure without adnexal mass has probability of ectopic pregnancy is 0.02% [9].

When free fluid is seen on ultrasound, it is not a pinpointing feature of ectopic pregnancy. A small amount of anechoic fluid in the pouch of Douglas may be found physiologically in normal pregnancy and may be seen with ectopic pregnancies. Which may signify tubal rupture, Most commonly the echogenic fluid has been reported is due to blood leaking from the fimbrial end of the fallopian tube but it may be tubal rupture. Culdocentesis was used in the past to diagnose hemoperitoneum. Fluid with old blood clots and blood does not clot points to hemoperitoneum. If the blood sample clots it may have been drawn from nearby blood vessel or from profound bleeding ectopic pregnancy. Nowadays culdocentesis is not advised it is replaced by usg.

3. Cervical pregnancy

Cervical ectopic pregnancy is diagnosed by following usg criteria:

1. Empty Uterus

2. a barrel-shaped cervix,

3. a gestational sac is seen below the level of the internal cervical Os,

4. 'Sliding sign' usually absent

5. On colour Doppler, Blood flow around the gestational sac

The 'sliding sign' distinguishes cervical ectopic pregnancies and miscarriages that are within the cervical canal. It is present in cervical miscarriage but absent in cervical ectopic gestation.

When pressure is applied to the cervix using the probe, in a miscarriage, the gestational sac slides against the endocervical canal, but does not in an cervical ectopic gestation.

Cervical Ectopic Gestation usually develops in fibrous wall of the cervix. Risk factors includes previous dilatation and curettage operation and pregnancy due to ART may be implanted in cervical canal [10, 11]. Usually the women present with painless vaginal bleeding and sometimes with massive haemorrhage [12].

Clinical criteria for diagnosis of cervical pregnancy [13].

- Pregnancy with painless vaginal bleeding.
- Soft and expanded cervix with length is equal or more than fundus wasp like or hourglass shape.
- Product of conception firmly attached to cervical canal.
- Closed internal os and partially opened external os (**Figure 3**).

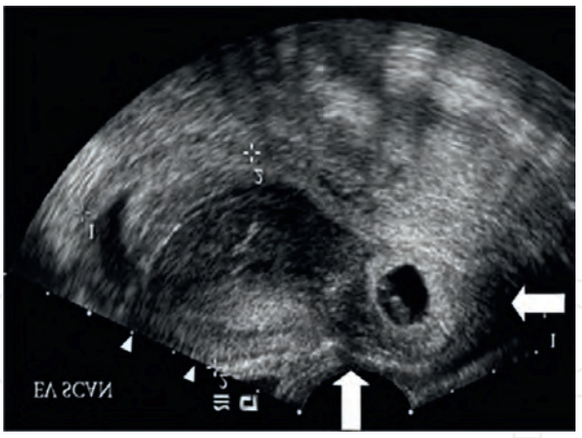

Figure 3.
Cervical pregnancy.

4. Caesarean scar pregnancy

The diagnosis of Caesarean scar pregnancy made by using transvaginal usg sometimes supplemented by trans-abdominal imaging if required.

Magnetic resonance imaging (MRI) can be used as a second-line investigation if the diagnosis is suspicious. Usually women with CSP present with painful bleeding PV and nearly half of women are asymptomatic.

Caesarean scar pregnancy is defined as implantation into the myometrial defect occurring at the site of the previous uterine scar.

The diagnostic criteria described for caesarean scar implantation on transvaginal ultrasound include: [14].

1. Empty uterine cavity and endocervical canal

2. Gestational sac or solid mass of trophoblast located anteriorly at the level of the internal Os embedded at the site of the previous lower uterine segment caesarean section scar

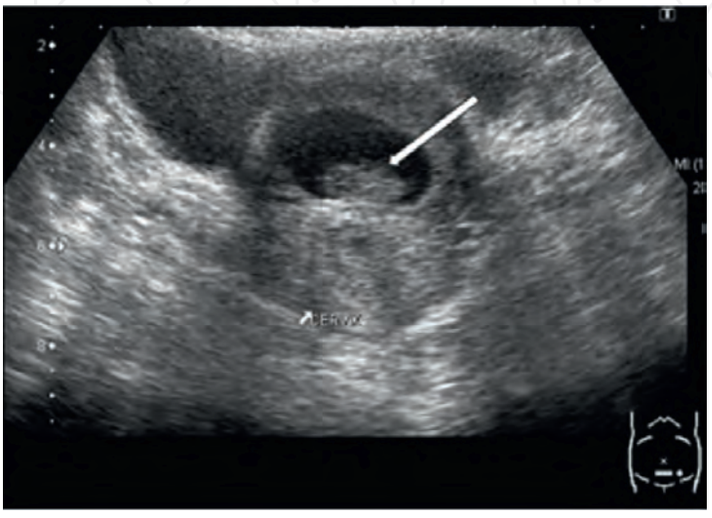

Figure 4.
Caesarean scar pregnancy.

3. Myometrial layer between bladder and gestational sac is absent or thin.

4. Evidence of prominent trophoblastic/placental circulation on Doppler examination.

5. Pregnancy less than 8wks triangular gestational sac is seen previous caesarean scar defect but after 8 weeks of gestation the gestational sac become rounded or oval.

The true prevalence of caesarean scar pregnancies is likely to be somewhat higher than estimated in the literature as some cases end in the first trimester, either by miscarriage or termination, and go unrecorded. A few percentages of reported cases of caesarean scar pregnancy were wrongly diagnosed as intrauterine or cervical pregnancies at presentation (**Figure 4**).

5. Interstitial pregnancy

When the implantation occurs in the proximal part of fallopian tube that lies within the muscular layer of uterus. Ipsilateral salpingectomy is a risk factor for interstitial pregnancy.

The following ultrasound scan criteria may be used for the diagnosis of interstitial pregnancy:

1. Empty uterine cavity, eccentric implantation,>1 cm away from the most lateral edge of uterine cavity.

2. Gestational sac surrounded by less than 5 mm of myometrium in all imaging planes,

3. And presence of the 'interstitial line sign'. An echogenic line extends from gestational sac to uterine cavity. It is highly sensitive and specific.

Dimensional ultrasound may be used if available to avoid misdiagnosis.

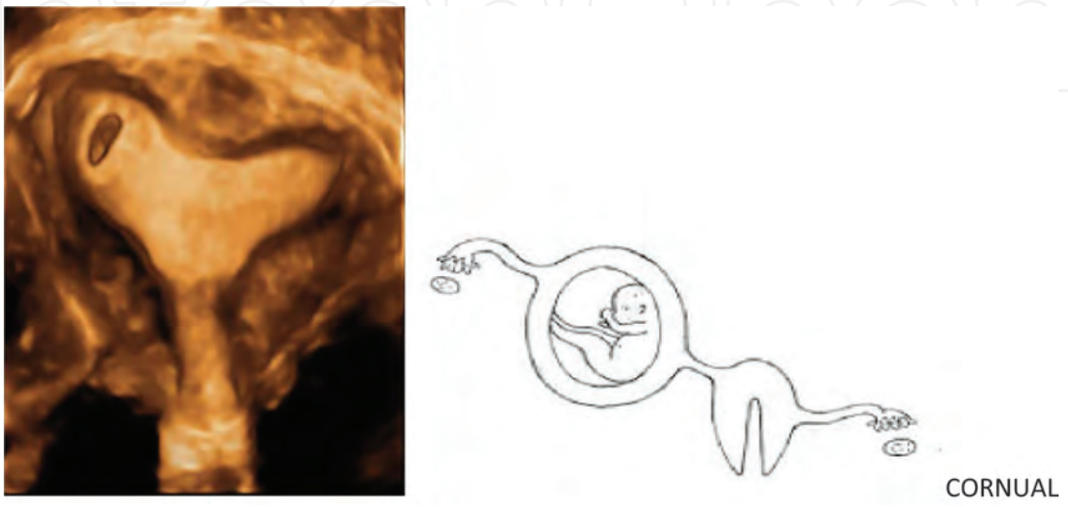

Figure 5.
Interstitial pregnancy.

MRI may be useful in addition to ultrasonography in the diagnosis of interstitial pregnancy (**Figure 5**).

6. Cornual pregnancy

The implantation occurs in the rudimentary horn of uterus it may be communicating or non communicating. It is a confusing terminology. Some authors prefer the cornual pregnancy when implantation occurs in upper lateral part of uterine cavity of normal uterus.

Ultrasound scan criteria are used for the diagnosis of cornual pregnancy:

1. Visualisation of a single interstitial portion of fallopian tube in the main uterine body,

2. gestational sac/products of conception seen mobile and separate from the uterus and completely surrounded by myometrium,

3. And a vascular pedicle adjoining the gestational sac to the unicornuate uterus.

7. Ovarian pregnancy

Findings suggestive of an ovarian ectopic pregnancy on transvaginal ultrasound with an empty uterus are:

1. A wide echogenic ring with an internal anechoic area on the ovary is seen commonly. A yolk sac or embryo is rarely seen [15].

2. It is not possible to separate the cystic structure or gestational sac from the ovary on gentle palpation (negative sliding organ sign).

3. Corpus luteum is identified separately from the suspected ovarian pregnancy.

4. Colour Doppler might be useful to detect foetal heart pulsation within the ovary.

A complex echogenic adnexal mass with free fluid in the pouch of Douglas may be the ruptured ovarian ectopic pregnancy.

Usually it is difficult to distinguish ovarian ectopic pregnancies from corpus luteal cysts, tubal ectopic pregnancy stuck to the ovary, a second corpus luteum, ovarian germ cell tumours and other ovarian pathologies and the diagnosis is confirmed surgically and histologically in most of the cases.

8. Abdominal pregnancy

When the implantation occurs in intraperitoneal cavity excluding tubal,ovarian and intraligamentous pregnancy. Usually the women have vague symptoms or no symptoms. Abnormal foetal position may be palpated.

MRI might be a useful diagnostic adjunct in advanced abdominal pregnancy and can help to plan the surgical approach.

1. Early abdominal Pregnancy, no intrauterine gestational sac.

2. Tubes and ovary are normal

3. A gestational sac surrounded by loops of bowel and separated from them by peritoneum and there is no myometrium between anterior abdominal wall and gestational sac.

4. A wide mobility similar to fluctuation of the sac, particularly evident with pressure of the transvaginal probe toward the posterior cul-de-sac.

Sonographic diagnosis may not be useful. MRI is very much useful to confirm the diagnosis and to identify placental implantation because placenta may be implanted over vital structures, such as major blood vessels and bowel [16]. This can help to make preoperative preparedness for perioperative considerations, such as the surgical approach, requirement of blood products, preoperative angiographic embolisation, bowel preparation and insertion of ureteral catheters. Precise mapping of the location of the placenta by using ultrasound and/or MRI prior to laparotomy to avoid incising the placenta and the associated risk of uncontrollable haemorrhage is necessary.

9. Heterotopic pregnancy

When there are both intrauterine and extrauterine implantation it is called heterotropic gestation it can be diagnosed with ultrasonography.

Heterotopic pregnancy should be suspected in if conception is after assisted reproductive technologies, with an intrauterine pregnancy and complaining of persistent pelvic pain and in those.

women with a persistently raised beta-hCG level following miscarriage or termination of pregnancy. A higher than expected level of serum beta-hCG in relation to gestational age may be suspicious of heterotopic pregnancy but, the presence of a complete or partial mole must be ruled out. Two corpora lutea found on laparoscopy or laparotomy. Sometimes patient may present with hemoperitoeum after termination of normal pregnancy or persistence of enlarged uterus and amenorrhoea after excision of ectopic pregnancy.

10. Conclusion

Ectopic pregnancy is associated with high maternal mortality and morbidity. With early diagnosis complications can be avoided. Primary modality of diagnosis is Ultrasound Scan. Hence Obstetrician should be well trained to diagnose ectopic pregnancy, and clinician should have high index of suspicion to diagnose ectopic pregnancy.

Diagnosis of Ectopic Pregnancy
DOI: http://dx.doi.org/10.5772/intechopen.101715

Author details

Subrat Panda*, Ananya Das, Kaushiki Singh, Prateeti Baruah and Anusuya Sharma NEIGRIHMS, Shillong, Meghalaya, India

References

[1] Della-Giustina D, Denny M. Ectopic pregnancy. Emergency Medicine Clinics of North America. 2003;**21**:565-584

[2] Gurel S, Sarikaya B, Gurel K, Akata D. Role of sonography in the diagnosis of ectopic pregnancy. Journal of Clinical Ultrasound. 2007;**35**:509-517

[3] Kirk E, Papageorghiou AT, Condous G, Tan L, Bora S, Bourne T. The diagnostic effectiveness of an initial transvaginal scan indetecting ectopic pregnancy. Human Reproduction. 2007;**22**:2824-2828

[4] Condous G, Van Calster B, Kirk E, Haider Z, Timmerman D, Van Huffel S, et al. Prediction of ectopic pregnancy in women with a pregnancy of unknown location. Ultrasound in Obstetrics & Gynecology. 2007;**29**:680-687

[5] Condous G, Okaro E, Khalid A, Lu C, Van Huffel S, Timmerman D, et al. The accuracy of transvaginal ultrasonography for thediagnosis of ectopic pregnancy prior to surgery. Human Reproduction. 2005;**20**:1404-1409

[6] Shepherd RW, Patton PE, Novy MJ, Burry KA. Serial beta-hCG measurements in the early detection of ectopic pregnancy. Obstetrics and Gynecology. 1990;**75**:417

[7] Yeh HC, Goodman JD, Carr L, Rabinowitz JG. Intradecidual sign: A US criterion of early intrauterine pregnancy. Radiology. 1986;**161**:463-467

[8] Bradley WG, Fiske CE, Filly RA. The double sac sign of early intrauterine pregnancy: Use in exclusion of ectopic pregnancy. Radiology. 1982;**143**:223-226

[9] Doubilet PM, Benson CB. Double sac sign and intradecidual sign in early pregnancy: Interobserver reliability and frequency of occurrence. Journal of Ultrasound in Medicine. 2013;**32**:1207-1214

[10] Ginsburg ES, Frates MC, Rein MS, Fox JH, Hornstein MD, Friedman AJ. Early diagnosis and treatment of cervical pregnancy in an in vitro fertilization program. Fertility and Sterility. 1994;**61**: 966

[11] Jeng CJ, Ko ML, Shen J. Transvaginal ultrasound-guided treatment of cervical pregnancy. Obstetrics & Gynecology. 2007;**109**:1076

[12] Ushakov FB, Elchalal U, Aceman PJ, Schenker JG. Cervical pregnancy: Past and future. Obstetrical & Gynecological Survey. 1997;**52**:45

[13] Paalman R, McElin T. Cervical pregnancy. American Journal of Obstetrics and Gynecology. 1959;**77**:126

[14] Timor-Tritsch IE, Monteagudo A, Santos R, Tsymbal T, Pineda G, Arslan AA. The diagnosis, treatment and follow-up of cesarean scar pregnancy. American Journal of Obstetrics and Gynecology. 2012;**207**:44e1

[15] Comstock C, Huston K, Lee W. The ultrasonographic appearanceof ovarian ectopic pregnancies. Obstetrics & Gynecology. 2005;**105**:42-45

[16] Aliyu LD, Ashimi AO. A multicentre study of advanced abdominal pregnancy: A review of six cases in low resource settings. European Journal of Obstetrics & Gynecology and Reproductive Biology. 2013;**170**:33-38

Chapter

Non-tubal Ectopic Pregnancy: Diagnosis and Management

Adebayo A. Adeniyi and Christopher A. Enakpene

Abstract

Ectopic pregnancy is the leading cause of maternal mortality in the first trimester, and prompt diagnosis and intervention are essential to ameliorate its associated complications. A majority of ectopic pregnancies are tubal, but extra-tubal pregnancy may pose more challenges in diagnosis and treatment. Early diagnosis of extra-tubal pregnancies requires high index of suspicion using transvaginal ultrasound and at times complemented with the help of magnetic resonance imaging. Similar to tubal pregnancy, extra-tubal ectopic pregnancies can be treated using surgical approach via laparotomy versus laparoscopy, or medical intervention with methotrexate, potassium chloride and most recently, mifepristone and epidermal growth factor inhibitor (gefitinib). For abdominal and ovarian ectopic pregnancies, the best surgical approach is via laparotomy or laparoscopy, while for cervical ectopic pregnancy and cesarean scar pregnancy (CSP), initial medical treatment with methotrexate, then suction curettage under ultrasound guidance, or hysteroscopic resection can suffice. All patients with extra-tubal pregnancy should be well counseled about the associated complications, fertility preserving intervention, and need for prolong monitoring especially those that choose medical therapy.

Keywords: cervical, ovarian, abdominal, cesarean section scar, interstitial, pregnancy, medical, surgical, treatment

1. Introduction

Ectopic pregnancy is defined as the implantation of a fertilized ovum outside the normal endometrial lining of the uterine cavity, and it accounts for 1–2% of all pregnancies [1, 2]. The true incidence of ectopic pregnancy is unknown but it accounts for 18% of women seen in the emergency room for first trimester vaginal bleeding, or abdominal pain, or both [3]. Moreover, ruptured ectopic pregnancies are responsible for 2.7% of all pregnancy-related deaths, and it is the leading cause of hemorrhage-related mortality [4]. About 95% of ectopic pregnancies occur in the oviduct or the Fallopian tube, while the remaining 5% occur in different locations such as the cervix, ovary, abdominal cavity and previous uterine scar especially cesarean section scar [5]. There have also been reported cases of ectopic pregnancy in unusual locations such as the intrahepatic ectopic pregnancy.

2. Etiology and risk factors

The risk factors for tubal ectopic pregnancy are well known, and this include poorly treated pelvic inflammatory disease (PID) mostly due to chlamydia and gonorrhea, history of ectopic pregnancy, tubal surgeries including tubal sterilization procedure, pelvic surgery and congenital anomalies of the Mullerian duct such as abnormally long fallopian tubes, unicornuate or bicornuate uterus. Other risk factors include infertility, smoking, use of intrauterine contraceptive device (Levonorgestrel impregnated or Copper IUD), and utero exposure to diethylstilbestrol. While the causes of extra-tubal pregnancy are less defined, it is clear that assisted reproductive techniques have contributed significantly to the incidence of all ectopic pregnancies especially the extra-tubal pregnancies [6].

3. Ovarian pregnancy

Ovarian ectopic is also a rare variant of extra-tubal ectopic pregnancy. It accounts for about 0.5% of all ectopic pregnancies [7]. The incidence of ovarian ectopic pregnancy after natural conception ranges from 1 in 2000 to 1 in 60,000 deliveries and accounts for 3% of all ectopic pregnancies among intrauterine devices users [7]. Most ovarian ectopic pregnancy (OEP) will rupture before the end of the first trimester, but few cases that progressed to term have been reported.

Risk factors for ovarian ectopic pregnancy:

1. Embryo migration related to the presence of certain conditions that cause fallopian tube epithelial damage that alters tubal motility [8].

2. A hindrance in the release of the ovum from the ruptured follicle [9].

3. Inflammatory thickening of the tunica albuginea [10].

4. IUD insertion is the most significant risk factor for primary OEP in 57–90% of the cases [8, 9]. This is because IUD provider protection for intrauterine implantation, but it does not prevent ovarian implantation [11].

Criteria for diagnosis of ovarian pregnancy as described by Spiegelberg in 1878:

1. Fallopian tube on the ipsilateral (affected) side must be intact.

2. The gestational sac must occupy the normal anatomical position of the ovary in the ovarian fossa (see **Figure 1**) [12].

3. The gestational sac is connected to the uterus by the ovarian ligament.

4. Ovarian tissue must be found on the wall of ectopic pregnancy on histological examination [13].

3.1 Treatment

The classical management of ovarian pregnancies is surgical. Early bleeding for small lesson has been managed by ovarian wedge section or cystectomy [14]. With larger lesions, ovariectomy is most often performed and this can be performed via laparotomy or laparoscopy which can be used to excise the gestational sac, to perform laser ablation or use of bipolar electrocoagulation. Methotrexate has been used successfully to treat unruptured ovarian ectopic [15].

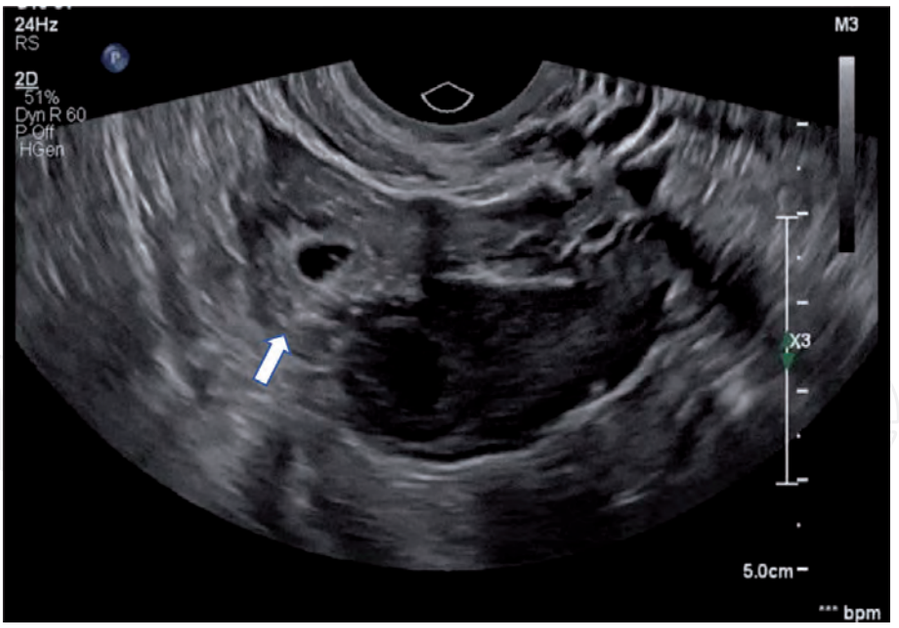

Figure 1.
Ovarian ectopic pregnancy. Transvaginal ultrasound showing a gestational sac located within the ovarian stroma (white arrow) [12].

4. Abdominal pregnancy

Abdominal pregnancy is almost always due to secondary implantation, with the primary sites being the tube, ovary or even the uterus. The conceptus result from tubal abortion into the peritoneal cavity or escapes through a rent in the uterine scar [16]. However, there have been reports of rare pseudo-abdominal pregnancies where women have abdominal pregnancy after hysterectomy with intact ovaries. This is most likely to have occurred via a fistula in the vaginal cuff in fertile women following total hysterectomy or via cervical canal following supracervical hysterectomy. The average incidence is above 1 in 3000 pregnancies. With the used of ART, the incidence is found rising [17]. Primary implantation of the fertilized ovum on the peritoneum is so rare that its existence is questionable.

4.1 Diagnosis

The diagnostic criteria of abdominal pregnancy as described by Studdiford in 1942:

1. Both the tubes and ovaries are normal without evidence of recent injury.

2. Absence of utero-peritoneal fistula.

3. Presence of a pregnancy related exclusively to the peritoneal surface and early enough to eliminate the possibility of secondary implantation following primary nidation in the tube [18].

Apart from symptoms of lower abdominal pain and amenorrhea, symptoms of normal uterine pregnancy are often exaggerated such as nausea, vomiting, constipation and increased fetal movements. The fetal parts are felt easily and persistent abdominal attitude and position of the fetus on repeated examination is quite common. While abdominal high position the fetus is commonly found in intraperitoneal pregnancy, though the fetus may be lying low in intraligamentary pregnancy. The cervix is not typically soft and is usually displaced

depending upon the position of the sac. Investigations done in case of suspected abdominal ectopic pregnancy include abdominopelvic ultrasound which shows absence of uterine wall around the fetus with close approximation to maternal abdominal wall and visualization of the uterus separately. Magnetic resonance imaging (MRI) can confirm the diagnosis and may be very accurate. Computed Tomography (CT) is diagnostic and superior to MRI [19]. CT has the risk of radiation. Lateral X-ray on standing position shows superimposition of fetal shadow with the maternal spine shadow.

4.2 Treatment

Once the diagnosis is made the opinion is almost crystallized in favor of urgent laparotomy irrespective of period of gestation. The risks of continuation of pregnancy are; catastrophic hemorrhage, fetal death, increased fetal malformation and increased neonatal loss [20]. Thus, continuation of pregnancy for few weeks hoping the baby to become mature enough to survive can only be justified in exceptional circumstances such as a case where the pregnancy continued up to 30 weeks and eventually resulted in a live born baby [21]. The patient and her relatives should be informed about the eventuality. During the period, the patient should be in the hospital. The ideal surgery is to remove the entire sac, fetus, the placenta and the membranes. This may be achieved if the placenta is attached to a removable organ like uterus or broad ligament. However, if the placenta is attached to vital organs, it is better to take the fetus and leave behind the placenta and the sac after tying and cutting the umbilical cord close to the placental attachment. In such a situation, placental activity is to be monitored by quantitative serum βHCG level and ultrasound. Complete resorption of the placenta occurs through aseptic autolysis. Complications include secondary hemorrhage, intestinal obstruction and infection.

5. Other types of non-tubal pregnancy

The most notable of other extra-tubal ectopic pregnancy are cervical pregnancy, cesarean section scar pregnancy (CSP), interstitial pregnancy and also a recently reported case of intrahepatic pregnancy.

6. Cervical pregnancy

Cervical ectopic pregnancies (CEP) probably the rarest of all ectopic pregnancies and it occurs in about 1:16,000 pregnancies, with implantation occurring in the cervical canal at or below the internal cervical os (see **Figures 2** and **3**) [7, 12, 22–24]. The etiology and risk factors for cervical ectopic pregnancy are similar to those enumerated above, but previous overzealous uterine curettage with associated Asherman syndrome and in-vitro fertilization are probably the most important risk factors. Previous cesarean section has also been implicated as a possible risk factor.

The condition is commonly confused with cervical abortion. In cervical pregnancy, the bleeding is painless and the uterine body lies above the distended cervix. Intractable bleeding following evacuation or expulsion of the products brings about suspicion. The morbidity and mortality are high because of profuse hemorrhage due to paucity of smooth muscles in the cervix, hence unable to contract to stop this bleeding.

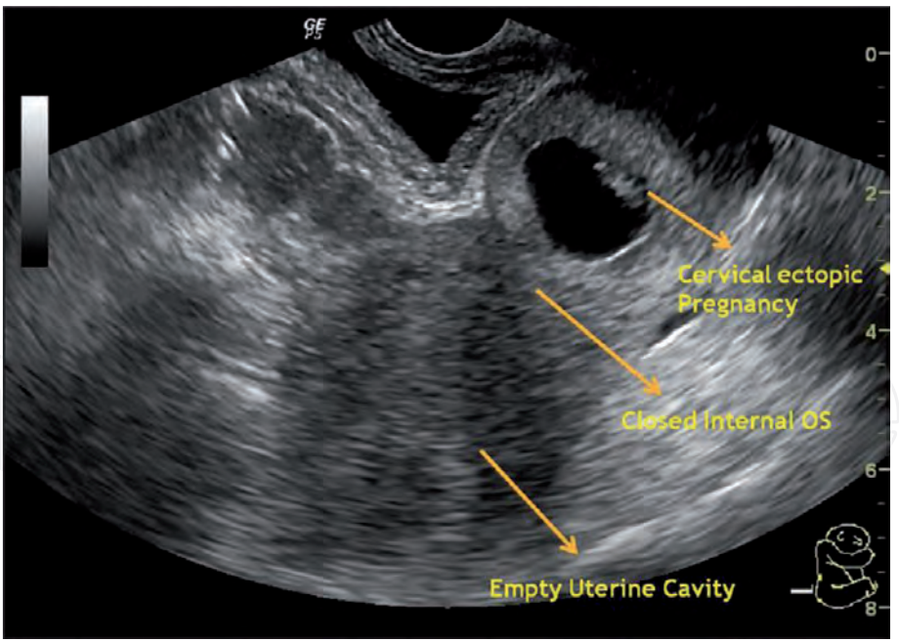

Figure 2.
Early cervical ectopic pregnancy with embryonic pole. Transvaginal ultrasound shows: (1) an empty and normal uterine cavity and (2) a cervical ectopic pregnancy with gestational sac and an embryonic pole (arrows) [23].

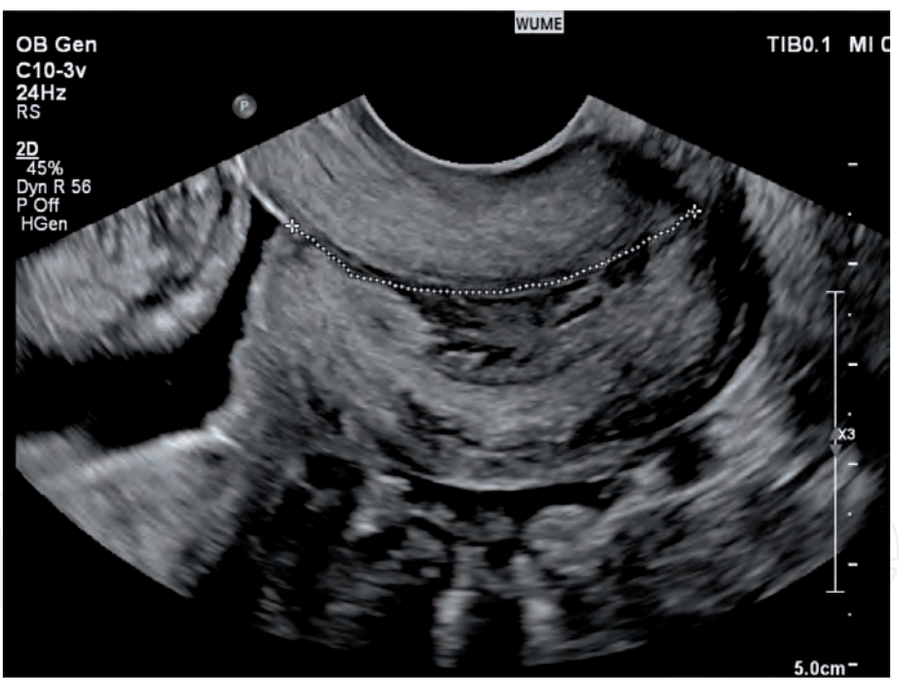

Figure 3.
Cervical ectopic pregnancy with no definite gestational sac. Transvaginal ultrasound showing an organized area with no definite gestational sac located within the posterior cervical stroma (white arrow) [24].

6.1 Diagnosis

Many criteria have been proposed for the diagnosis of ectopic pregnancy which include mostly the anatomical and histological criteria described by Rubin in 1911 but later modified in 1983, the more practical criteria by Paalman and McElin and finally, the sonographic criteria by Raskin et al.

The (Rubin, 1983) anatomical and histological criteria for cervical pregnancy include

1. Cervical gland must be opposite the placental attachment.

2. The placenta attachment to the cervix must be situated below the entrance of the uterine vessels or below the peritoneal reflections of the anterior or posterior surface of the uterus.

3. The fetal elements must be absent from the corpus uteri.

Rubin criteria require a hysterectomy specimen to satisfy these criteria.
Clinical diagnostic criteria as described by Paalman and McElin (1959)

1. Uterine bleeding without cramping pain following a period of amenorrhea.

2. Soft, enlarged cervix equal or larger than the fundus, (the "hourglass" appearance of uterus).

3. Products of conception entirely confined within and firmly attached endocervix.

4. A closed/ snug internal cervical os.

5. A partially opened external os.

Raskin (1978) proposed ultrasound diagnostic features but later modified by Timor-Tritsch et al.

1. Cervical enlargement.

2. Uterine enlargement.

3. Diffused intrauterine echoes.

4. Absence of intrauterine pregnancy.

5. Empty uterus or absence of gestational sac or embryo.

6. The entire product of conception (placenta and chorionic villi) must be located below the internal os and the cervical canal must be dilated and barrel shaped.

Jurkovic (1996) criteria were introduced to distinguish primary cervical ectopic pregnancy from an aborting intra-uterine pregnancy:

1. The "sliding sign" seen on transvaginal examination must be absent.

2. The demonstration of peri-trophoblastic blood flow to the fetus by color Doppler flow must be present.

7. Cesarean scar ectopic pregnancy

Cesarean scar pregnancy (CSP) accounts for 0.04–0.05 of all pregnancies [1]. The prenatal diagnosis of CSP is by the presence of gestational sac at the site of the previous uterine incision and the presence of an empty uterine cavity and cervix, as well as thin myometrium adjacent to the bladder (see **Figure 4**) [25, 26]. Cesarean

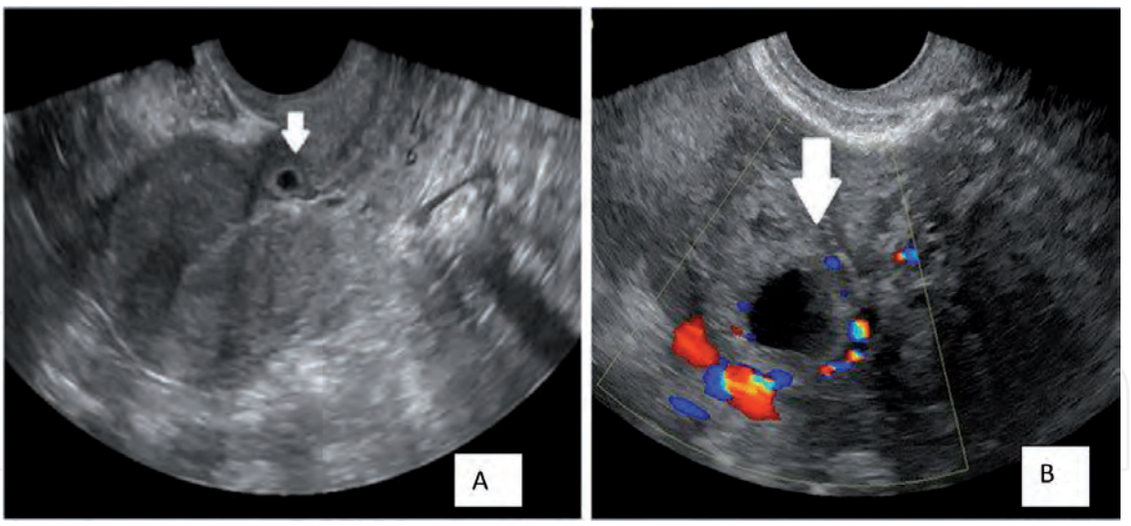

Figure 4.
Cesarean section scar ectopic pregnancy. Transvaginal ultrasound with 2-D and power Doppler showing: (1) normal uterine cavity and endometrium, (2) gestational sac in the cesarean section scar anteriorly, and (3) the vasculature around the gestational sac (white arrows) [25]. (A) shows cesarean ectopic pregnancy on a gray-scale ultrasound, and (B) shows the same pregnancy on color Doppler showing ring of fire of vessels around the gestational sac.

scar pregnancy can be classified based on the degree of invasion of amniotic sac into the myometrium, gestational age at diagnosis, presence of positive fetal heart beats and myometrial thickness of the lower uterine segment. The management of these rarer forms of ectopic pregnancy is just evolving.

Diagnostic criteria of cesarean scar ectopic pregnancy:

1. Empty uterus with clearly visualized endometrium.

2. Empty cervical canal.

3. Gestational sac within the anterior portion of the lower uterine segment at the presumed site of the cesarean scar.

4. Thinned or absent myometrium below the gestational sac and bladder (< 5 mm in two-thirds of cases) [27].

8. Cornual pregnancy

One of the most intriguing of ectopic pregnancies is the cornual or interstitial pregnancy, though not strictly extra-tubal pregnancy. It is neither located in the normal endometrial cavity nor in the normal fallopian tubes, but in the proximal portion of the tube and within the musculature of the uterus. The discussion on extra-tubal pregnancy cannot be complete without pointing out the implications of late diagnosis or misdiagnosis of cornual pregnancy; a potentially dangerous ectopic pregnancy. Often times, it can be mistaking for an intrauterine pregnancy thereby continuing till late first trimester, about 10–12 weeks of gestation. When it ruptures, it can result in rapid catastrophic hemorrhage because of the involvement of the well-vascularized muscular myometrium, and can cause significant maternal morbidity or mortality.

Diagnostic criteria of cornual ectopic pregnancy, 1992 [28]:

1. An empty uterine cavity.

2. A chorionic sac found separated (> 1 cm) from the lateral edge of the uterine cavity.

3. A thin (< 5 mm) myometrial layer surrounding the chorionic sac.

9. Diagnosis of non-tubal ectopic pregnancies

9.1 Pregnancy of unknown location (PUL)

Usually, the absence of intrauterine pregnancy, adnexal mass or abnormally rising serum beta hCG without evidence of intrauterine gestation are not always a confirmation of ectopic pregnancy. In the absence of any ultrasound evidence of visible pregnancy, the terminology of pregnancy of unknown location (PUL) is use. The prevalence of PUL is between 8 and 31% and it can be influenced by the quality of ultrasonography in the given unit, and the experience of the ultrasonographer [29, 30]. Even when PUL is being suspected, there is usually no place for diagnostic suction and curettage to determine the location of the pregnancy because this will disrupt a potential intrauterine pregnancy. Sometimes, some cases of PUL may evolve into ectopic pregnancy; tubal or non-tubal that may cause life threatening complications.

9.2 Ectopic pregnancies

Transvaginal ultrasound (TVUS) is the first line tool and the gold standard diagnostic apparatus of ectopic pregnancy. Ectopic pregnancy is usually diagnosed on TVUS as the presence of a mass with hyperechoic ring around the gestational sac ("bagel sign") or a gestational sac with a fetal pole with or without cardiac activity. The sensitivity and specificity of TVUS in detecting ectopic pregnancy are 90.9 and 99.9%, respectively, with positive and negative predict values of 93.5 and 99.8%, respectively. Another ultrasound feature of ectopic pregnancy is the trilaminar pattern of endometrial thickness with sensitivity of 38% and specificity of 94% for detecting ectopic pregnancy [31]. Magnetic resonance imaging is useful as a troubleshooting tool when ultrasound is equivocal or inconclusive before intervention or therapy [27]. Sagittal, coronal, and transverse sections of T1- and T2-weighted magnetic resonance imaging sequences can be used to show the gestational sac embedded in the anterior lower uterine segment, better evaluate pelvic anatomy, improve intra-operative orientation, and assess the possibility of myometrial invasion and bladder involvement [27, 32, 33]. Magnetic resonance imaging can also be used to measure the volume of the lesion so as to help assess whether methotrexate will be indicated and to predicts its success as medical intervention [27].

10. Management of non-tubal pregnancy

The management of extra-tubal ectopic pregnancy depends on the location, size of the gestational sac, presence of fetal heart beats and symptoms at presentation. The definitive management of extra-tubal ectopic pregnancy involves surgical extermination of the gestational sac via laparotomy, laparoscopy, hysteroscopy or suctional curettage under ultrasound guidance. Another advantage of surgical extermination is that there is confirmation of ectopic pregnancy by histological evidence of the presence of villi within the stroma of the affected structure.

Preservative procedures such as placement of cerclage; a pulse-string suture or cervical plugging have been proposed as adjunct treatment for cervical ectopic

pregnancy. Methotrexates therapy either systemic and /or local injections directly into the gestational sac or intracardiac potassium chloride injection have also been used especially when there is associated embryonic cardiac activity. Uterine artery embolization with Gelfoam has also been used successfully to control hemorrhage. However, hysterectomy is often required to control intractable bleeding. Occasionally, there may be no need for intervention due to declining serum beta hCG levels in asymptomatic patients; however, these patients are usually closely monitored to ensure spontaneous resolution of the pregnancy.

11. Medical management

11.1 Methotrexate

Methotrexate is a chemotherapeutic anti-metabolite that affects rapidly dividing cells, and it is use in the treatment of cancers and connective tissues disorders such as rheumatoid arthritis. The use of Methotrexate in the medical management of ectopic pregnancy has to be thoroughly given serious consideration to avoid inadvertent administration in patient with intrauterine pregnancy. Hence, careful selection of appropriate candidate for Methotrexate treatment to improve success rate is advised. In most instances, Methotrexate should only be given to patients with confirmed or presumed ectopic pregnancy who are hemodynamically stable with an unruptured gestational sac. The success rate is also dependent on the level of serum beta hCG because single-dose systemic Methotrexate had approximately 90% success rate if the initial serum hCG level is less than 5000 mIU/ml [34].

The indications and contraindications of Methotrexate should be reviewed before every use. For some extra-tubal pregnancies like CSP and cervical pregnancies, use of Methotrexate may be considered as the first and only option before surgical intervention to minimize catastrophic hemorrhage. The higher the level of serum beta hCG, the more likely the failure rate of using methotrexate in medical management of all ectopic pregnancies. In view of this, some experts have recommended use of two-dose or multiple-dose regimens for such patients if they are not surgical candidates and medical management is warranted. Lipscomb et al. demonstrated that a high serum hCG level is the most important factor associated with failure of treatment with single-dose MTX protocol among women with tubal ectopic pregnancy [35].

Contraindications to methotrexate therapy [36, 37].

Absolute contraindications

1. Pregnancy of unknown location of only one evaluation.

2. Peptic ulcer disease.

3. Intrauterine pregnancy.

4. Sensitivity to methotrexate.

5. Breastfeeding.

6. Suspected tubal rupture.

7. Immunodeficiency.

8. Active pulmonary disease.

9. Unwilling or unable to return for follow up visits.

Relative contraindications

1. Gestational sac >3.5 cm.

2. Embryonic cardiac motion.

3. Hepatic, renal, or hematologic dysfunction.

4. Serum beta hCG > 5000 mIU/ml.

11.2 Pre-treatment evaluation

Blood type, serum hCG (to be used as "Day 1" level).

Safety labs: full blood counts, complete metabolic panel consisting of AST/ALT, BUN/Cr, also to be repeated prior to additional MTX dosing.

11.3 Systemic methotrexate treatment protocol

Systemic methotrexate is usually given as a single-dose or two-dose or fixed multi-dose regimens. The single-dose regimen of 50 mg of methotrexate per body surface area (BSA, m^2) is usually given only on the first day, then followed by serial monitoring of serum hCG on days 4 and 7. There is the possibility of repeating the same dose on days 7 and 11 if there is less than 15% drop in the levels of hCG between days 4 and 7 or between days 7 and 11. The two-dose regimen also uses 50 mg of methotrexate per BSA (m^2) and it is predetermined to be given on days 1 and 4, then followed by serial serum hCG levels on days 4 and 7 or 11. There is also a possibility of repeating the same dose on days 7 and 11 if the drop in serum hCG levels between days 4 and 7 or days 7 and 11 are less than 15% respectively [36, 37].

The fixed multi-dose regimen uses 1 mg of methotrexate per kilogram body weight for a total of four doses given on alternate days; on the first, third, fifth, and seventh days while Folinic acid rescue is given on the second, fourth, sixth, and eighth days. This regimen requires serial serum hCG monitoring on the days of methotrexate injections until there is more than 15% drop from the previous level. Thereafter, continue weekly to every 4 weeks monitoring until the serum hCG levels is less than 5 mIU/ml [36, 37].

Methotrexate can also be injected locally into the gestational sac or in the fetal intracardiac space to enhance resolution of the pregnancy. This is usually done under ultrasound guidance and it is given in combination with systemic injection in various dosing regimens. Timor-Tritsch et al. suggested using a fixed dose of 75 mg of methotrexate; 25 mg intracardiac injection, 25 mg inside the gestational sac while the remaining 25 mg is given intramuscularly (**Table 1**).

11.4 Adjuvant medical treatments and other interventions

Give anti-D immunoglobulin injection if patient is rhesus negative.

Advise patient to discontinue folic acid supplementation during MTX treatment.

Avoid pelvic exams and sexual intercourse during treatment period.

Caution patients: to reduce gastrointestinal side-effects, avoid alcohol and non-steroidal anti- inflammatory drugs (NSAIDs).

Avoid prolonged exposure to sun due to sun hypersensitivity while on MTX.

Single-dose regimen	
Days	**Activities performed**
1	MTX 50 mg/m^2 IM injection.
4 and 7	Measure hCG levels, a rise may be seen on Day 4 compared to baseline Day 1.
If ≥15% drop from Days 4 to 7, continue to follow weekly until hCG < 5 mIU/ml. If <15% drop from Days 4 to 7, repeat MTX 50 mg/m^2, repeat serum hCG on Day 11.	
Two-dose regimen	
Days	**Activities performed**
1	MTX 50 mg/m^2 IM injection.
4	MTX 50 mg/m^2 IM injection and serum hCG level.
7	Serum hCG level, if ≥15% from Days 4 to 7, continue weekly until hCG < mIU/ml.
If <15% drop from Days 4 to 7, repeat MTX 50 mg/m^2 and check hCG on Day 11; if ≥15% drop from Days 7 to 11, continue to follow up weekly until hCG < 5 mIU/ml. If <15% drop from Days 7 to 11, repeat MTX 50 mg/m^2 and check hCG on Day 14; if ≥15% drop from Days 11 to 14, continue to follow weekly until hCG < 5 mIU/ml.	
Fixed multi-dose regimen	
Days	**Activities performed**
1, 3, 5, 7	MTX 1 mg/kg body weight.
2, 4, 6, 8	Folinic acid 0.1 mg/kg body weight.
Measure serum levels of hCG on MTX dose days; continue dosing until hCG decreases ≥15% from previous measurement. Follow hCG until <5 mIU/ml.	

MTX, methotrexate; hCG, human chorionic gonadotropin; IM, intramuscular.

Table 1.
Different regimens of systemic methotrexate.

Avoid new conception until serum hCG is undetectable.
Combination of systemic and local injection of methotrexate.
Timor-Tritsch recommendation of combined local and systemic injection:

A. 25 mg intragestational sac.

B. 25 mg into the placental site as the needle is being withdrawn.

C. 25 mg intramuscular prior to patient discharge from the hospital.

University of Illinois at Chicago protocol (unpublished):

A. Half dose of 50 mg/m2 BSA injected into the intragestational sac.

B. The remaining half dose of MTX is injected intramuscularly.

11.5 Potassium chloride

In the presence of cardiac activity, intracardiac injection of potassium chloride with 2 mEq/L under ultrasound guidance, and repeat until there is no longer

cardiac activity. It usually requires 2–3 ml injections for the procedure. Potassium chloride can be used as a stand-alone treatment intervention in ectopic pregnancy or in combination with any of the methotrexate injection regimens. In a study of 18 ectopic pregnancies with active embryonic cardiac activity, mean serum beta hCG levels of 33,412 IU/L and mean gestational age of 6 weeks and 6 days, 10 were assigned to KCL injection in the gestational sac while 8 were in the methotrexate group. There was no difference in time to resolution of ectopic pregnancies between those injected with KCL and those with methotrexate [38]. Verma et al. in a three-case series of women with concurrent injection of local KCL and systemic injection of methotrexate, they demonstrated that complete resolution of ectopic pregnancy was achieved and surgery avoided in all 3 cases [39].

11.6 Newer treatment combinations

The use of selective progesterone reception modulator (Mifepristone) as an adjuvant for medical therapy has been tried. In a randomized trial by Rozenberg et al., there was no benefit from the systematic addition of mifepristone except in women with progesterone level of 10 ng/L or more [40]. However, in a larger study involving 72 patients; 30 with combined methotrexate-mifepristone and 42 with methotrexate alone by Perdu et al., the failure rate was lower in the combined group, 1/30 (33.3%) compared to 11/42 (26.2%) in the methotrexate alone group [41]. Use of epidermal growth factor receptor inhibition in combination with methotrexate has been tried in an in vitro experiment and it showed inhibition of growth of placental cells. These results were confirmed in vivo in mouse models, and it revealed faster rate of fetal resorption when the two drugs were combined [42]. In a phase 1 nonrandomized open label study involving 12 women with ectopic pregnancy and 71 controls, the median level of serum beta hCG by day 7 and the time of pregnancy resolution were significantly lower in the combined methotrexate and epidermal growth factor receptor blocker (gefitinib) compared with methotrexate alone group [43]. Hence, the future goal of medical management of extra-tubal ectopic pregnancies should be combination therapy ab initio with various methotrexate regimen.

12. Surgical management of non-tubal pregnancy

To ensure complete removal of a tubal ectopic pregnancy, a British surgeon, Robert Lawson Tait performed a laparotomy with ligation of ruptured tube and board ligament in April 1883. By the 1920s, laparotomy and ligation of the bleeding vessels with removal of the affected tube had become the standard of care, and it remained so until the late 1970s, when operative laparoscopy and salpingectomy replaced laparotomy and salpingectomy. For CSPs, nearly 50% of clinically diagnosed cases miscarriage during the first trimester but most of them will require additional surgical intervention to stop bleeding [44]. Surgical management of any ectopic pregnancy is associated with a high success rate; low complication rate and short post-treatment follow up [19]. In a national cohort study in the UK by Hart et al. of 102 cases of CSP, the success rates of expectant, medical and surgical management were 43% (9/21), 46% (7/15) and 96% (54/56), respectively. The complication rates were 15/21 (71%) with expectant, 9/15 (60%) with medical and 20/56 (36%) with surgical management. Discharge from care (median number of days) was 82 (range 37–174) with expectant, 21 (range 10–31) with medical and 11 (range 4–49) with surgical management [45].

12.1 Suction curettage

This surgical intervention has been used to treat appropriately selected suitable patients with cervical ectopic or cesarean scar ectopic pregnancies. It is usually done under transabdominal or transrectal ultrasound guidance to ensure direct visualization of the pregnancy sac during the procedure. This procedure has been used for cervical ectopic pregnancy (CEP) and CSP despite the fear of potential catastrophic hemorrhage that may warrant emergency hysterectomy or may result in significant maternal morbidity and mortality. When suction curettage is being considered as a treatment option, you also need to plan for possible use of adjuvant interventions to reduce excessive blood loss. Adjuvant methods that have used so far include but not limited to intracervical balloon tamponade, angiographic embolization, cervical cerclage, ligation of uterine arteries or local hysteroscopic endocervical resection of the gestational sac with local use of different substances. Among these, arterial embolization has gained more recognition than any other interventions to decrease potentially dangerous massive hemorrhage thought to be associated with suction curettage of CSP or cervical ectopic pregnancy. However, there have been reports of suction curettage used successfully to evacuate CEP or CSP with minimal complications. In a study by Jurkovic et al. of 232 women with CSP, suction curettage was an effective method for the treatment of 191 pregnancies implanted into the lower uterine segment cesarean section scar because of the 116 women who had a follow up visit, only 7 (6.0%), 95% CI 1.7–10.3% required a repeat surgical procedure for retained products of conception. It was associated with a low risk of blood transfusion and hysterectomy. Of the 191 women, 9 (4.7%) required blood transfusion, 95% CI 1.7–7.7, and 1 (0.5%) women had life-saving hysterectomy due to uncontrollable intraoperative hemorrhage [46].

12.2 Wedge resection

Wedge resection of gestational sac can be used for many extra-tubal pregnancies such as CSP, ovarian or cornual pregnancies. There have been multiple case reports on the safety and effectiveness of wedge resection of CSP via laparotomy. Wedge resection should be considered when the diagnosis is made early, there is no involvement of vital contiguous structures and need for preservation of fertility. In a case report by Vial et al. of 28 years old G3P2002 at 6 weeks gestation, wedge resection of the gestational mass via a Pfannenstiel incision resulted in complete resolution of the pregnancy and subsequent full-term pregnancy delivered by cesarean section [47]. Traditionally, wedge resections of the gestational sac or hysterectomy via laparotomy is the treatment of choice of interstitial or cornual or angular pregnancy. However, laparoscopic cornuotomy is the removal of ectopic pregnancy tissue with preservation of uterine architecture. This increases incidence of persistent and recurrent interstitial pregnancy, but can potentially maintain patient fertility and decrease risk of future uterine rupture. Patients with cornual resection are often delivered at 36–37 weeks of gestation via cesarean section in subsequent pregnancies because of their increased risk of uterine scar rupture. In a study of 29 patients by Liao et al., the incidence of subsequent uterine rupture and dehiscence was 30% [48]. However, there is still controversy in regards to the recommended surgical technique to treat interstitial pregnancies; cornual resection and cornuectomy are both important considerations.

A small ovarian ectopic pregnancy (OEP) or early bleeding can be treated with wedge resection or cystectomy with the intention to preserve some of the affected ovarian tissues. There have been anecdotal case reports of the

effectiveness of wedge resection in the treatment of OEP. A case report by Kraemer et al. showed a 29-year-old G1P0 at 8 weeks gestation with confirmed ovarian pregnancy and she was managed by laparoscopic wedge resection of the OEP. She subsequent was pregnant with a normal intrauterine pregnancy 6 months after her surgery [49].

12.3 Laparotomy/laparoscopy in extra-tubal pregnancy

Directly visualization of the pregnancy via laparotomy or laparoscopy may be helpful in the definitive diagnosis of OEP and abdominal pregnancy. Surgical management of either of the two pregnancies is influenced by the size of the lesion, the proximity or attachment to vital organs, associated symptoms and the patient's desire for future fertility [46]. Small OEP are usually treated conservatively with wedge resection, enucleation, cystectomy, or trophoblast curettage with electrocoagulation or hemostatic suture to preserve fertility. However, large OEP may require oophorectomy when there are no apparent normal ovarian tissues left [47].

12.4 Adjuvant surgical interventions

The use of adjuvant interventions is to accelerate the efficacy of primary treatment or to minimize potential life-threatening complications. Intracervical balloon tamponade or cervical cerclage have been used during cervical curettage for cervical ectopic pregnancy to decrease bleeding. Direct ultrasound-guidance is helpful for all extra-tubal pregnancy to enable injection of methotrexate or KCL or hyperosmolar glucose into the gestational sac. Misoprostol and Methergine are uterotonic agents that cause vasoconstriction, thereby reducing the amount of blood loss during surgical intervention. Careful and appropriate use of these adjuvant treatments can improve successful outcome of primary treatment of extra-tubal pregnancy.

13. Conclusion

Ectopic pregnancy is the leading cause of first trimester maternal mortality, and it is mostly located in the fallopian tubes. When it is located outside the tubes, the need for high index of suspicious and prompt intervention is advised because the more advanced extra-tubal pregnancies can result in catastrophic hemorrhage or maternal death. Different surgical techniques that are unique to individual type of ectopic pregnancy, the use of methotrexate and combination therapy have all demonstrated proven benefits for the treatment of extra-tubal pregnancy.

Author details

Adebayo A. Adeniyi[1,2] and Christopher A. Enakpene[3*]

1 Afe Babalola University, Ado Ekiti, Ekiti State, Nigeria

2 Federal Medical Center, Ido Ekiti, Ekiti State, Nigeria

3 Texas Tech University Health Sciences Center, School of Medicine, Permian Basin, Texas, USA

References

[1] Rota M, Haberman S, Levgur M. Cesarean scar ectopic pregnancies, etiology, diagnosis and management. Obstetrics and Gynecology. 2006;**107**:1373-1381

[2] Kwawukume EY, Idrisa A, Ekele BA. Ectopic pregnancy In: Kwawukume EY, Emuveyan EE, editros. Comprehensive Obstetrics in the Tropics 2nd Edition. Accra-North Ghana: Assemblies of God Literature Centre Limited; 2015. pp. 282-287

[3] Barnhart KT, Sammel MD, Gracia CR, Chittams J, Hummel AC, Shaunik A. Risk factors for ectopic pregnancy in women with symptomatic first-trimester pregnancies. Fertility and Sterility. 2006;**86**:36-43

[4] Bouyer J, Coste J, Fernandez H, Pouly JL, Job-Spira N. Sites of ectopic pregnancy: A 10-year population-based study of 1800 cases. Human Reproduction. 2002;**17**:3224-3230

[5] Ann-Marie S, Samantha MD. Early pregnancy risks. In: Alan HD, Nathan L, editors. Current Obstetric & Gynecologic Diagnosis & Treatment. 11th ed. New York: McGraw-Hill; 2013. pp. 687-700

[6] Cepni I, Ocal P, Erkan S, Erzik B. Conservative treatment of cervical ectopic pregnancy with transvaginal ultrasound-guided aspiration and single-dose methotrexate. Fertility and Sterility. 2004;**81**:1130-1132

[7] Odejimi F, Rizzuto MI, MacRae R, Olowu O, Hussain M. Diagnosis and laparoscopic management of 12 consecutive cases of ovarian pregnancy and review of literature. Journal of Minimally Invasive Gynecology. 2009;**16**(3):354-359

[8] Mathur SK, Parmar P, Gupta P, Kumar M, Gilotra M, Bhatia Y. Ruptured primary ovarian ectopic pregnancy: Case report and review of the literature. Journal of Gynecologic Surgery. 2015;**31**(6):354-356

[9] Melcer Y, Maymon R, Vaknin Z, et al. Primary ovarian ectopic pregnancy: Still a medical challenge. The Journal of Reproductive Medicine. 2016;**61**(1-2):58-62

[10] Birge O, Erkan MM, Ozbey EG, Arslan D. Medical management of an ovarian ectopic pregnancy: A case report. Journal of Medical Case Reports. 2015;**9**(290):1-4

[11] Goyal LD, Tondon R, Goel P, Sehgal A. Ovarian ectopic pregnancy: A 10 years' experience and review of literature. Iranian Journal of Reproductive Medicine. 2014;**12**(12):825-830

[12] Huber WJ, Frishman GN. Ovarian ectopic pregnancy. In: Tulandi T, editor. Ectopic Pregnancy. Cham: Springer; 2015. pp. 93-99

[13] Hosni MM, Herath RP, Mumtaz R. Diagnostic and therapeutic dilemmas of cervical ectopic pregnancy. Obstetrical & Gynecological Survey. 2014;**69**(5):261-276

[14] Cunningham FG, Leveno KJ, Bloom SI, Hauth JC, Rouse DJ, Spong CY. Williams obstetrics. In: Ectopic Pregnancy. 23rd ed. New York City, USA: McGraw Hill Professional; 2010. p. 251

[15] Agonistini A, Blanc K, Ronda I. Prognostic value of human chorionic gonadotropin changes after methotrexate for ectopic pregnancy. Fertility and Sterility. 2007;**88**(2):504-506

[16] Ayinde OA, Aimakhu CO, Adeyanju OA, Omigbodun AO. Abdominal pregnancy at university

college hospital, Ibadan; a ten-year review. African Journal of Reproductive Health. 2005;**9**(1):123-127

[17] Zhang J, Sheng Q. Full term abdominal pregnancy: A case report and review of literature. Gynecologic and Obstetric Investigation. 2008;**65**(2):139-141

[18] Studdiford WE. Primary peritoneal pregnancy. American Journal of Obstetrics and Gynecology. 1942;**44**:487-491

[19] Karat LS. Viable abdominal pregnancy. The Journal of Obstetrics and Gynecology of India. 2007;**57**(2):169-170

[20] Stevens CA. Malformations and deformations in abdominal pregnancy. American Journal of Medical Genetics. 1993;**47**(8):1189-1195

[21] Baffoe P, Fofie C, Gandau BN. Term abdominal pregnancy with healthy newborn: A case report. Ghana Medical Journal. 2011;**45**(2):81-83

[22] Shrestha A, Chawla CD. Ruptured primary ovarian pregnancy: A rare case report. Kathmandu University Medical Journal. 2012;**10**:76-77

[23] Ching H-C, Chiu T's-H, Hsieh T's-T's, Lo L-M. Early cervical ectopic pregnancy: A case report and review of literature. Journal of Medical Ultrasound. 2014;**22**(2):117-119

[24] Singh S. Diagnosis and management of cervical ectopic pregnancy. Journal of Human Reproductive Sciences. 2013;**6**(4):273-276

[25] Panelli DM, Phillips CH, Brady PC. Incidence, diagnosis and management of tubal and nontubal ectopic pregnancies: A review. Fertility Research and Practice. 2015;**1**:15

[26] D'Antonio F, Palacios-Jaraquemada J, Lim PS, Forlani F, Lanzone A, Timor-Tritsch I, et al. Counseling in fetal medicine: Evidence-based to clinical answers to clinical questions on morbidly adherent placenta. Ultrasound in Obstetrics & Gynecology. 2016;**47**:290-301

[27] Ash A, Smith A, Maxwell D. 2wn location. Human Reproduction. 2006;**21**(10):2706-2710

[28] Arleo EK, DeFilippis EM. Cornual, interstitial, angular pregnancies: Clarifying the terms and a review of the literature. Clinical Imaging. 2014;**38**:763-770

[29] Condous G, Kirk E, Lu C, et al. There is no role for uterine curettage in the contemporary diagnostic workup of women with a pregnancy of unknown location. Human Reproduction. 2006;**21**(10):2706-2710

[30] Hahlin M, Thorburn J, Bryman I. The expectant management of early pregnancies of uncertain site. Human Reproduction. 1995;**10**:1223-1227

[31] Hammoud AO, Hammoud I, Bujold E, et al. The role of sonographic endometrial patterns and endometrial thickness in the differential diagnosis of ectopic pregnancy. American Journal of Obstetrics and Gynecology. 2005;**192**:1370-1375

[32] Rosen T. Placenta accreta and cesarean scar pregnancy: Overlooked costs of the rising cesarean section rate. Clinics in Perinatology. 2008;**35**:519-529

[33] Maymon R, Halperin R, Mendlovic S, Schneider D, Herman A. Ectopic pregnancies in a caesarean scar: Review of the medical approach to an iatrogenic complication. Human Reproduction Update. 2004;**10**:515-523

[34] Stovall TG, Ling FW, Gray LA. Single-dose methotrexate treatment of ectopic pregnancy. Obstetrics and Gynecology. 1991;**77**:754-757

[35] Lipscomb GH, McCord ML, Stovall TG, Huff G, Portera SG, Ling FW. Predictors of success of methotrexate treatment in women with tubal ectopic pregnancies. The New England Journal of Medicine. 1999;**341**:1974-1978

[36] Protocol of Gynecological Service, University of Alabama at Birmingham, December 2011

[37] Barnhart KT, Franasiak JM. American College of Obstetrician and Gynecologist Practice Bulletin Number 193. Tubal ectopic pregnancy. Obstetrics and Gynecology. 2018;**121**(3):e91-e103

[38] Monteagudo A, Minior VK, Stephenson C, Monda S, Timor-Tritsch IE. Non-surgical management of live ectopic pregnancy with ultrasound-guided local injection: A case series. Ultrasound in Obstetrics & Gynecology. 2005;**25**(3):282-288

[39] Verma U, Jacques E. Conservative management of live tubal pregnancies by ultrasound-guided potassium chloride injection and systematic methotrexate treatment. Journal of Clinical Ultrasound. 2005;**33**(9):460-463

[40] Rozenberg P, Chevrets S, Camus E, De Tayrac R, Garbin O, de Poncheville L, et al. Medical treatment of ectopic pregnancies: A randomized clinical trial comparing methotrexate-mifepristone and methotrexate – Placebo. Human Reproduction. 2003;**18**:1802-1808

[41] Perdu M, Camus E, Rozenberg P, Goffinet F, Chastang C, Philippe HJ, et al. Treating ectopic pregnancy with combination of mifepristone and methotrexate: A phase II nonrandomised study. American Journal of Obstetrics and Gynecology. 1998;**179**(3 pt 1):640-643

[42] Nilsson UW, Johns TG, Wilmann T, Kaitu'u-Lino T, Whitehead C, Dimitriadis E, et al. Effects of gefitinib, an epidermal growth factor receptor inhibitor, on human placental cell growth. Obstetrics and Gynecology. 2013;**122**(4):737-744

[43] Skubisz MM, Horne AW, Johns TG, Nilsson UW, Duncan WC, Wallace EM, et al. Combination gefitnib and methotrexate compared with methotrexate alone to treat ectopic pregnancy. Obstetrics and Gynecology. 2013;**122**(4):745-751

[44] Jurkovic D, Hillaby K, Woelfer B, Lawrence A, Salim R, Elson CJ. First-trimester diagnosis and management of pregnancies implanted into the lower uterine segment cesarean section scar. Ultrasound in Obstetrics & Gynecology. 2003;**21**:220-227

[45] Harb HM, Knight M, Bottomley C, Overton C, Tobias A, Gallos ID, et al. Caesarean scar pregnancy in the UK: A national cohort study. BJOG. 2018;**125**:1663-1670

[46] Jurkovic D, Knez J, Appiah A, Farahani L, Mavrelos D, Ross JA. Surgical treatment of cesarean scar ectopic pregnancy: Efficacy and safety of ultrasound-guided suction curettage. Ultrasound in Obstetrics & Gynecology. 2016;**47**(4):511-517

[47] Vial Y, Petignat P, Hohlfeld P. Pregnancy in a cesarean scar. Ultrasound in Obstetrics & Gynecology. 2000;**16**(6):595-593

[48] Liao CY, Tse J, Sung SY, Chen SH, Tsui WH. Cornual wedge resection for interstitial pregnancy and postoperative outcome. Australian and New Zealand Journal of Obstetrics and Gynaecology. 2017;**57**(3):342-345

[49] Kraemer B, Kraemer E, Guengoer E, Juhasz-Boess I, Solomayer EF, Wallwiener D, et al. Ovarian ectopic pregnancy; diagnosis, treatment to Carnegie stage 16 and review based on clinical case. Fertility and Sterility. 2009;**9**:393.e13-393.e15

7

The Use of Ultrasonography in Conservative Management of Cervical Pregnancy

Bing Xu[1], Jo Kitawaki[2], Yuying Duan[1] and Jilian Ding[3]
[1]*Department of Obstetrics and Gynecology,*
The Affiliated Hospital of Medical College, Qingdao University,
[2]*Department of Obstetrics and Gynecology, Kyoto Prefectural University of Medicine,*
[3]*Department of Obstetrics and Gynecology,*
Shanghai East Hospital Affiliated Tongji University,
[2]*Japan*
[1,3]*P.R.China*

1. Introduction

Cervical pregnancy is defined as an implantation of a fertilized ovum in the cervical canal. It is a very rare and dangerous form of ectopic pregnancy. The incidence ranges from 1/2500 to 1/12,000 pregnancies, which accounts for approximately 0.15% of all ectopic pregnancies. Rapid crossing of the fertilized ovum through the endometrial cavity and the travel speed of the ovum could be the cause of cervical implantation. An unfertilized ovum may reach the cervical canal and implantation occurs. Although the etiology of cervical pregnancy is unclear, previous uterine procedures such as dilation and curettage (D & C) and cesarean section, pelvic inflammatory disease, use of an intrauterine device (IUD), and in vitro fertilization (IVF) are likely causative or contributing factors. Particularly, with the use of assisted reproductive technology in recent years, the incidence of cervical pregnancy is expected to rise.

Cervical pregnancy is characterized by profuse, even life-threatening hemorrhage, which may lead to an emergency hysterectomy. In cervical pregnancy, the trophoblastic tissue directly invades into the cervix which is predominantly composed of fibrous connective tissue, with only 15% of smooth muscle. Such a cervical environment cannot satisfy the needs of the growing ovum. Pregnancy may eventually terminate when invasion, erosion, or rupture of large vessels results in bleeding. Clinically, the patients present a history of amenorrhea followed by uterine bleeding without cramping pain.

Before the routine use of ultrasound in gynecologic care, cervical pregnancy is rarely diagnosed at early gestational age. Prior to late 1980s, clinical diagnosis of cervical pregnancy was usually made when curettage for misdiagnosed incomplete spontaneous abortion resulted in uncontrollable hemorrhage. Such a condition often presented with life-threatening hemorrhage that frequently required an emergent hysterectomy and even resulted in maternal death. To avoid heavy bleeding and preserve uterus it is crucial to obtain an early and accurate diagnosis. In recent years, the widespread use of high

resolution ultrasound, particularly of the transvaginal sonography, has enabled the early diagnosis of cervical pregnancy, thereby allowing the application of conservative measures for women who desire to preserve fertility and/or obviate hysterectomy. Treatments tend to be more conservative and minimally invasive. In various conservative measures for cervical pregnancy, ultrasonography has progressively become an indispensable tool in diagnosis, interventional guidance, follow-up monitoring and clinical outcomes assessment.

2. Diagnosis of cervical pregnancy

Transvaginal or transabdominal ultrasound has become a standard and indispensible tool in the diagnosis of cervical pregnancy. An ultrasound examination will reveal a gestational sac in a widened cervical canal, with the absence of a gestational sac in the uterus (Figures 1, 2 and 3). The diagnosis is commonly established according to the following criteria described by Hofmann and Timor-Tritsch:

1. Presence of gestational sac or placental texture dominantly within the cervix;
2. No evidence of intrauterine pregnancy;
3. Visualization of an endometrial stripe;
4. Hourglass uterine shape with ballooned cervical canal;
5. Sac with active cardiac motion below the internal os for viable pregnancy.

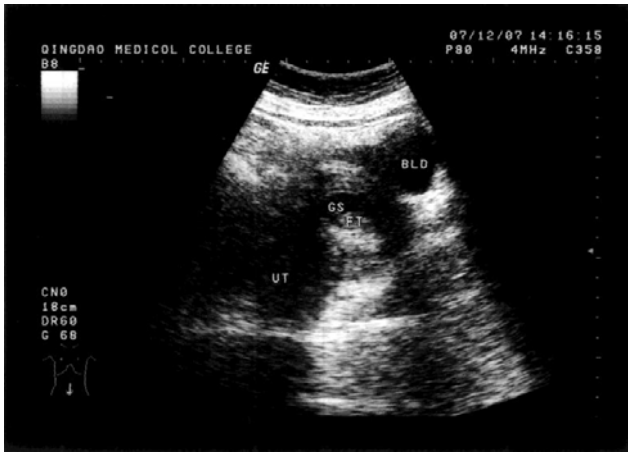

Fig. 1. Transabdominal ultrasound image of the cervical pregnancy. A 45-year-old woman, gravida 3, para 1 was admitted at 7 weeks and 5 days' gestation, presenting with a small amount of bloody vaginal discharge. Transabdominal sonography revealed normal-sized uterus with empty cavity. The gestational sac with a viable fetus is evident under the closed internal os. The β-hCG level was 59,313 mIU/L. UT: uterus; BLD: bladder; GS: gestational sac; FT: fetus

Ultrasound is used to localize and measure the gestational mass. Color Doppler imaging is applied to detect the blood flow of the gestational mass and surrounding tissues (Figure 4A and 4B). For the cases with acute bleeding or the cases that have been treated improperly with misdiagnosis, the combination use of transvaginal and transabdominal ultrasound will

supply more accurate information. Besides, serum β-hCG value is important for the diagnosis and assessment of treatment effect. A cautious vaginal speculum examination should be performed when the patient's physical condition permits.

Fig. 2. Tranvaginal ultrasound image of the cervical pregnancy. The same case as described in Figure 1. An empty cavity of uterus with a 35 mm gestational sac containing fetal cardiac activity is evident under the closed internal os. EN: endometrium; FT: fetus

Fig. 3. Tranvaginal ultrasound image of the cervical pregnancy. The same case as described in Figure 1. An enlarged cervix with a viable fetus in a gestational sac is evident under the closed internal os. CX: cervix; FT: fetus

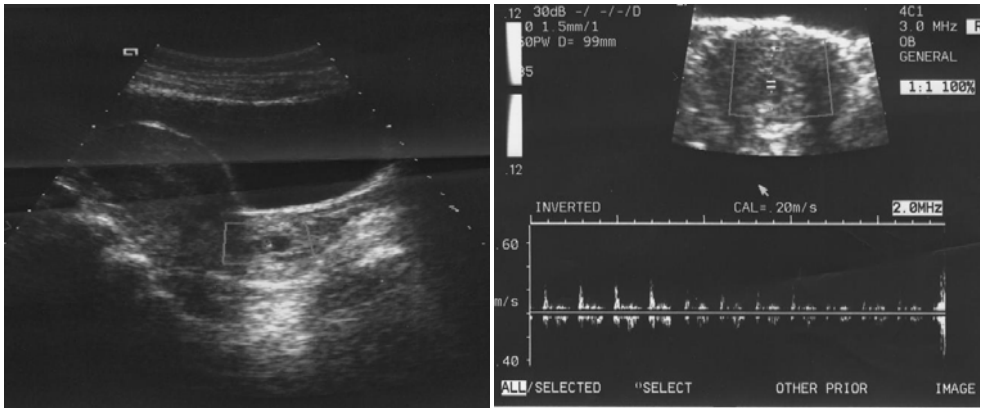

(a) (b)

Fig. 4. (a) Ultrasonographic scan of a case of cervical pregnancy. The gestational sac is evident under the closed internal os. (b) Doppler flow velocimetry depicting fetal cardiac activity. (Xu, et al. J Obstet Gynaecol Res. 2007;33:190-4)

2.1 Differential diagnosis of cervical pregnancy

The differential diagnosis of a cervical pregnancy includes other possible abnormal implantations, such as cesarean scar, low uterine corpus and abortion in progression pregnancies.

Caesarean scar pregnancy

A cesarean scar pregnancy is a gestation separated from the endometrial cavity and completely surrounded by the myometrium and the fibrous tissue of the scar. It is also a very rare form of ectopic pregnancy. However, with the caesarean deliveries increased all over the world, the incidence is rising in recent years. The most possible mechanism of cesarean scar pregnancy is because the invasion of the myometrium through a microscopic tract. The microscopic tract is believed to develop from trauma from previous uterine surgeries like caesarean section, myomectomy, and dilatation and curettage. Early diagnosis can promptly offer treatment options to decrease the likelihood of uterine rupture and heavy bleeding. Therefore, it is important to suspect the possibility of scar pregnancy when the gestational sac is found at the level of the uterine isthmus in a patient with a previous caesarean section. Transvaginal ultrasonography combined with Doppler is a reliable tool for diagnosis. Ultrasound imaging presents a gestational sac located in the anterior uterine wall at the isthmus (Figure 5).

Spontaneous abortion in progress

Differentiation from a spontaneous abortion of an early pregnancy can be accomplished by the shape of the uterus, which is generally globular in an intrauterine pregnancy, as well as by the absence of a "sliding sign," where an aborted gestational sac slides against the endocervical canal in response to gentle pressure by the sonographer. On transvaginal scan the gestational sac should be seen in the cervical canal and the sac should appear avascular, reflecting the fact that the sac has been detached from its implantation site.

Fig. 5. Transvaginal ultrasound image of a cesarean scar pregnancy. Transvaginal scan revealed a 26 mm gestational sac with fetal pole outside the lower uterine cavity at the level of the isthmus in the anterior uterine wall

Low uterine corpus pregnancy

Low uterine corpus pregnancy should be differentiated from cervical pregnancy. The implantation usually takes place in the lower part of the cavity of the uterus. The gestational sac is located above the internal os of the cervix (Figure 6).

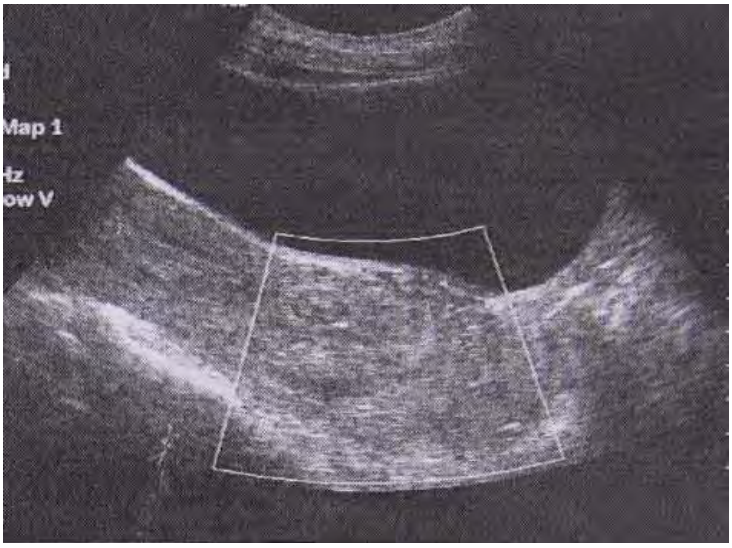

Fig. 6. Transabdominal ultrasound image of pregnancy in low uterine corpus

3. Conservative treatments of cervical pregnancy

The treatment options for cervical pregnancy largely depend on the severity of vaginal bleeding, gestational age, initial serum hCG levels, absence or presence of fetal heartbeat, and the woman`s desire to preserve fertility and/or to obviate hysterectomy. Treatments tend to be more conservative and minimally invasive in recent years. Hysterectomy is performed only as a radical treatment in cases of intractable hemorrhage.

Various conservative treatments have been reported previously, such as local or systemic administration of methotrexate (MTX), Foley catheter tamponade, curettage and local prostaglandin injection, cervical cerclage and intra-cervical injections of vasoconstricting agents, laparoscopy-assisted uterine artery ligation combined with hysteroscopic endocervical resection, angiographic uterine artery embolization (UAE). These procedures are used either alone or in combination. However, there is no consensus to date about the best approach mainly due to a lack of evidence derived from large series of clinical cases. Moreover, a risk of hemorrhage accompanies all options available.

UAE has been widely used as a highly effective technique for treating cervical pregnancy. However, recent studies indicate that rebleeding or delayed bleeding can occur after UAE. It is speculated that after complete occlusion of the uterine arteries by UAE, the extensive collateral circulation to the cervix will be established within hours. If the cervical pregnancy is not evacuated soon after UAE, some gestational tissues may remain alive and result in bleeding once again. We recently reported a promising conservative modality treatment--UAE followed by immediate curettage. We recommend this method for the cases with fetal cardiac activity, high serum hCG levels and late gestational age when fertility capacity is desired. The procedure is performed as the following: the UAE procedure is performed using digital subtraction angiography. After the bilateral arteries embolization is confirmed, an experienced gynecologist performed vacuum evacuation and curettage of the cervical canal under ultrasound guidance. After the procedure, vaginal bleeding is closely monitored for at least 48 hours. Outpatient follow-up, including sonographic examinations and β-hCG measurements are performed routinely twice in the first week after the procedure, and then once a week until decreased to normal range. After follow-up, the UAE and curettage technique, complications, vaginal bleeding, the changes of serum hCG level, regression of the uterine cervical mass, recovery of menses, pregnancy and pregnancy outcome are evaluated for the assessment of clinical outcomes. Of the patients treated by this method, quick regression of serum hCG level and cervical mass, fertility preservation, and a short hospital stay are observed.

4. Ultrasound guidance during medical and surgical intervention

During the medical or surgical intervention, ultrasound is used to accurately locate the gestational mass and guide medical injection. Direct injection of potassium chloride (KCl) or MTX into the gestational sac or fetal heart under ultrasound guidance is often used to kill embryo and destruct trophoblast tissues in cervix. It has been proved effective in clinical practice. Combined medical treatment with UAE has been proved to reduce the risk of bleeding. Local injection of prostaglandin and vasoconstricting agents are reported to effectively reduce bleeding. In the recently reported new treatment modality--UAE followed

by immediate curettage, under ultrasound guidance an experienced gynecologist performs vacuum evacuation and curettage of the cervical canal immediately after the bleeding is controlled by the bilateral arteries embolization. With a special emphasis on the clinical outcome, an advantage of this procedure is to complete bleeding control and evacuate gestational tissue in one step, which can lead to a quick recovery.

5. Ultrasound examination in follow-up and clinical outcomes assessment

After the medical or surgical treatment, the vaginal bleeding, the changes of serum hCG level and regression of the uterine cervical mass should be closely monitored. The clinical outcome assessment should be made. Thus, serial sonographic examinations and β-hCG measurements are required in follow-up routinely until cervical contour is recovered to a normal shape on sonogram and gynecological examination, serum β-hCG is reduced to undetectable, and normal menstrual cycle returns. In our previous report, a case of cervical pregnancy treated with UAE only presented intermittent vaginal bleeding again although serious bleeding was successfully controlled by UAE. The ultrasound images consistently revealed a heterogeneous mass in the cervix (Figure 7).

By contrast, in the patients treated by UAE followed by immediate curettage, a quick regression of cervical mass and serum hCG level, fertility preservation and a short hospital stay are observed (Figure 8).

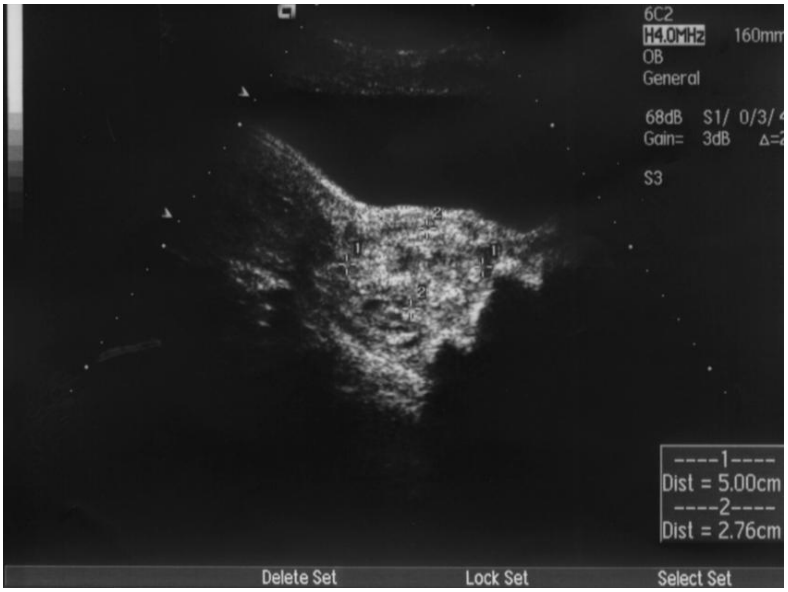

Fig. 7. A failure case of cervical pregnancy treated by UAE only. The sonography consistently revealed a heterogeneous mass in the cervix although serious bleeding was successfully controlled by UAE. The patient presented intermittent vaginal bleeding again. The patient underwent second UAE followed by immediate curettage and obtained complete solution. (Xu, et al. J Obstet Gynaecol Res. 2007;33:190-4)

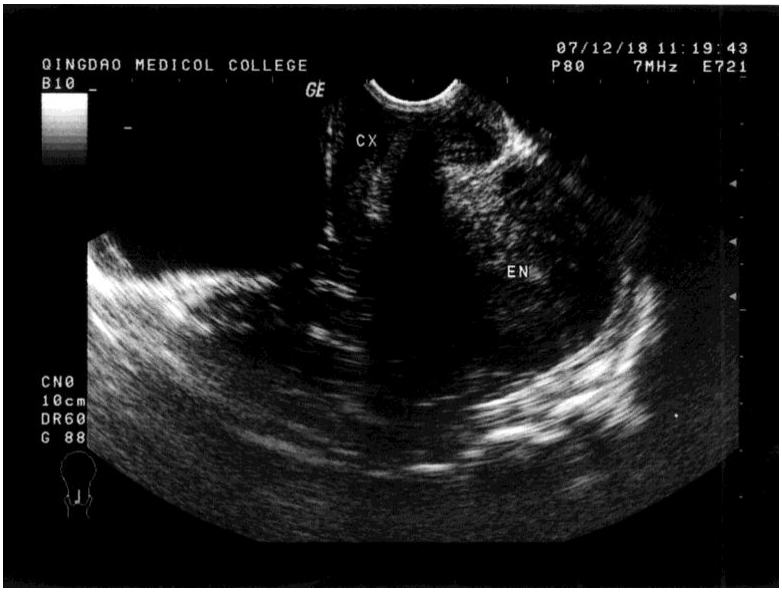

Fig. 8. Tranvaginal ultrasound image of the cervical pregnancy after treatment. The same case as described in Figure 1. Eight days after treatment by UAE followed by curettage, the cervix recovered to normal in contour

6. Conclusion

Cervical pregnancy is a very rare and dangerous form of ectopic pregnancy. It is characterized by profuse, even life-threatening hemorrhage, which may lead to an emergency hysterectomy. Recent widespread use of high-resolution ultrasound has enabled the early and accurate diagnosis of cervical pregnancy, thereby allowing the application of conservative measures for women who desire to preserve fertility. In various conservative measures for cervical pregnancy, ultrasonography has progressively become an indispensable tool in diagnosis, interventional guidance, follow-up monitoring and clinical outcomes assessment.

7. References

[1] Ushakov, FB, Elchalal U, Aceman PJ, Schenker JG. Cervival pregnancy: past and future. Obstet Gynecol Surv 1997;52:45-59.

[2] Frates MC, Benson CB, Doubilet PM et al. Cervical ectopic pregnancy: results of conservative treatment. Radiology 1994; 191: 773-5.

[3] Sherer DM, Dalloul M, Santoso P et al. Complete abortion of a nonviable cervical pregnancy following methotrexate treatment. Am J Perinatol 2004; 21: 223-6.

[4] Hofmann HM, Urdl W, Höfler H, Hönigl W, Tamussino K. Cervical pregnancy: case reports and current concepts in diagnosis and treatment. Arch Gynecol Obstet. 1987;241:63-9.

[5] Timor-Tritsch IE, Monteagudo A, Mandeville EO et al. Successful management of viable cervical pregnancy by local injection of methotrexate guided by transvaginal untrasonography. Am J Obstet Gynecol 1994; 170: 737-9.
[6] Gun M, Mavrogiorgis M. Cervical ectopic pregnancy: a case report and literature review. Ultrasound Obstet Gynecol 2002;19:297–301.
[7] Jurkovic D, Hacket E, Campbell S. Diagnosis and treatment of early cervical ectopic pregnancy: a review and report of two cases treatedconservatively. Ultrasound Obstet Gynecol 1996;8:373– 80.
[8] Sherer DM, Lysikiewicz A, Abulafia O. Viable cervical pregnancy managed with systemic Methotrexate, uterine artery embolization, and local tamponade with inflated Foley catheter balloon. Am J Perinatol 2003; 20: 263-7.
[9] Spitzer D, Steiner H, Graf A et al. Conservative treatment of cervical pregnancy by curettage and local prostaglandin injection. Hum Reprod 1997;12:860-6.
[10] Davis LB, Lathi RB, Milki AA, Dahan MH. Transvaginal ligation of the cervical branches of the uterine artery and injection of vasopressin in a cervical pregnancy as an initial step to controlling hemorrhage: a case report. J Reprod Med. 2008;53:365-8.
[11] Kung FT, Lin H, Hsu TY, Chang CY, Huang HW, Huang LY, Chou YJ, Huang KH. Differential diagnosis of suspected cervical pregnancy and conservative treatment with the combination of laparoscopy-assisted uterine artery ligation and hysteroscopic endocervical resection. Fertil Steril. 2004;81:1642-9.
[12] Trambert JJ, Einstein MH, Banks E, Frost A, Goldberg GL. Uterine artery embolization in the management of vaginal bleeding from cervical pregnancy: a case series. J Reprod Med. 2005 ;11:844-50.
[13] Cosin JA, Bean M, Grow D et al. The use of methotrexate and arterial embolization to avoid surgery in a case of cervical pregnancy. Fertil Steril 1997;67:1169-71.
[14] Vedantham S, Goodwin CS, Mclucas B et al. Uterine artery embolization: an underused method of controlling pelvic hemorrhage. Am J Obstet Gynecol 1997; 176: 938-48.
[15] Xu B, Wang YK, Zhang YH, Wang S, Yang L, Dai SZ. Angiographic uterine artery embolization followed by immediate curettage: an efficient treatment for controlling heavy bleeding and avoiding recurrent bleeding in cervical pregnancy. J Obstet Gynaecol Res. 2007;33:190-4.
[16] Wang Y, Xu B, Dai S, Zhang Y, Duan Y, Sun C. An efficient conservative treatment modality for cervical pregnancy: angiographic uterine artery embolization followed by immediate curettage. Am J Obstet Gynecol. 2011 Jan;204(1):31.e1-7.
[17] Nakao Y, Yokoyama M, Iwasaka T. Uterine artery embolization followed by dilation and curettage for cervical pregnancy. Obstet Gynecol. 2008;111:505-7.
[18] Yu B, Douglas NC, Guarnaccia MM, Sauer MV. Uterine artery embolization as an adjunctive measure to decrease blood loss prior to evacuating a cervical pregnancy. Arch Gynecol Obstet. 2009;279:721-4.
[19] Hajenius PJ, Roos D, Ankum WM, Van der Veen F. Are serum human chorionic gonadotropin clearance curves of use in monitoring methotrexate treatment in cervical pregnancy? Fertil Steril.1998;70:362-5.
[20] Akutagawa N, Nishikawa A, Saito T, Sagae S, Kudo R. Conservative vaginal surgery for cervical pregnancy. BJOG. 2001;108:888-9.

[21] Ash S, Farrell SA. Hysteroscopic resection of a cervical ectopic pregnancy. Fertil Steril. 1996;66:842-4.

[22] Suzumori N, Katano K, Sato T et al. Conservative treatment by angiographic artery embolization of an 11-week cervical pregnancy after a period of heavy bleeding. Fertil Steril 2003; 80:617-619.

[23] Nappi C, D'Elia A, Di Carlo C et al. Conservative treatment by angiographic uterine artery embolization of a 12 week cervical ectopic pregnancy. Hum Reprod. 1999; 14: 1118-21.

[24] Takano M, Hasegawa Y, Matsuda H et al. Successful management of cervical pregnancy by selective uterine artery embolization: a case report. J Reprod Med 2004; 49: 986-8.

[25] Hirakawa M, Tajima T, Yoshimitsu K, Irie H, Ishigami K, Yahata H, Wake N, Honda H. Uterine artery embolization along with the administration of methotrexate for cervical ectopic pregnancy: technical and clinical outcomes. AJR Am J Roentgenol. 2009;192;6:1601-7.

[26] Einarsson JI, Michel S, Young AE. Delayed spontaneous expulsion of a cervical ectopic pregnancy: a case report. J Minim Invasive Gynecol 2005; 12: 165-7.

[27] Hidalgo LA, Peñafiel J, Chedraui PA. Management of cervical pregnancy: risk factors for failed systemic methotrexate. J Perinat Med. 2004;32:184-6.

[28] Hung TH, Shau WY, Hsieh TT, Hsu JJ, Soong YK, Jeng CJ. Prognostic factors for an unsatisfactory primary methotrexate treatment of cervical pregnancy: a quantitative review. Hum Reprod. 1998;13:2636-42. Review.

[29] Song MJ, Moon MH, Kim JA, Kim TJ. Serial transvaginal sonographic findings of cervical ectopic pregnancy treated with high-dose methotrexate. J Ultrasound Med. 2009;1:55-61.

[30] Jeng CJ, Ko ML, Shen J. Transvaginal ultrasound-guided treatment of cervical pregnancy. Obstet Gynecol. 2007;5:1076-82.

[31] Leeman L, Wendland C. Cervical ectopic pregnancy: diagnosis with endovaginal ultrasound examination and successful treatment with methotrexate. Arch Fam Med 2000;9:72–7.

[32] Sherer DM, Lysikiewicz A, Abulafia O. Viable cervical pregnancy managed with systemic Methotrexate, uterine artery embolization, and local tamponade with inflated Foley catheter balloon. Am J Perinatol 2003; 20: 263-7.

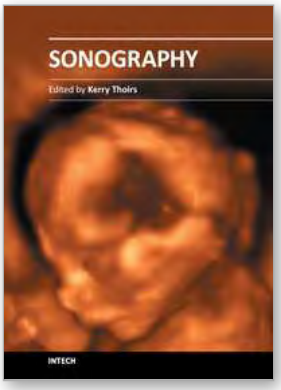

Sonography

Edited by Dr. Kerry Thoirs

ISBN 978-953-307-947-9
Hard cover, 346 pages
Publisher InTech
Published online 03, February, 2012
Published in print edition February, 2012

Medical sonography is a medical imaging modality used across many medical disciplines. Its use is growing, probably due to its relative low cost and easy accessibility. There are now many high quality ultrasound imaging systems available that are easily transportable, making it a diagnostic tool amenable for bedside and office scanning. This book includes applications of sonography that can be used across a number of medical disciplines including radiology, thoracic medicine, urology, rheumatology, obstetrics and fetal medicine and neurology. The book revisits established applications in medical sonography such as biliary, testicular and breast sonography and sonography in early pregnancy, and also outlines some interesting new and advanced applications of sonography.

INTECH
open science | open minds

InTech Europe
University Campus STeP Ri
Slavka Krautzeka 83/A
51000 Rijeka, Croatia
Phone: +385 (51) 770 447
Fax: +385 (51) 686 166
www.intechopen.com

InTech China
Unit 405, Office Block, Hotel Equatorial Shanghai
No.65, Yan An Road (West), Shanghai, 200040, China
中国上海市延安西路65号上海国际贵都大饭店办公楼405单元
Phone: +86-21-62489820
Fax: +86-21-62489821

Chapter

Haemodynamic Changes during Preterm Birth Treatment

Szymon Bednarek, Małgorzata Głogiewicz, Rafał Adamczak and Mariusz Dubiel

Abstract

The well-being of the fetus depends on the efficiency of its circulatory system and the proper maternal-fetal exchange. Hemodynamic changes can occur due to disturbance of fetal and maternal homeostasis, malformations, pregnancy pathology, and medications. Preterm labor directly affects maternal-fetal haemodynamics, both due to uterine contractions and medications used to inhibit it. Research on maternal-fetal haemodynamics in preterm labor is currently focused mainly on the safety of the used tocolytics. In this chapter, we will discuss the basic principles of fetal haemodynamics, ultrasound methods of maternal-fetal circulation assessment, and the influence of preterm labor on maternal-fetal haemodynamics, with particular emphasis on medications used in threatening and progressive preterm labor.

Keywords: preterm labor, maternal-fetal haemodynamics, doppler

1. Introduction

During pregnancy, the maternal body undergoes significant hemodynamic changes to ensure normal fetal growth. On average, maternal cardiac output can increase up to 30%–45%, resulting mostly from the intensified metabolism, increased circulating blood mass, the appearance of an accessory placental circulatory system, and finally, a gradual increase in body weight during pregnancy. Although blood volume increases, the systemic blood pressure in a healthy mother undergoes no significant changes. This is mainly due to a decrease in total peripheral vascular resistance, primarily at the arteriolar level. The mammalian placenta is also important for the regulation of both the maternal and fetal circulations. Adequate uterine blood flow is critical to fetal growth and development [1]. Fetal heart undergoes functional changes: throughout gestation, the fetal myocardium becomes more compliant and making ventricular filling less dependent on atrial contraction. Both the increase in size and the maturational changes lead to a tremendous increase in cardiac output [2].

2. Maternal-fetal circulation

The primary heart and vascular system appear in the middle of the third week of development. On about 22nd-23rd day, the heart begins its systolic action.

Oxygenated blood, rich in nutrients, flows through the umbilical vein from the placenta to the portal sinus. The portal sinus is a wide L-shaped vessel at the terminal end of the umbilical vein, connecting two main vessels termed the right and left intrahepatic portal veins perfusing the right and left hepatic lobes. It then goes into the ductus venosus. The ductus venosus originated from the portal sinus as the latter turned at an almost right angle into the right lobe of the liver. The ductus venosus is a branchless, hourglass-shaped vessel that ascends steeply in the direction of the diaphragm. The blood flow in the ductus venosus is regulated by the sphincter mechanism. The blood then flows in the inferior vena cava and enters the right atrium of the heart. Most of the blood from the inferior vena cava is directed to the secondary septum through the oval foramen to the left atrium. There it mixes with a relatively small amount of poorly oxygenated blood returning through the pulmonary veins from the lungs. The blood from the left atrium flows into the left ventricle and leaves it through the ascending aorta. The arteries that supply the heart, head, neck and upper limbs receive well-oxygenated blood. The small amount of well-oxygenated blood from the inferior vena cava that remains in the right atrium of the heart mixes with the poorly oxygenated blood from the superior vena cava and coronary sinus and flows into the right ventricle. This blood leaves the right heart through the pulmonary trunk. Due to the high pulmonary vascular resistance during fetal life, blood flow through the lungs is low. About 10% of the blood flows to the lungs and most of it flows through the arterial duct to the fetal aorta. The blood returns to the placenta through the umbilical arteries [3, 4].

3. Vascular flow testing using Doppler ultrasonography

Doppler examination assessing the vascular flow of the maternal-fetal circulation is an important diagnostic tool in the assessment of the well-being of the fetus. The analysis of vascular flows is also used to make decisions about the further duration of pregnancy. It is often a pregnancy complicated by diseases that threaten the life of the mother and the fetus. Due to the high risk of iatrogenic prematurity, the experience of the person performing the ultrasound examination is extremely important, taking into account the factors that may affect the parameters of the vascular flow wave. Overinterpretation of the Doppler results may expose both parents and the perinatological team to unnecessary stress, medical activities and costs [5, 6].

The safety of ultrasound examinations is based on the degree of fetal exposure, which depends on the amount and duration of ultrasound examinations and the energy used for the examination. It takes into account the control of the thermal and mechanical index and the superior principle of using the lowest dose of energy that allows correct imaging - ALARA (as low as reasonably achievable). The term thermal index describes the quotient of the power lost to the reference power that increases the tissue temperature by 1 °C. The mechanical index describes the amplitude of the ultrasound wave. Ensuring the safety of ultrasound examination is only possible through excellent knowledge of anatomy and embryology, as well as regular index control when changing the settings of the ultrasound machine.

The table contains the most frequently assessed vascular flows along with their correct imaging.

Vessel	Visualization	Doppler sample volume (mm)	Insonation angle	Flow velocity/ waveforms
Umbilical artery	Free loop of the umbilical cord, without fetal breathing movements	2–3	<30°	4–6 waveforms
Middle cerebral artery	Cross-section of the brain, visualization of the Willis circle, mapping on the proximal side of the transducer, Doppler gate in the 1/3 proximal course of the vessel, as little pressure as possible on the fetal head - high risk of change of intracranial pressure and flow velocity	2–3	<30°	3–10 waveforms
Ductus venosus	Sagittal or transverse section of the fetus	0,5–1	<30°	3–6, velocity > 30 cm/s
Uterine arteries	Measurement on the right and left side of the patient, after visualizing the junction with the iliac vessels, cephalic direction	2	<30°	3–6, velocity > 50 cm/s

The special structure of the fetal uteroplacental, umbilical and cerebral circulation ensures a constant vascular flow in the fetus, independent of the mother's heart cycle. This system gradually develops in the utero-fetal circulation. The significant effect of this phenomenon consists not only in the gradual increase in the end-diastolic velocity of the flow wave, but also in the accompanying decrease in pulsation, which is the difference between the components of the maximum systolic and end-diastolic velocity.

The correct shape of the flow wave of both the fetal middle cerebral artery and the umbilical cord artery is not characterized by the disappearance of the flow wave or its inversion. It is one of the disparities in the fetal circulatory system that does not give a compensatory break in the heart's work. If it occurs, it is called absent flow or reverse flow. Both of these phenomena are among the alarm signals of poor fetal condition [7].

3.1 Mistakes in Doppler examination

Due to incomplete bone calcification, the head of a premature fetus is susceptible to pressure. Excessive pressure with the transducer may indicate the disappearance of the end-diastolic wave in the assessed fetal middle cerebral artery [7, 8].

The assessment of the vascular flow spectrum should cover several fetal heartbeat cycles. One of the reasons for doing this are the breathing movements of the fetus, which can disrupt the normal flow spectrum. Similar phenomena can be observed when a pregnant woman breathes too deeply. In order to verify the correctness of the vascular flow, a patient should be asked to shorten her breath or even temporarily stop breathing.

Incorrect parameters of the ultrasound device settings may falsify the Doppler measurements.

Corticosteroids administered to the mother to stimulate the maturation of the fetal lungs in the event of impending preterm labor may temporarily "improve" the

flow waves. In that case, it is reasonable to repeat the Doppler examination approximately 48 hours after administering the medications [7, 9].

4. Medications used in the preterm labor

The use of medications should take place primarily in compliance with the principles of patient safety and the minimum risk of side effects. The problem of therapy in pregnancy is related to the limited possibility of testing the effects of the medication on the pregnant woman and the fetus, and often the lack of consent to perform such tests. Therefore, medications used in pregnancy often have limited indications and are administered taking into account the individual risks and benefits of therapy. The pharmacological action of the medication in the fetus must take into account the kinetics of its transformations in the mother's organism as well as in the placenta. The distribution of the medication and its metabolism in the mother's body determine its availability to the fetus. Since pregnancy involves profound physiological and biochemical changes, the metabolism of many medications is also significantly altered. Data from animal studies suggest that the rate of metabolism of medications in the liver decreases during pregnancy and their availability to the fetus may be greater than expected. The transfer of the medication from the mother's body to the fetus takes place from arterial blood through the intervillous spaces to the fetal capillaries in the villi and further through the umbilical vein.

Despite the fact that the placenta is treated as a specific protective barrier for the fetus, it has little ability to metabolize medications. Many medications can reach the fetus in the form of metabolites, often more toxic [10]. The safety of the use of tocolytics is still a significant perinatological problem. The duration of tocolysis should be short enough to allow the full effect of steroid therapy on the fetus, with the least negative impact on the health of the mother and child [11].

The most commonly used medications that inhibit uterine contractions are discussed below, with particular emphasis on their effects on the circulatory system of the mother and the fetus.

4.1 Calcium channel blockers – nifedipine

Nifedipine contains the formula of a short- and long-acting 1,4-dihydropyridine calcium channel blocker. It prevents contraction of calcium-dependent myocytes and their vessels by blocking the influx of calcium into smooth muscle cells. The second possible vasodilatory mechanism is the inhibition of pH-dependent calcium influx by inhibiting smooth muscle carbonic anhydrase. Nifedipine is used to treat high blood pressure and chronic stable angina. At therapeutic sub-toxic concentrations, it has little effect on myocardium and conducting cells. Inhibition of calcium influx lowers smooth muscle contraction, which causes dilation of the coronary and systemic arteries, increased oxygen delivery to the muscle tissue, reduced total peripheral resistance, blood pressure and afterload.

The most common side effect of nifedipine reported by mothers is headache associated with a transient reduction in blood pressure after initiating therapy. The second common effect is tachycardia. In addition, dizziness, drowsiness, nausea, a sharp drop in blood pressure, slurred speech and weakness may occur. One in ten patients may experience palpitations and hot flushes. Severe side effects, such as myocardial infarction, maternal dyspnea, patient hypoxia, severe maternal hypotension with intrauterine fetal death, atrial fibrillation were also observed during nifedipine therapy. Pulmonary edema has been reported in a group of pregnant patients after taking nifedipine.

It is not recommended for use in patients with twin pregnancies due to the more frequent occurrence of dyspnea. It is absolutely contraindicated in the group of patients with heart disease, maternal hypertension and intrauterine infection. Dyspnea occurring in twin pregnancy is explained by a reduced blood flow and the degree of lung ventilation due to the higher elevated diaphragm dome [11–15]. Nifedipine has no effect on motor activity, heart rate and blood flow in the fetus. The occurrence of side effects is not related to the level of this medication in the patient's blood serum, so there is no need to adjust its dose based on body weight, body mass index (BMI) or gestational age [14].

In a study carried out on laboratory animals, the effect of nifedipine on the normal development of pregnancy was assessed. After administration of three and thirty times higher doses of nifedipine than recommended for humans, dilatation of blood vessels, increased vascularization of the uterus and placenta, and trophoblast hyperplasia were observed in both groups. Higher placental weights were seen in the higher dose group, but this had no effect on fetal survival or an increased risk of birth defects. Fetal weight did not differ from the control group at the lower dose, but statistically significantly lower weight was reported for the group with the higher dose of the drug. As expected, there were changes in the uterine muscle and collagen structure of the cervix during tocolysis. The authors concluded that the use of nifedipine in pregnancy in acceptable doses should not have a negative impact on the condition of fetuses and newborns, and that this therapy often improves the prognosis [16].

The optimal dose of nifedipine is still being determined. The starting dose in most studies was 10 mg either orally or sublingually. If uterine contractions were maintained, the dose was repeated every 15–20 minutes, until a dose of 40 mg was obtained in the first hour. Then, maintenance therapy is 20 mg every 6–8 hours for two to three days [14].

In a comparative study of nifedipine and another tocolytic combined with steriodotherapy, no significant risk to the fetuses was observed [17].

4.2 Beta-adrenergic receptor agonists

Ritodrine stimulates the beta-2-adrenergic receptor, increasing the level of cAMP and decreasing the concentration of intracellular calcium, which in turn leads to the relaxation of uterine smooth muscles and a reduction in the frequency of uterine contractions.

Terbutaline is a relatively selective bronchodilator with little or no effect on alpha-adrenergic receptors. It appears to have a greater effect on stimulating the beta receptors of the bronchi, vessels and smooth muscle, including the uterus (beta-2 receptors), than at the heart receptors (beta-1). This drug relaxes smooth muscles and inhibits uterine contractions, but it can also have a stimulating effect on the heart and central nervous system.

The mechanism of action is based on the stimulation of beta-adrenergic receptors in intracellular adenylate cyclase, the enzyme that catalyses the conversion of adenosine triphosphate (ATP) to cyclic adenosine 3 ', 5'-monophosphate (c-AMP). Elevated levels of c-AMP are associated with relaxation of bronchial smooth muscles and inhibition of the release of immune system mediators, especially from mast cells.

Fenoterol stimulates beta-2 receptors in the lungs and causes bronchial smooth muscle relaxation, bronchodilation and increased air flow. Symptoms of overdose are chest pain, dizziness, dry mouth, fatigue, flu-like symptoms, headaches, heart abnormalities, high or low blood pressure, high blood glycemia, insomnia, muscle spasms, nausea, nervousness, rapid heartbeat, seizures and tremors.

4.3 Prostaglandin synthesis inhibitors – indomethacin

As an analgesic and antipyretic drug, indomethacin inhibits the secretion of prostaglandins involved in the pain reaction, fever and inflammation. Symptoms of overdose: nausea, vomiting, severe headache, dizziness, confusion or lethargy. There have been reports of paraesthesia, numbness and convulsions.

4.4 Magnesium sulfate

Magnesium sulfate reduces striated muscle contraction and blocks neuromuscular transmission, reducing the release of acetylcholine. In addition, magnesium inhibits the inflow of calcium, enhancing the relaxing effect of vascular smooth muscles [12]. It is currently treated as a mild tocolytic. Used in fetal neuroprotection in preterm labor below 32 weeks of pregnancy.

4.5 Oxytocin receptor antagonist – atosiban

It is a competitive antagonist of human oxytocin at the receptor level. In rats and guinea pigs, atosiban has been observed to bind to oxytocin receptors, reducing the frequency of contractions and the tension of the uterine muscles, thereby reducing uterine contractions. Atosiban has also been observed to bind to vasopressin receptors, reducing its effect. In animals, atosiban had no effect on the cardiovascular system. In women at risk of preterm labor, atosiban, at the recommended doses, prevents uterine contractions and induces a resting state of the uterus. Uterine relaxation following atosiban administration is rapid, uterine contractions are significantly reduced within ten minutes, and uterine quiescence of less than four contractions per hour is achieved and stable for twelve hours.

In women at risk of preterm labor receiving atosiban by intravenous infusion (300 micrograms per minute for six to twelve hours), steady-state plasma concentrations were reached within one hour of starting the infusion.

The use of atosiban below 24 and above 33 weeks of pregnancy is contraindicated. There was no evidence of fetal toxicity. Small amounts of the drug are excreted into breast milk, no effect of the drug on breastfeeding has been acknowledged.

The most common side effects of treatment with this preparation include nausea, headache and dizziness, hot flushes and an increase in heart rate [18].

4.6 Medications that relax the uterine muscles

Scopolamine (hyoscine) is an alkaloid. Along with its derivatives, it resembles atropine and has a similar effect, but with a greater influence on the nervous system. Hyoscine belongs to a group of medications called parasympatholytics. The action of cholinolytic medications is to block the stimulation of cholinergic receptors (activated by acetylcholine). Hyoscine acts on muscarinic receptors and relaxes smooth muscles of the gastrointestinal, biliary and urogenital tract.

Side effects may include dry mouth, atonic constipation, increased urination disorders, urinary retention, decreased sweat secretion, increased heart rate (tachycardia), hypotension, and visual disturbances [12, 18].

Drotaverine inhibits the activity of the phosphodiesterase IV enzyme, which leads to an increase in the concentration of cAMP and a further cascade of intracellular reactions that result in the relaxation of the muscle cell. It may also have calcium channel blocking abilities.

The relaxant effect affects the smooth muscles of the gastrointestinal tract, urogenital system, cardiovascular system and bile ducts and is stronger than that of papaverine. It is used in the case of contraction of smooth muscles of both nervous and muscular origin. Side effects are rare and similar to scopolamine [12, 18].

5. Effect of preterm labor and its treatment on maternal-fetal hemodynamics

5.1 Patient's body position

Khatib et al. analyzed changes in vascular flow in the fetal circulation when changing the left lateral to supine position in pregnant women in the third trimester. Test time was approximately fifteen minutes. The authors noted a statistically significant decrease in the value of the pulsation index in the middle cerebral and umbilical artery, as well as a decrease in the maximum systolic velocity of the middle cerebral artery and the systolic-diastolic index of the umbilical artery [19]. It is most likely related to the symptom of brain sparring of the fetal circulation. As can be seen from the above studies, the mechanisms of circulatory centralization are not only activated by the pathological condition, but also by a stressful situation for the fetus, such as changing the position from a comfortable left-lateral or vertical position to a supine position, limiting the correct placental-fetal flow. The mechanism of fetal circulation centralization protects the fetus in a situation of persistent limited blood flow. Vascular resistance in the cerebral circulation is reduced, which allows blood flow to the brain to be increased.

Katwijk and Wladimiroff analyzed changes in the value of flows in the umbilical artery when the body position changes. When changing the patient's body position from vertical to lying, they noted an increase in the umbilical artery pulsation and resistance index, regardless of the gestational age, and this is explained by the flow mechanism of a lock [20].

Kinsella et al. in the group of twenty pregnant women in the third trimester did not observe any changes in the flow in the fetal umbilical artery when the patient's body position was changed [21].

Similarly, Armstrong et al. in the group of twenty-five full-term pregnant women qualified for elective cesarean section did not observe changes in vascular flow depending on the different positions of the patient's body. The authors assume that the degree of compression of the inferior vena cava and aorta in different body positions is not significant enough to disturb the vascular flow in the umbilical artery, or that these changes are so subtle that Doppler devices are unable to capture them [22].

Marx et al. monitored the vascular flow in the umbilical cord in various body positions in the early stage of labor. The systolic-diastolic index of the umbilical artery was significantly higher in the supine position compared to the left-lateral position of the patient, which in turn led to an increase in vascular resistance in the umbilical artery [23].

Inferior vena cava syndrome most often occurs in the third trimester of pregnancy, when a large weight of the pregnant uterus presses on the inferior vena cava, especially in the supine position, which disturbs the maternal-fetal flow and may lead to fainting, and consequently the fetus to hypoxia. Ryo et al. undertook studies to determine the risk of inferior vena cava syndrome in the second trimester of pregnancy and its consequences for the fetus. In a group of ninety Japanese pregnant women between the twenty-fourth and twenty-seventh weeks of pregnancy, they assessed umbilical artery flow and its relationship with uteroplacental flow.

There were no changes in the umbilical artery resistance index during the five-minute supine position of the patient [24].

In a study by Qu et al. on a group of fifty pregnant women between the twenty-seventh and forty weeks of gestation, no changes in the umbilical artery flow values were found when the patient's body position was changed [25], similarly to Backe et al. [26], while Sorensen et al. did not report changes in the systolic-diastolic index in patients with normal blood pressure [27].

Kinsella et al. and Witter and Besinger did not find statistically significant changes in uterine artery flows depending on the patient's body position and the duration of the study [21, 28].

In the group between thirty-seven and forty weeks of pregnancy, Qu et al. observed a statistically significant increase in the resistance index in the uterine arteries after changing the position of the pregnant woman [25].

Sohn et al. proved that uterine flow clearly decreases in the sitting and standing position of the pregnant woman, which is associated with an increase in vascular resistance. In the conclusions, the authors emphasize that apart from uterine contractions, there are also other factors influencing uterine flow, which may be important in the monitoring of fetuses with limited growth rate [29]. In another work, the author presents the concept of selecting a safe position of the patient's body based on the results of measurements of vascular flows in the maternal-placental circulation [30]. Similar conclusions were presented by Easterling et al. in each trimester of pregnancy [31], as well as by Ryo et al. [24].

5.2 The influence of tocolytics on vascular flows

In the study by Bednarek et al. on the safety of tocolytic medications in preterm labor, mean values of vascular flow measurements before the initiation of therapy that inhibits premature uterine contraction and at least one day after their initiation, subjected to statistical analysis, did not show significant changes in most of the parameters studied. The changes mainly concerned the systolic-diastolic index in the umbilical artery, where its decrease was noted, the peak systolic velocity in the middle cerebral artery increased, and the pulsation index decreased. The patients' therapy mainly included nifedipine. The lack of statistically significant changes in the value of vascular flows may indirectly confirm the safety of this medication and the lack of negative impact on the well-being of the mother and the fetus. No patients experienced life-threatening or health-threatening symptoms, and the reported side effects were mainly periodic headache during the first day of therapy and transient reddening of the skin. There was no significant decrease in blood pressure in patients undergoing treatment. This significantly increases the benefits associated with the use of this therapy, especially in relation to therapy with beta-mimetics, especially fenoterol.

Cornette et al. analyzed the effect of nifedipine on the values of vascular flow in the cerebral and placental-fetal circulation. They found no statistically significant changes in the vascular flow of the fetal middle cerebral artery, umbilical cord, uterine arteries and ductus venous. The study was conducted in pregnant women between the thirty-fifth and thirty-seventh week of gestation in a group of fifteen healthy pregnant women, after administering 20 milligrams of nifedipine orally and assessing vascular flow one hour after dosing. The authors emphasize the mechanisms counteracting the disturbance of the uterine circulation despite the significant reduction of maternal afterload under the influence of nifedipine, which means that in healthy pregnant women with normal arterial pressure, trophoblast invasion lowers uterine vascular resistance to such an extent that administration of nifedipine, which has the ability to lower peripheral vascular resistance, is no longer

able to lower uterine resistance. Adverse effects of nifedipine have been reported in the situation of significantly lowered blood pressure in pregnant women, therefore it is important that the use of this medication as an inhibitor of uterine contractions ought to be considered only in pregnant women with normal blood pressure [32].

The study by Lima et al. was based on the administration of nifedipine in a dose of 20 milligrams sublingually every twenty minutes to a pregnant woman with uterine contraction, until the activity subsided. Thereafter, 20 milligrams of nifedipine was orally administered every six hours, until a total dose of 120 milligrams per day. Vascular flow in the fetal and maternal circulation was assessed before the initiation of nifedipine, five and twenty-four hours after the initiation of the therapy. Five and twenty-four hours after the initiation of the therapy, there was no change in the resistance index from pre-treatment measurements, while a decrease in the resistance index in the fetal central artery was observed between five and twenty-four hours after the initiation of the therapy.

The value of the peak systolic velocity of the middle cerebral artery was also analyzed. In the Lima study, there was a decrease after five hours, while comparing the measurements before and 24 hours after starting the treatment, no statistically significant changes were noted [33]. In the study by Bednarek et al., the peak systolic velocity of the middle cerebral artery increased statistically significantly after the initiation of the therapy. It is noteworthy, however, that the measurements were made at least twelve hours after the initiation of the therapy. Similarly, Grzesiak et al. reported a decrease in the peak systolic velocity in the middle cerebral artery, with no changes in the remaining parameters during the day after the initiation of oral nifedipine therapy [34].

The special structure of the fetal uteroplacental, umbilical and cerebral circulation ensures constant vascular flow independent of the heart cycle. This system gradually develops in the utero-fetal circulation. A significant effect of this phenomenon consists not only in the gradual increase in the velocity of the end-diastolic flow wave, but also in the accompanying decrease in the pulsation index, which is the difference between the components of the maximum systolic velocity and the end-diastolic velocity [33].

Similarly, Guglu et al. observed a decrease in the pulse index of the central cerebral artery one day after the initiation of nifedipine therapy. The authors note that nifedipine reduces blood pressure while keeping the maternal heart rate unchanged. Moreover, they acknowledged a decrease in resistance in the uterine circulation. The mechanism of increased resistance in the umbilical artery with an accompanying decrease in the pulse index in the central artery of the brain prevents diastolic changes in the fetal heart [35, 36]. It is noteworthy that the maternal-fetal circulation has mechanisms that protect the fetus against changes in flow that may be a real threat to its well-being.

Beta-memetic therapy is now used much less frequently in suppressing preterm labor. Despite the lack of obvious adverse effects on vascular flow in the fetal circulation, side effects in the mother are significant enough to minimize this method of treatment [37–39]. In a study with ritodrine, an increase in the pulse index in the middle artery of the fetal brain was noted, with a decrease in the pulse index in the umbilical artery [40]. Friedman et al. claim that therapy with ritodrine does not increase the resistance to placental circulation, does not lead to fetal hypoxia, changes in the fetal heart rate or preload on the fetal heart, but shortens the systolic fraction of the heart, which may lead to an increase in vascular resistance in the fetal circulation or reduce contractility of the heart muscle [41, 42]. Similarly, terbutaline increases vascular flow through the fetal heart, thus increasing its load [43]. Beta-agonist therapy should be limited as much as possible due to the side effects of these medications on both the mother and the fetus.

Oxytocin receptor blockers are a new class of tocolytic drugs. The oxytocin antagonist atosiban has less side effects than beta-agonists [44]. Atosiban crosses the placenta. Drug concentrations in the fetal circulation do not increase with longer infusion rates, suggesting that the drug does not accumulate in the fetus. Atosiban has the best maternal and fetal safety profile; however, its costs are considerable. Maternal heart rate and blood flow in (R-UtA/L-UtA) were not altered significantly during atosiban administration. No significant changes in FHR as well as Doppler parameters (resistance index, pulsality index, peak systolic velocity) in umbilical artery and middle cerebral artery were recorded after 24/48 hours of tocolytic treatment. The mean values of cerebroplacental ratio (CPR) remained unaltered during treatment. Detailed evaluation of fetal cardiac function parameters (E/A, SF, MPI) calculated independently for both ventricles, revealed no significant changes over the time [45].

Tocolytic treatment with atosiban is associated with elevation of oxidative stress markers after a 48 hours administration. This effect of atosiban may reduce its potency as a tocolytic agent and therefore should be considered with respect to its clinical use, especially because of its connection with the occurrence of premature birth [46].

Indomethacin used as a substance inhibiting premature uterine contractile activity does not negatively affect the cerebral flow in the fetus, however, it should be remembered that long-term therapy with non-steroidal anti-inflammatory medications may lead to blood flow disorders in the arterial duct [47, 48].

Intravenous magnesium sulfate is also allowed in the treatment of preterm labor. Keeley et al. analyzed the effect of this medication on vascular flow and found a decrease in the flow velocity in the fetal middle cerebral artery and an increase in flow velocity in the uterine arteries. There were no disturbances in the flow in the umbilical artery. During the study, the blood circulation was normalized, which the authors associate with the beneficial effects of magnesium sulphate also on the fetus and the tocolytic effect [49]. This is also confirmed by the studies of Pezzati et al., who assessed the fetal and neonatal circulation in the first hours of life of children in the therapy of magnesium sulphate and ritodrine [50].

When analyzing the safety of tocolytic medications, it should be remembered that in most patients, steroid therapy is started parallel to stimulate the fetal respiratory system. In the study by Bednarek et al. no significant haemodynamic changes were found after steroid therapy, however, other authors observed a transient decrease in the pulse index of the fetal middle cerebral artery [51, 52]. It cannot be ruled out that these differences result from the different tocolitics analyzed. Corticosteroids administered to the mother to stimulate the maturation of the fetal lungs in the event of impending preterm labor may temporarily "improve" the flow waves. In such a situation, it is reasonable to repeat the Doppler examination approximately 48 hours after administration [34].

Brar et al. reported lower efficacy of tocolysis in patients with abnormal flows in the maternal-fetal circulation before the therapy, which increases the risk of preterm labor [53].

Summing up, it should be emphasized that drugs inhibiting uterine contractions do not have a significant, long-term and permanent effect on the vascular flow of the maternal-fetal circulation. When considering the efficacy of tocolysis, other factors disrupting normal vascular flow should be taken into account, which may reduce the effectiveness of tocolytic drugs and increase the risk of preterm labor.

5.3 Preterm labor ended with cesarean section

Nakayi et al. analyzed the vascular flow of the uterine arteries on the third, sixth and ninth day after cesarean section. They found no significant changes in the resistance index in these vessels [54].

The assessment of uterine artery flow seems to be useful in vaginal bleeding in puerperal patients after cesarean section, as one of the complications of this operation may be rupture of the intraoperatively developed pseudoaneurysm of the uterine artery [55].

5.4 Infection in preterm labor

Caroll et al. assessed the flow in the middle cerebral and umbilical arteries of fetuses and in the uterine arteries of patients with premature rupture of the membranes with or without intrauterine infection. They found no changes in vascular flow, which means that Doppler examination is not useful for monitoring the developing intrauterine infection associated with premature drainage of amniotic fluid [56].

Different results were obtained by Yücel et al. They analyzed vascular flows in patients after premature drainage of amniotic fluid with histopathologically confirmed placental inflammation. The researchers proved that an increase in the systolic-diastolic index in the uterine artery can be considered as a marker of developing intrauterine infection [57].

5.5 Ultrasound features of the cervix shortening

Bednarek et al. observed no statistically significant changes depending on the length of the cervix. Similar results were established by Klemm et al. analyzing uterine flows after radical trachelectomy. There were no changes in the uterine arterial resistance index in relation to the control group [58].

The three-dimensional evaluation of the cervical circulation accounts for a new diagnostic possibility. Samutchaikij et al. established reference values for certain measurements of the cervical vascular bed, and De Diego et al. analyzed three-dimensional images of the cervix in patients at risk of preterm labor. The authors found differences in the parameters of cervical vascularization in patients with preterm labor in comparison to asymptomatic patients with a comparable length of the cervix. It is possible that three-dimensional ultrasound will become a practical tool for the actual assessment of cervical insufficiency [59, 60].

5.6 Pregnancy duration and vascular flows

The study by Bednarek et al. involved the division of the study group into preterm labor below and above 32 weeks of pregnancy. Vascular flow differences were found in the umbilical artery. The pulsation, resistance and systolic-diastolic index values were higher in the younger group. Similar conclusions were presented by Chanprapaph et al. in the analysis of measurements in over three hundred healthy pregnant women. This phenomenon should be explained by the progressive increase in end-diastolic velocity with increasing gestational age, which directly translates into a decrease in the pulsation index. The authors draw attention to the fact that the value of the systolic-diastolic index above three, in a pregnancy above the thirtieth week, is more often associated with complications of low fetal body weight and birth disorders - the presence of meconium in the amniotic fluid, cesarean section and worse birth condition of the newborn [61–64].

Mari and Deter draw attention to the parabolic shape of the curve of changes in the flow rates of the central artery of the brain, the values of which are maintained in newborns until the first month of life. The curves established by the authors are applicable to the monitoring of fetuses with low body weight [65].

Degani found a clear decrease in the value of the middle cerebral artery pulsation index after the thirty-sixth week of pregnancy, which is related to the compensation mechanism that protects the fetus against a progressive decrease in oxygen tension [66].

Gadelha da Costa et al. assessed the increase in fetal middle cerebral artery resistance index up to the twenty-sixth week of pregnancy, and then a decrease to the period of full-term pregnancy [67, 68].

The lack of vascular changes in the uterine arteries in pregnant women with pre-term labor confirms the assumption that the assessment of the flow of these vessels is justified in pregnancies with placental abnormalities, such as intrauterine growth restriction, arterial hypertension or diabetes [69, 70].

6. Summary

Research on maternal-fetal haemodynamics in preterm labor is currently focused mainly on the safety of the used tocolytics. The reduction of the use, and often the elimination of beta-agonists, undoubtedly increased the safety of the mother and the fetus. The above literature review proves that despite some influence of medications on maternal-fetal blood flow values, tocolysis does not significantly disturb haemodynamics. However, it is worthwhile to remember about safety rules during ultrasound examinations with the use of Doppler technique.

Author details

Szymon Bednarek, Małgorzata Głogiewicz, Rafał Adamczak and Mariusz Dubiel*
Department of Obstetrics and Gynecology, Nicolaus Copernicus University, Bydgoszcz, Poland

Available from https://dx.doi.org/10.5772/intechopen.96923

References

[1] Zhao H, Wong R, Doyle T, Nayak N, Vreman H, Contag C, Stevenson D. Regulation of Maternal and Fetal Hemodynamics by Heme Oxygenase in Mice, Biology of Reproduction, Volume 78, Issue 4, 1 April 2008, Pages 744-751.

[2] Van Mieghem T, Deprest J, Verhaeghe J. Fetal and maternal hemodynamics in pregnancy: new insights in the cardiovascular adaptation to uncomplicated pregnancy, twin-to-twin transfusion syndrome and congenital diaphragmatic hernia. Facts Views Vis Obgyn. 2011;3(3):205-213.

[3] Moore K. et al. Embriologia i wady wrodzone. Edra Urban&Partner. Wrocław. 2013.

[4] Mavrides E, Moscoso G, Carvalho JS, Campbell S, Thilaganathan B. The anatomy of the umbilical, portal and hepatic venous systems in the human fetus at 14-19 weeks of gestation. Ultrasound Obstet Gynecol. 2001 Dec;18(6):598-604. doi: 10.1046/j.0960-7692.2001.00581.x. PMID: 11844197.

[5] Robson SC. Assessment of hemodynamics usin Doppler ultrasound. Ultrasound Obstet Gynecol. 2000;15:456-459.

[6] Maulik D. Doppler Ultrasound in Obstetrics and Gynecology. Springer, Berlin, Heidelberg 2005.

[7] Dubiel M, Bednarek S, Bernard P. Najczęstsze błędy w badaniu dopplerowskim w ciąży. Ginekologia po dyplomie 2015; 17(6): 62-78.

[8] Vyas S, Campbell S, Bower S, Nicolaides K. Maternal abdominal pressure alters fetal cerebral blood flow. Brit J Obstet Gynaecol.1990;97:740-747.

[9] Thuring A, Malcus P, Maršál K. Effect of maternal betamethasone on fetal and uteroplacental blood flow velocity waveforms. Ultrasound Obstet Gynecol. 2011;37(6):668-672.

[10] Kostowski W. red. Farmakologia. Podstawy farmakoterapii. PZWL. Warszawa. 1998.

[11] Wielgoś M, Bomba-Opoń A. Tokoliza w porodzie przedwczesnym – aktualne wytyczne. Ginekol Pol 2014; 85(05):332-334.

[12] http://www.drugbank.ca/drugs/DB01115

[13] Gáspár R, Hajagos-Tóth J. Calcium channel blockers as tocolytics: principles of their actions, adverse effects and therapeutic combinations. Pharmaceuticals 2013, 6, 689-699.

[14] Conde-Agudelo A, Romero R, Kusanovic J P. Nifedipine for the menagement of preterm labor: a systematic review and metaanalysis. Am J Obstet Gynecol. 2011 February; 204(2):134.

[15] Bednarek S, Lauda-Świeciak A, Latoch I, Skórczewski J, Ludwikowski G, Dubiel M, Bręborowicz GH. The influence of nifedipine in pre-term labour therapy on blood flow parameters in fetus middle cerebral, umbilical artery and in maternal uterine arteries. APM 2016; 22(1): 48-52.

[16] Richichi J, Vasilenko P. The effects of nifedipine on pregnancy outcome and morphology of the placenta, uterus, and cervix during late pregnancy in the rat. Am J Obstet Gynecol. 1992 Sep;167(3):797-803.

[17] de Heus R, Mulder EJ, Derks JB, Visser GH. The effects of the tocolytics atosiban and nifedipine on fetal movements, heart rate and blood flow. J Matern Fetal Neonatal Med. 2009 Jun;22(6):485-490.

[18] http://bazalekow.mp.pl

[19] Khatib N, Weiner Z, Beloosesky R, Vitner D, Thaler I. The effect of maternal supine position on umbilical and cerebral blood flow indices. Eur J Obstet Gynecol Reprod Biol. 2014 Apr;175:112-114.

[20] van Katwijk C, Wladimiroff JW. Effect of maternal posture on the umbilical artery flow velocity waveform. Ultrasound Med Biol. 1991;17(7):683-685.

[21] Kinsella SM, Lee A, Spencer JA. Maternal and fetal effects of the supine and pelvic tilt positions in late pregnancy. Eur J Obstet Gynecol Reprod Biol. 1990 Jul-Aug;36(1-2):11-17.

[22] Armstrong S, Fernando R, Columb M, Jones T. Cardiac index in term pregnant women in the sitting, lateral, and supine positions: an observational, crossover study. Anesth Analg. 2011 Aug;113(2):318-322.

[23] Marx GF, Patel S, Berman JA, Farmakides G, Schulman H. Umbilical blood flow velocity waveforms in different maternal positions and with epidural analgesia. Obstet Gynecol. 1986 Jul;68(1):61-64.

[24] Ryo E, Okai T, Kozuma S, Kobayashi K, Kikuchi A, Taketani Y. Influence of compression of the inferior vena cava in the late second trimester on uterine and umbilical artery blood flow. Int J Gynaecol Obstet. 1996 Dec;55(3):213-218.

[25] Qu LR, Kan A, Masahiro N. Fetal circulation in relation to various maternal body positions. Zhonghua Fu Chan Ke Za Zhi. 1994 Oct;29(10):589-591, 635-6.

[26] Backe B, Brodtkorb CJ, Giltvedt J, Kvernes S, Brubakk AO, Torp H, Angelsen BA. Fetal and maternal aortic flow in two different maternal positions. An investigation with combined Doppler-velocimetry and ultrasonic multiple array. Ultrasound Med Biol. 1983 Nov-Dec;9(6):587-593.

[27] Sorensen TK, Hendricks S, Easterling TR, Carlson KL, Benedetti TJ. Effect of orthostatic stress on umbilical Doppler waveforms in normal and hypertensive pregnancies. Am J Obstet Gynecol. 1992 Sep;167(3):643-647.

[28] Witter FR, Besinger RE. The effect of maternal position on uterine artery flow during antepartum fetal heart rate testing. Am J Obstet Gynecol. 1989 Feb;160(2):379-380.

[29] Sohn C, Kesternich P, Fendel H. The effect of body position on uterine blood flow in the 3d trimester of pregnancy. Ultraschall Med. 1989 Feb;10(1):10-14.

[30] Sohn C Fendel H, Billet P, Werdin R, Kesternich P, Schonlau H. Changes in uterine circulation in relation to body position in pregnancy. Z Geburtshilfe Perinatol. 1987 Sep-Oct;191(5):169-173.

[31] Easterling TR, Schmucker BC, Benedetti TJ. The hemodynamic effects of orthostatic stress during pregnancy. Obstet Gynecol. 1988 Oct;72(4):550-552.

[32] Cornette J, Duvekot J, Roos-Hesselink J, Hop W, Steegers E. Maternal and fetal haemodynamic effects of nifedipine in normotensive pregnant women. BJOG. 2010 Dec 24.

[33] Lima MM, Souza AS, Diniz C, Porto AM, Amorim MM, Moron AF. Doppler velocimetry of the uterine, umbilical and fetal middle cerebral arteries in pregnant women undergoing tocolysis with oral nifedipine. Ultrasound Obstet Gynecol. 2009 Sep;34(3):311-315.

[34] Grzesiak M, Ahmed RB, Wilczynski J. 48-hours administration

of nifedipine in spontaneous preterm labor - Doppler blood flow assessment of placental and fetal circulation. Neuro Endocrinol Lett. 2013;34(7):687-692.

[35] Guclu S, Gol M, Saygili U, Demir N, Sezer O, Baschat AA. Nifedipine therapy for preterm labor: effects on placental, fetal cerebral and atrioventricular Doppler parameters in the first 48 hours. Ultrasound Obstet Gynecol. 2006 Apr;27(4):403-408.

[36] Guclu S, Saygili U, Dogan E, Demir N, Baschat AA. The short-term effect of nifedipine tocolysis on placental, fetal cerebral and atrioventricular Doppler waveforms. Ultrasound Obstet Gynecol. 2004 Dec;24(7):761-765.

[37] Grzesiak M, Hincz P, Forys S, Ahmed RB, Wilczynski J. 48-hours administration of fenoterol in spontaneous preterm labor - Doppler blood flow assessment of placental and fetal circulation. Neuro Endocrinol Lett. 2013;34(6):553-558.

[38] Grzesiak M, Forys S, Sobczak M, Ahmed RB, Wilczynski J. 48-hours administration of fenoterol in spontaneous preterm labor - does it affect fetal preload? Neuro Endocrinol Lett. 2013;34(6):549-552.

[39] Faber R, Ruckhäberle KE, Robel R. Comparison of Doppler ultrasound assessment of utero-placento-fetal perfusion in normal pregnancies and in those with threatened premature labor. Zentralbl Gynakol. 1993;115(1):27-32.

[40] Gokay Z, Ozcan T, Copel JA. Changes in fetal hemodynamics with ritodrine tocolysis. Ultrasound Obstet Gynecol. 2001 Jul;18(1):44-46.

[41] Friedman DM, Blackstone J, Young BK, Hoskins IA. Fetal cardiac effects of oral ritodrine tocolysis. Am J Perinatol. 1994 Mar;11(2):109-112.

[42] Park YK, Hidaka A. Effect of left-lateral position on maternal hemodynamics during ritodrine treatment in comparison with supine position. Nihon Sanka Fujinka Gakkai Zasshi. 1991 Jun;43(6):655-662.

[43] Grzesiak M, Ahmed RB, Wilczynski J. Doppler evaluation of blood flow in fetal inferior vena cava during 48-hours Atosiban administration in spontaneous preterm labor. Neuro Endocrinol Lett. 2013;34(8):787-791.

[44] Fabry I, Paepe P, Kips J, Bortel L. The influence of tocolytic drugs on cardiac function, large arteries, and resistance vessels. European Journal of Clinical Pharmacology, Springer Verlag, 2011, 67 (6), pp.573-580.

[45] Grzesiak M, Wilczynski J. Preliminary report of 48-hours Atosiban administration in spontaneous preterm labor - Doppler blood flow assessment of placental and fetal circulation. Neuro Endocrinol Lett. 2013;34(7):681-686.

[46] Grzesiak M, Gaj Z, Kocyłowski R, Suliburska J, Oszukowski P, Horzelski W, von Kaisenberg C, Banach M. Oxidative Stress in Women Treated with Atosiban for Impending Preterm Birth. Oxid Med Cell Longev. 2018 Dec 2;2018:3919106.

[47] Parilla BV, Tamura RK, Cohen LS, Clark E. Lack of effect of antenatal indomethacin on fetal cerebral blood flow. Am J Obstet Gynecol. 1997 Jun;176(6):1166-1169; discussion 1169-71.

[48] Pacifici GM. Clinical pharmacology of Ibuprofen and indomethacin in preterm infants with patent ductus arteriosus. Curr Pediatr Rev. 2014;10(3):216-237.

[49] Keeley MM, Wade RV, Laurent SL, Hamann VD. Alterations in maternal-fetal Doppler flow velocity waveforms in preterm labor patients undergoing

magnesium sulfate tocolysis. Obstet Gynecol. 1993 Feb;81(2):191-194.

[50] Pezzati M, Giani T, Gambi B, Dani C, Bertini G, Biagiotti R, Rubaltelli FF. Influence of maternal magnesium sulphate and ritodrine treatment on cerebral blood flow velocity of the preterm newborn. Acta Obstet Gynecol Scand. 2001 Sep;80(9):818-823.

[51] Piazze J, Anceschi MM, Cerekja A, Cosmi E, Meloni P, Alberini A, Pizzulo S, Argento T, Cosmi EV. The combined effect of betamethasone and ritodrine on the middle cerebral artery in low risk third trimester pregnancies. J Perinat Med. 2007;35(2):135-140.

[52] Bednarek S. Wpływ tokolityków na wartości prędkości przepływu krwi w tętnicy środkowej mózgu u płodu i w krążeniu matczyno-łożyskowym - rozpr. dok. CMUMK. Bydgoszcz. 2015.

[53] Brar HS, Medearis AL, DeVore GR, Platt LD. Maternal and fetal blood flow velocity waveforms in patients with preterm labor: prediction of successful tocolysis. Am J Obstet Gynecol. 1988 Oct;159(4):947-950.

[54] Nakai Y, Imanaka M, Nishio J, Maeda T, Ozaki A, Sun TT, Ogita S. Uterine blood flow velocity waveforms during early postpartum course following caesarean section. Eur J Obstet Gynecol Reprod Biol. 1997 Aug;74(2):121-124.

[55] Kulkarni SS, Teoh WH, Sia AT, Nair S. Ruptured uterine artery pseudoaneurysm: an overlooked cause of late postpartum haemorrhage. Acta Anaesthesiol Belg. 2013;64(4):159-162.

[56] Carroll SG, Papaioannou S, Nicolaides KH. Doppler studies of the placental and fetal circulation in pregnancies with preterm prelabor amniorrhexis. Ultrasound Obstet Gynecol. 1995 Mar;5(3):184-188.

[57] Yücel N, Yücel O, Yekeler H. The relationship between umbilical artery Doppler findings, fetal biophysical score and placental inflammation in cases of premature rupture of membranes. Acta Obstet Gynecol Scand. 1997 Jul;76(6):532

[58] Klemm P, Tozzi R, Köhler C, Hertel H, Schneider A. Does radical trachelectomy influence uterine blood supply? Gynecol Oncol. 2005 Feb;96(2):283-286.

[59] Samutchaikij T, Pitukkijronnakorn S, Panburana P. Normal reference of cervical blood perfusion in pregnancy. J Med Assoc Thai. 2014 Apr;97(4):369-373.

[60] De Diego R, Sabrià J, Vela A, Rodríguez D, Gómez MD. Role of 3-dimensional power Doppler sonography in differentiating pregnant women with threatened preterm labor from those with an asymptomatic short cervix. J Ultrasound Med. 2014 Apr;33(4):673-679.

[61] Chanprapaph P, Wanapirak C, Tongsong T. Umbilical Artery Doppler Waveform Indices in Normal Pregnancies. Thai Journal of Obstetrics and Gynaecology June 2000, Vol. 12, pp. 103-107.

[62] Hendricks SK1, Sorensen TK, Wang KY, Bushnell JM, Seguin EM, Zingheim RW. Doppler umbilical artery waveform indices--normal values from fourteen to forty-two weeks. Am J Obstet Gynecol. 1989 Sep;161(3):761-765.

[63] Erskine RL, Ritchie JW. Umbilical artery blood flow characteristics in normal and growth-retarded fetuses. Br J Obstet Gynaecol. 1985 Jun;92(6):605-610.

[64] Gadelha-Costa A, Spara-Gadelha P, Filho FM, Gadelha EB. Hemodynamic changes in the fetal arteries during

the second half of pregnancy assessed by Doppler velocimetry. Eur J Obstet Gynecol Reprod Biol. 2007 Jun;132(2):148-153.

[65] Mari G, Deter RL. Middle cerebral artery flow velocity waveforms in normal and small-for-gestational-age fetuses. Am J Obstet Gynecol 1992; 166: 1262-1270.

[66] Degani S. Evaluation of fetal cerebrovascular circulation and brain development: the role of ultrasound and Doppler. Semin Perinatol. 2009 Aug;33(4):259-269.

[67] Gadelha-Costa A, Spara-Gadelha P, Filho FM, Gadelha EB. Hemodynamic changes in the fetal arteries during the second half of pregnancy assessed by Doppler velocimetry. Eur J Obstet Gynecol Reprod Biol. 2007 Jun;132(2):148-153.

[68] Gadelha Da Costa A, Mauad Filho F, Spara P, Barreto Gadelha E, Vieira Santana Netto P. Fetal hemodynamics evaluated by Doppler velocimetry in the second half of pregnancy. Ultrasound Med Biol. 2005 Aug;31(8):1023-1030.

[69] Hofstaetter C, Dubiel M, Gudmundsson S, Marsal K. Uterine artery color Doppler assisted velocimetry and perinatal outcome. Acta Obstet Gynecol Scand. 1996 Aug;75(7):612-619.

[70] Simanaviciute D, Gudmundsson S. Fetal middle cerebral to uterine artery pulsatility index ratios in normal and pre-eclamptic pregnancies. Ultrasound Obstet Gynecol. 2006 Nov;28(6):794-801

15

Future Uses of Three/Four Dimensional Power Doppler Signal in Fetal Medicine

Juan Carlos Bello-Munoz[1], Mauricio Ayala[2],
Elena Carreras[1], Paula Oliveros[1], Nazareth Campo[1],
Alexandra Casasbuenas[1], Silvia Arévalo[1] and Lluis Cabero[1]
[1]*Department of Obstetrics, Vall d'Hebron University Hospital;*
Universitat Autónoma de Barcelona; Catalonia
[2]*Department of Applied Physics and Mathematics;*
Universitat Autónoma de Barcelona; Catalonia
Spain

1. Introduction

Three-dimensional Ultrasound (3DUS) has grown quickly and constantly over the last fifteen years. However, some of its best clinical uses remain to be defined. The three-dimensional Power Doppler (PD) is based on the ability to register the signal amplitude of the ultrasound wave, which allows us to depict most moving particles in a given Region of Interest (ROI). It is also based on the three-dimensional US principles, that permit the collection of signals from such particles in a given Volume of Interest (VOI) The inclusion of a time sequencing protocol or a Space-Time Image correlation (STIC) algorithm, developed and made available to last generation US machines, adds the additional possibility of following the signal evolution during a pre-established lap. At first, this promising tool was used to evaluate vascularisation and perfusion in a series of foetal organs, finding neither adequate accuracy nor repeatability. Nowadays, its use in Foetal Medicine is restricted to certain foetal conditions, although new research is on-going and further uses for this technology are being unveiled.

As is it largely understood (Burns 1992), there are compelling scientific and medical reasons to seek measuring the volumetric flow rate, which means to estimate the volume of flow delivered per minute to a tissue bed. No doubt, the success in delivering oxygen and nutrients to the tissues depends, mainly, on the amount of blood delivered to such tissues per unit of time. At the beginning of the Doppler ultrasound era, a number of attempts to achieve this calculation were done (Gill 1979; Eik-Nes et al. 1982; Sauders et al. 1980). The standard method for estimating volume flow using sonography consists on multiplying the mean spatial velocity by the luminal cross-sectional area. However, it is well known that this technique has many problems; these include the inherent variability of vessel geometry, inaccurate assumptions about flow profile, B-dimensional sampling, and other important technical limitations derived from the way pulsed and spectral Doppler signals are registered, not to mention an unsustainable amount of human interaction in the final

estimation (J M Rubin 1999). All of the abovementioned reasons caused those efforts to fail and led this pretension to be forsaken for two decades.

Then, the experimental analysis of the Doppler Effect was described – taking into account the amplitude of the wave and tracking the acoustic speckle pattern produced by the echoes from moving blood (J M Rubin et al. 1994; Forsberg et al. 1995; Harrington et al. 1996; J M Rubin 1999). From those initial approaches, the concept of Fractional Moving Blood Volume (FMBV) (J M Rubin et al. 1997) was developed, which was mainly a mathematical normalization process of the colour pattern obtained from the power Doppler signal acquisition (Tomas Jansson et al. 2003; A. Welsh 2004). Preliminary publications established a direct relationship between the data from FMBV acquired by registering the power Doppler signal in a given Region of Interest (ROI) and actual perfusion of the tissue as measured by invasive methods in animal models (E Hernandez-Andrade, T Jansson, et al. 2004; E Hernandez-Andrade, Thuring-Jönsson, et al. 2004). It has been recently described how, under certain foetal conditions such as foetal growth restriction, some perfusion patterns are objectively altered and significantly differ from "normal" patterns established by the authors (E Hernandez-Andrade et al. 2008; Rogelio Cruz-Martinez et al. 2009; R Cruz-Martinez et al. 2011).

Nonetheless, there are still enormous gaps between the information obtained by FMBV and the actual estimations of, either, flow or perfusion (A. Welsh 2004; Lai et al. 2010). There are some boundaries which will limit insurmountably the utility of this technique, such as the low repeatability when comparing one patient with the same in a better acquisition setting - or one patient with difficulties for exploration like obese or anxious mothers to a normal one. Additionally, it will be impossible to relate such magnitudes with flow whenever there is no time frame considered in the image quantification process (A. W. Welsh et al. 2005).

No additional experience in this technique has been published and very likely it will not in the future. The next logical step would be to evaluate the possibilities of three dimensional ultrasound and power Doppler as an alternative approach to this phenomenon.

2. Three-dimensional power Doppler signal and the vascular indexes

Three-dimensional power Doppler (PD) became available for medical purposes towards the end of the last century (Fenster, Lee, et al. 1998; Guo, Durand, et al. 1998). It exhibited some advantages, considering the higher sensitivity of the PD for detecting, and therefore depicting, moving particles. Its first clinical application was designed to evaluate vascularisation in compromised regions, trying to elucidate whether there was an obstruction or not in a given vessel (Guo & Fenster 1996). Considering its potential for depicting vascular structure accurately, it was employed as a tool for measuring potentially angiogenic structures as tumours (Bendick et al. 1998; Kupesic & Kurjak 2000). Also its potential for depicting vascular architecture and potential anomalies has been considered as promising (Fig. 1) (Heling, Chaoui, et al. 2000; Chaoui & Kalache 2001)

Nevertheless, the information given by this technique was rather limited, considering there was no quantification of the signal and no objective measurements would be done. Then, a mathematical algorithm was developed, firstly used in gynaecology (J M Rubin 1999; Pairleitner et al. 1999); based on the possibility of a direct correlation between PD signal

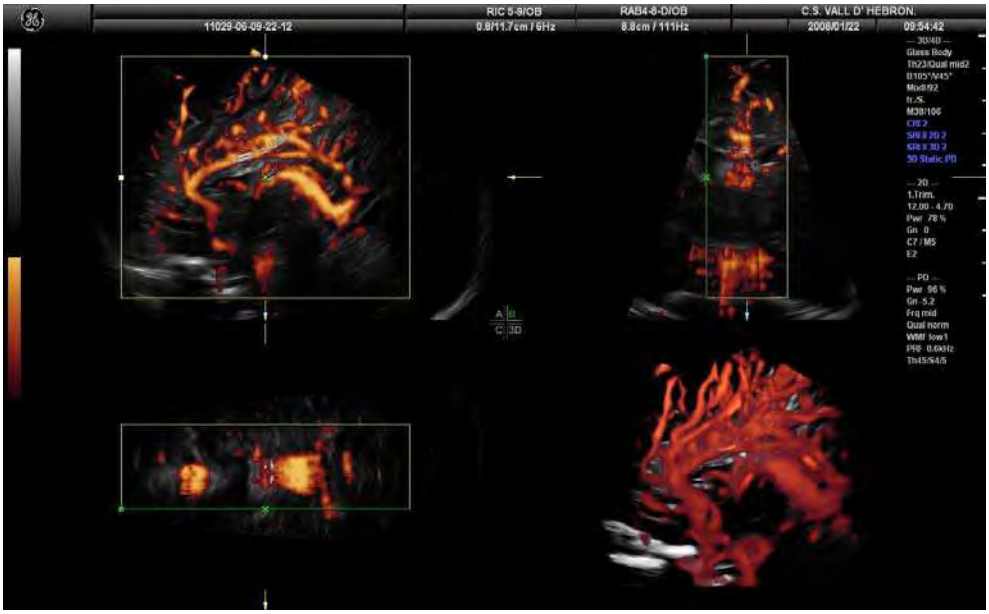

Fig. 1. Three dimensional PD angio mode rendering of intracranial blood vascularisation in a term fetus

intensity and, somehow, the velocity of the particles and the possible quantification of moving particles in a Volume of Interest (VOI) over the amount of grayscale, B-mode, particles in the same VOI. Three indexes were developed, which could indirectly give a mathematical expression of vascularisation and flow:

*Vascularization index (VI) = color voxels/(total voxels − background voxels)

$$VI = \frac{\sum_{c=1}^{100} hc(c)}{\sum_{g=1}^{100} hg(g) + \sum_{c=1}^{100} hc(c)} \tag{1}$$

Where
g= gray-scale value in the US image, normalized to 0-100: lowest intensity= 1; highest = 100
c= color value in the US image from power Doppler signal representation. Normalized to 0-100: lowest intensity= 1; highest = 100
hg(x) = frequency of gray-value x in US image
hc(x) = frequency of color value x in US image
*Flow index (FI) = weighted color voxels/color voxels

$$FI = \frac{\sum_{c=1}^{100} c \cdot hc(c)}{\sum_{c=1}^{100} hc(c)} \tag{2}$$

*Vascularization–flow index 1 (VFI) = weighted color voxels/(total voxels - background voxels)

$$VFI = \frac{\sum_{c=1}^{100} c \cdot hc(c)}{\sum_{g=1}^{100} hg(g) + \sum_{c=1}^{100} hc(c)} \quad (3)$$

Based on the above mentioned indexes, a number of research communications have been produced, evaluating the vascularity of benign versus malign ovarian masses (Kurjak et al. 1998; Juan Luis Alcázar & Jurado 2011) and prostatic tumours (Moskalik et al. 2001). Regarding the feto-placental unit, several attempts to correlate those indexes with regional perfusion of foetal brain (Hayashi et al. 1998; Nardozza et al. 2009), liver (C.-H. Chang et al. 2003), and lungs in normal (Dubiel et al. 2005) as well as pathologic *in-utero* conditions (Ruano et al. 2006). However, the clinical efficacy of this method remains unsupported by the evidence. No clinical findings can be drawn from those values so far. (Fig. 2)

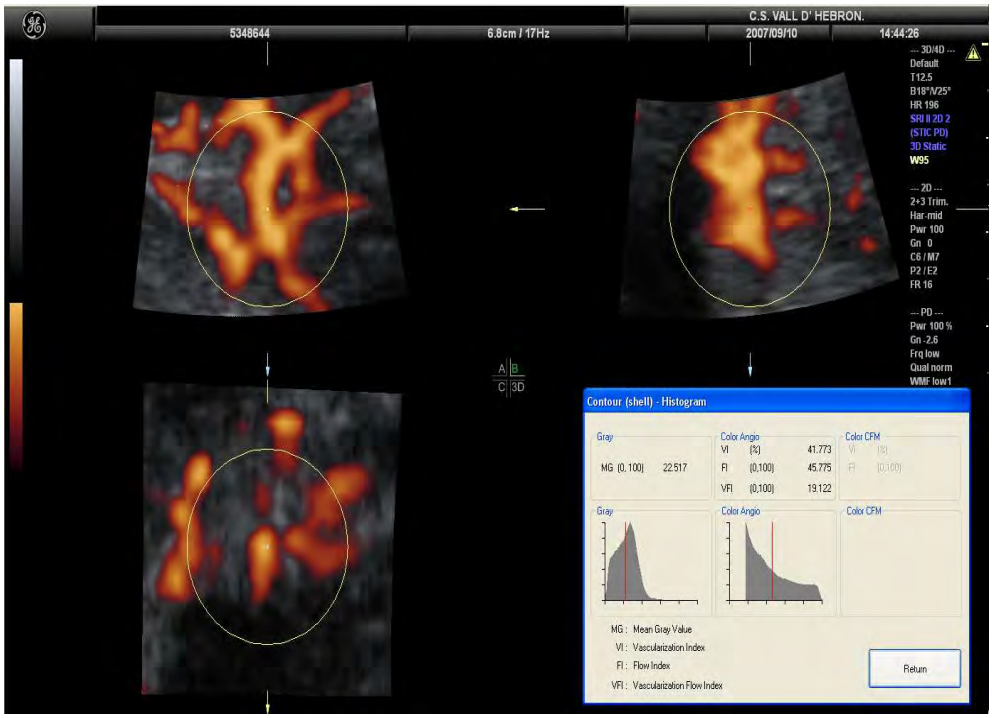

Fig. 2. Three dimensional PD angio mode rendering of intracranial blood vascularisation in a mid-trimester foetus with suspected brain sparing. In the right lower corner it is possible to visualize the histogram with the indexes obtained from the spherical shape –Volume of Interest

A promising field, still open to research, is the analysis of placental vasculature and its potential relationship to placental dysfunction (N. W. Jones et al. 2011). Some authors have found a positive correlation between low vascularisation indexes in early pregnancy and Fetal Growth Restriction (FGR) (Bozkurt, Başgül Yigiter, et al. 2010; Dar et al. 2010; Guimarães Filho et al. 2011; Morel et al. 2010; Negrini et al. 2011; A. O. Odibo et al. 2011;

Pomorski et al. 2011; Rizzo et al. 2009). It seems that the evaluation of first trimester placental vascularisation correlates, somehow, with a compromised placentation and therefore could predict some adverse perinatal outcomes of placental origin. Besides, the technique exhibits fairly good repeatability and accuracy (Tuuli et al. 2010; Martins & N J Raine-Fenning 2010; Yigiter et al. 2011).

The challenges for the future involve overcoming some of the technical problems that the three dimensional PD is plagued with and also to establish an adequate normalisation protocol, which it is currently lacking. (Fig. 3)

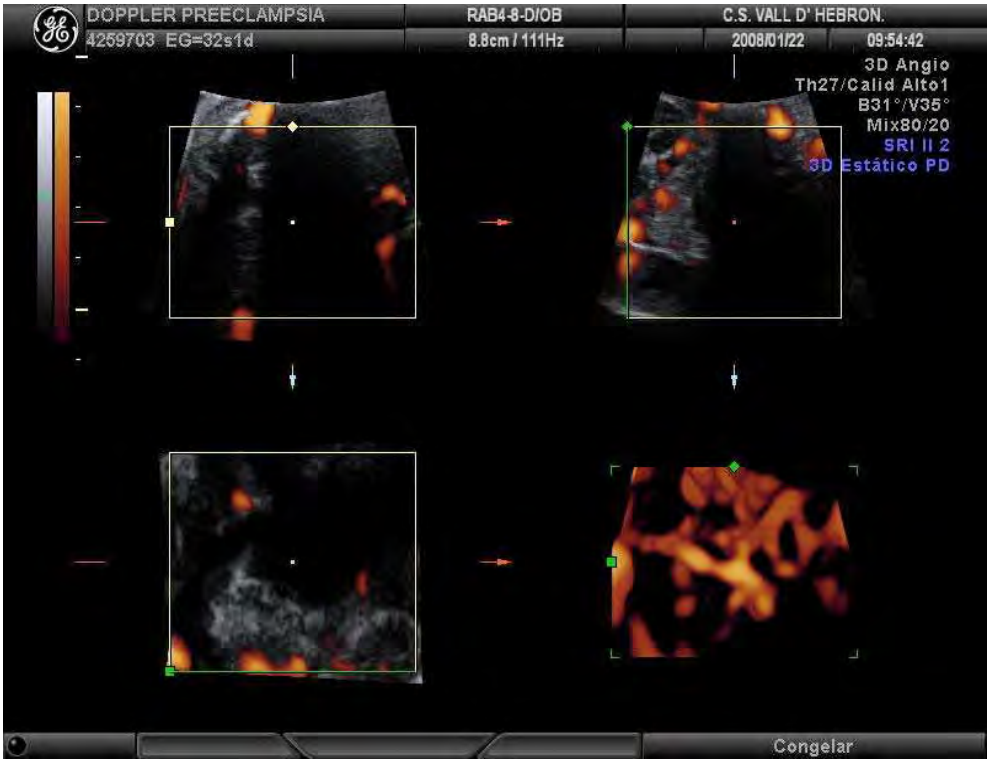

Fig. 3. Three dimensional angio mode rendering of placental vascularisation in a pre-eclampsia patient. Quantification of vascular branches suggests a lower flow in the corial plate when compared to volumes taken at the same gestational age from normal gestations

Another recently attempted and straightforward approach is to use 3D PD for the evaluation of progressive foetal conditions such as foetal goitrous hypothyroidism (Marín et al. 2010): In a given patient, under well-controlled conditions, it should be possible to evaluate the progression of either, an inflammatory response or the success of the treatment, which was thyroid hormone supplementation in that case. (Fig. 4).

Despite being rather promising, the 3D PD still has important limitations, some related to the power Doppler signal itself and some derived from acoustic impedance and mechanical interference. Some of these aspects are going to be discussed further in the next section.

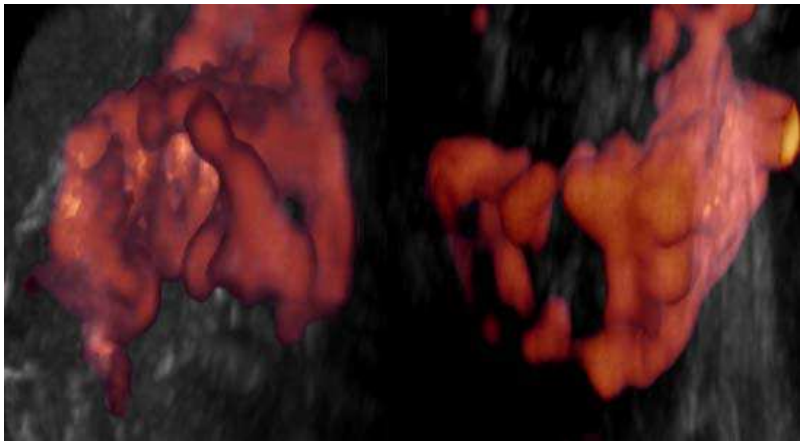

Fig. 4. Three dimensional PD angio mode rendered image of Thyroid gland of the same human foetus, before (left side) and after four weeks of intra-amniotic thyroid hormone supplementation (right side). Actual volume of the gland changed according to foetal growth, but vascularisation decreased markedly after treatment

2.1 The signal normalization problem and its consequences

To normalize the 3D PD signal, it is necessary to take into account three paramount boundaries:

- The signal can be altered by tissue impedance, which means that a low velocity flow in a deep vessel will produce completely different PD patterns depending on the mother's abdominal wall thickness, the amount of amniotic fluid and the position of the foetus (Schulten-Wijman et al. 2011).
- The settings of the machine can sensibly modify the amount of signal registered by the processor, and therefore, the amount of colour voxels inside the VOI: the algorithms for refining the B-mode signal, like the speckle reduction or the cross beam reduction post-process algorithms, mask the signal processed and "erase" a significant amount of moving particles. (N J Raine-Fenning, Nordin, Ramnarine, Campbell, Clewes, Perkins & Johnson 2008b)
- The post-processing software provided by the developers of the Volume Measurement software: 4DView and virtual organ computer-aided analysis (VOCAL®) by General Electric Medical division. Q-lab® by Philips Medical Division, as well as Sonoview® and Histogram by Samsung-Medison Co show no correlation in their measurements. Therefore, the same structure, under similar circumstances, draw off different results once measurement of the VOI is performed. (J L Alcázar 2008)

2.1.1 The biases behind the algorithm

Based on previous observations, we conducted a preliminary study, on five healthy foetuses on their 20th week of gestation, comparing the values obtained in the same foetus with different machines and adjusting settings as main gain in 600 Hz, medium wall filter in 60 Hz, cross beam reduction off and persistence of colour signal in 0. In all of them the

structure was the Willis' polygon at the cranial base. Figure 5 shows the images obtained from the machines and the histograms.

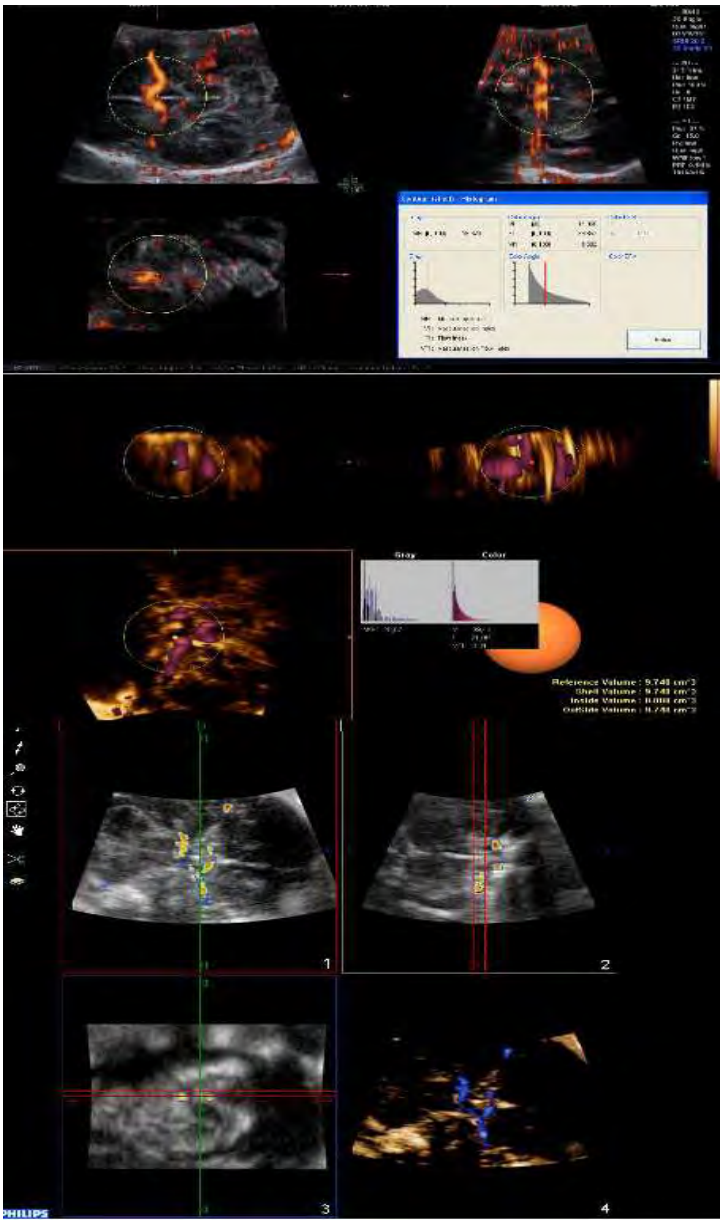

Fig. 5. Images obtained from a single foetus in cephalic presentation, from three different machines: General Electric Voluson E8 (Upper); Medison Accuvix V20 Prestige (Middle); Philips iU22 (Lower)

The results, summarized in the table 1, show how different the measurements are, depending on the brand. They also show how they differ among themselves, despite the same gestational age and similar maternal characteristics.

Foetus	GE Voluson E8			Philips iU22			Medison Accuvix V20		
	VI	FI	VFI	VI	FI	VFI	VI	FI	VFI
1	44.9	46.1	20.7	32.3	25..1	33.5	48.6	16.9	5.5
2	14.1	39.8	5.6	16.6	28.3	9.5	39.4	21.1	8.3
3	23.6	51.1	17.3	36.2	17.3	19.5	42.5	28.1	4.7
4	36.3	38.9	21.3	27.3	32.8	11.1	25.8	40.3	19.2
5	37.3	44.0	9.5	48.1	27.3	13.1	35.8	39.9	6.9

Table 1. Results from comparing similar VOI in three different machines, with the PD quantification application included in their software

In conclusion, normalizing the data from the 3D PD signal is currently not possible and reference ranges to discriminate normality from pathologic conditions are not available. Therefore, no feasibility for these indexes in obstetric clinical practice can be foreseen in the short term.

2.2 The regional normalization solution

Given that no decisions can be made from direct measurement of the abovementioned indexes, a possible approach could be to use two Regions of Interest (ROI) inside the same volume. The more reliable possibility after *in-vitro* testing was the VFI (N J Raine-Fenning, Nordin, Ramnarine, Campbell, Clewes, Perkins & Johnson 2008a). And the easier and more repeatable formula was a simple VFI index

$$VFI_1 / VFI_2 \tag{5}$$

2.2.1 The ductus venosus shunting as an example

In physiological conditions, few regions of foetal circulation can offer enough regional differences to be considered clinically relevant. But the most important of these is, no doubt, the physiological shunt in the ductus venosus which is not only a reliable indicator of preload, but also a sensitive mechanism of circulatory re-distribution in adverse circulatory conditions such as placental insufficiency (M Bellotti et al. 2000; Kiserud 2001).

The original description of Ductus Venosus Shunting (DVS) measurement was published by Belloti (Maria Bellotti et al. 2004), and was, simplifying, an index of estimated flow through Ductus Venosus (DV) over the one through Umbilical Vein (UV)

The classical way for estimating the flow through the UV is

$$Q_{UV} = 0.5 \times (V_{\max})_{UV} \times \pi \times (D_{UV}^2 / 4) \tag{6}$$

Where Vmax relates to the Umbilical Vein maximum velocity as measured by pulsed Doppler. 0,5 is a normalization constant related to foetal blood viscosity and DUV is the mean diameter of the umbilical vein in its abdominal portion.

Also, the calculation of DV flow, made by Belloti et al, is;

$$Q_{DV} = \left(-0.03 \times DR^2 + 0.189 \times DR + 0.43\right) \times (V_{\max})_{UV} \times \pi \times (D_{UV}^2 / 4) \quad (7)$$

Where Vmax DV is the maximum systolic velocity in the Ductus Venosus. DR respresents the ratio between the inlet (smaller) and the outlet (larger) of the ductus venosus, represented as part of a paraboloid equation

Therefore, the DVS could be expressed as

$$\left(Q_{DV} / Q_{UV}\right) \cdot \cdot 100 \quad (8)$$

A description of the ideal technique for measuring blood flow in both UV and DV has been published (Tchirikov et al. 2006). For UV blood volume flow measurement, a straight segment of the intra-abdominal part of the UV upstream of any hepatic branches should be selected, with the Doppler gate positioned so as to completely cover the vessel's diameter. The UV flow volume can also be measured in the umbilical cord. Authors suggest measuring blood flow volume following the 'maximum principle', which aims to determine the maximum diameter of the vessel, the maximum intensity weighted mean velocity (or time-averaged mean velocity, TAV) at the maximum vessel length in a straight longitudinal section. The inner vessel diameter is determined to the nearest tenth of a millimeter by placing the calipers at right angles to the vessel axis on a frozen B-mode image (without color). This is followed by the TAV measurement at the same vessel portion with a small insonation angle of insonation (less than 30°). The blood volume flow rate is calculated from diameter (D) and TAV as flow rate = TAV × π × (D/2)^2 mL/min. Regarding the DV, The inner diameter of the DV should be measured by insonating perpendicularly to the vessel wall at the isthmus. In order to reduce random error, the procedure must be repeated four or more times and the calculated mean diameter entered into the statistics (Kiserud et al. 2006). Doppler evaluations must be carried out in the absence of fetal breathing and body movements.

As it should become evident, the skills needed for achieving such measurements are prohibitively high; the time needed for every exploration is too long for a usual clinical exploration and the medical scope of this practice is quite reduced. Our proposal to address this issue is a far simpler, faster and repeatable approach, by using 3D PD. (Bello-Muñoz et al. 2009)

By taking a single volume of the foetal abdomen in Angio 3D PD mode, it was possible to measure the UV VFI by calculating it into a 1 cc sphere. After navigating through the volume, same measurement (DV VFI) was done in the DV, employing the same 1 cc sphere (Figure 6 summarizes both measurements)

Our study compared 162 volumes from normal foetuses and 36 from Foetal Growth Restriction (FGR) cases. In all of them we measured the DVS as described classically by Belloti et al (M Bellotti et al. 2007), and collected a volume of the foetal abdomen with 3D PD angio mode signal, always adjusting the same settings in the machine (General Electric Voluson E 8 GE Medical Systems Milwaukee USA) with a 3D RNA5-9-D Volume Convex Array Transducer Probe.

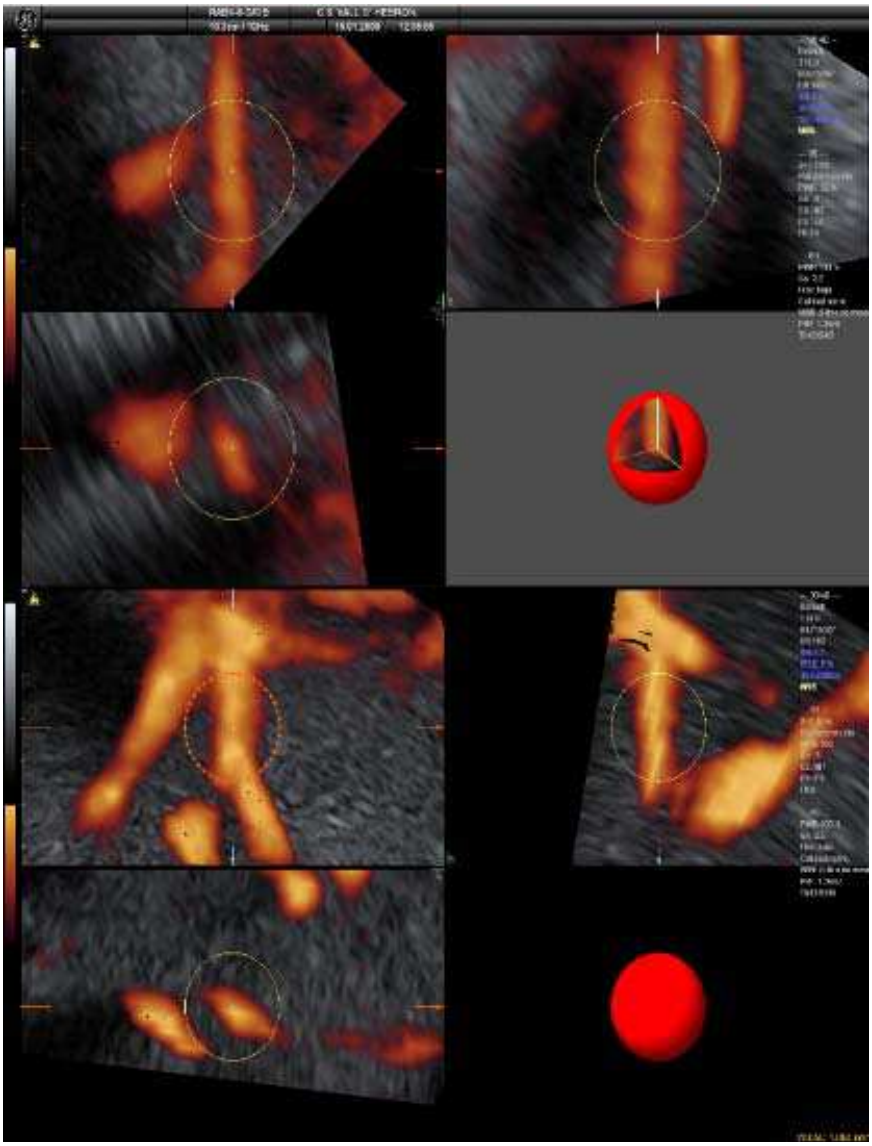

Fig. 6. VFI measurement in abdominal umbilical vein (upper) and in ductus venosus (lower). As the size of the sphere is exactly the same, the VOI remains unchanged

The calculation of the DV/UV VFI ratio was as simple as:

$$DV \cdot VFI \,/\, UV \cdot VFI. \cdot\cdot 100 \tag{9}$$

We found a significant positive correlation between DVS measured as described by Belloti et al and DVS measured as a ratio of DV/UV VFI (Figure 7)

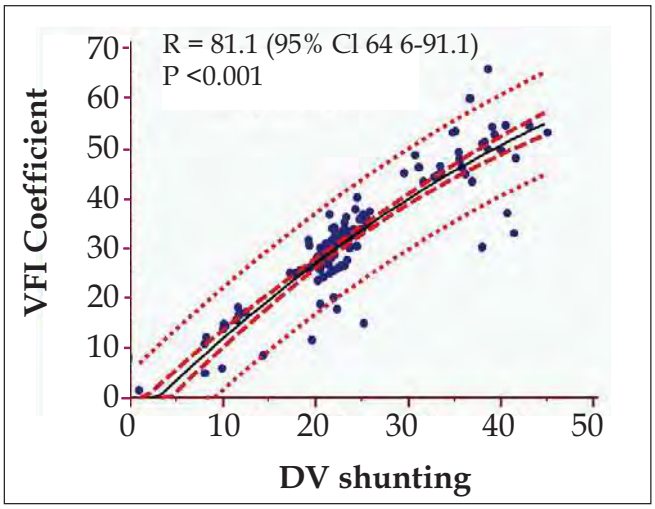

Fig. 7. Lineal regression plot comparing the DVS measured as classically described and the DV/UV VFI ratio r value = 0.81; P<0.001

Reference ranks equation $y = 0{,}6766 + 1{,}6542\ x + -0{,}007813\ x^2$

Also, as previously described, we found a significant difference in DV/UV VFI ratio between normal and FGR foetuses. Comparing results in growth restricted foetuses showed difference as plotted by gestational age mean (SD):39 (11,5) and 53(16,8) (p = 0,03). (Figure 8)

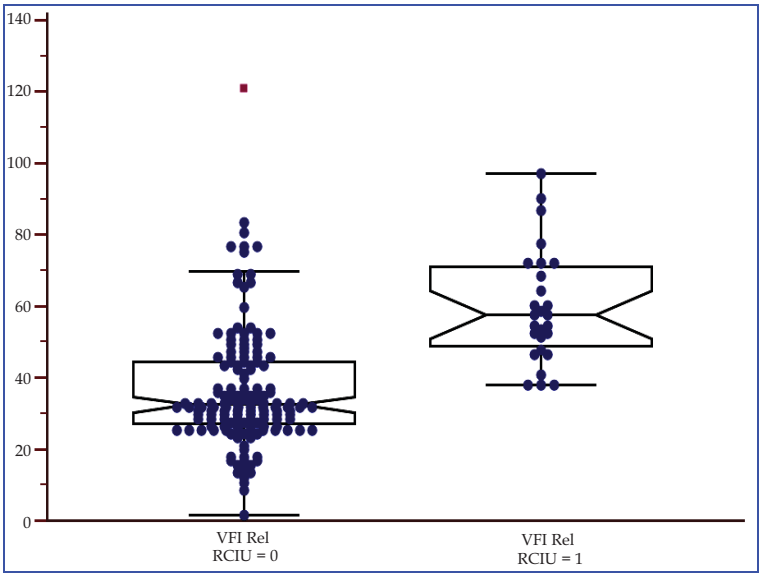

Fig. 8. Box Whisker plot of DV/UV VFI ratio comparing normal (left) to IUGR foetuses (right)

3. Four-dimensional power Doppler signal and the estimation of flow

3.1 The addition of a time sequence

Since the solution provided is already limited and only allows to estimate some regional changes in vascularity, applicable perhaps to the abovementioned DVS and to placenta (Odeh et al. 2011), but is still far away from depicting the flow phenomenon; it is necessary to move forward, towards two recently opened gates:

First is the integration of Power Doppler signal derived velocities profile, whose most reliable approach is the Surface Integration of Velocity Vectors, (Sun et al. 1995; J M Rubin et al. 2001; Berg et al. 2000) a clarifying concept which was developed for Color Dopler signal analysis, but has the handicap of the angle effect (Pemberton et al. 2005; Li et al. 2005), reason why it was left aside. Until the algorithms for calculating velocity of particles from power Doppler signals were developed (M. G. Jones et al. 2003; Kripfgans et al. 2006; Petersch & Hönigmann 2007)

Surface integration of velocity vectors is based on Gauss' theorem, which relates the divergence of the quantity (*v)* in an enclosed volume (*V)* to the flux through the surface (*S)* covering (*V)*. In other words, a surface integral of *v* over the enclosing boundary *S* will yield the volume flow *Q*:

$$Q = \int_S \vec{v} \cdot \overrightarrow{dA} \,. \tag{10}$$

The easiest way to implement SIVV is to choose a surface that is locally perpendicular to each Doppler beam. For this case, the right side dot product in Equation 1 will be replaced by a regular multiplication of the Doppler velocity and the size of the surface element. In other words, this surface has a constant depth geometry with respect to the Doppler beams. (Kripfgans et al. 2006)

The most general scanning geometry is the surface of a torus because the center of rotation for the axial-lateral and axial-elevational beams can differ). Volume flow can be computed by integrating all Doppler acquisitions on the defined surface, as expressed by Kripfgans et al:

$$Q = \sum_{i \in S} v_i a_i \tag{11}$$

Where, *Q* is the total flux through the surface *S*, which equals volume flow; *vi* is the local Doppler velocity; *ai* is the associated cross-sectional area on *S* for this voxel, and · is the dot product between the local velocity vector and the local surface normal. In this case, the detected velocity is parallel to the surface normal.

In Kripfgans et al experiment, for the depicted type of tube-to-transducer orientation, the left-/right-most Doppler beam has the smallest/largest Doppler angle, respectively. This causes the velocity maximum to shift toward the left. However, warping of velocity values does not affect the measured SIVV value. Inherent compensation of this warping is due to nonuniform distribution of surface elements over the tube cross section.

A very important matter, mainly derived from biophysical characteristics of blood is the Rouleaoux' effect (J M Rubin et al. 1997; A. W. Welsh et al. 2005; N J Raine-Fenning, Nordin,

Ramnarine, B. K. Campbell, Clewes, Perkins & Johnson 2008a). The local Doppler power is largest inside the vessel and smallest outside because of the effect of partial volume averaging and the Doppler wall filter effect, which gives the pixels inside the vessel a higher power. All Doppler data is wall filter processed internally in the scanner by the smallest setting possible on the machine. Therefore, it is mandatory to minimize filtering for the selected Doppler frequency range.

Authors define a solution for surface integration of velocity vectors, which was weighted on the basis of the Doppler power in the respective voxels. A velocity masking algorithm which was generated, using the Doppler power value pT to weight the velocity values of the integration surface.

Therefore, the modified SIVV method that was used by the authors was

$$Q = \sum_{i \in S} (v_i \cdot a_i) p_i \ . \tag{12}$$

Where, pi is a scaling factor based on the local Doppler power. Power weighting factors pi were set to 1 for all Doppler powers larger then pT. Values between 0 and pT were scaled between 0 and 1 on the basis of their Doppler power value. The justification for the selection/scaling process is that voxels near the wall, which partially contain flow and soft tissue, will show lower than- maximum Doppler power. Fractional power is therefore weighted by fractional scaling factors. So far, the threshold $pTwas$ set empirically by developers. However, it was set constant for all measurements, and it could be shown that the pT contour fills the lumen. User-selected Doppler gain was adjusted as needed to compensate for signal reduction due to large angles between flow and Doppler beams.

The next addition to the conceptual framework was the estimation of pulsatile conditions by Richards and Kripfgans (Richards et al. 2009), by adding to the model the potential signal fluctuations derived from the wall movements and the local velocity profile changes derived from particles acceleration. As a first issue, authors defined the possibility of collecting not one, but N number of velocity profiles according to the local variations in time and position. Such local velocities were expressed as:

$$\widehat{v_i} = E\left(v_i\left(X_i\right)\right) = \frac{\sum_{j=1}^{N} v\left(X_i, t_j\right)}{N}, \tag{13}$$

Where $E(vi(Xi))$ is the expected value of the local velocity estimates. $v(Xi,tj)$ are the local velocity estimates that are measured at randomly selected time increments defined by tj as follows:

$$t_{j+1} = t_j + t_s + t_r, \tag{14}$$

Authors defined an experiment to obtain the average volume flow in the presence of pulsatility: 50 random time points distributed across the equivalent of a cardiac cycle were collected and averaged at each location. Power Doppler data were then used to correct for partial volume effects as described in the previous paragraph. Then, using seven previously defined surfaces for flow estimate, the equation for the modified SIVV method, became:

$$Q = \frac{1}{M} \sum_{i \in S_M} s_i \bullet w_i \bullet \widehat{v_i} \ , \tag{15}$$

where *M* is the number of integration surfaces and the surface of integration *(S)* has been modified to include the *M* surfaces *(SM)*.

In our opinion, Richards & Kripfgans' works have achieved a breakthrough in this matter, and the experiment we have developed is nothing but a logical consequence of their postulations.

Before describing the experiment, next consequent step was to add a regular time frame to the algorithm. Fortunately, the tool for getting the initial data was already developed and seated on the machine: The Spatio Temporal Image Correlation (STIC) is an automated volume acquisition in which the array inside the transducer housing performs a slow, single sweep, recording one single 3D data set. This volume consists of a high number of 2D frames, one behind the other. Due to the small region of interest required to image the foetal heart, the B-mode frame rate during the acquisition of the volume scan is very high, in the range of 150 frames/s. Assuming a volume acquisition time of 10 s and sweeping over an area of 25° (both parameters can be adjusted), there are 1500 B-mode images in the volume memory. During this acquisition time the fetal heart beats 20–25 times, which means there are 20–25 images showing a systolic peak contained within these 1500 B-mode frames (DeVore et al. 2003; Chaoui & Heling 2005). Concerning this application, further studies have shown how, the mere analysis of intra-ventricular stroke volume in left and right heart gave information reliable enough for calculating the cardiac output in foetuses from 16 to 32 weeks (Molina, Faro, Sotiriadis, Dagklis & Nicolaides 2008a).

Basis of volume calculation in VOCAL are performed by integration of polygon areas marked in parallel planes. The method used for the integration of the polygon areas is given by the formula

$$Vol - \frac{\pi}{N} \cdot \left[\sum_{i=1}^{2 \cdot N} TA_i \cdot ds_i \right] \tag{16}$$

Where N = number of marked polygon areas Ai = polygon area in plane i di,j = distance between plane i and plane j the sort order of planes 1,..., N is given by d1,2 £ d1,3 £... £ d1,N. (Sohn 1993; Robb et al. 1997).

And the basis for stroke volume calculation and cardiac output calculation were (Molina, Faro, Sotiriadis, Dagklis & Nicolaides 2008b):

$$CO = \lim_{n \to \infty} \left(1 + \frac{1}{n} \right)^n \cdot Vs \ \vdots - \vdots \ \lim_{n \to \infty} \left(1 + \frac{1}{n} \right)^n \cdot VD \tag{17}$$

Where CO = Cardiac Output, VS is Systolic Volume and VD is Diastolic Volume.

The abovementioned approach provides some additional information on cardiac output and has proven to be repeatable and more accurate than previous methods (Messing et al. 2007; Hamill et al. 2011; Simioni et al. 2011). Notwithstanding, it still has a substantial amount of human interaction, and is rather time-consuming as for being used in an actual clinical setting.

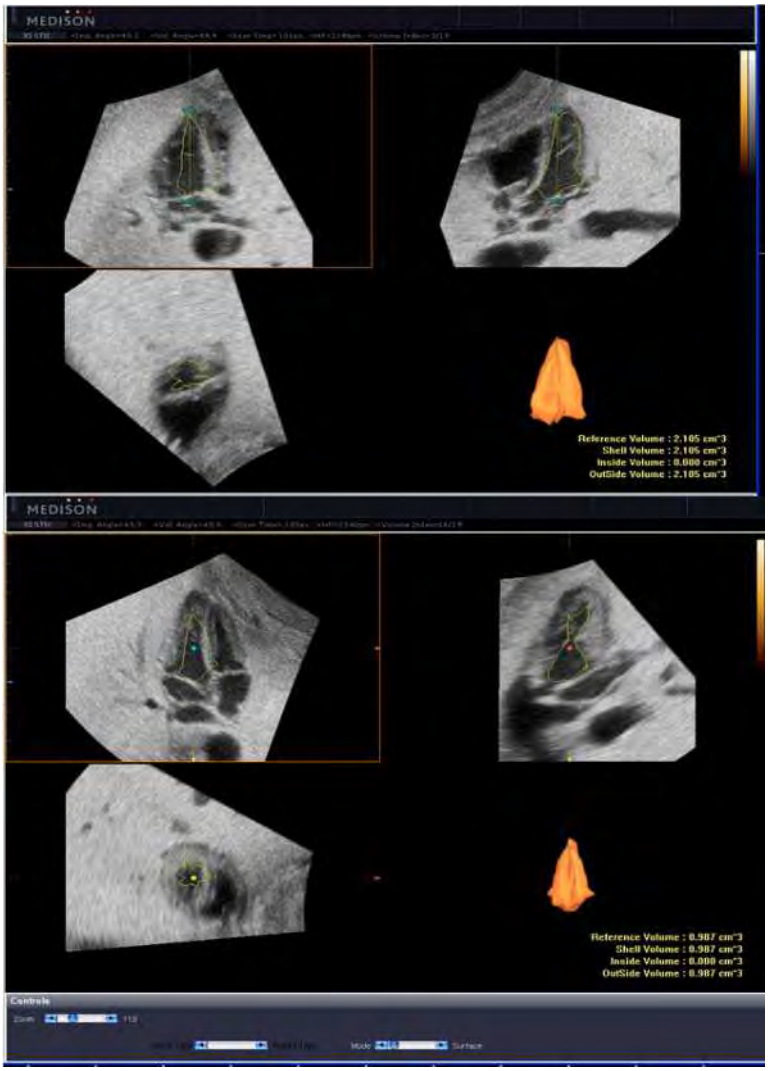

Fig. 9. Reproduction of STIC and VOCAL model for left ventricle output calculation in a term ovine foetus, taken by the authors during their experiment (Bello-Muñoz et al. 2010); as proposed by Molina et al.

3.1.1 The cardiac output model

Based on previous studies and encouraged by the works of Richards & Kripfgans, we decided to develop an algorithm of flow calculation, based on surface integration of velocity vectors and time frame sequences from STIC volumes. Volume datasets as obtained by the ultrasound machine Medison Accuvix V-20 prestige with a Medison 3D4-8ET 3D volumetric probe (Samsung Medical Co, Hoofddorp, Nz).

A total of eight foetuses from near term pregnant sheep (125-140 days) were exteriorized through a cesarean section and a modified central catheter inserted via umbilical cord and under direct echographic vision. An arterial line was also inserted in one of the umbilical arteries. Both transducers from the catheters were connected to a PICCO monitor for invasive testing (PULSION Medical Inc. Irving TX, USA). Continuous measurement of combined cardiac output was the registered as long as the experiment was carried out, meanwhile one of the authors (JB-M), recorded several volume datasets synchronizing the register of the data set with data obtained by monitorization. Analysis of all the data was made offline.

A complete spreadsheet of physiologic registers from the experimental subject was recorded for comparison and external validation of calculations. All images were processed by using the Mathematica® software (Wolfram Research Europe Ltd., Oxfordshire, UK). All data from VOI analysis was addded to the calculation spreadsheet and a polinomial regression fit model was designed

The mathematical background of this study was based on flow calculation:

$$Q = \sum_{i \in S} (v_i \cdot a_i) p_i \ . \tag{12}$$

And the concept of vector velocity profile described above. But with the addition of a time frame provided by the STIC algorithm, which means a continuous sum of velocity profiles, giving us a new profile of the area, represented as:

$$(1+A)^n = 1 + \frac{Ax}{1!} + \frac{A(n-1)x^2}{2!} + \cdots \tag{18}$$

And to the velocity profile, expressed also as

$$\sum \ vi(t1) + vi(t2) \ldots \ldots vi()tn \tag{19}$$

Where N is the entire amount of frames included in a cardiac cycle.

Once collected the sequences, information of velocity vector profile (VVP) form the VOI was collected in a series of frames, from the starting of the cardiac cycle (early start of diastole), denominated as t_0 until the end of same cycle (end of systole) hence called t_n. Information of VVP was then modified according to area variation in every frame. Therefore, the mathematical expression of this phenomenon could be expressed as a matrix of data:

$$\begin{aligned} \sum_{t=1}^{N} Qn = \big(& (A1.vi1)t1 \vdots (A2.vi2)t1 \vdots \cdots \vdots (Ax.vix)t1 \vdots (A1.vi1)t2 \vdots (A2.vi2)t2 \vdots \cdots \vdots \\ & (Ax.vix)t2 \vdots (A1.vi1)tn \vdots (A2.vi2)tn \vdots \cdots \vdots (Ax.vix)tn \big) \end{aligned} \tag{20}$$

Where A_x is an estimated area obtained by adding all the regional areas in the VOI and vi_x is the velocity vector profile in each sub-area, according to, previously described, sectorial variations in velocity. And t is the timeline described above.

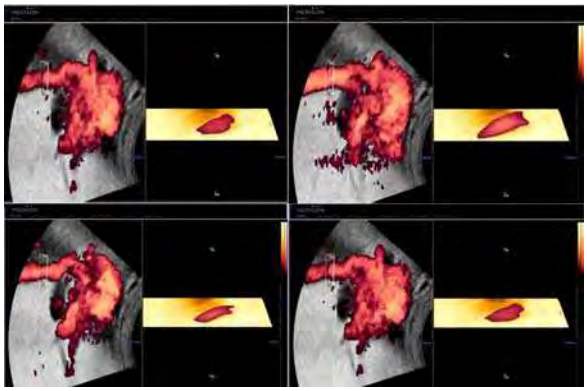

Fig. 10. Screen snapshot of descending aorta plane with selected volume of evaluation. Right side of the image is the VOI containing the $v_1 \ldots v_n$ information. A set of voxels like this one was added to the matrix, since t_1 till t_n where n=end of the cardiac cycle. (Actual experiment added measurements from the aortic isthmus, this image is for illustrative purposes)

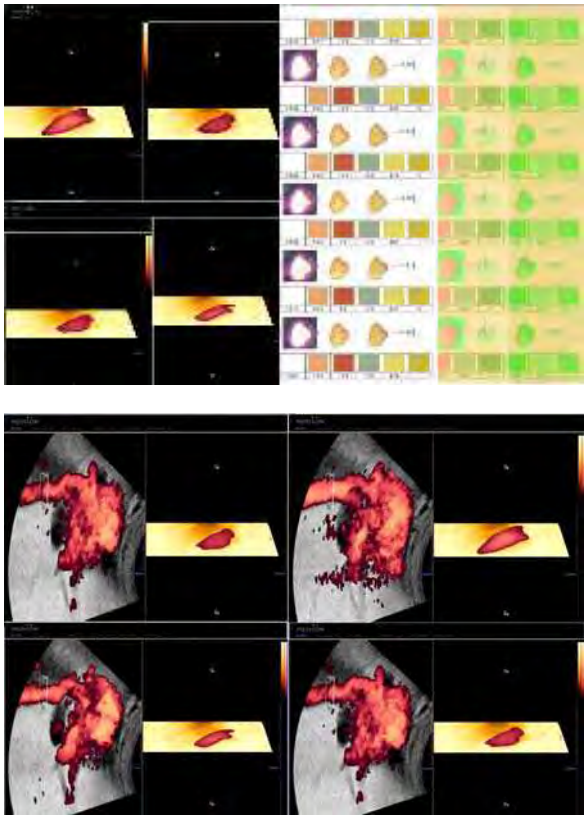

Fig. 11. Colour deconvolution algorithm as delivered by the Mathematica software ®

Regression analysis showed a strong correlation between actual measurement of Combined cardiac Output as obtained by invasive methods and the estimated flow 4D PD dataset as calculated by the authors. The reference polynomial equation and plot is showed in Figure 11

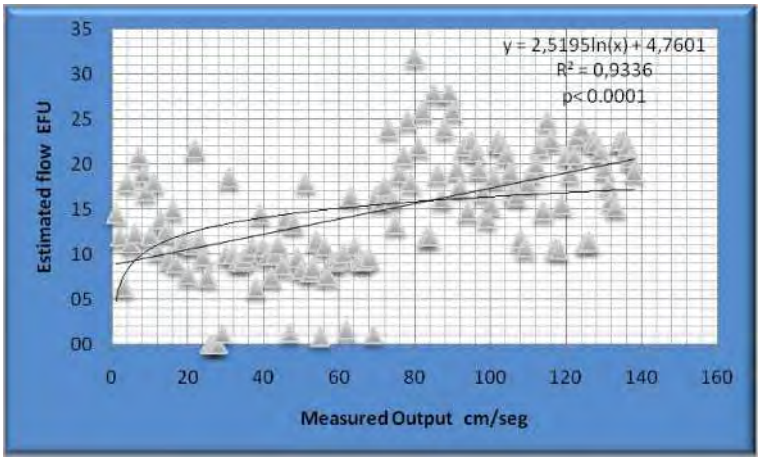

Fig. 12. Polinomial regression plot

4. Conclusion

Three dimensional power Doppler (3D PD), in its current state has no correlation with actual flow measurements, since there is no way of involving the time as a magnitude. Four dimensional power Doppler, by adding the surface integration of velocity vectors from power Doppler signal, and the Spatio Time Image correlation (STIC) might improve significantly its potential. An important amount of additional research on this field is mandatory in order to grant its utility in clinical conditions. But 4D PD could be, in the near future, the most reliable tool for non invasive assessment of physiological intrauterine magnitudes, as Cardiac Output, vascular shunting and flow variations, in normal as well as in pathological conditions

5. Acknowledgment

The authors wish to thank Drs Marielle Estevez and Carla Fonseca from the animal house of the Institut de Recerca de l'Hospital Universitari Vall d'Hebron for their invaluable help in animal care and preparation. They also wish to express their gratitude to Dr Jose Lluis Peiró for his surgical intervention on the mother sheep and the instrumentation of foetuses as well as for his generous teaching and support.

6. References

Alcázar, J L, 2008. Three-dimensional power Doppler derived vascular indices: what are we measuring and how are we doing it? Ultrasound in Obstetrics & Gynecology: The

Official Journal of the International Society of Ultrasound in Obstetrics and Gynecology, 32(4), págs.485-487.

Alcázar, Juan Luis & Jurado, M., 2011. Three-dimensional ultrasound for assessing women with gynecological cancer: a systematic review. Gynecologic Oncology, 120(3), págs.340-346.

Bello-Muñoz, J. et al., 2009. OP23.05: A three-dimensional power Doppler algorithm for ductus venosus shunting evaluation in normal and growth restricted fetuses. Ultrasound in Obstetrics & Gynecology, 34(S1), págs.136-137.

Bellotti, M, Pennati, G. & Ferrazzi, E., 2007. Re: ductus venosus shunting in growth-restricted fetuses and the effect of umbilical circulatory compromise. Ultrasound in Obstetrics & Gynecology: The Official Journal of the International Society of Ultrasound in Obstetrics and Gynecology, 29(1), págs.100-101; author reply 101-102.

Bellotti, M et al., 2000. Role of ductus venosus in distribution of umbilical blood flow in human fetuses during second half of pregnancy. American Journal of Physiology. Heart and Circulatory Physiology, 279(3), págs.H1256-1263.

Bellotti, Maria et al., 2004. Simultaneous measurements of umbilical venous, fetal hepatic, and ductus venosus blood flow in growth-restricted human fetuses. American Journal of Obstetrics and Gynecology, 190(5), págs.1347-1358.

Bendick, P.J. et al., 1998. Three-dimensional vascular imaging using Doppler ultrasound. American Journal of Surgery, 176(2), págs.183-187.

Berg, S. et al., 2000. Volumetric blood flow measurement with the use of dynamic 3-dimensional ultrasound color flow imaging. Journal of the American Society of Echocardiography: Official Publication of the American Society of Echocardiography, 13(5), págs.393-402.

Bozkurt, N., Başgül Yigiter, A., et al., 2010. Correlations of fetal-maternal outcomes and first trimester 3-D placental volume/3-D power Doppler calculations. Clinical and Experimental Obstetrics & Gynecology, 37(1), págs.26-28.

Burns, P.N., 1992. Measuring volume flow with Doppler ultrasound-an old nut. Ultrasound in Obstetrics & Gynecology: The Official Journal of the International Society of Ultrasound in Obstetrics and Gynecology, 2(4), págs.238-241.

Cruz-Martinez, R et al., 2011. Normal reference ranges of fetal regional cerebral blood perfusion as measured by fractional moving blood volume. Ultrasound in Obstetrics & Gynecology: The Official Journal of the International Society of Ultrasound in Obstetrics and Gynecology, 37(2), págs.196-201.

Cruz-Martinez, Rogelio et al., 2009. Cerebral blood perfusion and neurobehavioral performance in full-term small-for-gestational-age fetuses. American Journal of Obstetrics and Gynecology, 201(5), págs.474.e1-7.

Chang, C.-H. et al., 2003. Assessment of normal fetal liver blood flow using quantitative three-dimensional power Doppler ultrasound. Ultrasound in Medicine & Biology, 29(7), págs.943-949.

Chaoui, R. & Heling, K.S., 2005. New developments in fetal heart scanning: three- and four-dimensional fetal echocardiography. Seminars in Fetal & Neonatal Medicine, 10(6), págs.567-577.

Chaoui, R. & Kalache, K.D., 2001. Three-dimensional power Doppler ultrasound of the fetal great vessels. Ultrasound in Obstetrics & Gynecology: The Official Journal of the

International Society of Ultrasound in Obstetrics and Gynecology, 17(5), págs.455-456.

Dar, P. et al., 2010. First-trimester 3-dimensional power Doppler of the uteroplacental circulation space: a potential screening method for preeclampsia. American Journal of Obstetrics and Gynecology, 203(3), págs.238.e1-7.

DeVore, G.R. et al., 2003. Spatio-temporal image correlation (STIC): new technology for evaluation of the fetal heart. Ultrasound in Obstetrics & Gynecology: The Official Journal of the International Society of Ultrasound in Obstetrics and Gynecology, 22(4), págs.380-387.

Dubiel, M. et al., 2005. Computer analysis of three-dimensional power angiography images of foetal cerebral, lung and placental circulation in normal and high-risk pregnancy. Ultrasound in Medicine & Biology, 31(3), págs.321-327.

Eik-Nes, S.H. et al., 1982. Ultrasonic measurement of human fetal blood flow. Journal of Biomedical Engineering, 4(1), págs.28-36.

Fenster, A., Lee, D., et al., 1998. Three-dimensional ultrasound imaging of the vasculature. Ultrasonics, 36(1-5), págs.629-633.

Forsberg, F. et al., 1995. Volume flow estimation using time domain correlation and ultrasonic flowmetry. Ultrasound in Medicine & Biology, 21(8), págs.1037-1045.

Gill, R.W., 1979. Pulsed Doppler with B-mode imaging for quantitative blood flow measurement. Ultrasound in Medicine & Biology, 5(3), págs.223-235.

Guimarães Filho, H.A. et al., 2011. Reproducibility of three-dimensional power Doppler placental vascular indices in pregnancies between 26 and 35 weeks. Archives of Gynecology and Obstetrics, 283(2), págs.213-217.

Guo, Z. & Fenster, A., 1996. Three-dimensional power Doppler imaging: a phantom study to quantify vessel stenosis. Ultrasound in Medicine & Biology, 22(8), págs.1059-1069.

Guo, Z., Durand, L.G., et al., 1998. In vitro evaluation of multiple arterial stenoses using three-dimensional power Doppler angiography. Journal of Vascular Surgery: Official Publication, the Society for Vascular Surgery [and] International Society for Cardiovascular Surgery, North American Chapter, 27(4), págs.681-688.

Harrington, K., Deane, C. & Campbell, S., 1996. Measurement of volume flow with time domain and M-mode imaging: in vitro and in vivo validation studies. Journal of Ultrasound in Medicine: Official Journal of the American Institute of Ultrasound in Medicine, 15(10), págs.715-720.

Hayashi, T. et al., 1998. Three-dimensional reconstruction of the power flow Doppler imaging of intracranial vascular structures in the neonate. Journal of Neuroimaging: Official Journal of the American Society of Neuroimaging, 8(2), págs.94-96.

Heling, K.S., Chaoui, R. & Bollmann, R., 2000. Prenatal depiction of the angioarchitecture of an aneurysm of the vein of Galen with three-dimensional color power angiography. Ultrasound in Obstetrics & Gynecology: The Official Journal of the International Society of Ultrasound in Obstetrics and Gynecology, 15(4), pág.345.

Hernandez-Andrade, E et al., 2008. Changes in regional fetal cerebral blood flow perfusion in relation to hemodynamic deterioration in severely growth-restricted fetuses. Ultrasound in Obstetrics & Gynecology: The Official Journal of the International Society of Ultrasound in Obstetrics and Gynecology, 32(1), págs.71-76.

Hernandez-Andrade, E, Jansson, T, et al., 2004. Validation of fractional moving blood volume measurement with power Doppler ultrasound in an experimental sheep model. Ultrasound in Obstetrics & Gynecology: The Official Journal of the International Society of Ultrasound in Obstetrics and Gynecology, 23(4), págs.363-368.

Hernandez-Andrade, E, Thuring-Jönsson, A., et al., 2004. Fractional moving blood volume estimation in the fetal lung using power Doppler ultrasound: a reproducibility study. Ultrasound in Obstetrics & Gynecology: The Official Journal of the International Society of Ultrasound in Obstetrics and Gynecology, 23(4), págs.369-373.

Jansson, Tomas et al., 2003. Estimation of fractional moving blood volume in fetal lung using Power Doppler ultrasound, methodological aspects. Ultrasound in Medicine & Biology, 29(11), págs.1551-1559.

Jones, M.G., Shipley, J.A. & Robinson, T.M., 2003. Visualisation of 4-D colour and power Doppler data. Ultrasound in Medicine & Biology, 29(12), págs.1735-1747.

Jones, N.W. et al., 2011. Evaluating the intra- and interobserver reliability of three-dimensional ultrasound and power Doppler angiography (3D-PDA) for assessment of placental volume and vascularity in the second trimester of pregnancy. Ultrasound in Medicine & Biology, 37(3), págs.376-385.

Kiserud, T., 2001. The ductus venosus. Seminars in Perinatology, 25(1), págs.11-20.

Kiserud, T. et al., 2006. Ductus venosus shunting in growth-restricted fetuses and the effect of umbilical circulatory compromise. Ultrasound in Obstetrics & Gynecology: The Official Journal of the International Society of Ultrasound in Obstetrics and Gynecology, 28(2), págs.143-149.

Kripfgans, O.D. et al., 2006. Measurement of volumetric flow. Journal of Ultrasound in Medicine: Official Journal of the American Institute of Ultrasound in Medicine, 25(10), págs.1305-1311.

Kupesic, S. & Kurjak, A., 2000. Contrast-enhanced, three-dimensional power Doppler sonography for differentiation of adnexal masses. Obstetrics and Gynecology, 96(3), págs.452-458.

Kurjak, A. et al., 1998. The assessment of ovarian tumor angiogenesis: what does three-dimensional power Doppler add? Ultrasound in Obstetrics & Gynecology: The Official Journal of the International Society of Ultrasound in Obstetrics and Gynecology, 12(2), págs.136-146.

Lai, P.K., Wang, Y.A. & Welsh, A.W., 2010. Reproducibility of regional placental vascularity/perfusion measurement using 3D power Doppler. Ultrasound in Obstetrics & Gynecology: The Official Journal of the International Society of Ultrasound in Obstetrics and Gynecology, 36(2), págs.202-209.

Li, X. et al., 2005. A novel method for the assessment of the accuracy of computing laminar flow stroke volumes using a real-time 3D ultrasound system: In vitro studies. European Journal of Echocardiography: The Journal of the Working Group on Echocardiography of the European Society of Cardiology, 6(6), págs.396-404.

Marín, R.C. et al., 2010. Use of 3-dimensional sonography for prenatal evaluation and follow-up of fetal goitrous hypothyroidism. Journal of Ultrasound in Medicine: Official Journal of the American Institute of Ultrasound in Medicine, 29(9), págs.1339-1343.

Martins, W.P. & Raine-Fenning, N J, 2010. Analysis and acquisition reproducibility of 3D power Doppler. Ultrasound in Obstetrics & Gynecology: The Official Journal of the International Society of Ultrasound in Obstetrics and Gynecology, 36(3), págs.392-393; author reply 393-394.

Morel, O. et al., 2010. Correlation between uteroplacental three-dimensional power Doppler indices and true uterine blood flow: evaluation in a pregnant sheep model. Ultrasound in Obstetrics & Gynecology: The Official Journal of the International Society of Ultrasound in Obstetrics and Gynecology, 36(5), págs.635-640.

Moskalik, A.P. et al., 2001. Analysis of three-dimensional Doppler ultrasonographic quantitative measures for the discrimination of prostate cancer. Journal of Ultrasound in Medicine: Official Journal of the American Institute of Ultrasound in Medicine, 20(7), págs.713-722.

Nardozza, L.M.M. et al., 2009. Evolution of 3-D power Doppler indices of fetal brain in normal pregnancy. Ultrasound in Medicine & Biology, 35(4), págs.545-549.

Negrini, R. et al., 2011. Assessment of placental blood flow between 22 and 34 weeks of gestation by 3D-sonography power Doppler vascular indices. Archives of Gynecology and Obstetrics, 284(1), págs.53-57.

Odeh, M. et al., 2011. Placental volume and three-dimensional power Doppler analysis in prediction of pre-eclampsia and small for gestational age between Week 11 and 13 weeks and 6 days of gestation. Prenatal Diagnosis, 31(4), págs.367-371.

Odibo, A.O. et al., 2011. Placental volume and vascular flow assessed by 3D power Doppler and adverse pregnancy outcomes. Placenta, 32(3), págs.230-234.

Pairleitner, H. et al., 1999. Three-dimensional power Doppler sonography: imaging and quantifying blood flow and vascularization. Ultrasound in Obstetrics & Gynecology: The Official Journal of the International Society of Ultrasound in Obstetrics and Gynecology, 14(2), págs.139-143.

Pemberton, J. et al., 2005. The use of live three-dimensional Doppler echocardiography in the measurement of cardiac output: an in vivo animal study. Journal of the American College of Cardiology, 45(3), págs.433-438.

Petersch, B. & Hönigmann, D., 2007. Blood flow in its context: combining 3D B-mode and color Doppler ultrasonic data. IEEE Transactions on Visualization and Computer Graphics, 13(4), págs.748-757.

Pomorski, M. et al., 2011. Comparative analysis of placental vasculature and placental volume in normal and IUGR pregnancies with the use of three-dimensional Power Doppler. Archives of Gynecology and Obstetrics. Available at: http://www.ncbi.nlm.nih.gov/pubmed/21744006 [Accedido Julio 17, 2011].

Raine-Fenning, N J, Nordin, N.M., Ramnarine, K.V., Campbell, B.K., Clewes, J.S., Perkins, A. & Johnson, I.R., 2008a. Determining the relationship between three-dimensional power Doppler data and true blood flow characteristics: an in-vitro flow phantom experiment. Ultrasound in Obstetrics & Gynecology: The Official Journal of the International Society of Ultrasound in Obstetrics and Gynecology, 32(4), págs.540-550.

Raine-Fenning, N J, Nordin, N.M., Ramnarine, K.V., Campbell, B.K., Clewes, J.S., Perkins, A. & Johnson, I.R., 2008b. Evaluation of the effect of machine settings on quantitative three-dimensional power Doppler angiography: an in-vitro flow phantom experiment. Ultrasound in Obstetrics & Gynecology: The Official Journal of the

International Society of Ultrasound in Obstetrics and Gynecology, 32(4), págs.551-559.

Richards, M.S. et al., 2009. Mean volume flow estimation in pulsatile flow conditions. Ultrasound in Medicine & Biology, 35(11), págs.1880-1891.

Rizzo, G. et al., 2009. First-trimester placental volume and vascularization measured by 3-dimensional power Doppler sonography in pregnancies with low serum pregnancy-associated plasma protein a levels. Journal of Ultrasound in Medicine: Official Journal of the American Institute of Ultrasound in Medicine, 28(12), págs.1615-1622.

Ruano, R. et al., 2006. Quantitative analysis of fetal pulmonary vasculature by 3-dimensional power Doppler ultrasonography in isolated congenital diaphragmatic hernia. American Journal of Obstetrics and Gynecology, 195(6), págs.1720-1728.

Rubin, J M, 1999. Flow quantification. European Radiology, 9 Suppl 3, págs.S368-371.

Rubin, J M et al., 1994. Power Doppler US: a potentially useful alternative to mean frequency-based color Doppler US. Radiology, 190(3), págs.853-856.

Rubin, J M et al., 1997. Normalizing fractional moving blood volume estimates with power Doppler US: defining a stable intravascular point with the cumulative power distribution function. Radiology, 205(3), págs.757-765.

Rubin, J M, Tuthill, T.A. & Fowlkes, J B, 2001. Volume flow measurement using Doppler and grey-scale decorrelation. Ultrasound in Medicine & Biology, 27(1), págs.101-109.

Sauders, J.B., Wright, N. & Lewis, K.O., 1980. Measurement of human fetal blood flow. British Medical Journal, 280(6210), págs.283-284.

Schulten-Wijman, M.J. et al., 2011. Re: Three-dimensional power Doppler: validity and reliability. Ultrasound in Obstetrics & Gynecology: The Official Journal of the International Society of Ultrasound in Obstetrics and Gynecology, 37(5), págs.620-621.

Sun, Y. et al., 1995. Estimation of volume flow rate by surface integration of velocity vectors from color Doppler images. Journal of the American Society of Echocardiography: Official Publication of the American Society of Echocardiography, 8(6), págs.904-914.

Tchirikov, M., Schröder, H.J. & Hecher, K., 2006. Ductus venosus shunting in the fetal venous circulation: regulatory mechanisms, diagnostic methods and medical importance. Ultrasound in Obstetrics & Gynecology: The Official Journal of the International Society of Ultrasound in Obstetrics and Gynecology, 27(4), págs.452-461.

Tuuli, M.G. et al., 2010. Validation of placental vascular sonobiopsy for obtaining representative placental vascular indices by three-dimensional power Doppler ultrasonography. Placenta, 31(3), págs.192-196.

Welsh, A., 2004. Quantification of power Doppler and the index «fractional moving blood volume» (FMBV). Ultrasound in Obstetrics & Gynecology: The Official Journal of the International Society of Ultrasound in Obstetrics and Gynecology, 23(4), págs.323-326.

Welsh, A.W. et al., 2005. Standardization of power Doppler quantification of blood flow in the human fetus using the aorta and inferior vena cava. Ultrasound in Obstetrics & Gynecology: The Official Journal of the International Society of Ultrasound in Obstetrics and Gynecology, 26(1), págs.33-43.

Yigiter, A.B. et al., 2011. Placental volume and vascularization flow indices by 3D power Doppler US using VOCAL technique and correlation with IGF-1, free beta-hCG, PAPP-A, and uterine artery Doppler at 11-14 weeks of pregnancy. Journal of Perinatal Medicine, 39(2), págs.137-141.

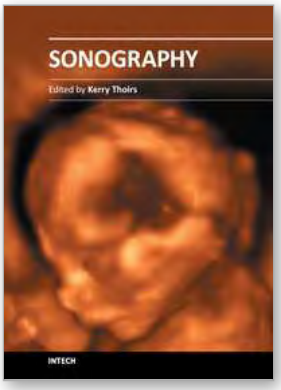

Sonography

Edited by Dr. Kerry Thoirs

ISBN 978-953-307-947-9
Hard cover, 346 pages
Publisher InTech
Published online 03, February, 2012
Published in print edition February, 2012

Medical sonography is a medical imaging modality used across many medical disciplines. Its use is growing, probably due to its relative low cost and easy accessibility. There are now many high quality ultrasound imaging systems available that are easily transportable, making it a diagnostic tool amenable for bedside and office scanning. This book includes applications of sonography that can be used across a number of medical disciplines including radiology, thoracic medicine, urology, rheumatology, obstetrics and fetal medicine and neurology. The book revisits established applications in medical sonography such as biliary, testicular and breast sonography and sonography in early pregnancy, and also outlines some interesting new and advanced applications of sonography.

INTECH
open science | open minds

InTech Europe
University Campus STeP Ri
Slavka Krautzeka 83/A
51000 Rijeka, Croatia
Phone: +385 (51) 770 447
Fax: +385 (51) 686 166
www.intechopen.com

InTech China
Unit 405, Office Block, Hotel Equatorial Shanghai
No.65, Yan An Road (West), Shanghai, 200040, China
中国上海市延安西路65号上海国际贵都大饭店办公楼405单元
Phone: +86-21-62489820
Fax: +86-21-62489821

18

Fetal Yawning

Olivier Walusinski
Family Physician. Private Practice
France

1. Introduction

The introduction of ultrasound exploration during pregnancy has led to very important conclusions concerning fetal behavioural milestones. For example, the development of oral sensorimotor functions such as swallowing (essential for survival) can be assessed from normal or abnormal neurobehavioral development during the fetal period. While the assessment of these functions takes a long time, another daily behaviour can be detected during an ultrasound examination: yawning. Before the development of real-time imaging techniques, it was impossible to assess facial movements, swallowing and thus yawning. Only the overall movements of the trunk and limbs could be perceived by the mother or by someone touching her belly with their hand. In this chapter, we will show the usefulness of ultrasound in exploring facial mobility, particularly yawning, and in drawing conclusions on harmonious fetal cerebral development.

The phenomenon of yawning is just as intriguing and fascinating as sleep, yet understanding of its causes and consequences has defied the human mind for centuries. Phylogenetically and ontogenetically primitive, this motor behaviour has been remarkably well preserved during evolution and is nearly universal in vertebrates. It appears closer to an emotional stereotypy than to a reflex. Yawning is a stereotyped and often repetitive motor act characterized by gaping of the mouth accompanied by a long inspiration of air or fluid, followed by a brief acme and a short expiration. It is not merely a simple opening of the mouth, but a complex coordinated movement bringing together a flexion followed by an extension of the neck, a wide dilatation of the laryngopharynx with strong stretching of the diaphragm and anti-gravity muscles. Highly stereotypical because no environmental input changes the sequence of movements, it is observed in cold-blooded and warm-blooded vertebrates, from reptiles with rudimentary 'archaic' brains to human primates, in water, air and land environments. The ethology, neurophysiology and neuropsychology literature describes yawning as a transitional behaviour associated with wake/sleep rhythms and hunger/satiety fluctuations, where it externalizes a group of possible vigilance-stimulating mechanisms and attests to the central role of the diencephalon and notably the hypothalamus in homeostasis (Walusinski, 2004; Guggisberg, 2010).

All the movements that a newborn is able to produce originate during the fetal phase and are performed throughout the life span. The fetus exhibits a wide range of behaviours starting with slow flexion and extension of the spine and limbs at around 7 weeks gestation. The variety of movements increases rapidly over the next three to four weeks and many

different movement patterns have been described, including breathing, truncal rotation, limb flexion/extension, sucking and yawning (de Vries, 1982).

2. How to recognize a fetal yawn during ultrasound examination

During ultrasound facial examination, yawning can be seen accidentally. Yawning consists of a slow opening of the mouth with simultaneous downward movements of the tongue and is usually combined with retroflexion of the head. This phase occupies 50 to 75% of the

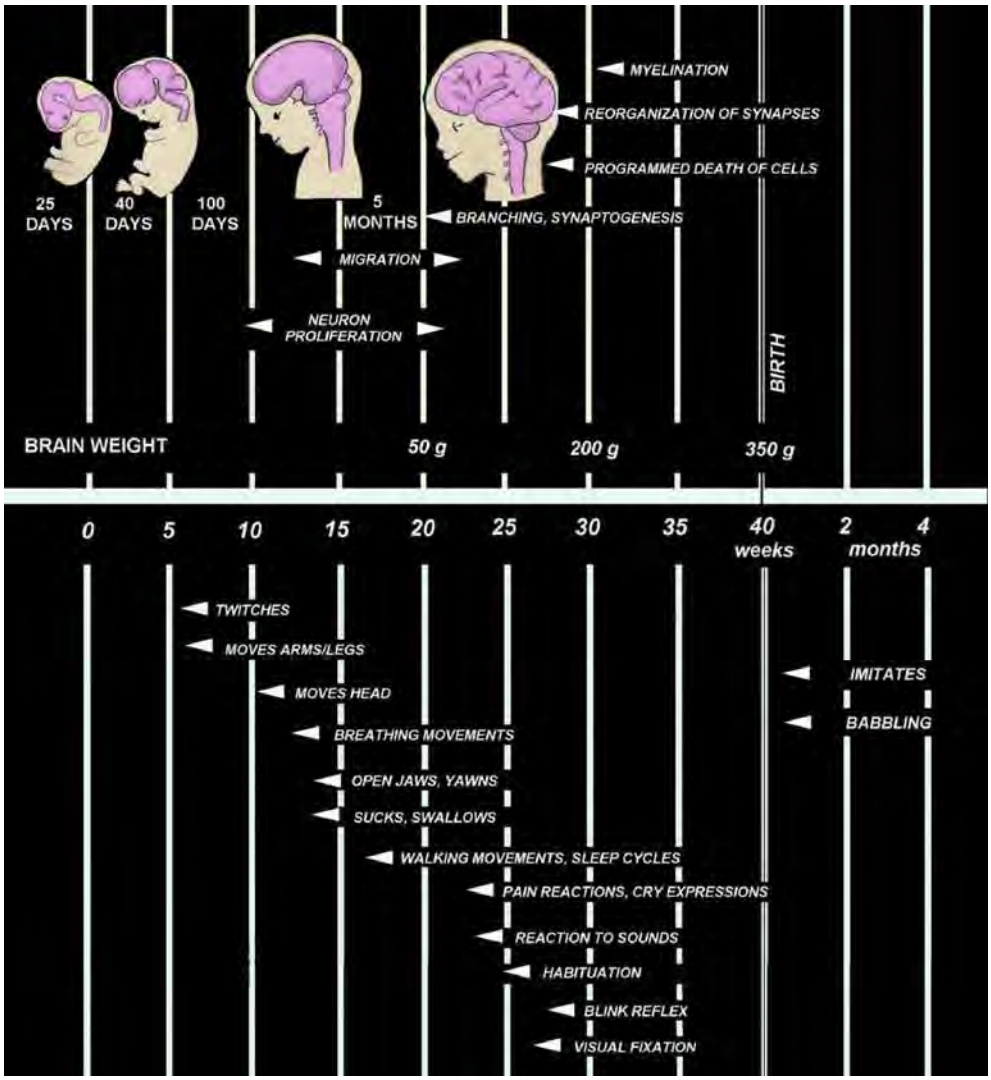

Fig. 1. Development of brain and fetal central nervous system and chronology of the functional development of fetal movements

yawning cycle. After reaching its maximum opening, the mouth remains wide open for 5 to 15 s and returns to its resting closed position within seconds. This harmonious sequence is markedly different from a brief swallowing episode. Using a colour Doppler technique, it is possible to observe the flow of amniotic fluid through the fetal mouth, oropharynx and trachea to the lungs. Contrary to adults, yawning is non-repetitive in the fetus. It is part of a generalized stretch, not just a matter of opening one's mouth. It especially involves the muscles of the respiratory tract (diaphragm, intercostals), face and neck. Fetal yawning can be recognized as one of the movement patterns consistently present starting at around 11-12 weeks of pregnancy (fig. 2). The frequency of yawning gradually increases between 12 and 24 weeks (fig. 3 and 4). During this time, it is possible to observe 40 to 60 yawns per day, and it is the best time to assess yawning with ultrasound examination. A plateau is reached, after which the number of yawns decreases slightly until term. Thus, yawning occurs regularly at a rate of about 1 to 3 yawns per hour. It is obviously by chance or after a long investigation that a yawn can be observed. Furthermore, occiput anterior fetal position unfortunately impedes adequate observation of yawning (Sepulveda, 1995; Masuzaki, 1996).

3. Yawning and neurodevelopmental assessments

Yawning is a phylogenetically old, stereotyped phenomenon. Its survival without evolutionary variations suggests a particular importance as far as development. The strong muscular contraction during yawning has a metabolically high cost. If we agree with Darwin's evolutionary propositions, the costs of brain activity must be outweighed by the developmental advantages. Thus, one structural hypothesis is activation of neurotrophins, which leads to a cascade of new synapse formation or recruitment as well as activation through the diencephalon, brainstem and spinal cord. Activity-dependent development has been clearly shown to be one mechanism by which early sensory or motor experience can affect the course of neural development. This mechanism may be a ubiquitous process in brain maturation, by which activity in one brain region can influence development of other regions. Fetal yawning can be seen as a mechanism that influences functional determination of the moving parts of the musculoskeletal system and contributes to joint development and maintenance.

Fetal movements become more regular and coordinated as a result of increased maturation of the nervous system. At the beginning of the third month, the embryo becomes a fetus with the occurrence of the first oral and pharyngeal motor sequences, controlled by neurological brainstem development and the development of the suction-swallowing activity and yawning. Indeed, suction and yawning have the same embryological origin, which shows the importance of the brainstem in the neurophysiological development of oropharyngeal activity coordinated by respiratory, cardiac and digestive regulations, which have the same neuroanatomical location. The cephalic pole comprises an original embryological encephalo-facial and encephalo-cervical segmentation with a strict topographical correspondence: the naso-frontal and premaxillary structures are connected to the forebrain; the maxillo-mandibular and anterior cervical structures are connected to the 41 brainstem and its nerves. The major structures of the brainstem are formed by the 7-8th postconceptional week, although brainstem maturation continues until the 8th postconceptional month. In addition to its many subnuclei, the brainstem gives rise to a variety of descending spinal motor tracts and hosts the nuclei of five cranial nerves (VIII-XII). Formation of the pons begins almost simultaneously, but its maturation is more prolonged. The structures of the pons include cranial nerves V-VIII and the medial

Fig. 2. Fetal yawn at 12 weeks of pregnancy (3D). Fetus weighing 80g

Fig. 3. Fetal yawn at 23 weeks of pregnancy (3D). Fetus weighing 200g

Fig. 4. Fetal yawn at 23 weeks of pregnancy (2D). Fetus weighing 200g

longitudinal fasciculus (MLF), pontine tegmentum, raphe nucleus and locus coeruleus, which exert widespread influence on arousal, including the sleep-wake cycle. Therefore, these structures exert tremendous influence on gross body movements, head turning, heart rate, and respiratory movements, as well as swallowing, yawning, suckling, hiccups, and 7 facial grimacing movements (Santagati, 2003; Kontges, 1996; Jacob, 2000; Sadler, 2009) (Fig. 1).

The emergence of different behavioural states is one of the most significant aspects of early brain maturation in the fetus. In early intra-uterine life, a diffuse collection of phasic and cyclic motor events occur that gradually coalesce. For the fetus, wakefulness and sleep are reliably characterized, respectively, by periods of myoclonic twitching and movements of the limbs against a background of muscle atonia. Periods of twitching are almost always followed by the abrupt onset of high-amplitude, wakeful behaviours. The emergence of distinct states is followed by dramatic changes in the level, duration and cyclicity. An ultradian rhythm may be observed: during a 60 to 90 minute period, there is an alternation of movement characterized by motor activity and movement characterized by rest, as in newborns. The switchover from periods of rest to periods of activity is accompanied by a yawn. Thus, a periodicity of one or two yawns per hour can be seen. Repetitive motions gradually determine the shape and composition of moving structures, as well as their associated neural control pathways. The precociousness and stability of yawning suggest that these characteristics contribute to such development. Furthermore, since a forced inspiration is a critical component of yawning, a potential role for expanding fetal terminal alveoli by the inspired fluid is possible (Marder, 2005).

4. Yawning as a testimony to safe neurological development

In pregnant women, the methods of assessing fetal wellbeing include the biophysical profile; however, this method is limited. Thus, infants must develop safe and effective

respiration and oral feeding skills after birth if they are to survive. For this to occur, infants must have the necessary anatomical structures and adequate central control to coordinate swallowing, ventilation, sleep and arousal. Yawning is associated with all of these behaviours and thus is useful to observe. Fetal facial expressions and movements are known to be an indirect expression of cerebral functional maturity during the fetal period. Facial expressions during this period correspond to facial expression during the neonatal period. Ultrasound has become essential for assessing neurophysiological development as well as detecting anatomical pathology. 4D ultrasound makes it straightforward to comprehend morphological dynamics such as yawning or sucking. As we have seen, yawning can provide information about neurodevelopment and the development of behavioural rhythms (alternation between motor activity, rest and sleep). When fetal activity appears abnormal, nervous system development may be disturbed. Yawning indicates harmonious development of both the brainstem and the peripheral neuromuscular function, testifying to the induction of an ultradian rhythm of vigilance (Rogers, 2005; Einspieler, 2005; Kurjak, 2008). (Ultradian rhythms are recurrent periods or cycles repeated throughout a 24-hour circadian day. In contrast, infradian rhythms, such as the human menstrual cycle, have periods longer than a day. The descriptive term ultradian is used in sleep research in reference to the 90–120 minute cycling of the sleep stages during human sleep).

5. Fetal pathologies assessed by yawning exploration

Yawns recur regularly, about one or two per hour. When a yawn is observed during a 4D US examination, it is obviously by chance or after very long investigation. Yawning appears preferentially after a period of rest, and indicates waking. If normal swallowing is seen (much more frequent), yawning seems of no additional interest with regard to harmonious brainstem maturation. Inversely, the lack or dysfunction of swallowing requires taking the time to understand the set of phasic and cyclic motor events characterizing the ultradian fetal rhythm, thereby increasing the opportunity to observe a yawn. If the ultrasound examination suggests the absence of yawning and swallowing, it is imperative to search for developmental and anatomical abnormalities (van Woerden, 1988).

The lack of fetal yawning, frequently simultaneous to the lack of associated swallowing may be a key to predicting brainstem dysfunction after birth. It is thus imperative to search for mandibular hypoplasia and glossoptosis, often associated with cleft palate (Luedders, 2011; Palit, 2008). For example, Pierre Robin sequence is characterized by a posterior U-shaped cleft palate, retrognatia and glossoptosis. Several arguments favour an embryonic origin consisting of an anomaly in caudal hind brain development. Feeding disorders are the most important functional symptom. Mother testimonies are consistent with the lack of yawning at birth and its progressive appearance during the first year of life, simultaneous to the acquisition of the swallowing reflex necessary for feeding. Pierre Robin syndrome can be seen as the prenatal brainstem dysfunction responsible for orofacial maldevelopment, which can be diagnosed at 23 weeks gestation during a 4D ultrasound examination (Bromley, 1994; Rotten, 2001).

Petrikovsky et al. (1999) report that clusters of yawns were observed in a series of anaemic fetuses and suggest that yawning repetitiveness helps to track fetal anaemia, although fetal yawning has no effect on O2 pressure. Yawning can be seen as the exteriorization of a homeostatic process, the balance between adrenergic and cholinergic stimulation of the autonomic nervous system. We believe this function is already active in the fetus.

Although no data has actually been collected, we have made a non-exhaustive inventory of congenital pathologies in which yawning research is relevant:

- Mandibular hypoplasia is a frequently encountered craniofacial difference and can be classified into congenital and developmental types:
  - Mandibulofacial dysostosis with a variety of limb abnormalities
- Any syndrome (primary bilateral or unilateral growth anomalies), associated or not with temporo / mandibular joint ankylosis, aglossia / microglossia: Francheschetti syndrome, Goldenhar syndrome, Richner-Hanhart syndrome.
- Moebius syndrome comprises a congenital facial diplegia and bilateral abducens nerve palsies by degenerative and involved nuclei of the VI, VII, and XII nerves. Simultaneous occurrence of limb malformations with cranial nerve dysfunction suggests a disruption of normal morphogenesis during a critical period in embryonic brainstem development, most likely starting at 4 to 7 weeks of gestation. Instances of bilateral paresis of the soft palate and scattered instances of dysphagia (some of which resolve in infancy) have been reported. In this type of functional problem, the inability to close the mouth is constant.
- Watershed infarcts in the fetal and neonatal brainstem are clinically expressed as multiple cranial neuropathies, failure of central respiratory drive and dysphagia.
- Goldenhar Syndrome includes malformations primarily involving the jaw, mouth and ears and, in most cases, affects one side of the body. It represents defects in the embryonic first and second brachial arches, the first pharyngeal pouch and brachial cleft, and the primordia of the temporal bone.
- Joubert syndrome is a rare, genetic disorder characterized by absence or underdevelopment of the cerebellar vermis and a malformed brainstem. The most common features include ataxia, an abnormal breathing pattern, sleep apnea, abnormal eye and tongue movements, and hypotonia.
- It is possible to complete this catalogue by referring to Congenital trismus, Crisponi syndrome, Stüve-Wiedemann syndrome, etc.

6. Conclusion

An entirely new paradigm has emerged in fetal medicine, given that the advances in prenatal imaging allow one to see and diagnose disease not previously detected. Clinicians can better plan for the delivery of the neonate, with identified anomalies being optimally managed and the impact on the neonate's health minimized. There exists a sound rationale for including systematic observations of spontaneous motor activity in the neurological assessment of fetuses. Yawning, as spontaneous motility linked to brainstem activities, appears to be a good parameter for indicating such wellbeing and harmonious development. Thus, brainstem maturation could be associated with changes in the yawning pattern. A difficult task is qualitative evaluation of general and partial movements in order to distinguish normal from abnormal performance. Yawning is a basic behaviour that is easy to recognize and highly valuable in assessing brainstem activity. It is advisable to include the fetal yawning examination in the systematic week 23 ultrasound scan. Future studies will improve its diagnostic value in detecting neuromuscular developmental abnormalities as well as fetal behavioural abnormalities.

A complete review on yawning can be founded in the book: “The Mystery of Yawning in Physiology and Disease”. Walusinski O. ed. Basel. Karger. 2010. 160p.

7. References

Bromley B, Benacerraf BR. Fetal Micrognathia: Associated Anomonalies and Outcome. *J Ultrasound Med*. 1994;13:529-533.

de Vries JI, Visser GH, Prechtl FM. The emergence of fetal behaviour. *Early Hum Dey* 1982;7:301-322.

Einspieler C, Prechtl HF. Prechtl's assessment of general movements: a diagnostic tool for the functional assessment of the young nervous system. *Ment Retard Dev Disabil Res Rev*. 2005;11:61-67.

Guggisberg AG, Mathis J, Schnider A, Hess CW. Why do we yawn? *Neurosci Biobehav Rev.* 2010;34:1267-1276

Jacob J, Gutrhie S. Facial visceromotor neurons display specific rhombomere origin and axon pathfinding behavior. *J Neuosci* 2000;20:7664-7671.

Kontges G, Lumsden A. Rhombencephalic neural crest segmentation is preserved throughout craniofacial ontogeny. *Development* 1996,122:3229-3242.

Kurjak A, Tikvica A, Stanojevic M, Miskovic B, Ahmed B, Azumendi G, Di Renzo GC. The assessment of fetal neurobehavior by three-dimensional and four-dimensional ultrasound. *J Matern Fetal Neonatal Med*. 2008;21:675-684.

Luedders DW, Bohlmann MK, Germer U, Axt-Fliedner R, Gembruch U, Weichert J. Fetal micrognathia: objective assessment and associated anomalies on prenatal sonogram. *Prenat Diagn*. 2011;31:1461-51.

Marder E, Rehm KJ. Development of central pattern generating circuits. *Curr Opin Neurobiol*. 2005;15:86-93.

Masuzaki H, Masuzaki M. Color Doppler imaging of fetal yawning. *Ultrasound Obstet Gynecol* l996;8:355-356.

Palit G, Jacquemyn Y, Kerremans M. An objective measurement to diagnose micrognathia on prenatal ultrasound. *Clin Exp Obstet Gynecol*. 2008;35:121-123.

Petrikovsky BM, Kaplan GP, Holsten N. Fetal yawning activity in normal and high-risk fetuses: a preliminary observation. *Ultrasound Obstet Gynecol* 1999;13:127-130.

Rogers B, Arvedson J.Assessment of infant oral sensorimotor and swallowing function. *Ment Retard Dev Disabil Res Rev*. 2005;11:74-82.

Rose RJ. Prenatal programming of behavior. *Neurosci Biobehav Rev*. 2005;29:321-327.

Rotten D, Levaillant JM, Martinez H., Ducou le Pointe H, Vicaut E. The fetal mandible: a 2D and 3D sonographic approach to the diagnosis of retrognathia and micrognathia. *Ultrasound Obstet Gynecol*. 2002;19:122-130.

Sadler, T.W. Langman's Medical Embriology. Williams & Wilkins, Baltimore. 2009. 414p.

Santagati F, Rijli F. Cranial neural crest and the building of the vertebrate head. *Nature Rev Neurosci* 2003;4:806-8l8.

Sepulveda W, Mangiamarchi M. Fetal yawning. Ultrasound Obstet Gynecol 1995;5:57-59.

van Woerden EE, van Geijn HP, Caron FJ, van der Valk AW, Swartjes JM, Arts NF. Fetal mouth movements during behavioural states 1F and 2F. *Europ J Obstet Gynecol Reprod Biol* 1988;29:97-105.

Walusinski 0, Deputte B. The phylogeny, ethology and nosogeny of yawning. *Rev Neurol* 2004;l60:1011-1021.

Yigiter AB, Kavak ZN. Normal standards of fetal behavior assessed by four-dimensional sonography. *J Matern Fetal Neonatal Med*. 2006;19:707-721.

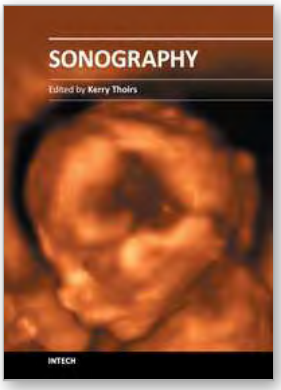

Sonography

Edited by Dr. Kerry Thoirs

ISBN 978-953-307-947-9
Hard cover, 346 pages
Publisher InTech
Published online 03, February, 2012
Published in print edition February, 2012

Medical sonography is a medical imaging modality used across many medical disciplines. Its use is growing, probably due to its relative low cost and easy accessibility. There are now many high quality ultrasound imaging systems available that are easily transportable, making it a diagnostic tool amenable for bedside and office scanning. This book includes applications of sonography that can be used across a number of medical disciplines including radiology, thoracic medicine, urology, rheumatology, obstetrics and fetal medicine and neurology. The book revisits established applications in medical sonography such as biliary, testicular and breast sonography and sonography in early pregnancy, and also outlines some interesting new and advanced applications of sonography.

How to reference

In order to correctly reference this scholarly work, feel free to copy and paste the following:

Olivier Walusinski (2012). Fetal Yawning, Sonography, Dr. Kerry Thoirs (Ed.), ISBN: 978-953-307-947-9, InTech, Available from: http://www.intechopen.com/books/sonography/fetal-yawning

INTECH
open science | open minds

InTech Europe
University Campus STeP Ri
Slavka Krautzeka 83/A
51000 Rijeka, Croatia
Phone: +385 (51) 770 447
Fax: +385 (51) 686 166
www.intechopen.com

InTech China
Unit 405, Office Block, Hotel Equatorial Shanghai
No.65, Yan An Road (West), Shanghai, 200040, China
中国上海市延安西路65号上海国际贵都大饭店办公楼405单元
Phone: +86-21-62489820
Fax: +86-21-62489821

Chapter 7

Follicle Detection and Ovarian Classification in Digital Ultrasound Images of Ovaries

P. S. Hiremath and Jyothi R. Tegnoor

Additional information is available at the end of the chapter

http://dx.doi.org/10.5772/56518

1. Introduction

Some of the successful applications of the image processing techniques are in the area of medical imaging. The development of sophisticated imaging devices coupled with the advances in algorithms specific to the medical image processing both for diagnostics and therapeutic planning is the key to the wide popularity of the image processing techniques in the field of medical imaging. Ultrasound imaging is one of the methods of obtaining images from inside the human body through the use of high frequency sound waves. The reflected sound wave echoes are recorded and displayed as a real time visual image. It is a useful way of examining many of the body's internal organs including heart, liver, gall bladder, kidneys and ovaries. The detection of follicles in ultrasound images of ovaries is concerned with the follicle monitoring during the diagnostic process of infertility treatment of patients.

For women undergoing assisted reproductive therapy, the ovarian ultrasound imaging has become an effective tool in infertility management. Among the many causes, ovulatory failure or dysfunction is the main cause for infertility. Thus, an ovary is the most frequently ultrasound scanned organ in an infertile woman. Determination of ovarian status and follicle monitoring constitute the first step in the evaluation of an infertile woman. Infertility can also be associated with the growth of a dominant follicle beyond a preovulatory diameter and subsequent formation of a large anovulatory follicle cyst. The ovary is imaged for its morphology (normal, polycystic or multicystic), for its abnormalities (cysta, dermoids, endometriomas, tumors etc), for its follicular growth in ovulation monitoring, for evidence of ovulation and corpus luteum formation and function. Ovulation scans allow the doctor to determine accurately when the egg matures and when it ovulates. Daily scans are done to visualize the growing follicle, which looks like a black bubble on the screen of the ultrasound imaging machine.

1.1. Ovarian types

The outcome of ovarian evaluation is the classification of the ovary into one of the three types of ovaries, namely, normal ovary, cystic ovary and polycystic ovary, which are described below :

i. Normal ovary with antral/dominant follicles

A normal ovary consists of 8-10 follicles from 2mm to 28mm in size [1]. The group of follicles with less than 18mm in size are called antral follicles, and the size in the range of 18-28mm are known as dominant follicles. In a normal menstrual cycle with ovulation, a mature follicle, which is also a cystic structure, develops [2]. The size of a mature follicle that is ready to ovulate is about 18-28mm in diameter. During the past 50 years, it has been accepted that folliculogenesis begins with recruitment of a group or cohort of follicles in the late luteal phase of the preceding menstrual cycle followed by visible follicle growth in the next follicular phase [3]. The group or cohort of follicles begins growth and by the mid-follicular phase, around day 7, a single dominant follicle appears to be selected from the group for accelerated growth [4]. The dominant follicle continues to grow at a rate of about 2mm per day. In women, a preovulatory follicle typically measures 18–28mm when a surge of luteinizing hormone (LH) is released from the pituitary to trigger ovulation; ovulation occurs approximately 36 hours after LH release [5]. The Figure 1 shows an ultrasound image of normal ovary with dominant follicles.

ii. Ovarian cyst

An ovarian cyst is simply a collection of fluid within the normal solid ovary. There are many different types of ovarian cysts, and they are an extremely common gynaecologic problem. Because of the fear of ovarian cancer, cysts are a common cause of concern among women. But, it is important to know that the vast majority of ovarian cysts are not cancer. However, some benign cysts will require treatment, in that they do not go away by themselves, and in quite rare cases, others may be cancerous [6]. The most common types of ovarian cysts are called functional cysts, which result from a collection of fluid forming around a developing egg. Every woman who is ovulating will form a small amount of fluid around the developing egg each month. The combination of the egg, the special fluid-producing cells, and the fluid is called a follicle and is normally about the size of a pea. For unknown reasons, the cells that surround the egg occasionally form too much fluid, and this straw colored fluid expands the ovary from within. If the collection of fluid gets to be larger than a normal follicle, about three-quarters of an inch in diameter, a follicular cyst is said to be present. If fluid continues to be formed, the ovary is stretched as if a balloon was being filled up with water. The covering of the ovary, which is normally white, becomes thin and smooth and appears as a bluish-grey. Rarely, though, follicular cysts may become as large as 3 or 4 inches [7]. The Figure 2 shows an ultrasound image of cystic ovary.

iii. Polycystic ovary

The typical polycystic appearance is defined by the presence of 12 or more follicles measuring less than 9mm in diameter arranged peripherally around a dense core of stroma [8]. Other ultrasound features include enlarged ovaries, increased number of follicles and density of

http://dx.doi.org/10.5772/56518

Figure 1. Ultrasound image of a normal ovary with dominant follicles

ovarian stroma. The current ultrasound guidelines supported by ESHRE/ASRM consensus characterize the polycystic ovary as containing 12 or more follicles measuring 2–9mm [9]. The basic difference between polycystic and normal ovaries is that, although the polycystic ovaries contain many small antral follicles with eggs in them, the follicles do not develop and mature properly, and hence, there is no ovulation [10]. The infertility incidence with polycystic ovaries is very high. These women usually will have difficulty in getting pregnant and, hence, invariably require treatment to improve chances for pregnancy. In a polycystic ovary, the numerous small cystic structures, also called antral follicles, give the ovaries a characteristic "polycystic" (many cysts) appearance in ultrasound image. It is referred to as polycystic ovarian syndrome (PCOS/PCOD) [11]. Since women with polycystic ovaries do not ovulate regularly, they do not get regular menstrual periods. The Figure 3 shows an ultrasound image of ovary with PCOD.

A computer assisted diagnostic procedure is desirable because of tedious and time consuming nature of the manual follicle segmentation and ovarian classification done by medical experts. In the present book chapter, the objective of study is to design algorithms for follicle detection and ovarian classification in ultrasound ovarian images in order to assist medical diagnosis in infertility treatment using digital image processing techniques.

Figure 2. Ultrasound image of a cystic ovary

1.2. Background literature

In [12,13], follicular ultrasound images are segmented using an optimal thresholding method applied to coarsely estimated ovary. However, this fully automated method, using the edges for estimation of ovary boundaries and thresholding as a segmentation method, doesn't give optimal results. In [14], this method has been upgraded using active contours and, consequently, the segmentation quality of recognized follicles is considerably improved. Edges of recognized objects were much closer to the real follicle boundaries. However, the determination of suitable parameters for snakes automatically is problematic. In [15], region growing based segmentation method is used for the follicle detection. In [16], a semi automated method is proposed for the outer follicle wall segmentation, wherein a frequent manual tracing of the inner border of all follicles is done. In [17], cellular automata and cellular neural networks are employed for the follicle segmentation. The results are found to be very promising but an obvious drawback of these two methods is the difficulty in determination of the required parameters for follicle segmentation. In [18], the authors have determined the inner border of all follicles using watershed segmentation techniques. Watershed segmentation was applied on smoothed image data which merged some small adjacent follicles. Therefore binary mathematical morphology was employed to separate such areas adhoc in some steps. In [19],

http://dx.doi.org/10.5772/56518

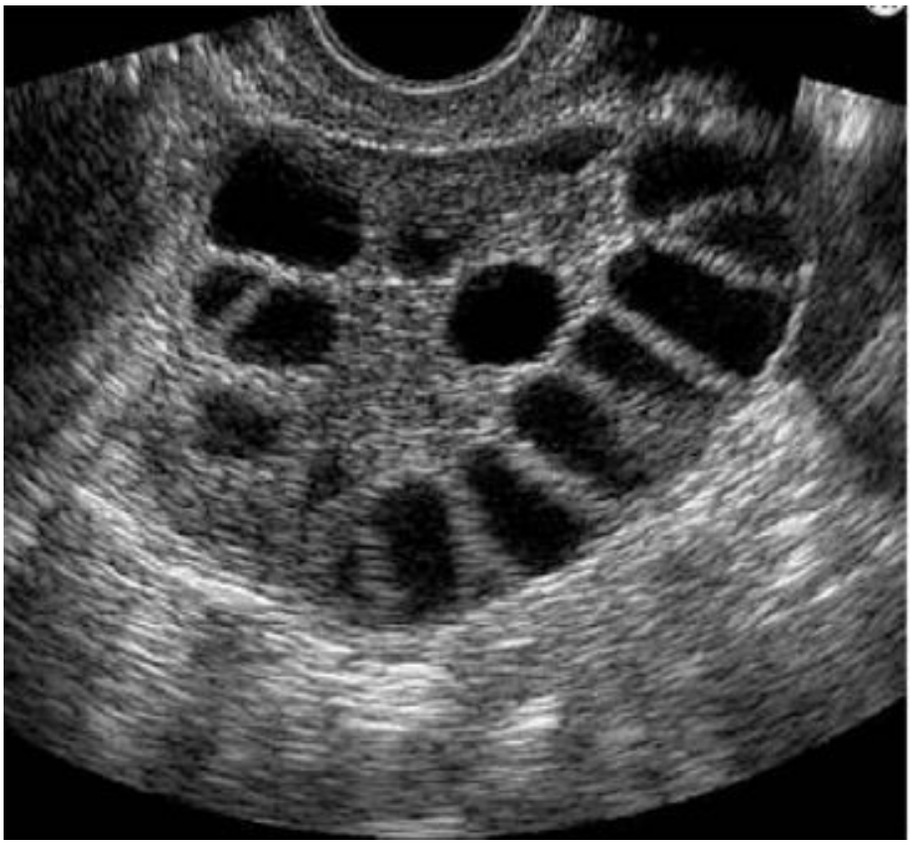

Figure 3. Ultrasound image of an ovary with PCOD

the authors have reported follicle segmentation based on modified region growing method for the follicle segmentation and linear discriminant classifier for the purpose of classification. In [20], the scanline thresholding method is used for the follicle detection and the segmentation performance is measured in terms of the mean square error (MSE).

The follicles are the regions of interest (ROIs) in an ovarian ultrasound image, which need to be detected by using image processing techniques. This is basically an object recognition problem. Thus, the basic image processing steps, namely, preprocessing, segmentation, feature extraction and classification, apply. In the literature, the authors have employed various techniques for ultrasound image processing, as shown below:

1. Preprocessing

- Gaussian low pass filter
- Homogeneous region growing mean filter (HRGMF)
- Contourlet transform

2. Segmentation

- Optimal thresholding
- Edge based method

– Watershed transform

– Scanline thresholding

– Active contour method

3. Feature extraction

– Geometric features

– Texture features

4. Classification

– 3σ interval based classifier.

– K-NN classifier

– Linear discriminant classifier

– Fuzzy classifier

– SVM classifier

1.3. Image data set

For the purpose of experimentation, the databases D1, D2 and D3, of ultrasound images of ovaries are prepared in consultation with the medical expert, namely, Radiologist and Gyneocologist, for the present study of the follicle detection and ovarian classification in ovarian images. Some of the images are captured by the Toshiba [Model SSA-320A/325A] diagnostic ultrasound system with the transvaginal transducer frequency 26 Hz. Some of the images are obtained from the publicly available websites [www.radiologyinfo.com; www.ovaryresearch.com]. The image dataset D1 consists of the 80 ultrasound ovarian images, with the size 256x256. The image dataset D2 consists of the 90 ultrasound ovarian images, with the size 512x512. The image dataset D3 consists of the 70 ultrasound ovarian images, with the size 512x512. It contains the images of 30 normal (healthy) ovaries, 20 polycystic ovaries and 20 cystic ovaries.

2. Follicle detection

The methods employed by [Hiremath and Tegnoor] for follicle detection based on different segmentation, feature extraction and classification techniques are described below:

a. Edge based method

The automatic method for the detection of follicles in ultrasound images of ovaries using edge based method uses, Gaussian lowpass filter for preprocessing, canny operator for edge detection for segmentation, 3σ-intervals around the mean for the purpose of classification [21]. The experimentation has been done using sample ultrasound images of ovaries and the results

http://dx.doi.org/10.5772/56518

are compared with the inferences drawn by medical expert. Initially, the image is processed with Gaussian low pass filter yielding denoised image. Then canny operator is applied to detect the edges from the denoised image. Morphological dilation is performed by using the disk shaped structuring element with radius 1 to fill the weak edges. which yields the segmented image. Possible holes inside the segmented regions are filled. Any spurious regions due to noise are eliminated by morphological erosion. The regions in segmented image having smaller area than the threshold T (empirical value) are removed. The segmented regions are labeled. Set all the nonzero pixels of the border of segmented image to zero, which yields the final segmented image. Thus the plausible follicle regions are the labeled segments.

The geometric features are extracted for the known follicle regions. The main aim of geometric feature extraction is to recognize geometric properties of ovarian follicles in ultrasound images. The ovarian follicles are oval shaped compact structures, which resemble the circular/ellipse and are, thus, characterized by the seven geometric features, namely, the area A, the ratio R of majoraxislength to minoraxislength, the compactness Cp, the circularity Cr, the tortousity Tr, the extent E and the centriod $Y = \frac{1}{B^2}\sum_{i,j=1}^{B} CS_{-i,-j}\left(F^{-1}\left(\lambda\left(F\left(CS_{i,j}(X)\right)\right)\right)\right)$.

The classification stage comprises two steps, namely, the training phase and the testing phase.

Training phase : In the training phase, the geometrical features, are computed for regions known to be follicles in the training images in consultation with the medical expert. Then, the sample means and standard deviations of the geometric parameters R, Cp, Cr, Tr, E and, $C = (Cx, Cy)$ are computed which are used to set the rules for classification of labelled segments into follicles and non-follicles. The $\overline{R}$, $\overline{Cp}$, $\overline{Cr}$, $\overline{Tr}$, $\overline{E}$, $(\overline{Cx}, \overline{Cy})$ denote the mean values, and, the σ_R, σ_{Cp}, σ_{Cr}, σ_{Tr}, σ_E, $(\sigma_{Cx}, \sigma_{Cy})$ denote the standard deviation values, of the geometric parameters R, Cp, Cr, Tr, E and C=(Cx,Cy).

Now, the classification rules for follicle recognition are formulated as following: A region with area A, ratio R, compactness Cp, circularity Cr, Tortousity Tr, extent E, and centriod $C = (Cx, Cy)$, is classified as a follicle, if the following conditions are satisfied:

$$A > T_A \tag{1}$$

$$\overline{R} - \alpha\sigma_R < R < \overline{R} + \alpha\sigma_R \tag{2}$$

$$\overline{Cp} - \alpha\sigma_{Cp} < Cp < \overline{Cp} + \alpha\sigma_{Cp} \tag{3}$$

$$\overline{Cr} - \alpha\sigma_{Cr} < Cr < \overline{Cr} + \alpha\sigma_{Cr} \tag{4}$$

$$\overline{Tr} - \alpha\sigma_{Tr} < Tr < \overline{Tr} + \alpha\sigma_{Tr} \tag{5}$$

$$\overline{E} - \alpha\sigma_{E} < \mathrm{E} < \overline{E} + \alpha\sigma_{E} \tag{6}$$

$$\overline{Cx} - \alpha\sigma_{Cx} < Cx < \overline{Cx} + \alpha\sigma_{Cx} \tag{7}$$

$$\overline{Cy} - \alpha\sigma_{Cy} < Cy < \overline{Cy} + \alpha\sigma_{Cy} \tag{8}$$

The constants T_A and α are empirically determined. In our experiments, we have determined that the empirical values are T_A =30, α=3. The equations (1) to (8) constitute the 3σ-classifier, which is to be used in the testing phase.

Testing phase : During the testing phase, the area A, the ratio R, the compactness Cp, the circularity Cr, the tortousity Tr, the extent E and the centriod, $C=(Cx, Cy)$ are computed for a region of the segmented image and apply the above classification rules to determine whether it is a follicle or not. The comparison of the experimental results for the two sample images with the manual segmentation done by medical expert is presented in the Figure 4. There is good agreement between the segmented image and the manual segmentation done by the medical expert, which demonstrates the efficiency of the edge based method. The manual segmentation is done by the team of three medical experts (Radiologists (2) and Gynaecologist (1)).

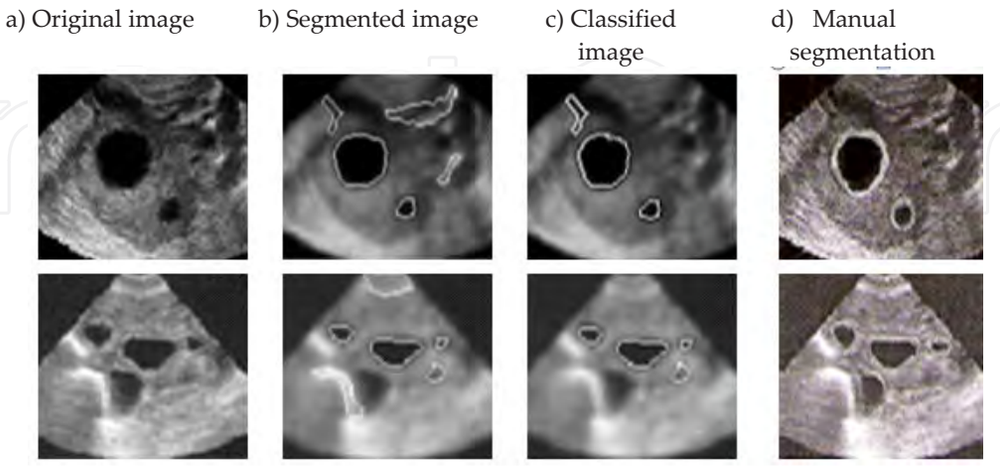

Figure 4. Some typical results: a) Original images, b) Segmentation by edge based method, c) Classified image, d) Manual segmentation by medical expert.

b. Watershed segmentation method

The follicle detection in ultrasound images of ovaries using watershed segmentation method uses the watershed transform for segmentation, geometric features for feature extraction and 3σ-intervals around the mean for the purpose of classification [22]. We follow three steps in the segmentation, first, the internal marker image is obtained, second, external marker image is obtained, and third, modifying gradient of the original image, by mask. In next phase, segmentation is carried out by applying marker controlled watershed transform to modified gradient image, region filling and clearing the border. Finally, preserve the regions which are most probably appear as follicles, while all other regions are removed. The feature extraction is based on seven geometric parameters of the follicles and the classification of regions for follicle detection is based on 3σ intervals around the mean. The experimental results are in good agreement with the manual follicle detection by medical experts.

c. Optimal thresholding method

In the automatic detection of follicle in ultrasound images of ovaries using optimal thresholding method, sobel operator and morphological opening and closing is used for preprocessing, optimal thresholding for segmentation and 3σ-intervals around the mean for classification are used [23]. Initially, the image is processed with finding the gradient by using sobel operators in horizontal direction. For the gradient image morphological opening and closing is applied by using appropriate structuring element. Then thresholding is applied to the filtered image by optimal thresholding method [24]. In the process, many undesired spurious regions are also obtained (e.g., regions inside the endometrium). These spurious regions must be removed as much as possible and all regions touching the borders are removed, which yields the segmented image. The feature extraction is based on seven geometric parameters of the follicles and the classification of regions for follicle detection is based on 3σ intervals around the mean. The experimental results are in good agreement with the manual follicle detection by medical experts.

2.1. HRGMF and thresholding

Ultrasound ovary images show planar sections through the follicles. These images are characterized by specular reflections and edge information, which is weak and discontinuous. Therefore, traditional edge detection techniques (e.g. Sobel, Prewitt) are susceptible to spurious responses when applied to ultrasound imagery. The main reason, that the follicle segmentation using solely edge information is rather unsuccessful, is a high level of added speckle noise [25]. The follicles being fluid-filled sacs appear as dark oval regions because they display similar fluid echotextures, which are more or less darker than their neighbourhood. The follicles could therefore be treated as homogeneous dark regions.

The main idea behind the HRGMF based method is as follows: [26]: In the first phase, the homogeneous region growing mean filter (HRGMF) is applied [27]. By using this filter, first homogeneous region can be identified and then this region is grown until it satisfies the similarity criteria. The value of filtering point is replaced by arithmetic mean of the grown region. In next phase, segmentation is carried out, by binarising the filtered image with three

different thresholds, T1, set as standard deviation of the input image, T2, set as mean of the input image, T3, set as abs(T2-T1). The resultant images are combined after thresholding. The components are labelled, the holes inside the regions are filled, the borders if any are cleared. Finally, the regions which most probably appear as follicles are preserved, while all other regions are removed. The feature extraction is based on seven geometric parameters of the follicles and the classification of regions for follicle detection is based on 3σ intervals around the mean.

The experimentation has been done using two datasets D1 and D2. The D1 set consists of the 80 sample ultrasound ovarian images of size 256x256, out of which 40 images are used for training and 40 for testing. The D2 set consists of 90 sample ultrasound images of ovaries of size 512x512, out of which 45 images are used for training and 45 for testing. The ten-fold experiments are performed for the classification and the average follicle detection rate is computed.The Table 1 shows the classification results of the proposed method after ten-fold experiments for both the data sets D1 and D2. The average detection rates for the proposed method with D1 and D2 sets are 79.77% and 68.86%, false acceptance rates (FAR) are 25.99% and 28.41%, and false rejection rates (FRR) are 20.52% and 31.12%, respectively.

	Classification results for ten-fold experiments	
Data set	D1 set	D2 set
Classification rate	79.77%	68.86%
Type I error (FAR)	25.99%	28.41%
Type II error(FRR)	20.52%	31.12%

Table 1. Classification results of proposed method after ten-fold experiments.

The proposed HRGMF based method for follicle detection is more effective as compared to the edge based method, watershed based segmentation method and optimal thresholding methods. The experimental results are in good agreement with the manual follicle detection by medical experts, and thus demonstrate efficacy of the method. Thus, the proposed HRGMF based method for follicle segmentation is effective in computer assisted fertility diagnosis by the experts.

2.2. Contourlet transform and scanline thresholding

The follicle detection rate in the homogeneous region growing mean filter (HRGMF) based method is considerably improved. However, due to speckle noise, finding the object boundaries is difficult and thus leads to poor segmentation. To improve the segmentation accuracy, the contourlet transform is used for despeckling the ultrasound image followed by histogram equalization, and, thereafter, the horizontal and vertical scanline thresholding (HVST) method is employed for follicle detection using geometric parameters.

Contourlet transform : The first step of the algorithm is denoising the image, since ultrasound images are invariably noisy due to the mode of the image acquisition itself. (e.g. head of the

http://dx.doi.org/10.5772/56518

ultrasound device is not moist enough). Especially, a disturbing type of noise is the speckle noise. Therefore the more efficient speckle reduction method based on the contourlet transform is used for denoising medical ultrasound images [28]. The contourlets can be loosely interpreted as a grouping of nearby wavelet coefficients since their locaters are locally correlated due to smoothness of the boundary curve [29, 30]. The contourlet transform is a multiscale and multidirectional framework of discrete image [31]. It is the simple directional extension for wavelet that fixes its subband mixing problem and improves its directionality. In this transform, the multiscale and multidirectional analyses are separated in a serial way. The laplacian pyramid (LP), is first used to capture the point discontinuities followed by a directional filter bank (DFB) to link point discontinuities into linear structure. Thus, we perform a wavelet like transform for edge detection, and then a local directional transform for contour segment detection. In other words, the contourlet transform comprises a double filter bank approach for obtaining sparse expansions for typical images with contours.

The contourlet transform exploits smoothness of contour effectively by considering variety of directions following contour. The contourlet transform can be designed to be a tight frame along with thresholding in order to achieve denoising of the image more effectively. The algorithm for contourlet transform method is as follows [32,33] : Firstly, apply the log transform to the input ultrasound image. Then, apply the contourlet transform on the log transformed image upto n levels of Laplacian pyramidal decomposition and m directional decompositions at each level, where n and m depend on the image size. Next, perform thresholding of contourlet transformed image. Lastly, the despeckled image is obtained by performing inverse contourlet transform on the thresholded image. Then, histogram equalization is applied to enhance the contrast of the despeckled image.

i. Horizontal and Vertical Scanline (HVST) based method

Firstly, all the pixels which are darker than their neighborhood row wise (horizontal scan) and then column wise (vertical scan) is collected. Then, the two resultant images are added to yield a segmented image. The regions with area less than a threshold value are removed. The holes inside the region are filled. The nonzero pixels touching the image border are set to zero [34,35].

Horizontal Scanline Thesholding (HST) : The follicle region will have more or less same grey level value for all the pixels within it. The horizontal scanline thresholding method is described as follows; Consider the input image f of the size MxN. The sample mean m_i and standard deviation σ_i of the ith row subimage of f are given by the equations 9 and 10 :

$$m_i = \frac{1}{N}\sum_{j=1}^{N} f(i,j) \tag{9}$$

$$\sigma_i = \sqrt{\left(\frac{1}{N}\sum_{j=1}^{N}(f(i,j)-m_i)^2\right)} \tag{10}$$

Now, set T4 = m_i and T5 = σ_i. Then multiply T4 and T5 by positive scale factors K1 and K2 (empirically fixed). Binarize ith row subimage using the thresholds K1T4 and K2T5 separately. This procedure is carried out for the rows i=1,...,M and obtain the horizontal mean (standard deviation) thresholded image fhm (fhsd).

Vertical Scanline Thresholding (VST): The VST method is described as follows; Consider the input image f of the size MxN. The sample mean m_j and standard deviation σ_j of the jth column subimage are given by the equations 11 and 12:

$$m_j = \frac{1}{M}\sum_{i=1}^{M} f(i,j) \tag{11}$$

$$\sigma_j = \sqrt{\frac{1}{M}\sum_{i=1}^{M}(f(i,j) - m_j)^2} \tag{12}$$

Now, set T6 = m_j and T7 = σ_j. Then multiply T6 and T7 by positive scale factors K3 and K4 (empirically fixed), respectively. Binarize jth column subimage using thresholds K3T6 and K4T7 separately. This procedure is carried out for the columns j=1,...,N and obtain the vertical mean (standard deviation) thresholded image fvm (fvsd).

Image Fusion: The resultant images fhm and fvm are combined, to yield the image fhvm. Any region touching the borders are removed. The resultant images fhsd and fvsd are combined, to yield the image fhvsd. Any region touching the borders are removed. Finally, the resultant images fhvm and fhvsd are combined, to yield the segmented image fseg, which contains segmented regions in it. The regions in fseg having smaller area than the threshold T8 are removed. The regions are labeled (identified) and possible holes inside them are filled.

The geometric features are extracted and then 3σ-intervals around the mean are used for classification. The Table 2 shows the classification results of the HVST based method after ten-fold experiments for both the data sets D1 and D2. The average detection rates for the proposed Method I with D1 and D2 sets are 90.10% and 92.76%, false acceptance rates (FAR) are 11.71% and 9.89%, and false rejection rates (FRR) are 21.55% and 7.23%, respectively.

	Classification results for ten-fold experiments	
Data set	D1 set	D2 set
Classification rate	90.10%	92.76%
Type I error (FAR)	11.71%	21.55%
Type II error(FRR)	9.89%	7.23%

Table 2. Classification results of proposed method after ten-fold experiments.

ii. *Edge based method:* The edge based segmentation method, which is described in the section 2 (a), is applied to the histogram equalized image obtained after despeckling the input image using contourlet transform [36]. The follicle detection rate is improved in the edge based segmentation after applying contourlet transform and histogram equalization, as compared to the method in the section 2(a) which employs Gaussian low pass filter and edge based segmentation.

The HVST based method for the follicle detection is more effective as compared to edge based segmentation after applying contourlet transform and histogram equalization.

3. Active contour method for follicle detection

The active contour method is used for segmentation of ultrasound image to increase the follicle detection accuracy. Either 3σ intervals based classifier or fuzzy classifier may be employed for follicle detection.

i. Active contour method with 3σ intervals based classification

The follicle detection in ultrasound images of ovaries using active contour method uses the contourlet transform based method for preprocessing, active contour method for segmentation and 3σ-intervals around the mean for classification [37]. Initially, the input image is despekled by using the contourlet transform method. Next, histogram equalization is applied to enhance the contrast of the despeckled image. Further, the negative transformation is applied on the histogram equalized image [38], as the proposed segmentation method works on high intensity valued objects. In the segmentation stage, the active contour without edges method is used [39]. The resulting image after applying active contour method contains segmented regions with it. The geometric features are extracted and then 3σ-intervals around the mean is used for classification.

The Figure 5 (a) depicts sample original ultrasound image of the ovary. The resultant images obtained at different steps of the proposed method are shown in the Figure 5 (b)-(e). Many undesired spurious regions are also obtained (e.g., regions inside the endometrium). These spurious regions must be removed as much as possible. Therefore, the regions having an area less than T (empirical value) are removed (Figure 5(f)). The Figure 5(g) depicts the segmented follicles (outlined in white) superimposed on the original image. The Figure 5(h) depicts the recognized follicles after applying the classification rules and the Figure 5(i) shows the follicles annotated manually by the medical expert.

The Figure 6 depicts comparison of the active contour method with the HVST based segmentation method. In the Figure 6, (a) and (e) are two original images, while (b) and (f) are their corresponding segmented images by HVST method. Similarly, (c) and (g) are segmented images of active contour method. It is observed that the follicles, which were not detected by HVST based segmentation method (Figure 6 (b) and (f)), are correctly identified by the active contour method (Figure 6 (c) and (g)). The Figure 6 (d) and (h) show the manual segmentation rendered by the medical expert. Hence, the classification accuracy is improved in the active

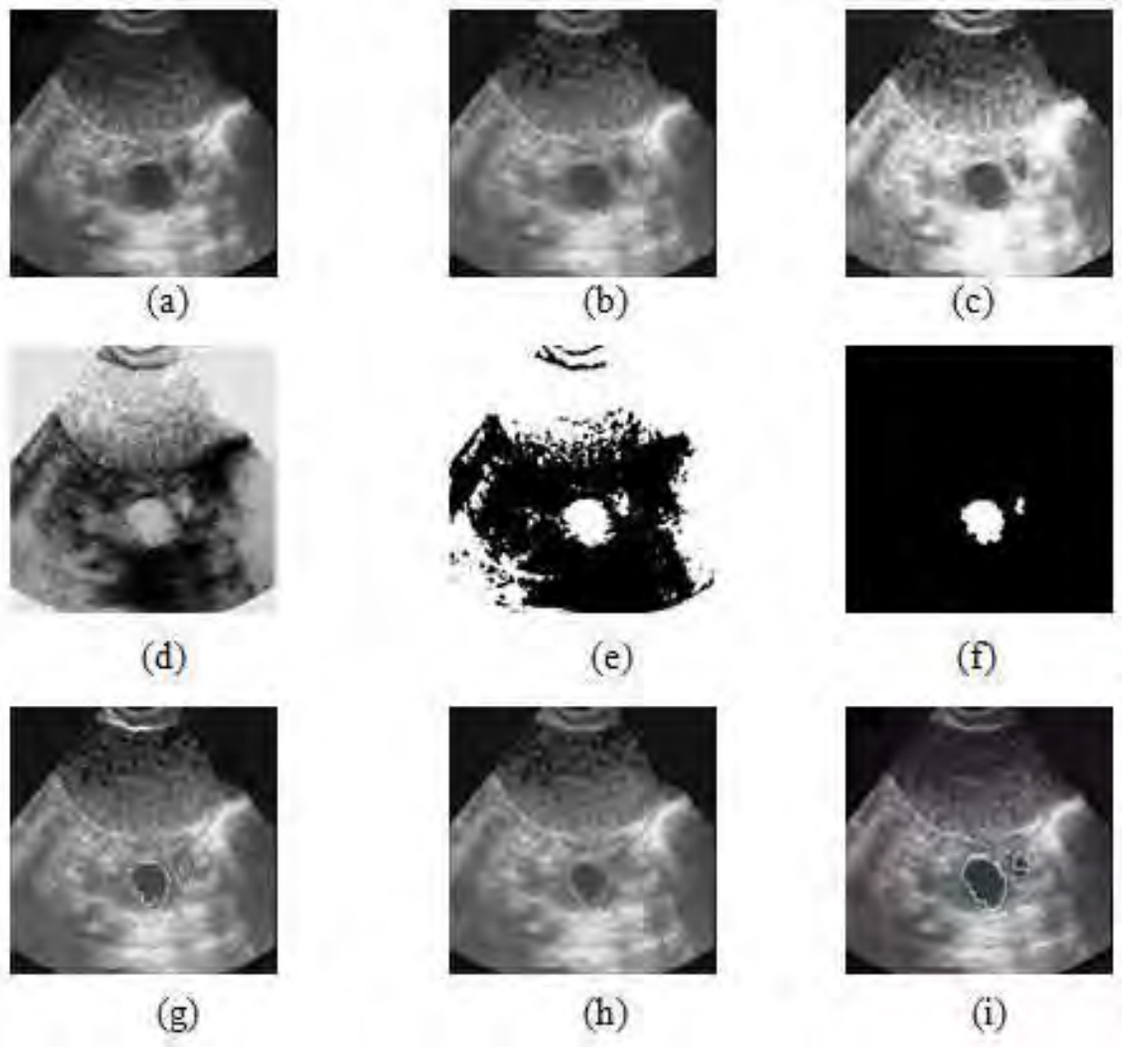

Figure 5. Original ultrasound image of the ovary and resultant images at different steps of proposed method. a) Original image, b) Contourlet transformed image (despeckling), c) Histogram equalized image, d) Image after applying negative transformation, e) Image after applying active contour without edges method, f) Segmented image after clearing the border, filling the holes and removing the small regions, g) Image showing recognized follicles(outlined in white) super imposed on the original image, h) Output image after classification, i) Manual segmentation of follicles by medical expert.

contour method as compared to HVST based segmentation method. The Table 3 presents the comparison of the experimental results of active contour method and HVST based method obtained for the original images in Figure 6. It is observed that the HVST based method leads to higher false acceptance rate (FAR) and false rejection rate (FRR). Further, the active contour method is found to yield more accurate results.

The Table 4 shows the comparison of classification results of the active contour method and the HVST based method after performing ten-fold experiments for both the data sets D1 and D2. The average detection rates for the active contour method using D1 and D2 sets are 92.3% and 96.66%, false acceptance rates (FAR) are 13.90% and 15.04%, and false rejection rates (FRR)

http://dx.doi.org/10.5772/56518

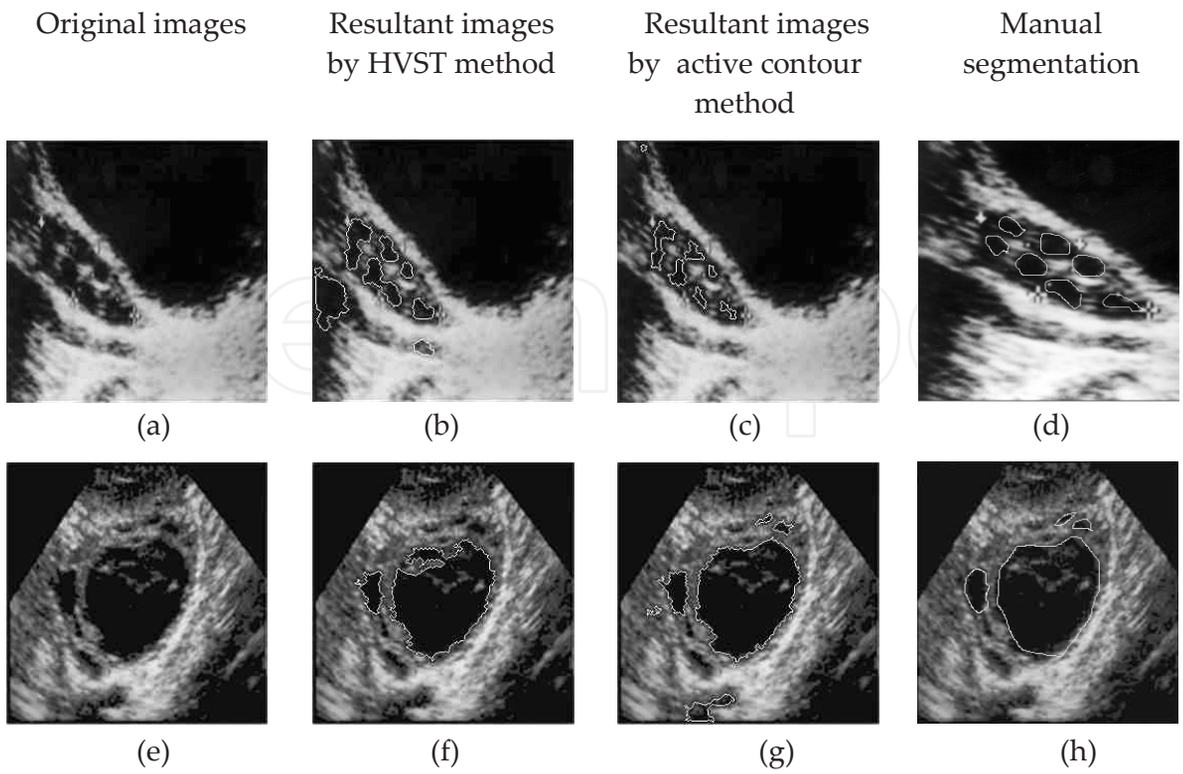

Figure 6. Comparison of resultant images of the active contour method with the HVST based method for two different original images. (a) and (e) original image, (b) and (f) resultant images of HVST method, (c) and (g) resultant images of the active contour method, (d) and (h) manual segmentation by medical expert.

Original Image	Number of follicles detected						
	Active contour method			HVST based method			Manual (by medical expert)
	Total	Correct	False	Total	Correct	False	
Figure 6 (a)	6	6	-	6	5	1	7
Figure 6 (e)	6	4	2	2	2	-	4

Table 3. Comparison of experimental results of active contour method and HVST based method for original images in Figure 6.

are 7.62% and 3.33%, respectively. The average detection rates for the HVST based method using D1 and D2 sets are 90.29% and 92.76%, false acceptance rates (FAR) are 14.10% and 21.55%, and false rejection rates (FRR) are 9.60% and 7.23%, respectively. Clearly, the method based on active contours outperforms the HVST based method.

	Classification results			
Data set	**D1 set**		**D2 set**	
Method	Active contour method	HVST based method	Active contour method	HVST based method Based Method
Classification rate	92.3%	90.29%	96.66%	92.76%
Type I error (FAR)	13.90%	14.10%	15.04%	21.55%
Type II error (FRR)	7.62%	9.60%	3.33%	7.23%

Table 4. Comparison of average classification results of the active contour method with the HVST based method after performing ten-fold experiments.

ii. Active contour method with fuzzy classification

To improve the performance of follicle detection in ultrasound images of ovaries, a new algorithm using fuzzy logic is developed. The method employs contourlet transform for despeckling, histogram equalization and negative transformation in the preprocessing step, the active contours without edges method for segmentation and fuzzy logic for classification. The seven geometric features are used as inputs to the fuzzy logic block of the Fuzzy Inference System (FIS). The output of the fuzzy logic block is a follicle class or non follicle class. The fuzzy-knowledge-base consists of a set of physically interpretable if-then rules providing physical insight into the process. The experimentation has been done using sample ultrasound images of ovaries and the results are compared with the inferences drawn by 3σ interval based classifier and also those drawn by the medical expert. The experimental results demonstrate the efficacy of the fuzzy logic based method [40].

Fuzzy set theory has been successfully applied to many fields, such as pattern recognition, control systems, and medical applications [41,42]. It has also been effectively used to develop various techniques in image processing tasks including ultrasound images [43]. The existence of inherent "fuzziness" in the nature of these images in terms of uncertainties associated with definition of edges, boundaries, and contrast makes fuzzy set theory an interesting tool for handling the ultrasound imaging applications [44]. Fuzzy logic was initiated in 1965 by L. A. Zadeh [45-48].

Training phase: The fuzzy inference system (FIS) of sugeno type is employed using the fuzzy input variables the ratio R of majoraxislength to minoraxislength, the compactness Cp, the circularity Cr, the tortuousity Tr, the extent E and the centriod C= (Cx, Cy) and output variables: follicle and non follicle classes. The Gaussian membership function is used for each of the fuzzy input variables with mean and standard deviation of the corresponding variables. Let mfr, mfcp, mfcr, mftr, mfe, mfcx and mfcy be the Gaussian membership functions of the fuzzy input variables R, Cp, Cr, Tr, E and C=(Cx,Cy), respectively, belonging to the follicle class. Let mfr1, mfcp1, mfcr1, mftr1, mfe1, mfcx1 and mfcy1 be the Gaussian membership functions of these input variables belonging to the non-follicle class.

http://dx.doi.org/10.5772/56518

During the training phase, the geometrical features, namely, R, Cp, Cr, Tr, E and C=(Cx,Cy), are computed for regions known to be follicles in the training images in consultation with the medical expert. Then, the mean and standard deviation of each of the geometric parameters R, Cp, Cr,Tr, E and C=(Cx,Cy), are computed which are used to set the rules for classification of follicles. The mean and standard deviation of these parametric values are stored as knowledge base which is shown in the Table 5. These values are used as the pattern (parameters) in FIS membership function design.

	Mean value	**Standard deviation**
Ratio(R)	1.82	0.58
Compactness (C_p)	37.35	10.16
Circularity (C_r)	0.37	0.09
Tortousity (T_r)	0.27	0.03
Extent (E)	0.51	0.09
Centriod C=(Cx,Cy)	(251, 55)	(201,70)

Table 5. The knowledge base of mean and standard deviation of parametric values of geometric features or the follicle regions

The construction of the membership functions for the output variables is done in the similar manner. Since this is Sugeno-type inference (precisely, zero-order Sugeno), constant type of output variable fits the best to the given set of outputs (1 for follicle and 0 to non-follicle classes). Based on the descriptions of the inputs (the ratio R of majoraxislength to minoraxislength, the compactness Cp, the circularity Cr, the tortousity Tr, the extent E and the centriod C=(Cx,Cy)) and output variables (follicle and non follicle). The fuzzy rules for classification procedure in verbose format are as follows:

i. IF (R is input to mfr) AND (Cp is input to mfcp) AND (Cr is input to mfcr) AND (Tr is input to mftr) AND (E is input to mfe) AND (Cx is input to mfcx) AND (Cy is input to mfcy) THEN (class is follicle)

ii. IF (R is input to mfr1) AND (Cp is input to mfcp1) AND (Cr is input to mfcr1) AND (Tr is input to mftr1) AND (E is input to mfe1) AND (Cx is input to mfcx1) AND (Cy is input to mfcy1) THEN (class is non-follicle).

At this point, the fuzzy inference system has been completely defined, in that the variables, membership functions and the rules necessary to determine the output classes are in place.

Testing phase: During the testing phase, the geometric features R, Cp, Cr, Tr, E and C= (Cx, Cy) are computed for each segmented region of the input image and then the above fuzzy classification rules are applied to determine whether the region is a follicle or not a follicle.

Experimental results: The ten-fold experiments are performed for the classification and the average follicle detection rate is computed. The Figure 7 (a) depicts an original ultrasound

image of the ovary and the resultant images at different steps of fuzzy based method are shown in Figure 7(b)-(e). Many undesired spurious regions are also obtained (e.g., regions inside the endometrium). These spurious regions must be removed as much as possible. Therefore, the regions having an area less than T are removed (Figure 7(f)). The Figure 7 (g) depicts the segmented follicles (outlined in white) superimposed on the original image. The Figure 7 (h) depicts the recognized follicles after applying classification rules and Figure 7 (i) shows the follicles annotated manually by the medical expert.

The Figure 8 depicts comparison of the fuzzy logic based classification with the 3σ intervals based classification [section 3(i)]. In the Figure 8 (a) and (d) are two original images, (b) and (e) are their corresponding resultant images by the 3σ intervals based method. and, (c) and (f) are resultant images of fuzzy based method. It is observed that the regions which are misclassified as follicles, by the method in [section 3(i)] (Figure 8 (b) and (e)), are correctly classified by the fuzzy logic based method (Figure 8 (c) and (f)). Hence, the classification accuracy of the fuzzy logic based method is improved as compared to the method in [section 3(i)]. The Table 6 presents number of follicles detected in the results of the fuzzy based method and the method in [section 3(i)] corresponding to the original images in the Figure 8.

	Number of follicles detected						
Method	**fuzzy based method**			**3σ intervals based method [section 3(i)]**			**Manual (by medical expert)**
Input original image	Total	Correct	False	Total	Correct	False	
Figure 8(a)	3	3	-	5	3	2	3
Figure 8(d)	1	1	-	3	1	2	1

Table 6. Comparison of experimental results of proposed fuzzy logic based classification and 3σ interval based classification based method for original images in the Figure 8.

The Table 7 shows the comparison of classification results of fuzzy based method and the method in [section 3(i)] after ten-fold experiments for both the data sets. The average detection rates for the fuzzy based method with D1 and D2 sets are 98.18% and 97.61%, false acceptance rates (FAR) are 4.52% and 9.05%, and false rejection rates (FRR) are 1.76% and 2.37%, respectively. The average detection rates for the method in the Section 3(i) with D1 and D2 sets are 92.3% and 96.66%, false acceptance rates (FAR) 13.6% and 15.04%, and false rejection rates (FRR) are 7.62% and 3.33%, respectively. It is observed that the false acceptance rate (FAR) is reduced and the classification accuracy is improved in case of the fuzzy logic based method as compared to that in the 3σ intervals based method [section 3(i)] for classification.

http://dx.doi.org/10.5772/56518

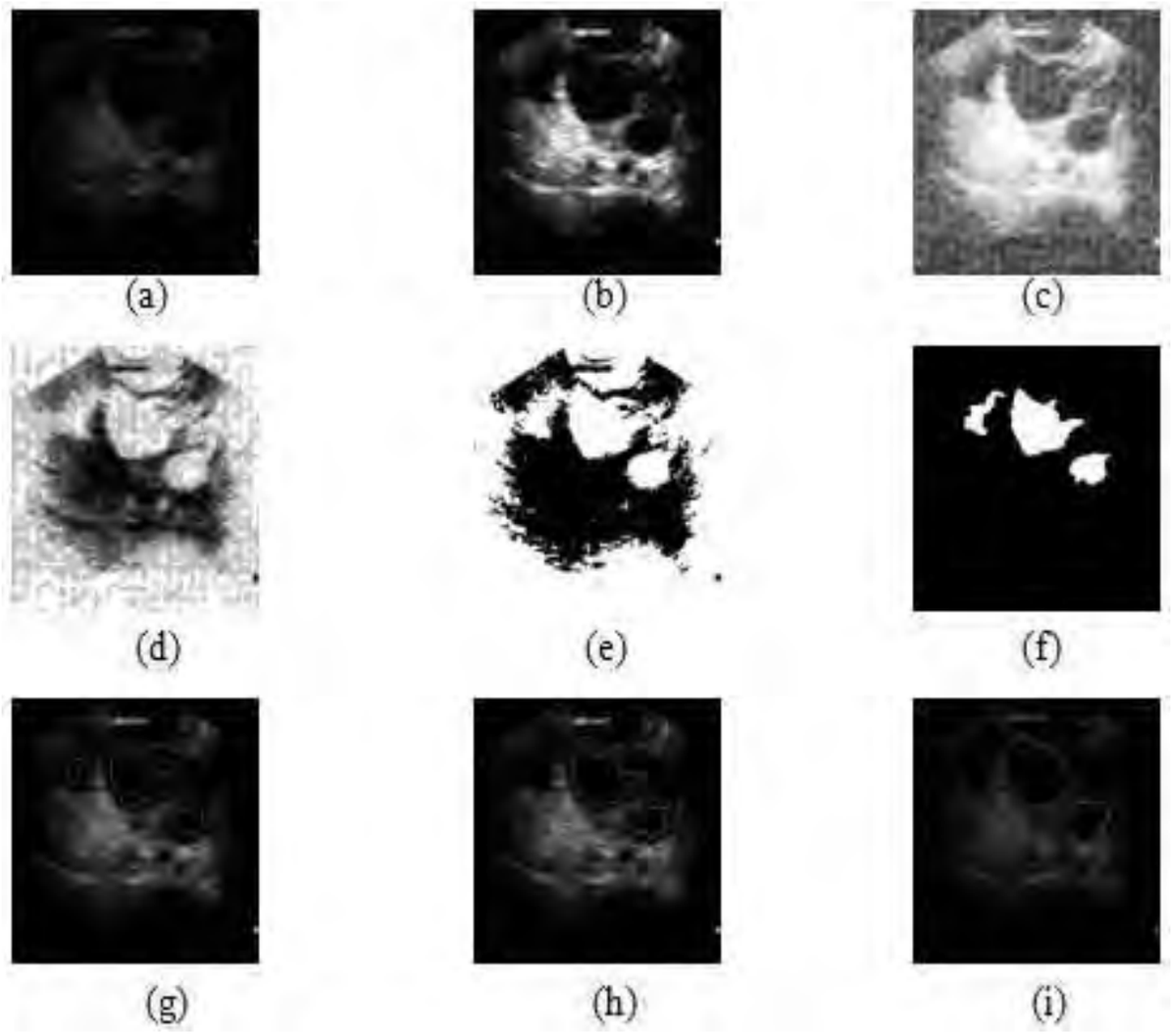

Figure 7. Original ultrasound image of the ovary and resultant images at different steps of fuzzy based method. a) Original image, b) Contourlet transformed image (despeckling), c) Histogram equalized image, d) Image after applying negative transformation, e) Image after applying active contour without edges method, f) Segmented image after clearing the border, filling the holes and removing the small regions, g) Image showing recognized follicles(outlined in white) super imposed on the original image, h) Output image after fuzzy classification, i) Manual segmentation of follicles by medical expert.

4. Ovarian classification

The ovaries are classified into three types based on the number and size of the follicles. Ovary is scanned, follicles are identified by using the method described the section 3, and the size of the follicles are measured and the number of follicles are counted.

There are three categories :

- The ovary containing 1-2 follicles with size measuring greater than 28mm in size, is a cystic ovary.

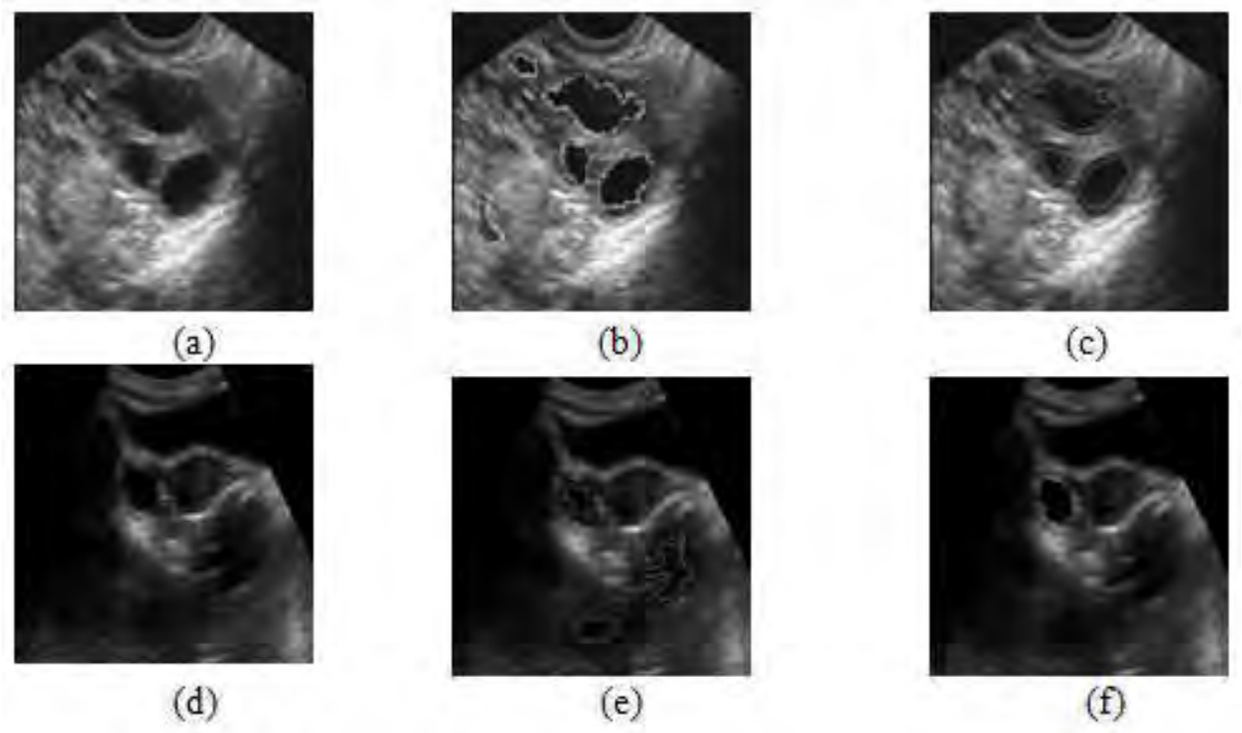

Figure 8. Comparison of resultant images of the fuzzy based method with the 3σ intervals based classification for two different original images. (a) and (d) original images, (b) and (e) resultant images of 3σ intervals based, (c) and (f) resultant images of fuzzy based method.

- The ovary containing 12 or more follicles with size measuring less than 10mm, is a polycystic ovary.
- The ovary containing 1-10 follicles with size measuring 2-10mm, are antral follicles and with the 10-28mm size, are dominant follicles, is a normal ovary with m number of antral follicles and n number of dominant follicles.

The two ovarian classification methods are discussed below [Hiremath and Tegnoor, 2012]:

i. Fuzzy ovarian classification

Training phase: The fuzzy inference system (FIS) of sugeno type is employed using the fuzzy input variables the number of follicles NN and the size of the follicle S and output variables: normal, cystic and polycystic ovarian classes. The Trapezoidal membership function is used for each of the fuzzy input variables with minimum and maximum value of the corresponding variables. Let mfn1 and mfs1, mfn2 and mfs2, and mfn3 and mfs3, be the trapezoidal membership functions of the fuzzy input variables NN and S respectively, belonging to the normal ovarian class, cystic ovarian class, polycystic ovarian class.

During the training phase, the parameters, namely, NN and S, are computed for the ovarian images known to be healthy, cystic and polycystic ovary in the training images in consultation with the medical expert, which are used to set the rules for classification of ovarian images.

We denote,

http://dx.doi.org/10.5772/56518

n1 - number of follicles of normal ovary

sz1 - size of the follicles in the normal ovary

n2 - number of follicles of cystic ovary

sz2- size of the follicles in the cystic ovary

n3 - number of follicles of polycystic ovary

sz3 - size of the follicles in the polycystic ovary

The number of follicles and size of follicles of these three classes are stored as knowledge base which is shown in the Table 8.

	Classification results			
Data set	**D1 set**		**D2 set**	
Methods	Fuzzy logic method	3σ interval based method [section 3(i)]	Fuzzy logic method	3σ interval based method [section 3(i)] Based Method
Classification rate	98.18 %	92.3 %	97.61%	96.66%
Type I error (FAR)	4.52 %	13.6 %	9.05%	15.04%
Type II error (FRR)	1.76 %	7.62 %	2.37 %	3.33 %

Table 7. Comparison of classification results of fuzzy based classification method with 3σ intervals based method after ten-fold experiments.

The construction of the membership functions for the output variables is done in the similar manner. Since this is Sugeno-type inference (precisely, zero-order Sugeno), constant type of output variable fits the best to the given set of outputs (0 for normal ovary and 0.5 for cystic ovary and 1 for polycystic ovary). Based on the descriptions of the inputs (the number of the follicles NN and size of the follicles S) and output variables (normal ovary, cystic ovary, polycystic ovary). The fuzzy rules for classification procedure in verbose format are as follows:

i. IF (n1 is input to mfn1) AND (sz1 is input to mfs1) THEN (class is normal ovary)

ii. IF (n2 is input to mfn2) AND (sz2 is input to mfs2) THEN (class is cystic ovary)

iii. IF (n2 is input to mfn3) AND (sz3 is input to mfs3) THEN (class is polycystic ovary)

At this point, the fuzzy inference system has been completely defined, in that the variables, membership functions and the rules necessary to determine the output classes are in place.

Image type	Number of follicles	Size of the follicle
Normal ovary	1-10	15-10000
Cystic ovary	1-2	4300-75000
Polycystic ovary	12-20	15-9000

Table 8. The knowledge base of number of follicles and size of follicles of all the three classes

Testing phase: During the testing phase, we compute the number of follicles NN, and the size of each follicle S, for an ovary with the detected follicles and apply the above classification rules to determine whether an ovary is normal, cystic, and polycystic.

Experimental results: The experimentation is done using image data set D3. The D3 set consists of 70 sample ultrasound ovarian images of size 512x512, out of which 35 images are used for training and 35 for testing. In the first step, the ten-fold experiments for the follicle detection are done and then the average follicle detection rate is computed. Further, in the second step, for the ovary classification, 70 sample images of the detected follicles are used, of which 35 are used for training and 35 are used for testing. The ten-fold experiments for the ovarian classification are done and the average classification rate for the ovarian type is computed. The Figure 9 shows the sample results for the ovarian classification method. detection method after performing ten-fold experiments for the image data set. The Table 9 shows the average classification results of follicle detection method after performing ten-fold experiments for the image data set. The follicle detection method (Section 3(ii)) yields the average detection rate for the fuzzy based method 98.47%, false acceptance rate (FAR) 2.61% and false rejection rate (FRR) 1.47%.

Classification rate	Type I error (FAR)	Type II error (FRR)
98.47%	2.61%	1.47%

Table 9. Average classification results after ten-fold experiments

The Table 10 shows the ten-fold experimental results of the ovarian classification based on fuzzy inference rules. It is observed that the average normal ovary cyst ovary and polycystic ovary is 100%, with zero false acceptance rate is (FAR) and false rejection rate (FRR). Although, the proposed ovarian classification method yields 100% classification results, it is to be noted that these results are with reference to the limited data set used for experimentation. However, in case of different data sets, with varying image resolution, image sizes and numbers, the classification accuracy may be less than 100%.

http://dx.doi.org/10.5772/56518

Ovarian class	Number of images	Number of correctly classified images	Manual detection	Type I error	Type II error
Normal ovary	15	15	15	-	-
Cystic ovary	10	10	10	-	-
Polycystic ovary	10	10	10	-	-

Table 10. Experimental results for classification accuracy for all the three classes

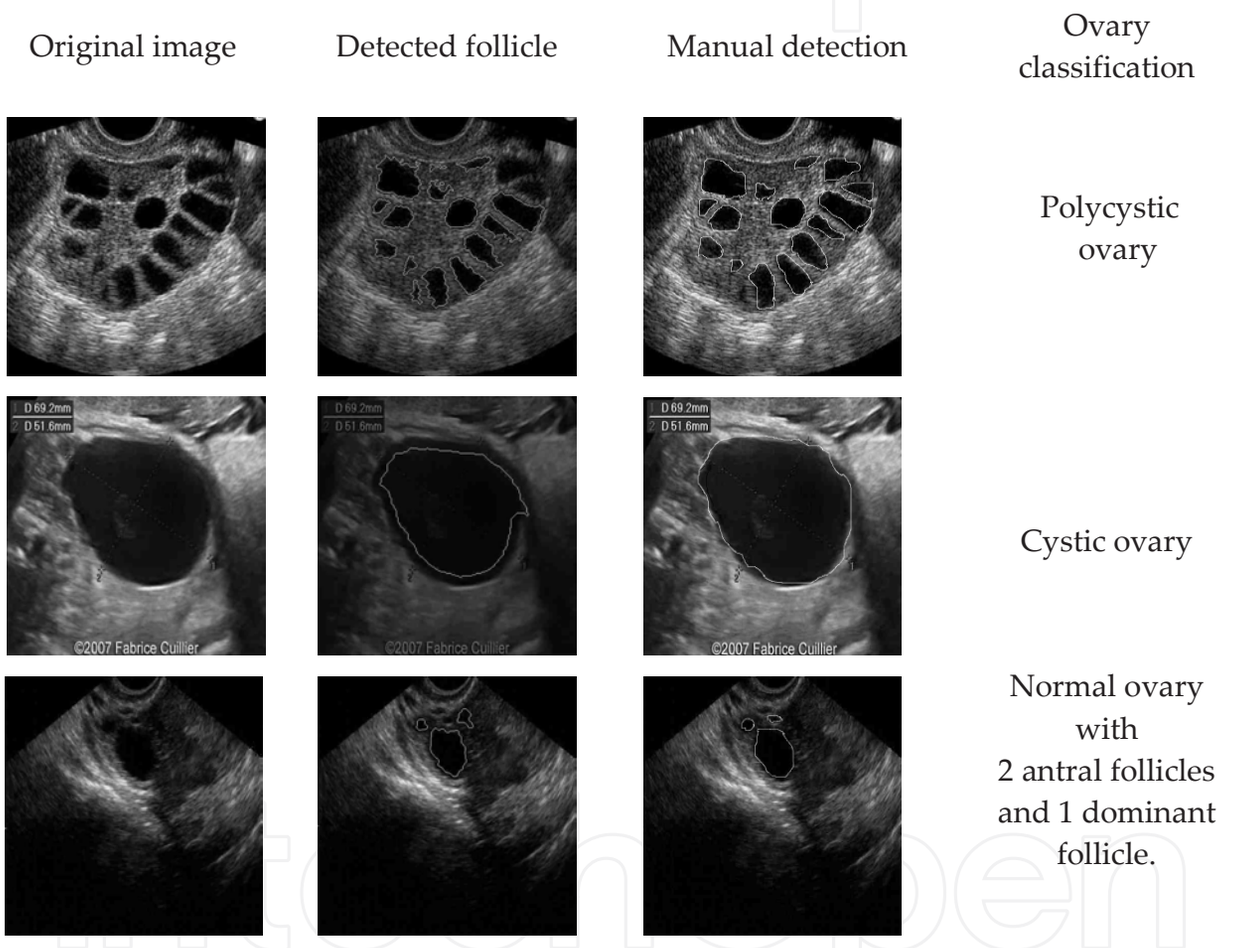

Figure 9. Sample results for proposed ovarian classification method

ii. Ovarian classification by using SVM

The aim of support vector machine (SVM) is to devise a computationally efficient way of learning separating hyper planes in a high dimensional feature space [49]. The SVMs have been shown to be an efficient method for many real-world problems because of its high generalization performance without the need to add a priori knowledge. Thus, SVMs have much attention as a successful tool for classification [50,51], image recognition [52,53] and

bioinformatics [54]. The SVM model can map the input vectors into a high-dimensional feature space through some non-linear mapping, chosen a priori. In this space, an optimal separating hyperplane is constructed. SVM is the implementation of the structural risk minimization principle whose object is to minimize the upper bound on the generalization error. Given a set of training vectors (l in total) belonging to separate classes, (x1, y1), (x2, y2), (x3, y3),..., (xl, yl), where $x_i \in R^n$denotes the ith input vector and $y_i \in \{+1, -1\}$ is the corresponding desired output. The maximal margin classifier aims to find a hyperplane w: wx + b = 0 to separate the training data. In the possible hyperplanes, only one maximizes the margin and the nearest data point of each class. The Figure 10 shows the optimal separating hyperplane with the largest margin. The support vectors denote the points lying on the margin border. The solution to the classification is given by the decision function in the equation 13.

$$f(x) = sign\left(\sum_{i=1}^{N_{SV}} \alpha_i y_i k(s_{i,} x) + b\right) \tag{13}$$

where $\alpha_i$is the positive Lagrange multiplier, s_i is the support vector (N_{SV} in total) and k(s_i, x) is the function for convolution of the kernel of the decision function. The radial kernels perform best in our experimental comparison, and, hence, are chosen in the proposed diagnosis system. The radial kernels are defined as (equation 14).

$$k(x, y) = \exp\left(-\gamma\left(x - y\right)^2\right) \tag{14}$$

By using the SVM method, firstly, follicles are detected and secondly, the ovarian classification is performed [55]. During the training phase, the parameters, namely, the number of follicles NN and the size of the follicle S, are determined for the ovarian images known to be normal, cystic and polycystic ovary in the training images in consultation with the medical expert. The quadratic kernel is used for training the three-class SVM classifier; normal, cystic and polycystic ovary being the three classes.

During the testing phase, the parameters, namely, the number of follicles NN and the size of follicles S, are determined, and then, the SVM classifier is used to determine whether an ovary is normal, cystic, or polycystic.

Experimental results: The Table 11 shows the comparison of classification results of SVM based method and the fuzzy based method in [section 4(i)] after ten-fold experiments. The average follicle detection rate for the SVM method is 98.89%, false acceptance rate (FAR) is 1.61 % and false rejection rate (FRR) is 1.10%. The average detection rate for the method in [section 4(i)] is 98.47%, false acceptance rate (FAR) is 2.61% and false rejection rate (FRR) is 1.47%. It is observed that the classification accuracy is improved in the SVM based method as compared to the fuzzy based method [section 4(i)].

http://dx.doi.org/10.5772/56518

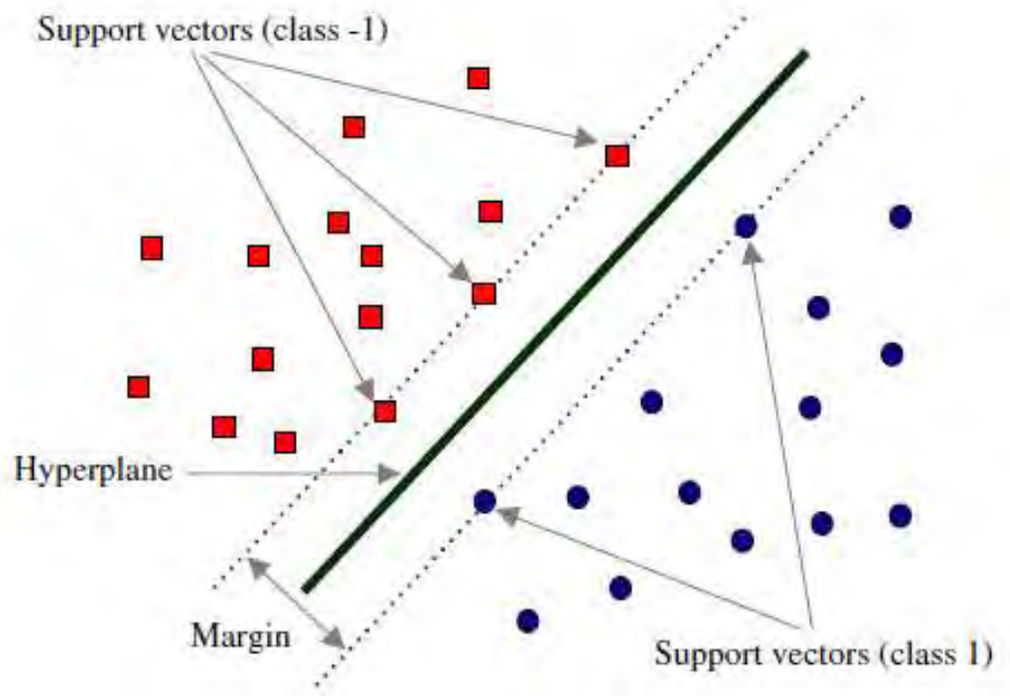

Figure 10. Optimal hyperplane for support vector machine

	Classification accuracy (%) of follicle detection	
Method	**SVM based method**	**Fuzzy based method [4(i)]**
Classification rate	98.89 %	98.47%
Type I error (FAR)	1.61 %	2.61%
Type II error (FRR)	1.10 %	1.47%

Table 11. Comparison of classification results of SVM based method and fuzzy based method [section 4(i)] for follicle detection after ten-fold experiments

The Table 12 shows the ten-fold experimental results of the ovarian classification based on SVM. It is observed that the average classification rates for normal ovary, cystic ovary and polycystic ovary are 100%, with zero false acceptance rate (FAR) and zero false rejection rate (FRR). It is observed that both the proposed SVM based method and the fuzzy based method [section 4(i)] yield 100% accuracy in ovarian classification, although the SVM outperforms the fuzzy method [section 4(i)] in follicle detection.

The Table 13 shows the comparison of all the follicle detection and ovarian classification methods developed in the present study and the other follicle detection methods available in the literature.

Ovary type	Number of images	Number of correctly classified images		Manual detection by expert	Type I error (FAR)		Type II error (FRR)	
		SVM	Fuzzy [4(i)]		SVM	Fuzzy [4(i)]	SVM	Fuzzy [4(i)]
Normal ovary	15	15	15	15	0	0	0	0
Cystic ovary	10	10	10	10	0	0	0	0
Polycystic ovary	10	10	10	10	0	0	0	0

* Type I Error: Regions are not follicles, but they are recognized as follicles.

**Type II Error: Regions are follicles, but they are not recognized as follicles.

Table 12. Experimental results for classification accuracy of the SVM based method for the three classes of ovaries in comparison with the fuzzy based method [section 4(i)]

Method	Data set used	Classification accuracy
Edge based method with Gaussian lowpass filter	D1	62.3%
	D2	45.2%
Watershed segmentation method	D1	49.55%
	D2	50.68%
Optimal thresholding method with Sobel operator	D1	50.77%
	D2	61.82%
HRGMF based thresholding method	D1	79.47%
	D2	68.86%
Edge based method with contourlet transform method	D1	75.2%
	D2	59.95%
HVST based method	D1	90.10%
	D2	92.76%
Active contour with 3σ interval based method	D1	92.37%
	D2	96.66%
Active contour with fuzzy classification	D1	98.18%

http://dx.doi.org/10.5772/56518

Method	Data set used	Classification accuracy
	D2	97.61%
Active contour with fuzzy classification of ovary	D3	98.47%
Active contour with SVM classification of ovary	D3	98.47%
Modified region growing and LD classifier [Maryruth et al., 2007]	(70)	83.25%
Region growing method [Potocnik and Zazula, 2000]	(50)	78%
Cellular neural network [Cigale and Zazula, 2000]	(50)	60%
Edge based method [Potocnick et al., 2002]	(50)	61%
Prediction based method [Potocnick and Zazula, 2002]	(50)	78%

Note : D1, D2 and D3 are image data sets.

Table 13. Comparison of the proposed method with all the other methods proposed in the present study and also with the other methods in the literature.

5. Conclusion

The main significant research contributions that fulfill the objectives set in the present chapter are :

i. Automatic detection of follicles using better segmentation and classification methods.

ii. Automatic ovarian classification into three categories, namely: normal ovary, cystic ovary and polycystic ovary.

The performance comparison of the various methods proposed in the present study and other methods in the literature is summarized in the Table 13. It is observed that :

i. the proposed method using contourlet transform based despeckling, active contour without edges based segmentation, geometric feature extraction and fuzzy logic or SVM based classifier, has yielded better follicle detection results; and,

ii. the proposed method for ovarian classification using fuzzy or SVM has yielded better classification results.

These research contributions are expected to be useful for the design and development of the software tool to support the medical experts, namely, Gynecologists and Radiologists, in their effort for ovarian image analysis and to implement the same in automated diagnostic systems. Further, these research contributions serve as the basis for design of automatic systems for the detection of the follicles inside the ovary under the examination during the entire female cycle and to study the ovarian morphology and, thus, help the medical experts for monitoring follicles and identifying the ovarian type during the course of infertility treatment of patients. The burden of the experts is significantly reduced in their everyday routine, without sacrificing the accuracy of diagnosis and prognosis.

The future research in this direction would be to take up the analysis of ovarian images captured at regular intervals for various subjects undergoing drug susceptibility tests. Further, the image processing methods could be developed in the detection of ovarian cancer stages.

Acknowledgements

Authors are thankful to Mediscan Diagnostics Care, Gulbarga, for providing the ultrasound images of ovaries. We are indebted to Dr. Suchitra C. Durgi, Radiologist, Dr. Chetan Durgi, Radiologist and Dr. Suvarna M. Tegnoor, Gynaecologist, Gulbarga, for helpful discussions and for rendering manual detection of follicles and ovarian classification in ultrasound images of ovaries.

Author details

P. S. Hiremath* and Jyothi R. Tegnoor*

Dept of Computer Science, Gulbarga University, Gulbarga, India

References

[1] Gougeon A. and Lefevre B. Evolution of the Diameters of the Largest Healthy and Atretic Follicles During the Human Menstrual Cycle, Reproduction and Fertility 1983;69: 497-502.

[2] Gougeon A., Adashi E. and Leung P. Dynamics of Human Follicular Growth, a Morphologic Perspective: Comprehensive Endocrinology, The Ovary, Raven Press, New York, 1993: 21-39.

[3] Pellicer A., Gaitán P., Neuspiller F., Ardiles G., Albert C., Remohí J. and Simón C., Ovarian Follicular Dynamics: From Basic Science to Clinical Practice, Journal of Reproductive Immunology 1998; 39(1-2) 29-61.

[4] Hanna M. D., Chizen D. R. and Pierson R. Characteristics of Follicular Evacuation During Human Ovulation, J Ultrasound Obstet Gynaecol 1994; 4(6) 488-493.

[5] Pierson R. and Chizen D. Ultrasonography of Normal and Aberrant Ovulation. Imaging in Infertility and Reproductive Endocrinology, 1994;155-166.

[6] Bal A. and Mohan H. Malignant Transformation in Mature Cystic Teratoma of the Ovary: Report of Five Cases and Review of the Literature, Arch Gynecol Obstet, 2007; 275(3)179-182.

[7] Yamanaka Y. and Tateiwa Y. Preoperative Diagnosis of Malignant Transformation in Mature Cystic Teratoma of The Ovary, Eur J Gynaecol Oncol 2005; 26(4)391-392.

[8] Battaglia C., Artini P. G., Genazzani A. D., Gremigni R., Slavatori M. R. and Sgherzi M. R., Color Doppler Analysis in Oligo and Amenorrheic Women with Polycystic Ovary Syndrome. Gynecolog Endocrinto, 1997;11:105-110.

[9] Balen Adam H., Joop S. E. Laven, Seang-Lin Tan and Didier Dewailly, Ultrasound Assessment of the Polycystic Ovary: International Consensus Definitions, Human Reproduction, 2003;9(6)505-511.

[10] Pache T. D., Wladimiroff J. W., Hop W. C. and Fauser B. C. How to Discriminate Between Normal and Polycystic Ovaries: Transvaginal US Study. Radiology 1992;183(2) 421-423.

[11] Kelsey T.W. and Wallace W. H. B. Ovarian Volume Correlates Strongly with Number of Non Growing Follicles in the Human Ovary, Obstretics and Gynocology International, 2012; Article-id 305025.

[12] Potocnik B., Zazula D., Korze D. Automated Computer-Assisted Detection of Follicles in Ultrasound Images of Ovary. Journal of Medical Systems 1997; 21(6) 445-457.

[13] Potocnik B., Viher B. and Zazula D. Computer assisted detection of ovarian follicles based on ultrasound images, Proc. of a szamitastechnika orvosies biological alkalmazasai, Verzprem, Hungary, pp. 24-34; 1998.

[14] Potocnik B. and Zazula D. Aktivne krivulje-nadgradnja razpoznavalnih sistemov (Active contours-an extension of recognition systems). Proceedings of 7th Electrotechnical and Computer Science Conference ERK 98, Portoroz, Slovenia, Vol. B, 1998; 249-252.

[15] Potocnik B. and Zazula D. Automated Analysis Of Sequence of Ovarian Ultrasound Images, Part I: Segmentation of Single 2D Images. Image Vision and Computing 2002; 20(3) 217-225.

[16] Sarty G. E., Liang W., Sonka M. and Pierson R. A. Semiautomated Segmentation of Ovarian Follicular Ultrasound Images Using a Knowledge Based Algorithm. Ultrasound in Medicine and Biology, 1998; 24(1)27-42.

[17] Cigale B. and Zazula D. Segmentation of Ovarian Ultrasound Images Using Cellular Neural Networks, International Journal of Pattern Recognition and Artificial Intelligence, 2004; 18, 563-581.

[18] Krivanek and Sonka M. Ovarian Ultrasound Image Analysis Follicle Segmentation. IEEE Transactions on Medical Imaging, 1998; 17(6) 935-944.

[19] Maryruth, Lawrence J. and Eramian Mark G. Computer Assisted Detection of Polycystic Ovary Morphology, Ultrasound Images 2007; 23(2) 306-309.

[20] Mehrotra P., Chakraborthy C., Ghoshdastidar B. and Ghostidas S. Automated Ovarian Follicle Detection for Polycystic Ovarian Syndrome, Proc. of IEEE International Conference on Image Information Processing (ICIIP), 3-5 Nov 2011, Himachal Pradesh, India, 1-4; 2011.

[21] Hiremath P. S. and Tegnoor J. R. Automatic Detection of Follicles in Ultrasound Images of Ovaries, Proc. of Second International Conference on Cognition and Recognition (ICCR-08), 15-17 Apr. 2008, Mysore, India, pp 468-473; 2008.

[22] Hiremath P. S. and Tegnoor J. R. Automatic Detection of Follicles in Ultrasound Images of Ovaries, Proc. of Third International Conference on Systemic, Cybernetics and Informatics (ICSCI-09), 07-10 Jan. 2009, Hyderabad, India, pp. 327-330; 2009.

[23] Hiremath P. S. and Tegnoor J. R. Automatic Detection of Follicles in Ultrasound Images of Ovaries by Optimal Threshoding Method, International Journal of Computer Science and Information Technology 2010; 3(2) 217-220.

[24] Gonzalez R. C. and Woods R. E. Digital Image Processing, Second Edition, Pearson Edu; 2002.

[25] Jing Hanm B S., Shin D. V., Arthur G. L. and Chi-Ren Shyu, 2010, Multiresolution Tile Based Follicle Detection Using Colour and Textural Information of Follicular Lymphoma IHC Slides, Proc. of IEEE International Conference on Biomedicine Workshop., 18-21 Dec. 2010, Hong Kong, China, pp. 886-87; 2010.

[26] Hiremath P. S. and Tegnoor J. R. Automatic Detection of Follicles in Ultrasound Images of Ovaries using HRGMF Based Segmentation, International Journal of Multimedia, Computer Vision and Machine Learning (IJMCVML) 2010; 1(1) 83-87.

[27] Koo Ja. I. and Song B. Park. Speckle Reduction with Edge Preservation, Medical Ultrasonics 1991; 3(13) 211-237.

[28] Srinivasrao Ch., Srinivaskumar S. and Chattergi B. N. Content Based Image Retrieval Using Contourlet Transform, ICGST-GVIP Journal 2007;7(3) 9-15.

[29] Jainping Zhou, Arthur L. Cunha and Minh N. Do, Non subsampled Contourlet Transform: Construction and Application in Enhancement, Proc. of IEEE International Conference on Image Processing, 11-14 Sept. 2005, Genoa, Italy, pp. 469-72; 2005.

[30] Do Minh N. and Vetterli Martin, The Contourlet Transform: An Efficient Directional Multiresolution Image Representation, IEEE Transaction on Image Processing 2005; 14(12)2091-2106.

[31] Eslami Ramin and Hayder Radha, 2006, Translation invariant contourlet transform and its application image denoising, IEEE Transactions on Image Processing 2005;15(11) 3362-74.

[32] Hiremath P. S., Akkasaliger P. and Badiger S., 2009, Despeckling medical ultrasound images using the contourlet transform, Proc. of Indian International Conferance on Artificial Intelligence, 16-18 Dec. 2009, Tumkur, India, pp. 1814-1827.

[33] Hiremath P. S., Akkasaliger P. and Badiger S., Performance Comparision of Wavelet Transform and Contourlet Transform Based Method for Despekling Medical Ultrasound Images, International Journal of Computer Applications, 2011, 26(9)34-41.

[34] Hiremath P. S. and Tegnoor J. R. Automatic Detection of Follicles in Ultrasound Images of Ovaries using Horizontal and Vertical Scanline Thresholding Method, Proc. of Second International Conference on Signal and Image Processing (ICSIP-09), 12-14 Aug. 2009, Mysore, India, pp 468-473;2009.

[35] Hiremath P. S. and Tegnoor J. R. Recognition of Follicles in Ultrasound Images of Ovaries using Geometric Features, Proc. of Second IEEE International Conference on Biomedical and Pharmaceutical Engineering (ICBPE-09), 2-4 Dec. 2009, Singapore, ISBN 978-1-4244-4764-0/09; 2009.

[36] Hiremath P. S. and Tegnoor J. R. Automatic Detection of Follicles in Ultrasound Images of Ovaries using Edge based Method, International Journal of Computer Applications (IJCA), Special Issue on "Recent Trends in Image Processing and Pattern Recognition", RTIPPR, pp 120-125, ISSN 0975-8887; 2010.

[37] Hiremath P. S. and Tegnoor J. R. Automatic Detection of Follicles in Ultrasound Images of Ovaries using Active Contours Method, International Journal of Service Computing and Computational Intelligence (IJSCCI) 2011; 1(1) pp 26-30, ISSN 2162-514X.

[38] Jahne B., Digital Image Processing. Berlin, Germany Springer–Verlag; 1993.

[39] Chan Tony F. and Vese Luminita A., Active Contours Without Edges, IEEE Transactions on Image Processing 2001; 10(2) 266-277.

[40] Hiremath P. S. and Tegnoor J. R. Fuzzy Logic Based Detection of Follicles in Ultrasound Images of Ovaries, Proc. of Fifth Indian International Conference on Artificial

Intelligence (IICAI-2011), 14-16 Dec 2011, Tumkur, Karnataka, India, pp 178-189, ISBN: 978-0-9727412-8-6; 2011.

[41] Sourabh Dash, Raghunathan Rengaswamy and Venkat Subramanian. Fuzzy-Logic Based Trend Classification for Fault Diagnosis of Chemical Processes, International Journal of Computers and Chemical Engineering 2003; 27(3)347-362.

[42] Nedeljkovic I., Image Classification Based on Fuzzy Logic, The International Archives of the Photogrammetry, Remote Sensing and Spatial Information Sciences 2004, 34: 173-179,

[43] Kerre E. E. and Nachtegael M. Fuzzy Techniques in Image Processing. Springer, Heidelberg; 2000.

[44] Khademi A., Sahba F., Venetsanopoulos A. and Krishnan S., 2009, Region, Lesion and Border-Based Multiresolution Analysis of Mammogram Lesions, Proc. of the Sixth International Conference on Image Analysis and Recognition (ICIAR), 6-8 July 2009, Halifex, Canada, pp. 802-813.

[45] Zadeh L. A. Fuzzy Sets, Information and Control,1965; 8: 333-335.

[46] Zadeh L.A. Outline of a New Approach to the Analysis of Complex Systems and Decision Processes, IEEE Transactions on Systems, Man, and Cybernatics 1973; 3(1).

[47] Zadeh L.A. Fuzzy algorithms, Info and Ctl. 1968, 12: 94-102.

[48] Zadeh L.A. Making Computers Think Like People, IEEE. Spectrum 1984; pp. 26-32.

[49] Christianini N. and Shawe-Taylor J. An Introduction to Support Vector Machines and Other Kernel-Based Learning Methods. Cambridge University Press, UK 12; 2000.

[50] Kim K. I., Jung K., Park S. H. and Kim H. J. Support Vector Machines for Texture Classification, IEEE Trans Pattern Anal Mach Intell 2002; 24(11) 1542-1550.

[51] Song Q., Hu W. J. and Xie W. F., 2002, Robust Support Vector Machine With Bullet Hole Image Classification, IEEE Trans. Systems, Man and Cybenetics, Part C: Applications and Review 2002; 32(4) 440-448.

[52] El Naqa I., Yang Y. Y., Wernick M. N., Galatsanos N. P. and Nishikawa R. M. A Support Vector Machine Approach for Detection of Micro Calcifications. IEEE Trans Med Imaging 2002; 21(2)1552-1563.

[53] Yang M. H., Roth D. and Ahuja N. A tale of two classifiers: SNoW vs. SVM in visual recognition, Proc. of Seventh European Conference on Computer Vision, Copenhagen, Denmark, 27 May-2 June 2002, pp. 688-699; 2002.

[54] Sun Y. F., Fan X. D. and Li Y. D., Identifying Splicing Sites in Eukaryotic RNA: Support Vector Machine Approach, Comput. Biol. Med 2003, 33(1)17–29.

[55] Hiremath P. S. and Tegnoor J. R. Automated Ovarian Classification in Digital Ultrasound Images using SVM, International Journal of Engineering Research and Technology 2012; 1(6).

IntechOpen

IntechOpen

6

Normal and Abnormal Fetal Face

Israel Goldstein and Zeev Wiener
Rambam Health Care Campus, Haifa
Israel

1. Introduction

During the early stages of embryogenesis, genetic factors play the predominant role in the development of the fetal face. In later stages, environmental influences increase in importance. Facial malformation may be the result of chromosomal aberrations as well as teratogenic factors. Therefore, facial dysmorphism can provide important clues that suggest chromosomal or genetic abnormalities. The post-natal diagnosis of facial dysmorphism is a well-known pediatric diagnosis, primarily based on pattern diagnosis related to the appearance of one or a combination of facial features, such as low-set ears, hypo-hypertelorism, small orbits, micrognathia, retrognatia, and more. Some of these features are detectable prenatally (Benacerraf, 1998). More than 250 syndromes are associated with disproportional growth of abnormal features of the fetal face (Smith & Jones, 1988).

Indication	**N**	%
Other fetal anomalies detected by US	118	52.8
Familial history of craniofacial malformations	72	32.2
Maternal drug intake	25	11.2
Fetal chromosomal aberrations	8	3.6
Total	**223**	

Table 1. Indications for ultrasound examination of the fetal face (Pilu et al., 1986)

Sonographic assessment of the fetal face is part of the routine anatomic survey. Recently, three-dimensional ultrasound (3D) images of the fetus can be also obtained. However, two-dimensional ultrasonographic images are more easily, rapidly, efficiently, and accurately obtained. Imaging of the fetal face is possible in most ultrasound examinations beyond 12 weeks of gestation.

This chapter describes normal structural development and the sonographic approach to evaluation of the fetal face. Clinical applications are discussed in relation to perinatal management.

2. Fetal face profile

Sonographic imaging of the fetal face can provide information for the antenatal diagnosis of fetuses with various congenital syndromes and chromosomal aberrations, many of which are known to be associated with facial malformations. Deviation from the normal

proportions of the fetal face profile might be one of the 'soft sonographic signs' that can provide important clues that suggests congenital syndromes (Benacerraf, 1998).

Visualization of the curvature of the forehead is important to rule out a flat forehead, such as microcephaly, or bossing of the forehead, such as craniosynostosis (Goldstein et al., 1988). Visualization of the bridge of the nose could rule out Apert or Carpenter syndromes (Smith & Jones, 1988). Visualization of normal prominent lips can rule out cleft lip (Benacerraf, 1998). Finally, a normal jaw appearance is important to rule out microganthia or prognathia (Sivan et al., 1997).

Evaluation of the fetal face structures is suggested on the coronal and mid-sagittal views. The fetal face profile appearance should be obtained, while an imaginary line is passed through the nasion (bridge of the nose) and the gnathion (lower protrusion of the chin). This imaginary line is vertical to the maxillary bone. In this view, the following structures can be identified: the bridge and tip of the nose, the philtrum (area between the nose and the upper lip), upper and lower lips, and chin (Goldstein et al., 2010).

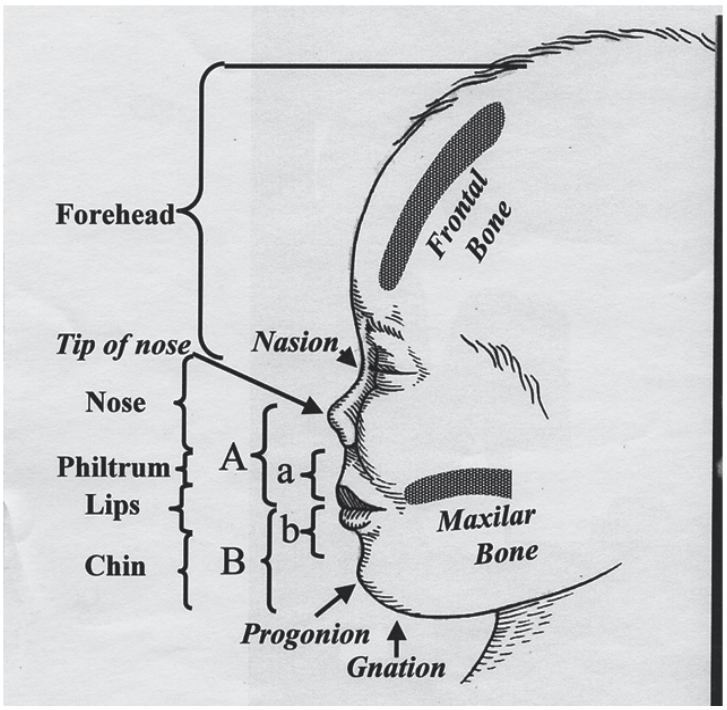

Fig. 1. **A** describes the distance from the tip of the nose to the mouth (line between the lips), **B** from the mouth to the chin, **a** describes the distances from the upper philtrum and the mouth**, b** from the mouth and the upper concavity of the chin.

The ratios between the following distances are independent of the gestational age and are almost constant: the distances between the tip of the nose and the mouth, and the distance from the mouth to the gnathion. In addition, a constant ratio was found between the upper philtrum and the mouth and from the mouth to the upper concavity of the chin (Goldstein et al., 2010).

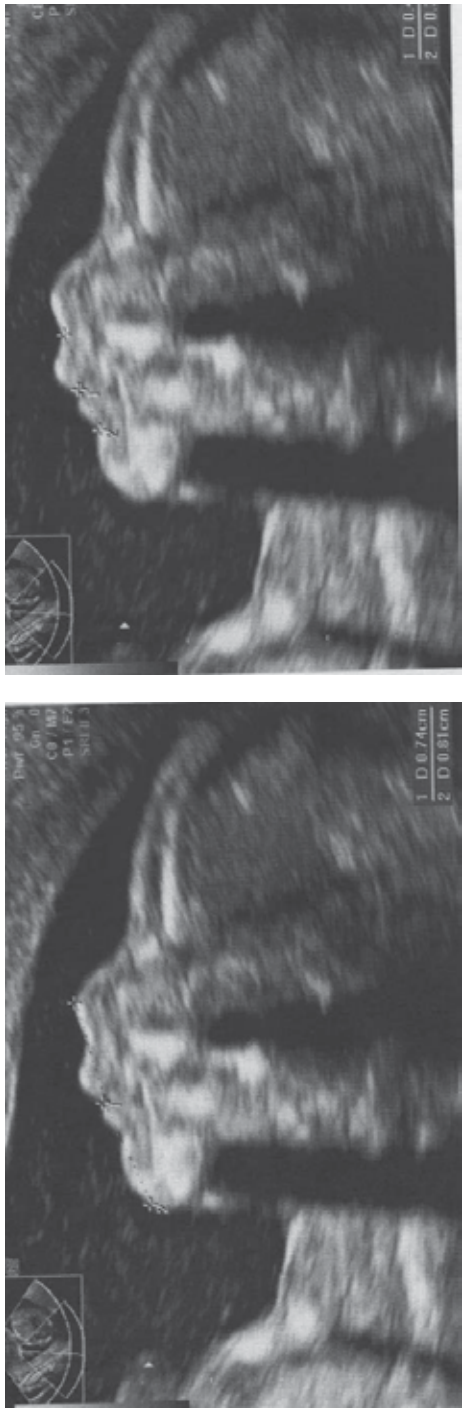

Fig. 2. Sonographic picture of the fetal face. Typical facial concavities and protrusions are presented. The calipers measured between the upper philtrum to the mouth (upper picture), and between the mouth to the chin (lower picture).

Fig. 3. 3D pictures of the fetal face. Mimics of face: a. kiss, b: open mouth and tongue, c: whistling, d: whistling, e: bye-bye

3. The forehead

Visualization of the curvature of the forehead is important to rule out a flat forehead (Figure 4). Investigators agree that microcephaly is associated with a decreased size of the frontal fossa and flattening of the frontal bone. Therefore, determination of the normal dimensions of the anterior cranial fossa and the frontal lobe of the fetal brain can provide normative

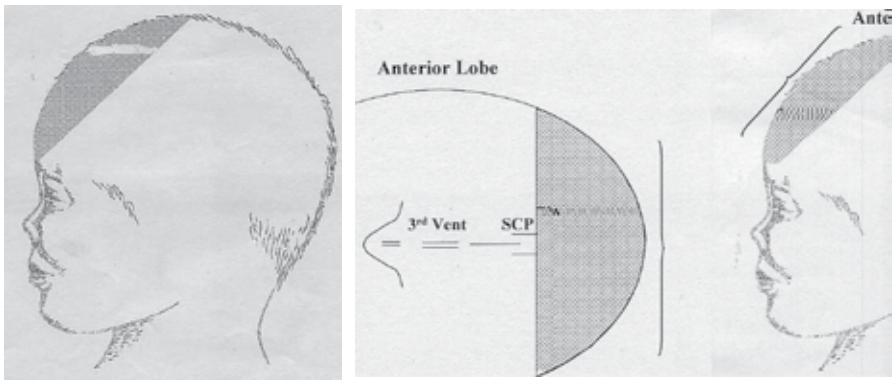

Fig. 4. Schematic picture of the anterior lobe on sagittal and axial planes

Fig. 5. A flat forehead in neonates with microcephaly

GA [weeks]	FLD [cm] mean±2SD		TFLD [cm] mean±2SD	
15	1.4	0.4	3.2	0.4
16	1.4	0.4	3.2	0.4
17	1.6	0.2	3.6	0.6
18	1.6	0.2	3.7	0.6
19	1.7	0.2	3.8	0.4
20	1.7	0.2	4.1	0.4
21	1.8	0.4	4.1	0.4
22	1.8	0.4	4.6	0.4
23	1.8	0.4	4.6	0.4
24	1.9	0.2	4.7	0.4
25	2.2	0.4	5.1	0.6
26	2.3	0.4	5.2	0.6
27	2.5	0.6	5.6	0.8
28	2.8	0.2	5.7	0.4
29	2.7	0.2	6.1	0.4
30	2.8	0.6	6.2	1.2
31	2.9	0.4	6.2	0.8
32	3.0	0.6	6.4	0.8
33	3.1	0.6	6.5	0.6
34	3.2	0.2	6.7	0.6
35	3.2	0.4	6.9	0.6
36	3.2	0.4	7.0	0.4
37	3.4	0.4	7.2	0.6
38	3.5	0.4	7.3	0.8
39	3.7	0.6	7.5	0.8
40	4.0	0.6	7.7	0.8

Table 2. Measurements of the mean±2SD of the frontal lobe distance and thalamic frontal lobe distance versus gestational age (Goldstein et al., 1988) (GA = gestational age, FLD = frontal lobe distance, TFLD = thalamic frontal lobe distance)

data against which fetuses suspected to have microcephaly or any other lesion affecting the anterior fossa can be evaluated. A dysmorphic sign with a high frequency appears to be a flat facial profile in neonates with trisomy 21 (Smith & Jones, 1988). Table 2 describes the normal dimensions of the frontal lobe of the fetal brain (Goldstein et al., 1988).

4. The nasal bone

Smallness of the nose is a common finding at postnatal examination of fetuses or neonates with trisomy 21, but also with more than 40 other genetic conditions. Measurements of the nasal bone were performed on a mid-sagittal profile in normal singleton fetuses at 14-34 weeks' gestation. It was found that the length of the nasal bones increased from 4 mm at 14 weeks to 12 mm at 35 weeks' gestation (Guis et al., 1995). Investigators examined the

Gestation [weeks]	Mean	SD
14	4.183	0.431
16	5.213	1.062
18	6.308	0.654
20	7.621	0.953
22	8.239	1.102
24	9.362	1.300
26	9.744	1.277
28	10.72	1.459
30	11.348	1.513
32	11.580	1.795
34	12.285	2.372

Table 3. Mean, standard deviation (SD), mean+2SD and mean-2SD for length of the nasal bones (mm) throughout gestation (Guis et al., 1995)

Gestation [weeks]	Mean [mm]	SD [mm]
11-11.9	1.7	0.5
12-12.9	2.0	0.5
13-13.9	2.3	0.5
14-14.9	3.4	0.7
15-15.9	3.3	0.8
16-16.9	4.4	0.7
17-17.9	5.0	0.7
18-18.9	5.5	0.9
19-19.9	5.7	0.1
20-20.9	6.2	0.1

Table 4. Fetal nasal bone length (mm), 11-20 weeks' gestation (Cuick et al., 2004)

Gestation [weeks]	Mean [mm]	SD [mm]
11-11+6	1.69	0.26
12-12+6	2.11	0.37
13-13+6	2.34	0.39
14-14+6	2.94	0.48

Table 5. Nomogram of fetal nasal bone length at 11-13 gestational weeks in fetuses (Sivri et al., 2006)

possible improvement in screening for trisomy 21 by examining the fetal nasal bone with ultrasound at 11-14 weeks of gestation (Cicero et al., 2001). The nasal bone was absent in 43 of 59 (73%) trisomy 21 fetuses, and in three of 603 (0.5%) chromosomally normal fetuses.

5. The nostrils

Smallness of fetal nose, often attributed to hypoplasia, is a common finding during postnatal examination of fetuses or neonates with trisomy 21 (Smith & Jones, 1988)

GA [weeks]	Centiles				
	10	25	50	75	90
14-15	5.5	7.2	7.6	8.3	10.2
16-17	6.5	7.3	7.9	8.5	10.5
18-19	8.5	8.9	10.0	10.5	11.0
20-21	10.2	11.0	12.0	12.0	13.0
22	13.0	13.0	14.0	15.0	15.0
23	13.0	13.0	14.0	15.0	15.0
24	13.0	14.1	15.0	16.0	16.0
25	14.2	15.0	16.3	17.0	17.0
26	14.1	15.0	16.3	17.4	18.4
27	13.4	15.4	17.2	18.4	19.0
28	15.1	16.9	17.6	18.2	20.2
29-30	16.5	17.4	18.1	19.2	20.6
31-32	16.6	17.9	19.6	20.7	21.4
33-34	17.4	19.1	20.5	21.4	23.1
35-37	17.6	20.0	20.5	22.0	23.3
38-40	17.4	17.9	18.9	20.5	23.4

Table 6. The fetal nose width (mm) (Goldstein et al., 1997)

GA [weeks]	Centiles				
	10	25	50	75	90
14-15	3.3	3.6	4.2	4.7	5.4
16-17	3.5	3.9	4.4	4.8	5.9
18-19	4.0	4.4	.6	5.0	5.8
20-21	4.2	5.0	5.0	5.7	6.0
22	5.0	5.0	6.0	6.4	7.0
23	5.0	5.6	6.0	7.0	7.0
24	5.8	6.0	6.2	7.3	7.9
25	5.9	6.0	6.4	7.0	7.7
26	5.1	6.2	7.7	8.0	9.0
27	6.4	6.8	7.8	8.4	9.4
28	6.4	7.0	7.9	8.6	9.4
29-30	5.4	7.0	7.0	8.2	9.6
31-32	4.6	7.4	7.9	9.2	10.7
33-34	5.4	6.4	8.1	9.0	9.7
35-37	5.8	6.6	8.5	9.6	10.2
38-40	6.0	6.8	8.5	9.5	10.5

Table 7. The fetal nostril distance (mm) (Goldstein et al., 1997)

6. The fetal eyes

The earliest sonographic visualization of the fetal orbit and lens has been considered to be in the beginning of the second trimester of pregnancy. On ultrasound, the orbits appear as echolucent circles in the face of the fetus, and the lens can be easily identified inside these structures. Imaging of these structures, which is possible on virtually all ultrasound examinations beyond the first trimester, is important because deviation in the relative size of the orbit and the lens can be associated with congenital malformations. The fetal orbits and lens eyes are best visualized by scanning the fetal face in coronal and axial planes. The fetal orbits should appear as two symmetrical structures on both sides of the fetal nose. Both lenses are depicted on the coronal or axial plane of the eye as circular hyperechogenic rings and with hypoechogenic areas inside the ring.

The coronal planes of the fetal face are the most important in the evaluation of the fetal orbits. Figure 6a shows the the outer orbital distance small hands, and Fig 6b the inner orbital distace the small arrows. The calipers measuring the outer orbital from the lateral mid-echogenicity to the lateral mid-echogenicity, and the calipers measuring the inner orbital distace from the middle mid-echogenicity to the middle mid-echogenicity of the orbits.

Fig. 6a. Coronal plane of the fetal orbits – small hands showing the outer orbital diameter measurement

Fig. 6b. Coronal plane of the fetal orbits – small arrows showing the inner orbital diameter measurement

GA [weeks]	N	Mean	95% CI	Centiles				
				10	25	50	75	90
14	10	5.2	4.8-5.7	4.5	5.0	5.3	5.7	90
15	26	6.1	5.9-6.3	5.4	5.5	6.2	6.5	6.7
16	25	6.6	6.3-6.9	5.8	6.2	6.5	7.0	7.6
17-18	19	7.3	6.7-7.8	6.2	6.5	6.7	9.0	9.0
19-20	23	9.8	9.3-10.2	8.6	9.0	10.0	10.1	11.3
21	19	10.5	10.0-10.9	9.4	9.9	10.0	11.0	12.0
22	26	10.4	10.0-10.7	9.5	9.6	10.5	11.0	11.3
23	21	10.7	10.4-11.1	9.6	10.0	10.5	11.4	11.5
24	19	11.6	11.3-11.8	10.7	11.0	11.5	12.0	12.5.
25	13	11.2	11.4-12.4	10.3	11.0	12.2	12.5	12.8
26	16	12.7	12.0-13.4	11.0	11.0	12.7	13.8	14.5
27	14	13.0	12.4-13.5	11.9	12.0	12.9	13.4	14.8
28	21	13.0	12.7-13.3	21.1	12.0	13.1	13.3	14.1
29	23	13.9	13.4-14.4	12.6	13.0	13.7	14.6	15.7
30-31	24	14.2	13.8-14.5	13.3	13.0	13.9	14.7	15.4
32-33	24	14.4	13.7-15.1	12.2	13.0	14.1	14.8	17.5
34-36	26	15.8	15.4-16.2	14.6	15.0	15.7	16.5	16.9

Table 8. The fetal orbital diameter (mm) (Goldstein et al., 1998) GA = gestational age; CI = confidence interval

GA [weeks]	n	Mean	95% CI	Centiles				
				10	25	50	75	90
14	10	2.5	23.3-2.7	2.1	2.4	2.5	2.7	2.9
15	26	2.9	2.9-3.0	2.7	2.8	2.9	3.1	3.2
16	25	2.9	2.8-3.0	2.7	2.8	2.9	3.1	3.2
17-18	19	3.3	3.0-3.6	2.8	2.9	3.0	3.3	5.0
19-20	23	4.1	4.0-4.3	3.6	4.0	4.0	4.3	5.0
21	19	4.4	4.1-4.6	3.7	3.9	4.0	5.0	5.0
22	26	4.4	4.2-4.7	3.9	4.0	4.3	5.0	5.0
23	21	4.6	4.3-4.8	3.8	4.0	5.0	5.0	5.0
24	19	4.6	4.4-4.8	4.0	4.3	4.6	5.0	5.0
25	13	4.8	4.6-5.0	4.2	4.6	5.0	5.1	5.2
26	16	5.0	4.8-5.2	4.4	4.8	5.1	5.2	5.5
27	14	5.0	5.0-5.2	4.5	5.0	5.2	5.2	5.5
28	21	5.1	5.0-5.2	4.5	5.0	5.2	5.2	5.5
29	23	5.3	5.1-5.5	4.6	5.2	5.2	5.5	5.9
30-31	24	5.3	5.2-5.5	4.8	5.1	5.5	5.5	5.7
32-33	24	5.6	5.4-5.8	4.8	5.2	5.5	5.9	6.2
34-36	26	5.8	5.6-6.0	5.4	5.5	5.7	6.0	6.5

Table 9. Diameter of orbital lens (mm) (Goldstein et al., 1998) GA = gestational age; CI = confidence interval)

6.1 Hypotelorism

Hypotelorism is a condition pertaining to abnormally close eyes.

GA [weeks]	OOD [mm]			IOD [mm]		
	5th	50th	95th	5th	50th	95th
12	8	15	23	4	9	13
13	10	18	25	5	9	14
14	13	20	28	5	10	14
15	15	22	30	6	10	14
16	17	25	32	6	10	15
17	19	27	34	6	11	15
18	22	29	37	7	11	16
19	24	31	39	7	12	16
20	26	33	41	8	12	17
21	28	35	43	8	13	17
22	30	37	44	9	13	18
23	31	39	46	9	14	18
24	33	41	48	10	14	19
25	35	42	50	10	15	19
26	36	44	51	11	15	20
27	38	45	53	11	16	20
28	39	47	54	12	16	21
29	41	48	56	12	17	21
30	42	50	57	13	17	22
31	43	51	56	13	18	22
32	45	52	60	14	18	23
33	46	53	61	14	19	23
34	47	54	62	15	19	24
35	48	55	63	15	20	24
36	49	56	64	16	20	25
37	50	57	65	16	21	25
38	50	58	65	17	21	21
39	51	58	66	17	22	26
40	52	59	67	18	22	26

Table 10. The outer orbital diameter (OOD) and inner orbital diameter (IOD), GA = gestational age (Jeanty et al., 1984)

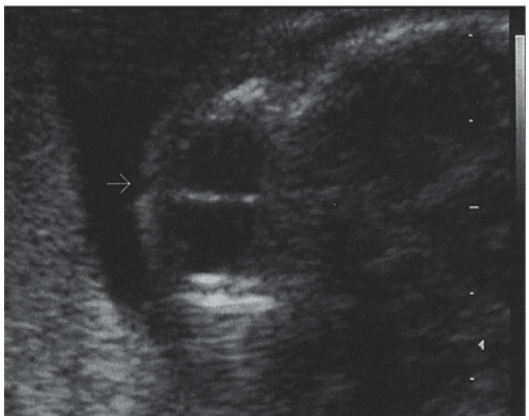

Fig. 7. Axial scan of a fetus at 25.3 weeks of gestation showing severe hypotelorism

BPD [cm]	Weeks' gestation	IOD [cm]	OOD [cm]
1.9	11.6	0.5	1.3
2.0	11.6	0.5	1.4
2.1	12.1	0.6	1.5
2.2	12.6	0.6	1.6
2.3	12.6	0.6	1.7
2.4	13.1	0.7	1.7
2.5	13.6	0.7	1.8
2.6	13.6	0.7	1.9
2.7	14.1	0.8	2.0
2.8	14.6	0.8	2.1
2.9	14.6	0.8	2.1
3.0	15.0	0.9	2.2
3.1	15.5	0.9	2.3
3.2	15.5	0.9	2.4
3.3	16.0	1.0	2.5
3.4	16.5	1.0	2.5
3.5	16.5	1.0	2.6
3.6	17.0	1.0	2.7
3.7	17.5	1.1	2.7
3.8	17.9	1.1	2.8
4.0	18.4	1.2	3.0
4.2	18.9	1.2	3.1
4.3	19.4	1.2	3.2
4.4	19.4	1.3	3.2
4.5	19.9	1.3	3.3
4.6	20.4	1.3	3.4
4.7	20.4	1.3	3.4
4.8	20.9	1.4	3.5
4.9	21.3	1.4	3.6
5.0	21.3	1.4	3.6

BPD [cm]	Weeks' gestation	IOD [cm]	OOD [cm]
5.1	21.8	1.4	3.7
5.2	22.3	1.4	3.8
5.3	22.3	1.5	3.8
5.4	22.8	1.5	3.9
5.5	23.9	1.5	4.0
5.6	23.3	1.5	4.0
5.7	23.8	1.5	4.1
5.8	24.3	1.6	4.1
5.9	24.3	1.6	4.2
6.0	24.7	1.6	4.3
6.1	25.2	1.6	4.3
6.2	25.2	1.6	4.4
6.3	25.7	1.7	4.4
6.4	26.2	1.7	4.5
6.5	26.2	1.7	4.5
6.6	26.7	1.7	4.6
6.7	27.2	1.7	4.6
6.8	27.6	1.7	4.7
6.9	28.1	1.7	4.7
7.0	28.6	1.8	4.8
7.1	29.1	1.8	4.8
7.3	29.6	1.8	4.9
7.4	30.0	1.8	5.0
7.5	30.6	1..8	5.0
7.6	31.0	1.8	5.1
7.7	31.5	1.8	5.1
7.8	32.0	1.8	5.2
7.9	32.5	1.9	5.2
8.0	33.0	1.9	5.3
8.2	33.5	1.9	5.4
8.3	34.0	1.9	5.4
8.4	34.4	1.9	5.4
8.5	35.0	1.9	5.5
8.6	35.4	1.9	5.5
8.8	35.9	1.9	5.6
8.9	36.4	1.9	5.6
9.0	36.9	1.9	5.7
9.1	37.3	1.9	5.7
9.2	37.8	1.9	5.8
9.3	38.3	1.9	5.8
9.4	38.8	1.9	5.8
9.6	39.3	1.9	5.8
9.7	39.8	1.9	5.9

Table 11. Predicted BPD and weeks' gestation from the inner orbital diameter (IOD) and outer orbital diameter (OOD) (Mayden et al., 1982)

6.2 Hypertelorism

Hypertelorism is an abnormally increased distance between two organs or body parts, usually referring to an increased distance between the eyes (orbital hypertelorism), seen in a variety of syndromes (Table 12).

Malformation	**Syndromes**
Anophthalmus	Trisomy 13 Vilaret, Weyers-Tier, ocular vertebral syndrome
Microphthalmus	Autosomal recessive or autosomal dominant Intrauterine infection Radiation Chromosomal aberration X-linked Associated with gingival fibromatosis Depigmentation
Ocular hypotelorism	Chromosome 5 p-syndrome Chromosome 15-p-proximal partial trisomy syndrome Chromosome 13 trisomy Craniosynostosis-medical aplasia syndrome Holoprosencephaly Meckel syndrome
Ocular hypetelorism	Aarshog syndrome Acrocephalosyndactyly Acrodystasis Auditory canal atresia Basal nevus syndrome Branchio-skeleto-genital syndrome Broad thumb-hallux syndrome Campomelic dysplasia Cerebro-hepato-renal syndrome Chromosome 18 p- syndrome Chromosome 5 p- syndrome Chromosome 4 p- syndrome Chromosome 14 p-proximal partial trisomy syndrome Coffin-Lowry syndrome Cranio-carpo tarsal dysplasia Cranio-facial dysostosis

Malformation	Syndromes
	Cranio-metaphyseal dysplasia Cranio-oculodental syndrome Deafness myopia cataract and saddle nose Ehlers-Danlos syndrome Fetal hydantoin syndrome Fetal warfarin syndrome G syndrome Hypertelorism–hypospadias syndrome Hypertelorism microtia facial clefting and conductive deafness Iris coloboma and canal atresia syndrome Larsen syndrome Multiple lentigines syndrome Cleft lip Marden-Walker syndrome Meckel syndrome Median cleft syndrome Noonan syndrome Nose and nasal septum defects Bifid nose Glioma of the nose Posterior atresia of the nose Ocular and facial anomalies with proteinuria and deafness Oculo-dento osseous dysplasia Opitz-Kaveggia FG syndrome Oto-palatodigital syndrome Bilateral renal agenesis Roberts syndrome Robinow syndrome Sclerosteosis Thymic agenesis Apert syndrome LEOPARD syndrome Crouzon syndrome Wolf-Hirschhorn syndrome Waardenburg syndrome Cri du chat syndrome DiGeorge syndrome Loeys-Dietz syndrome Morquio syndrome Hurler's syndrome Deafness

Table 12. Syndromes associated with fetal ocular malformation (Bergsma, 1979)

6.3 Cyclopia

Cyclopia is an anomaly characterized by a single orbital fossa, with fusion of bulbs, eyelids and lacrimal apparatus to a variable degree. Usually there is a single eye or partially divided eye in a single orbit and arhinia with proboscis. A normal nose is absent and a proboscis structure originating from the nasal root may be seen (Bergsma, 1979). The differential diagnosis in these cases includes ethmocephaly (extreme hypotelorism, arhinia and blinded proboscis located between the eyes) and ceboephaly (hypotelorism and a single nostril nose, without midline cleft). In ethmocephaly, the nasal bones, maxilla and nasal septum and turbinate are missing and lacrimal and palatine bones are united (Goldstein et al., 2003; McGahan et al., 1990).

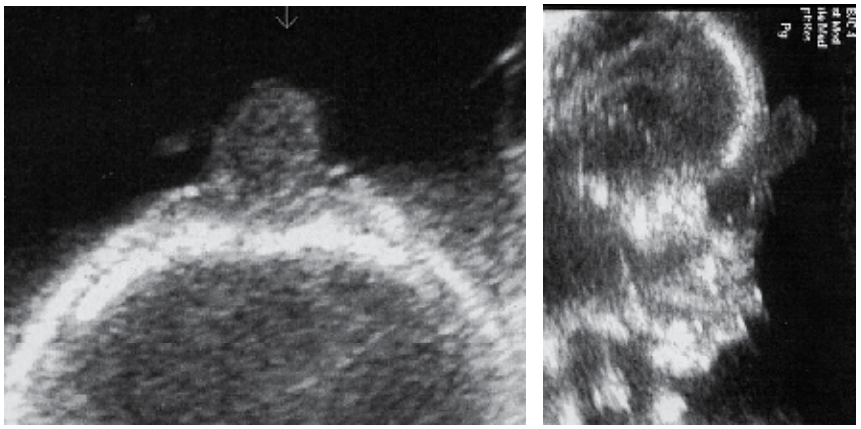

Fig. 8. Axial and sagittal scans of a fetus at 25.3 weeks of gestation show prominent forehead and proboscis

Fig. 9. Ethmocephaly – postmortem demonstrating hypotelorism and proboscis

6.4 Cataracts

A cataract is an opacity of the lens and accounts for 10% of the blindness seen in preschool age children in Western countries. Fetal cataracts may occur in association with infectious diseases, chromosomal anomalies or systemic syndromes.

Fig. 10. Sonographic pictures of fetal cataracts at 15 weeks of gestation. Coronal views of echogenic lens.

7. The ear

Abnormally small ears have been noted to be one of the findings in newborn and infants with trisomy 21 and other aneuploidies. Ears in these infants are often described as small, low-set, and malformed. Short ear length has been found to be the most consistent clinical characteristic in making the diagnosis of Downs' syndrome (Aase et al., 1973). Sonographically, a short fetal ear length may be a parameter in predicting fetal aneouploidy (Chitkara et al., 2002). Sonographic studies have suggested that short ear length measurements might be a useful predictor of fetal anomalies (Awwad et al., 1994; Lettieri et al., 1993; Shimizu et al., 1997; Yeo et al., 1998).

Investigators had suggested that the fetal ear length may be a useful measurement in prediction of aneuploidy in patients at high risk for fetal chromosomal abnormalities (Awwad et al., 1994; Lettieri et al., 1993; Shimizu et al., 1997; Yeo et al., 1998). However, it remains to be determined whether this measurement alone, or in combination with other aneuploidy markers, will prove to be a useful predictor of aneuploidy in a population of women at low risk for fetal chromosomal abnormalty.

GA (Weeks)	Mean [mm]	SD [mm]
14	8	0.7
15	9	1.8
16	10	0.9
17	11	1.0
18	13	0.7
19	14	1.1
20	15	1.1
21	17	1.0
22	18	1.5
23	19	1.4
24	20	1.1
25	22	1.7
26	23	2.1
27	25	1.7
28	26	1.8
29	26	1.6
30	27	2.3
31	29	2.6
32	29	1.9
33	30	1.8
34	31	1.6
35	31	2.1
36	33	2.6
37	33	2.0
38	33	4.1
39	34	4.3
40	37	2.1
41	38	1.9

Table 13. Fetal ear length (Yeo et al., 1998)

8. The maxillary bone

Imaging of the maxillary bone is possible in most ultrasound examinations and is important, because deviations in maxillary bone development can also be associated with a malformed face. The relationship between the maxillary, zygomatic and palatine bones provides a capacity for rapid movement of the fetal face. The etiology of hypoplasia of the maxillary bone may, in some cases, form part of well-established structural abnormalities in the fetus

such as choanal atresia, or genetic syndromes such as Marfan's syndrome. Sonographically, early prenatal detection of the maxillary bone is possible at 14 week of gestation. Hypoplasia of the maxillary bone can appear as an incidental finding. Table 14 depicts nomograms of the maxillary bone length.

Fig. 11. Sonographic picture of the maxillary bone

GA	Mean	SD	Centiles…….		
(Weeks)			10	50	90
14	9.97	1.12	8.32	10	11.52
15	10.64	1.07	9.4	10.6	11.8
16	10.6	1.73	7.6	10.4	12.98
17-19	10.07	2.75	7.0	10.9	13
20-22	11.48	3.42	7.0	11.0	17.35
23-24	13.19	3.34	8.60	13	16.76
25-26	12.85	1.74	10.2	13.0	15.92
27-28	12.61	2.11	10.0	12.0	16.2
29-30	13.63	1.67	11.67	13.50	16.23
31	13.16	1.25	11	13.0	15.48
32	13.49	1.25	11.9	13.45	15.0
33	13.7	1.37	11.11	14.0	15.95
34	13.87	1.72	11.96	14.0	16.15
35	14.15	1.27	12.54	14.0	16.0
36	14.31	1.4	12.63	14.35	16.15
37	14.08	1.26	12.93	14.0	16.73
38-39	14.84	1.77	11.74	14.8	17.47

Table 14. Maxillary bone length across gestational age (Goldstein et al., 2005)

The frontomaxillary facial (FMF) angle was studied in the first trimester in a Chinese population, demonstrating that the FMF angle decreases with fetal CRL increases. Similarity in the normal values of the FMF angle was found between the Chinese and Caucasian

populations (Chen et al., 2011). These authors previously studied the FMF angle in fetuses with trisomy 21 in the first trimester and found significant differences in the FMF angle between normal fetuses and fetuses with trisomy 21 in the Chinese population (Chen et al., 2009).

9. The tongue

Fetal macroglossia and microglossia are associated with several chromosomal defects. Table 15 describes the tongue circumference between 14 and 26 weeks of gestation.

GA (weeks)	Lower 95% CI	Mean	Upper 95% CI
14	24	28	31
15	26	33	36
16	33	36	38
17	37	37	38
18	40	43	46
19	47	48	51
20	47	51	56
21	51	55	61
22	52	58	62
23	58	62	68
24	60	64	67
25	68	70	73
26	71	73	76

Table 15. Tongue circumference (mm) by gestational age (weeks) and the 95% confidence interval (Achiron et al., 1997)

10. Cleft lips & palate

Cleft lip and palate is a common facial anomaly, with an incidence of 1 in 1000 live births. The incidence in fetuses is much higher, and many of these also have other malformations. Cleft palate alone occurs in about 1 of 2,500 white births. Cleft lip is more common in males, and cleft palate is more common in females. Cleft lip is one or more splits (clefts) in the upper lip. Cleft lip can range from a small indentation in the lip to a split in the lip that may extend up into one or both nostrils. Cleft lip develops in about the sixth to eighth week of gestation, when structures in the upper jaw do not fuse properly and the upper lip does not completely merge. Sometimes the nasal cavity, palate, and upper teeth are also affected in an opening in the roof of the mouth that develops when the cleft palate bones and tissues do not completely join during fetal growth, sometime between the 7^{th} and 12^{th} weeks of gestation. The severity and type of cleft palate vary according to where the cleft occurs on the palate and whether all the layers of the palate are affected. A mild form of cleft palate may not be visible because tissue covers the cleft. A complete cleft palate involves all layers of tissue of the soft palate, extends to and includes the hard palate, and may continue to the lip and nose. Sometimes problems associated with cleft palate also include deformities of the nasal cavities and/or the partition separating them (septum).

An ultrasound detection of cleft lip and palate may be seen as early as 14 to 16 weeks of gestation. Cleft palate and cleft lip may occur independent of each other or at the same time. The hard palate is the front part of the roof of the mouth, and the soft palate is the back part of the roof of the mouth. This description may include whether the uvulais affected. The latter is impossible to detect prenatally. Cleft lip is classified according to its location and severity. Unilateral cleft lip affects one side of the mouth; bilateral cleft lip affects both sides of the mouth. A complete cleft lip is a deep split in the upper lip extending into one or both sides of the nose; an incomplete cleft lip affects only one side of the upper lip. It may appear as a slight indentation or as a deep notch.

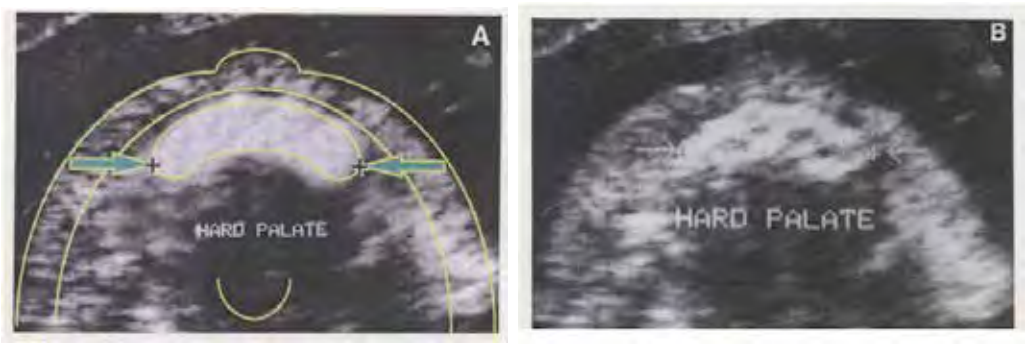

Fig. 12. Sonographic picture of normal primary palate (The alveolar ridge)

Fig. 13. Sonographic pictures of cleft lip

Ultrasonography can be used to identify clefting in the lip and primary palate (alveolar ridge). The ultrasound detecting rates of facial clefting have been reported as low as 21-30% using two-dimensional ultrasound (Crane et al., 1994). Accurate characterization of the fetal clefting is an important aspect of ultrasound diagnosis. Three-dimensional ultrasound may be useful in defining the location and extent of facial clefting *in utero* (Johnson et al., 2000). Although three-dimensional images of the fetal alveolar ridge can be obtained, two-dimensional sonographic images are obtained more easily, rapidly and accurately (Goldstein et al., 1999).

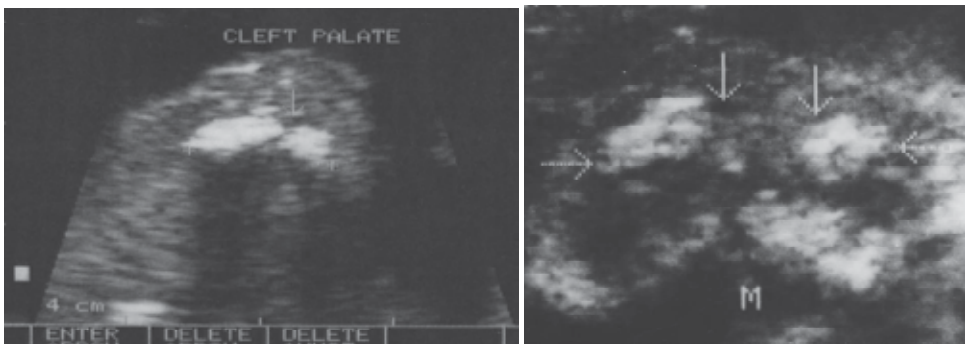

Fig. 14. Sonographic pictures of cleft palate (15 & 23 weeks of gestation)

Gestation [weeks]	Mean [mm]	±SD [mm]
14 -15	10.5	1.3
16	11.7	1.1
17	16.6	2.5
18	17.5	1.1
19	18.0	1.1
20	18.5	1.1
21	18.5	2.1
22	19.9	1.7
23	20.5	1.9
24	21.3	2.7
25	22.8	1.9
26	23.6	2.6
27-28	23.6	2.1
29	25.5	2.2
30	26.3	2.5
31	26.5	2.1
32	26.7	2.0

Table 16. Normal values of the fetal alveolar ridge width (Goldstein et al., 1999)

11. The chin: Microganthia-retroganthia or prognathia

Abnormal size of the chin, micrognathia and macrognathia, and abnormal length of the philtrum (short or long) are morphological features in numerous syndromes. Micrognathia is a common finding in many chromosome aberrations and dysmorphic syndromes (Gulla

et al., 2005). Investigators have reported a series with subjective micrognathia, 66% of whom had chromosomal abnormalities (Nicolaides et al., 1993). Others reported that micrognathia was associated with aneuploidy in 25% and 38% of cases (Benacerraf et al., 1984; Turner & Twining, 1993). Sivan et al. (1997) established normative dimensions for objective chin length. Measurements of the chin length, was performed between the lower lip and the apex of the chin in mid-sagittal plane.

Fig. 15. Chin length measured between the lower lip and the apex of the chin (Sivan et al., 1977)

GA	Mean	SD	Range
Age (weeks)	(mm)		
16-17.9	5	1	3-6
18-19.9	7	1	6-9
20-21.9	8	2	7-10
22-23.9	10	1	9-11
24-25.9	11	2	8-13
26-27.9	11	2	9-12
28-29.9	13	2	11-15
30-31.9	15	2	13-17
32-33.9	18	2	16-20
34.35.9	17	2	15-19
36-37.9 23	1	22-24	

Table 17. Chin length (Sivan et al., 1997)

Fig. 16. Sagittal scan and postmortem of a fetus at 16 weeks of gestation shows prominent forehead and retrognathia

12. References

Arai, T. & Kragic, D. (1999). Variability of Wind and Wind Power, In: *Wind Power,* S.M. Muyeen, (Ed.), 289-321, Scyio, ISBN 978-953-7619-81-7, Vukovar, Croatia

Lima, P.; Bonarini, A. & Mataric, M. (2004). *Application of Machine Learning,* InTech, ISBN 978-953-7619-34-3, Vienna, Austria

Li, B.; Xu, Y. & Choi, J. (1996). Applying Machine Learning Techniques, *Proceedings of ASME 2010 4th International Conference on Energy Sustainability*, pp. 14-17, ISBN 842-6508-23-3, Phoenix, Arizona, USA, May 17-22, 2010

Aase, J.M.; Wilson, A.C. & Smith, D.W. (1973). Small ear in Downs' syndrome: a helpful diagnosis aid. *Journal of Pediatrics*, Vol.82, No.5, (May), pp. 845-847.

Achiron, R.; Ben Arie, A.; Gabbay, U.; Mashiach, S.; Rotstein, Z. & Lipitz, S. (1997) Development of the fetal tongue between 14 and 26 weeks of gestation: in utero ultrasonographic measurements. *Ultrasound in Obstetrics & Gynecology*, Vol. 9, No.1, (January), pp. 39-41.

Awwad, J.T.; Azar, G.B.; Karam, K.S. & Nicolaides KH. (1994). Ear length: a potential sonographic marker for Down syndrome. *International Journal of Gynaecology and Obstetrics*, Vol.44, No. 3, (March), pp. 233-238.

Benacerraf, B.R. (1998). *Ultrasound of fetal syndromes*. Churchill Livingstone: New York, London, Philadelphia, San Francisco, pp. 83-223.

Benacerraf, B.R.; Frigoletto, F.D. Jr. & Bieber, F.R. (1984). The fetal face: ultrasound examination. *Radiology*, Vol.153, No.2, (November), pp. 495-497.

Bergsma, D. (1979). *Birth defects compendium*. 2nd ed., Macmillan.

Chen, M.; Wang, H.F.; Leung, T.Y.; Sahota, D.S.; Borenstein, M.; Nicolaides, K.; Lao, T.T. & Lau, T.K. (2011). Frontomaxillary facial angle at 11 + 0 to 13 + 6 weeks in Chinese population. *Journal of Maternal-Fetal and Neonatal Medicine*, Vol.24, No.3 (March), pp. 498-501.

Chen, M.; Yang, X.; Leung, T.Y.; Sahota, D.S.; Fung, T.Y.; Chan, L.W.; Lao, T.T. & Lau, T.K. (2009). Study on the applicability of frontomaxillary facial angle in the first-trimester trisomy 21 fetuses in Chinese population. *Prenatal Diagnosis*, Vol.29, No.12, (December), pp. 1141-1144.

Chitkara, U.; Lee, L.; Oehlert, J.W.; Bloch, D.A.; Holbrook, R.H.; El-Sayed, Y.Y. & Druzin, M.L. (2002). Fetal ear length measurement: a useful predictor of aneuploidy? Ultrasound in Obstetrics & Gynecology, Vol.19, No.2, (February), pp. 131-135.

Cicero, S.; Curcio, P.; Papageorghiou, A.; Sonek, J. & Nicolaides, K. (2001). Absence of nasal bone in fetuses with trisomy 21 at 11-14 weeks of gestation: an observational study. Lancet, Vol.358, No.9294, (November 17), pp. 1665-1667.

Crane, J.P.; LeFevre, M.L.; Winborn, R.C.; Evans, J.K.; Ewigman, B.G.; Bain, R.P.; Frigoletto, F.D. & McNellis, D. (1994). A randomized trial of prenatal ultrasonographic screening: impact on the detection, management, and outcome of anomalous fetuses. The RADIUS Study Group. *American Journal of Obstetrics and Gynecology*, Vol.171, No.2 (August), pp. 392-399.

Cuick, W.; Provenzano, L.; Sullvan, C.A.; Gallousis, F.M. & Rodis, J. (2004). Fetal nasal bone length in euploid and aneuploid fetuses between 11 and 20 weeks' gestation. A prospective study. *Journal of Ultrasound in Medicine*, Vol.23, No.10, (October), pp. 1327-1333.

Goldstein I., Jakobi P., Tamir A., & Goldstick O. (1999). Nomogram of the fetal alveolar ridge: a possible screening tool for the detection of primary cleft palate. *Ultrasound in Obstetrics & Gynecology*, Vol.14, No. 5, (November), pp. 333-337.

Goldstein I., Reece E.A., Gianluigi P., O'Connor T.Z., Lockwood C.J. & Hobbins J.C. (1988). Sonographic assessment of the fetal frontal lobe: A potential tool for prenatal diagnosis of microcephaly. *American Journal of Obstetrics & Gynecology*, Vol.158, No. 5, (May), pp. 1057-1062.

Goldstein I., Reiss A., Rajamim B.S. & Tamir A. (2005). Nomogram of maxillary bone length in normal pregnancies. *Journal of Ultrasound in Medicine*, Vol.24, No.9, (September), pp. 1229-1233.

Goldstein I., Tamir A., Itskovitz-Eldor J. & Zimmer E.Z. (1997). Growth of the fetal nose width and nostril distance in normal pregnancies. *Ultrasound in Obstetrics & Gynecology*, Vol. 9, No.1, (January), pp. 35-38.

Goldstein I., Tamir A., Weiner Z. & Jakobi P. (2010). Dimensions of the fetal facial profile in normal pregnancy. *Ultrasound in Obstetrics & Gynecology*, Vol.35, No.2, (February), pp. 191–194.

Goldstein I., Tamir A., Zimmer E.Z.& Itskovitz-Eldor J. (1998). Growth of the fetal orbit and lens in normal pregnancies. *Ultrasound in Obstetrics & Gynecology*, Vol. 12, No.3, pp. 175-179.

Goldstein I., Weissman A., Brill-Zamir R., Laevsky I. & Drugan A. (2003). Ethmocephaly caused by de novo translocation 18; 21 – prenatal diagnosis. *Prenatal Diagnosis*, Vol.23; No.10, (October), pp. 788-790.

Guis F., Vill Y., Vincent Y., Doumerc S., Pons J.C. & Frydman R. (1995). Ultrasound evaluation of the length of the fetal nasal bones throughout gestation. *Ultrasound in Obstetric Gynecology*, Vol.5, No.5, (May), pp. 304-307.

Gull I., Wolman I., Merlob P.,Jaffa A.J., Lessing J.B. & Yaron Y. (2005). Nomograms for the sonographic measurement of the fetal philtrum and chin. *Fetal Diagnosis and Therapy*, Vol.20, No. 2 (March-April), pp. 127–131.

Jeanty P., Cantraine F., Consaert E., Romero R. & Hobbins J.C. (1984). The binocular distance: A new way to estimate fetal age. *Journal of Ultrasound in Medicine*; Vol.3, No.6, (June), pp. 241-243.

Johnson, D.D.; Pretorius, D.H.; Budorick, N.E.; Jones, M.C.; Lou, K.V.; James, G.M. & Nelson, T.R. (2000). Fetal lip and primary palate: three-dimensional versus two-dimensional US. *Radiology,* Vol.217, No.1, (October), pp. 236-239.

Lettieri L., Rodis J.F., Vintzileos A.M., Feeney L., Ciarleglio .L & Craffey A. (1993). Ear length in second-trimester aneuploid fetuses. *Obstetrics and Gynecology*, Vol.18, No. 1, (January), pp. 57-60.

Mayden K.L., Totora M., Berkowitz R.L., Bracken M. & Hobbins J.C. (1982). Orbital diameters: a new parameter for prenatal diagnosis and dating. *American Journal of Obstetrics & Gynecology,* Vol.1;144 No.3, (October), pp. 289-297.

McGahan J.P., Nyberg D.A. & Mack L.A. (1990). Sonography of facial features of alobar and semilobar holoprosecephaly *American Journal of Roentgenol,* Vol.154, No.1, (January), pp. 143-148.

Nicolaides K.H., Salvesen D.R., Snijders R.J. & Gosden C.M. (1993). Fetal facial defects. Associated malformations and chromosomal abnormaties. *Fetal Diagnosis and Therapy*, Vol.8, No.1, (January-February) pp.1-9.

Pilu G., Reece R.A., Romero R., Bovicelli L. & Hobbis J.C. (1986). Prenatal diagnosis of craniofacial malformations with ultrasonography. *American Journal of Obstetrics & Gynecology,* Vol.155; No.1, (July), pp. 45-50.

Shimizu T., Salvador L., Hughes-Benzie R., Dawson L., Nimrod C. & Allanson J. (1977). The role of reduced ear size in the prenatal detection of chromosomal abnormalities. *Prenatal Diagnosis,* Vol.17, No.6, (June), pp. 545-549.

Sivan E., Chan L., Mallozzi-Eberle A. & Reece E.A. (1997). Sonographic imaging of the fetal face and the establishment of normative dimensions for chin length and upper lip width. *American Journal of Perinatology,* Vol.14, No. 4, (April), pp. 191-194.

Sivri D., Dane C., Dane B., Cetin A. & Yayla M. (2006) Nomogram of fetal nasal bone length at 11-13 gestational weeks in fetuses. *Perinatal Journal,* Vol.14, No.3, (September), pp.

Smith D. & Jones K.L. (1988). *Smith's recognizable patterns of human malformation*, 4th *ed*. Philadelphia, WB Saunders Company.

Turner G.M. & Twining P. (1993) The facial profile in the diagnosis of fetal abnormalities. *Clinical Radiology,* Vol.47, No.6 (June), pp. 389-95.

Yeo L., Guzman E.R., Day-Salvatore D., Vintzileos A.M. & Walters C. (1998). Prenatal detection of fetal aneuploidy using sonographic ear length. *American Journal of Obstetrics & Gynecology*, Vol.178:S141.

Available from https://dx.doi.org/10.5772/38369